Development of molecular probes acting on Tau/Tubulin and a-Synuclein/Tubulin interface

Kaliroi Peqini

▶ **To cite this version:**

Kaliroi Peqini. Development of molecular probes acting on Tau/Tubulin and a-Synuclein/Tubulin interface. Medicinal Chemistry. Université Paris-Saclay; Università degli studi (Milan, Italie). Dipartimento di Scienze della Terra, 2023. English. NNT : 2023UPASQ036 . tel-04662379

HAL Id: tel-04662379

https://theses.hal.science/tel-04662379

Submitted on 25 Jul 2024

HAL is a multi-disciplinary open access archive for the deposit and dissemination of scientific research documents, whether they are published or not. The documents may come from teaching and research institutions in France or abroad, or from public or private research centers.

L'archive ouverte pluridisciplinaire **HAL**, est destinée au dépôt et à la diffusion de documents scientifiques de niveau recherche, publiés ou non, émanant des établissements d'enseignement et de recherche français ou étrangers, des laboratoires publics ou privés.

THÈSE DE DOCTORAT

NNT : 2023UPASQ036

Development of molecular probes acting on Tau/Tubulin and α-Synuclein/Tubulin interface

Développement de sondes moléculaires agissant sur l'interface Tau / Tubuline et alpha-Synucléine / Tubuline

Thèse de doctorat de Università degli Studi di Milano et l'université Paris-Saclay
École doctorale n° 569, Innovation thérapeutique : du fondamental à l'appliqué (ITFA)
Spécialité de doctorat : Chimie thérapeutique; PhD Specialty : Therapeutic Chemistry
Graduate School : Santé et médicaments. Référent: Faculté de Pharmacie

Thèse préparée dans l'unité de recherche **DISFARM, Sezione di Chimica Générale e Organica "A.Marchesini" (Unimi),** sous la direction de Sara Pellegrino, Professeure Associoé et dans l'unité de recherche **BIOCIS Biomolécules: Conception, Isolement et Synthèse (Université Paris-Saclay, CNRS),** sous la direction de **Sandrine Ongeri** et la co-direction de **Julia Kaffy**

Thèse soutenue à Milano, le 11 Juillet 2023, par

Kaliroi PEQINI

Composition du Jury

Membres du jury avec voix délibérative

Giulio VISTOLI Professeur, Università degli Studi di Milano	Président
Sergio DALL'ANGELO Post-doctorant, University of Aberdeen	Rapporteur & Examinateur
Alessandro MORETTO Professeur agrégé, Università degli Studi di Padova	Rapporteur & Examinateur
Françoise OCHSENBEIN Professeur agrégé, Universitè Paris-Saclay	Examinatrice

Dipartimento di Scienze Farmaceutiche
PhD in Pharmaceutical Sciences XXXV cycle

Faculté de Pharmacie
PhD in Therapeutic innovation

Development of molecular probes acting on αSyn/Tubulin and Tau/Tubulin interaction

Kaliroi Peqini
R12788

Supervisor: Prof. Sara Pellegrino
(Università degli Studi di Milano)

Co-supervisor: Prof. Sandrine Ongeri
(Université Paris Saclay)

A.A. 2021/2022

This PhD takes part of Marie Curie Actions. It was funded by the H2020-MSCA-ITN-European Joint Doctorate "*Tuning Tubulin Dynamics and Interactions to Face Neurotoxicity: a Multidisciplinary Approach for Training and Research*", named with the acronym **TubInTrain,** Grant agreement n°: 860070.

www.tubintrain.eu

Table of contents

Abstract

Microtubules (MTs) are ubiquitous structures playing many roles in all eukaryotic cell types from fungi to mammals mainly consisting of conserved α/β tubulin heterodimers. Neurons are an impressive example of cells in which the contribution of MTs is fundamental to achieve their sophisticated cell architecture and to sustain their functional complexity. A growing body of evidence indicates that microtubule defects are linked to neurodegenerative diseases, such as Parkinson's Disease (PD). Several independent studies report a genome-wide crucial association with PD of single nucleotide polymorphisms in the MAPT locus, containing the gene coding for the Tau protein, a microtubule-binding protein that is predominantly expressed in neurons. The evidence of Tau pathology in PD is striking and contributes to neuronal dysfunction, impairment of axonal transport and cell death underlying PD. Recently another protein, α-Synuclein (αSyn), was put in the spotlight of various research groups since it was found aggregated in PD patients' brains. αSyn, composed of 140 amino acids, is in fact deeply involved in PD, as i) it is the main component of Lewy bodies, which are well-known as the histopathological hallmark of PD and ii) the gene that encodes it, SCNA, is mutated in familial PD. Even though, lots of new information regarding both αSyn/tubulin and Tau/tubulin have been obtained, their relevance over neuronal dysfunction remains unclear. For these reasons, their interaction is set at the center of my research project.

The first main aim of this PhD is the development of peptide based molecular probes able to modulate the Tau and α-Synuclein interaction with Tubulin. A library of peptides, both native and mutated sequences of αSyn, were synthesized and were used as molecular 'tools' for the conduction of *in vitro* experiments. The secondary structure of the peptides was characterized so to have a better idea of their possible activities during the *in vitro* experiments. Microscale Thermophoresis (MST) and the tubulin polymerization assay were employed using these peptides,

in conditions which were approximate to the physiological ones. From preliminary data, two mutants, seemed to affect the polymerization of tubulin *in vitro* and in a specific cell line. Moreover, we also aimed to stabilize a secondary conformation in the previously synthesized peptides, as a result a library of conformationally stable peptides was synthesized in order to obtain α-helically stable peptides. Their secondary structure was evaluated via CD and AT-IR experiments. In conclusion we could highlight that αSyn sequences tend to be difficult to be characterized conformationally since it is an intrinsically disordered protein, and in our case stapling strategies were completely successful. We, therefore, explored a less common stapling approach, by also designing a novel linker to afford the stapling. Unfortunately, our linker was not stable in standard SPPS conditions. Finally, Two Tau-deriving peptides were synthesized and used as molecular tools to detect their binding site on tubulin. The two peptides were then examined by our co-workers in PSI, Switzerland in soaking and co-crystallization experiments. The results have not been reported.

1.Introduction

1.1 Microtubules

Microtubules (MTs), the third principal component of the cytoskeleton, are rigid hollow rods approximately 25 nm in diameter, consisting of repeating α-tubulin and β-tubulin heterodimers (Figure 1). They function both to determine cell shape and in a variety of cell movements, including some forms of cell locomotion, the intracellular transport of organelles, and the separation of chromosomes during mitosis.[1] MTs also play a role in structural integrity, material transport, and force generation during mitosis.[1] MTs are dynamic structures, and their organization and dynamics are important for the development of processes and the maintenance of the structural and functional plasticity of neurons.[2,3] The dynamics of MTs show strong local variations and are regulated by a large number of associated proteins that modulate the assembly state, the organization, and the stability of the MT skeleton in a spatially restricted manner.[4] Such associated proteins include microtubule-associated proteins (MAPs), which bind to the MT polymer on one side, are proteins such as stathmin, which bind to soluble tubulin dimers on the other, thereby shifting the polymerization/depolymerization equilibrium either to the polymer or to the dimer state.[5,6] In addition, plus-end binding proteins (+TIPs) dynamically accumulate at the growing end of MTs, and MT severing enzymes such as katanin and spastin cause MT fragmentation.[7,8]

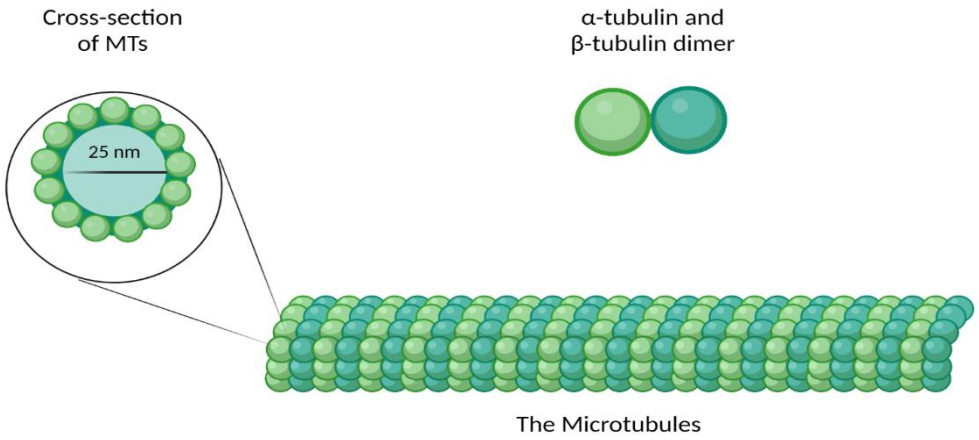

Figure 1. The microtubule consists of α-tubulin and β-tubulin that form hollow rigid rods with a diameter of approximately 25 nm.

1.1.1 Microtubules structure

As mentioned earlier, MTs consist of evolutionary conserved α/β tubulin heterodimers that assemble in a head-to-tail fashion into linear protofilaments whose lateral association forms polarized 25 nm wide hollow cylindrical polymers that are heterogeneous in length and highly dynamic *in vivo* and *in vitro* as they undergo a stochastic transition from polymerization to depolymerization, a process named dynamic instability (Figure 2).[9] This process allows MTs elongating and shrinking in response to local demands and is characterized by five parameters:

α) Polymerization rate,

β) Shrinkage rate

γ) Catastrophe (transition from polymerizing to depolymerizing phase) frequency

δ) Rescue (transition from depolymerizing to polymerizing phase),

ε) and pause (time spent neither polymerizing nor depolymerizing).

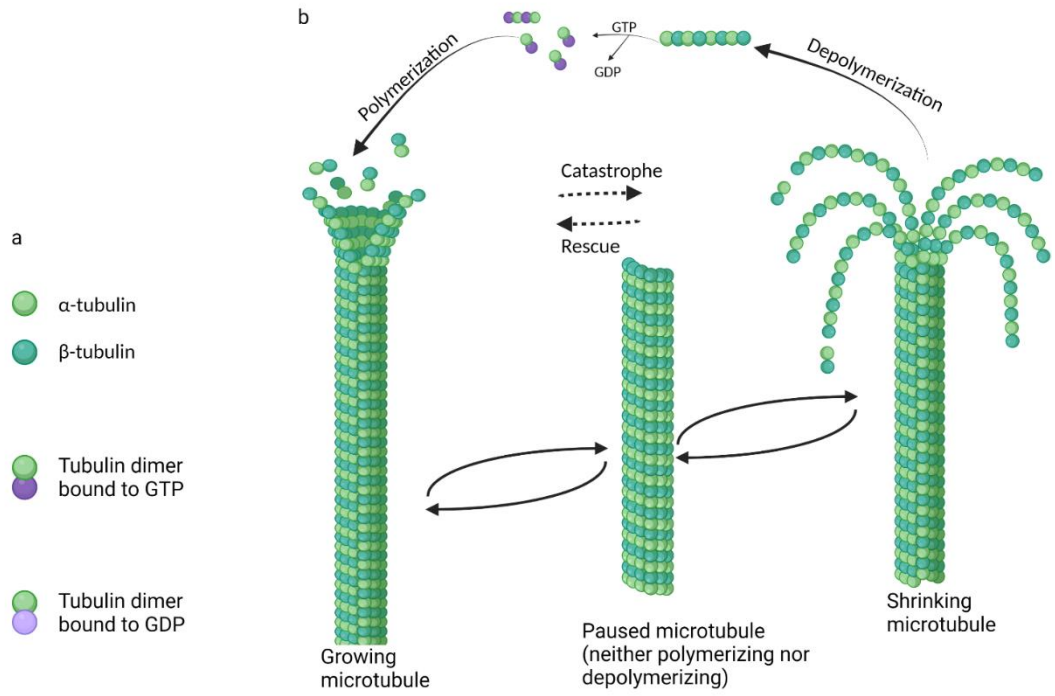

Figure 2. The microtubules and its dynamic instability process.

Dynamic instability is, indeed, crucial to many MT functions. [10] Although α - and β-tubulin display subtle differences, both comprise three separate structural domains[11]: the *N* terminal nucleotide-binding domain, the middle region involved in longitudinal and lateral dimers interaction and the *C*-terminal mainly responsible for the binding of microtubule-interacting proteins. This tripartite structure is of fundamental importance for the correct assembly of the MT and for the regulation of dynamic instability. The nucleotide-binding domain resides at the *N*-terminal half of the sequence (a little more than 200 amino-acids), containing alternated parallel β-strands and α -helices that form a true Rossmann fold. The Rossmnann fold is one of the most common and widely distributed super-secondary structures. It is composed of a series of alternating beta strand (β) and alpha helical (α) segments wherein the β-strands are hydrogen bonded forming a β-sheet.[12] There is a substantial difference between the α- and β monomer that leads to the intrinsic

polarity in the MT structure. Both monomers bind to GTP, but the binding domain of the α-tubulin is entrapped at the interface between the two monomers, known as non-exchangeable site (N-site) and avoids the exchange between GTP and GDP, whereas the site on the β-tubulin is exposed allowing GTP hydrolysis, and it is known as exchangeable site (E-site). These regions of tubulin are located at contact surfaces between α - and β-tubulin (N-site) or between heterodimers (E-site) and are highly complementary containing stretches of absolutely conserved residues; thus, a single amino acid substitution could be expected to significantly impede the formation of heterodimers, the overall ability of MTs to polymerize, or the conformational changes essential to the dynamic properties of the MTs. Thus, it is not surprising that the binding sites of two of the best-known microtubule-depolymerizing agents are in close proximity to these regions; indeed, the vinca domain is near the E-site whereas colchicine binds at the N-site. The middle part of the tubulin (around 150-180 amino acids) shows almost no sequence similarity with other proteins; it is involved in contacts between dimers both along and between protofilaments. The interaction surface between protofilaments involves the M-loop on one side with helix H3 along the other side. Although the helix appears rather rigidly locked into position, the flexibility of the M-loop suggests a simple mechanism for adapting the angle between protofilaments. Furthermore, this domain can also be considered the essential catalytic subunit of the molecule, being involved in GTP hydrolysis. The residue 254 appears to be the one with the catalytic activity and it is a glutamic acid in α- and a lysine in β-tubulin; thus, the opposite charge on these residues may help to explain the difference in the catalytic activity of the two monomers. Interactions between this region and the adjacent *N*-terminal domain participate in structural rearrangements resulting from the hydrolysis of GTP, which leads to two distinct protofilament geometries[13]: a GTP-bound state of straight protofilaments, as in the MT, and a GDP-bound state of curved

protofilaments (the 'relaxed' low-energy state of tubulin). When hydrolysis occurs after incorporation into the MT, the MT lattice maintains tubulin in the straight form and thus the energy of GTP hydrolysis is thought to be 'stored' within the lattice as structural constraint.[14] Upon loss of the GTP cap, energy is released causing the conversion into the curved low-energy state and MT depolymerization. The changes in the GTP/GDP state of the dimers, as well as their conformations and the resulting curvature of the protofilaments, can also modulate the interaction with MT interacting proteins.[15] The third domain (about 70 residues) is formed mainly by two long helices, a loop connecting them and a disordered short terminal sequence. This domain is the site of the major tubulin posttranslational modifications (PTMs) and is involved in the interaction with most of the MAPs, which share a binding motif with a basic character. The *C*-terminal region, in fact, is substantially acid, lying outsides the MTs and being highly flexible; thus, burying the *C*-terminus or shielding its charge is one of the dominant mechanisms to stabilize MTs. These residues mediate interactions with kinesin and dynein motors that facilitate intracellular transport in the anterograde and retrograde directions, respectively, as well as other MAPs that extrinsically regulate the dynamic properties of MTs. Certain residues found in this domain are also important for the stability of longitudinal protofilaments. MTs are intrinsically polar displaying plus and minus ends where the MT can grow and shrink; however, at the two MT ends the dynamics is different.[16] In each protofilament, the α/β heterodimers are oriented with their β-tubulin monomer pointing towards the faster-growing end (plus end) and their α-tubulin monomer exposed at the slower-growing end (minus end). Polymerization/depolymerization phases are also tightly associated with structural rearrangement of the terminal part of MTs, as polymerization occurs primarily by extension of protofilaments sheets[17] that eventually close to form the cylindrical body of MTs, whereas the depolymerizing MTs are often curved. Indeed, CryoEM

and X-ray scattering analysis indicated that the driving force for MT depolymerization is the curling up of protofilament[18], often associated with change in intradimer angle due to GTP hydrolysis.[19] Nowadays, the nature of the relationship between tubulin structure and MTs assembly and dynamics is becoming more and more evident. The plus end is a crucial site for the regulation of MT dynamics by the so-called plus-end tracking proteins (+TIPs). [16] Recent studies implicate a new category of proteins called calmodulin-regulated spectrin-associated proteins (CAMSAPs), sometimes referred to as minus-end binding proteins, that have been shown to bind to free minus-ends of MTs in various cell types, and thereby block the addition or subtraction of subunits from that end of the MT.[17]

MT assembly and dynamics are tightly regulated at multiple levels including the incorporation of alternative tubulin isotypes, the highly complex and diverse set of microtubule-interacting proteins, and the PTMs occurring on MTs.[20] In addition, the expression of different α- and β-tubulin genes and posttranslational modifications of tubulin are selectively combined, thus generating a tubulin code, that might regulate basic as well as higher-order cell functions.[21]

MTs were amongst the first targets to be studied by cryo-EM following its development. In the late 90s and early 2000s, 3D reconstructions of MTs with or without associated motor proteins via helical and pseudotomographic back-projection methods were limited to nanometer resolutions. This work gave information on the MT polymer not available from emerging crystallographic structures of α/βtubulin or protofilament subunits. An important and lasting shift was treating MT segments as single-particles in reference-matching approaches. A major challenge is differentiating between highly similar α and β-tubulin monomers during MT image processing, resulting in significant blurring of α and β-tubulin and

a failure to resolve the seam in more physiologically relevant pseudo-symmetric MTs.

This issue was particularly prominent in studies of MTs alone, while the presence of MT-bound proteins demarcating tubulin dimers would act as fiducials during processing, alleviating the severity of the artefact, particularly for pseudo-symmetric MT architectures. Combining statistical methods for seam-finding with pseudo symmetrical averaging approaches efficiently identified α and β tubulin register and seam-location with MT-binding proteins acting as fiducials. Nevertheless, CCD and film-derived reconstructions of pseudo-helical MTs and associated proteins could not break the ~4.5 Å resolution barrier required for the visualisation of the peptide backbone and side chains. The introduction of direct electron detectors was central to MT reconstructions achieving near-atomic resolutions. Ground-breaking work from the Nogales group, combining direct electron detector data with refined pseudo-helical processing methods achieved resolutions around 3.4 Å, allowing the authors to propose that small local nucleotide-dependent conformational changes leading to global changes in lattice compaction and twist govern dynamic instability. This and later work to near-atomic resolutions continued to use MT binding proteins as fiducials for differentiation of α and β-tubulin in processing when working on tubulin isoforms or nucleotide or drug-induced conformational changes in the MT lattice.[22]

1.1.2 Microtubules and Neurodegeneration

Neurons receive information and relay it along axons, to other neurons or muscles, through structures known as synapses. Neurodegeneration refers to the progressive loss of structure and/or function of neurons, often beginning at the synaptic distal ends of axons, a phenomenon termed as "dying-back neuropathy".[23,24] Neurodegeneration in humans can cause a variety of symptoms depending on the class of neurons affected and can lead to fatal outcomes. Some widely studied neurodegenerative diseases include Alzheimer's disease (AD), Parkinson's disease (PD), Huntington's disease (HD), and Amyotrophic Lateral Sclerosis (ALS). These, and other less well studied neurodegenerative diseases, exhibit a broad range of clinical symptoms, which nonetheless share several common pathological features.[25–28] One prominent cellular feature is the toxic aggregation of proteins that inhibit the protein quality control and the ubiquitin proteasome machinery of the neuron.[25,29] Other common characteristics include inflammatory responses[26], impaired ER calcium homeostasis[30], increased oxidative stress[31], and microtubule defects.[28] It is essential to recognize common underlying features that permit the degeneration of neurons to understand the most frequent mechanisms contributing to disease progression. Such an understanding can potentially lead to better therapeutic agents that can retard the progression of the most debilitating symptoms associated with neurodegeneration. Microtubules have often been thought to participate in neurodegenerative diseases through their well-established role in long-distance cargo transport. Examples include neurodegenerative diseases such as AD, HD, and several tauopathies that show compromised microtubule-dependent axonal transport in disease models.[28,32–38] However, these polymers play important roles in many aspects of neuronal cell biology that include establishing and conserving neuronal polarity, [39,40]maintaining neuronal morphology[41–43] and modulating signaling events.[40,44–46] In several neurodegenerative diseases, that include sporadic

rather than familial cases, we know little about the causes of disease onset. It is proposed that the disruption of microtubule dynamics may be a key mechanism contributing to neurodegeneration, since an alteration in dynamics can affect a number of the roles mentioned above. Therefore, modulating microtubule dynamics might help in retarding the progress of neurodegenerative diseases.

1.1.3 Microtubules-associated proteins (MAPS): α-Synuclein and Tau

MAPs are defined as proteins that bind MTs but are not molecular motors or severing enzymes and play a key role in regulating MT stability. This group of proteins is of particular interest because they play a critical role in maintaining cytoskeletal stability in neurons and other cells with complex three-dimensional structures. Based on their mode of action, MAPs can be classified into five categories:

a) Motile MAPs or motor proteins that generate forces and movement,[20,21]
b) Microtubule nucleators,[22]
c) Enzymes that break or depolymerize microtubules,[47]
d) End-binding proteins that specifically associate with plus- or minus-ends of microtubules,[48]
e) The so-called structural MAPs.

While the first four categories (a-d) of MAPs are clearly defined by their functions, the latter category (e) is a rather vaguely defined, heterogenous group of proteins that bind, and thus stabilize microtubules, but no systematic view on their functions has so far emerged. MAPs mutations, such as doublecortin (DCX), MAP2, MAP1A, MAP1B, and tau lead to varying degrees of central nervous system malformation and cognitive impairment in humans and in animal models.[49–57] One member of the MAP family, Tau, is also of particular interest because it has the unique ability to form toxic soluble oligomers, propagate and cause neurodegeneration in Alzheimer disease and related dementias.[58–62] It is the only MAP capable of this toxic gain-of-function and appears to do predominantly, but not exclusively, in humans.[63–72] The main role of Tau, which is known as one of the stabilizing MAPs, is to protect MTs against depolymerization by decreasing the dissociation of tubulin at both MT ends, resulting in an increased growth rate and decreased catastrophe frequency. *In vitro*, Tau induces MT formation at 37 °C and tubulin rings at 20 °C under experimental

conditions with no assembly of tubulin alone, suggesting that Tau is a MT inducer in addition to being a MT stabilizer. Tau was proposed to bind preferentially to the GDP-tubulin from the lattice, in detriment of the GTP-tubulin from the plus-end cap, and in agreement with a stabilizing role of Tau. However, monitoring of Tau binding to MTs by FRET has shown Tau decoration on MT tips, as well as on the lattice. Furthermore, the capacity of Tau to induce *in vitro* MT formation is lost when GDP-tubulin is used. In agreement, Tau depletion in rat cortical neurons results in the loss of MT mass in the axon, predominantly from the labile domain containing tyrosinated tubulin, rather than the stable domain of MTs. Green fluorescent protein (GFP)-tagged Tau was indeed observed to be more abundant on the labile domain of the MTs, or GTP-tubulin cap. Based on these observations obtained by quantitative immunofluorescence, the authors propose that Tau is not strictly a MT stabilizer, but rather allows the MTs to conserve long labile domains. However, a more likely explanation is that Tau is necessary to induce tubulin polymerization in the labile region. [72]

While for Tau protein there is an abundance of information over its interaction with MTs, little is known about alpha-Synuclein (αSyn), which has been lately proposed to be a MAP.

The first evidence of a link between αSyn and MT cytoskeleton dates to the beginning of this millennium, when αSyn was found to co-immunoprecipitate with α- and β-tubulin in zebra finch and murine forebrains.[73] During the last twenty years, this issue was not intensively addressed, but significant amounts of experimental evidence have been produced to strengthen this link and understand its meaning, thus adding little but important pieces to the puzzle. For example, the association between αSyn and different isoforms of tubulins was further supported by quantitative proteomics in rat MES cells. Further experimental evidence comes from the mouse and rat nervous systems and in post-mortem human brain. In detail,

αSyn co-localizes and is in close proximity to α-tubulin in the murine and human brain as revealed by confocal and electron microscopy analysis. Then, focusing on MTs, αSyn binding to *in vitro* assembled MTs has been revealed.[74] However, the specific effects of αSyn on tubulin polymerization and dynamics have been poorly investigated and the results are still somewhat controversial. Some authors have reported that monomeric αSyn does not influence tubulin polymerization in vitro, whereas others that it inhibits or promotes microtubules assembly, suggesting a regulatory role of the protein on MT formation. More recently, researchers suggested[75] that αSyn is not just a MAP, but rather a dynamase, i.e., a protein able to regulate both MT nucleation and catastrophe and regulates the partitioning between tubulin dimers and MTs at the neuronal growth cone. Finally, looking at the impact of αSyn on MT-dependent functions, recent papers show that αSyn promotes the formation of short transportable MTs that play an important role in axonal transport, and that WT αSyn induces vesicle endocytosis impairments via MT overassembly.[76]

2.Aim of the thesis

2.1 Development of molecular probes to study αSyn/Tubulin interaction and Tau/Tubulin

Nowadays, the molecular determinants in neurodegeneration are yet to be solved, much information is needed on how key proteins interact and which are the effects of these interactions. On one hand, αSyn is a very important protein involved in neurodegeneration, underlying those diseases termed synucleinopathies. Its propensity to interact with other proteins and structures renders the identification of neuronal death trigger extremely difficult. Conversely, the unbalance of MT cytoskeleton in terms of structure, dynamics and function is emerging as a point of convergence in neurodegeneration. Interestingly, αSyn and MTs have been shown to interact and mediate cross-talks with other intracellular structures. This is supported by an increasing amount of evidence ranging from their direct interaction to the engagement of in-common partners and culminating with their respective impact on microtubule-dependent neuronal functions. Last, but not least, it is becoming even more clear that αSyn and tubulin work synergically towards pathological aggregation, ultimately resulting in neurodegeneration.[74] However, understanding in detail which is the role of αSyn as a partner of tubulin and how it impacts on neuronal MT is crucial. On the other hand, Tau, is a MAP which is abundant in the axons of neurons where it stabilizes MT bundles. Together with other destabilizing MAPs, such as stathmin, Tau plays a central role in MT dynamics by regulating assembly, dynamic behavior, and the spatial organization of MTs. Tau and other MAPs that bind to MTs are tightly regulated by several factors, including post-translational modifications (PTMs), to ensure the appropriate dynamics of the system. However, the exact mechanism of assembly and stabilization of MTs by Tau remains challenging to characterize due to the inherent dynamics of the system and the disordered nature of Tau.[72]

In an attempt to address the current issue of lack of information on the interplay between αSyn and tubulin, the first part of this work was focused on the concerted action of αSyn and MTs both physiologically and pathologically. Hence, we first synthesized peptides that were domains of αSyn and performed *in vitro* assays to mimic the biological environment in order to obtain data about the direct interaction between αSyn and tubulin. Having, therefore, synthesized peptides from all the domains of αSyn our goal was to attempt to find the 'hot spot' of αSyn/tubulin interaction. In the library of peptides synthesized, we also included the PD mutated sequences to study the effects of the mutations on their interaction. The second part of this work was focused on Tau and tubulin. We synthesized Tau deriving peptides since one peptide, 2N, has been recently reported to bind near to the taxane-site at the luminal surface of MTs.[77] Moreover, a series of experiments were performed in order to illuminate the exact binding site of the peptides synthesized.

2.2 Synthesis of conformationally stable peptidomimetics deriving from αSyn

Based on the results of the *in vitro* assays that we conducted, we could derive as a preliminary result the fact that specific mutations decrease the polymerization of tubulin. We still lacked more detailed insight, though, of their interplay. Looking at the data obtained from the secondary structure characterization of the peptides in aqueous buffer pH 7 we observed that they are unstructured. Consequently, we hypothesized that probably a more stable conformation would help us to decipher better the interaction of the peptides with tubulin. As a result, we synthesized a library of conformationally stable peptides. Over the numerous strategies existing for the synthesis of peptides that adopt stable secondary structures, we chose to synthesize stapled peptides. We exploited the Lys/Glu lactamization for the

synthesis of the library. In addition to the lactams, taking under consideration numerous works published already on peptide stapling and a recently published review on stapling strategies[78],we thought that we could try a rather forgotten stapling pattern, the glutamic acid to glutamic acid one, since our sequences are rich in glutamic acids. We, therefore, designed a novel diazino linker to use to perform the stapling between the two glutamic acids.

The aim of the thesis is reassumed in Figure 3.

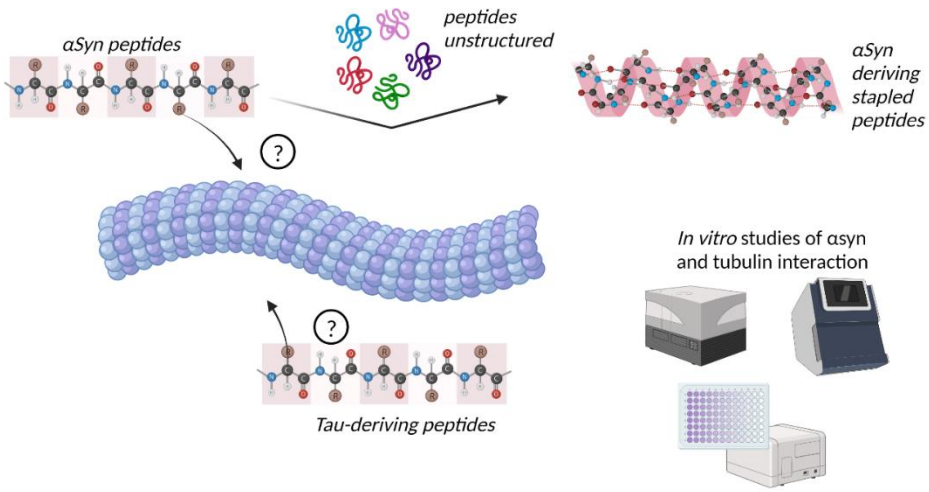

Figure 3. Aim of the thesis. Synthesis of αSyn peptides and Tau-deriving peptides and conduct in vitro assays with tubulin/MTs to investigate whether there is an interaction.

Chapter I

3.α-Synuclein

3.1 The synuclein family

Synucleins are proteins that exist in a great amount in the brain, but their exact mechanism of function is under question. The family of synucleins consists of three members— αSyn, β-synuclein and γ-synuclein — which are composed of 127 to 140 amino acids and present sequential similarities, with a resemblant domain organization (Figure 4).[79] Each synuclein protein in *N*-terminal half possesses an imperfect 11-amino-acids repeat that mainly contains the sequence **KTKEGV**. Right after these repeats, there is a hydrophobic intermediate region and a negatively charged carboxy-terminal domain; α- and β-synuclein have identical carboxyl termini. By immunohistochemistry, α- and β-synuclein are shown to be concentrated in nerve terminals, with little staining of somata and dendrites.

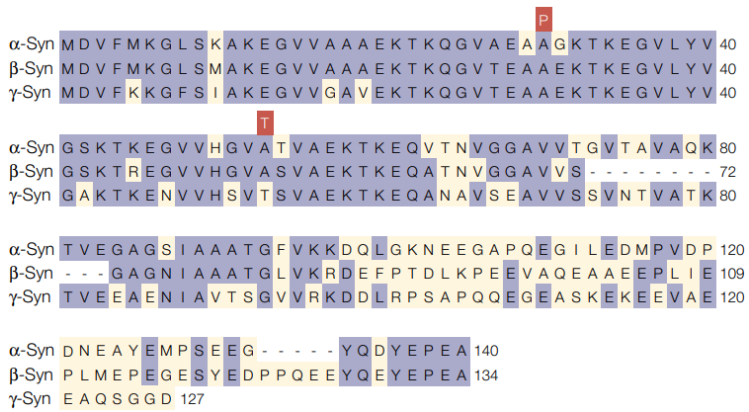

Figure 4. Sequence comparison of human αSyn, β-synuclein and γ-synuclein. Amino-acid identities between at least two of the three sequences are boxed (in blue). The α-Syn mutations of familial Parkinson's disease (A30P and A53T) are indicated (red). The amino-terminal half of the synucleins is taken up by 11-amino-acid repeats with the consensus sequence KTKEGV. αSyn assembles into filaments through these repeats. Despite similar repeat sequences, β-synuclein and γ-synuclein show poor assembly into filaments.

Sub-cellularly, they are found in nerve terminals, close to synaptic vesicles. In contrast, γ-synuclein seems to be present across nerve cells.[80] The first synuclein sequence was obtained from the electric organ of the Pacific electric ray (Torpedo californica) in 1988 by Maroteaux and colleagues.[81] The protein was named synuclein, because it was localized in the presynaptic nerve terminals and portions of the nuclear envelope. Subsequent studies have confirmed the presence of synuclein in nerve terminals but have not been successful in confirming its presence in the nucleus. However, the original name has survived for historical reasons. In 1992, the amino-acid sequence of one protein was defined, which was named phosphoneuroprotein-14 by Tobe et al.[82] and was found in plentitude in rat brains. In 1993, Uéda et al. described the amino-acid sequence of another protein, which they denominated 'non-amyloid-β component precursor' (NACP) because of the evident localization of a portion of this protein (the peptide NAC) in some amyloid plaques from the brains of patients with Alzheimer's disease.[83] However, subsequent work failed to confirm the presence of NAC in amyloid plaques.[84] In 1994, the amino-acid sequences of two homologous proteins from human brain that were identified because they reacted with an antibody raised against paired helical filament preparations from Alzheimer's disease brain.[85] The first protein was identical to NACP, whereas the second protein was the human homologue of rat phosphoneuroprotein-14. Both proteins were similar to synuclein from Torpedo californica, and consequently named them α- and β-synuclein, respectively. In 1997, Ji *et al*. reported the sequence of a protein, which they named breast-cancer-specific gene 1 (BCSG1) protein because of its high abundance in human breast cancer tissue.[86] Buchman *et al.*[87] independently identified the same protein and named it persyn. This molecule is also a synuclein that is now commonly referred to as γ-synuclein.

3.2 α-Synuclein functions

The function of αSyn is not entirely understood, but the following functions appear to be consistent with some of this protein's activities. These functions are also summarized in Table 1. Suppression of apoptosis in dopaminergic neurons by reducing protein kinase C activity Protein kinase C (PKC) is a serine-threonine kinase that phosphorylates different target proteins and therefore controls many mechanisms, such as apoptosis. This kinase is very sensitive to oxidative stress and triggers an apoptotic cascade in dopaminergic cells. αSyn seems to be a PKC down regulator that can protect dopaminergic cells against apoptosis. Particularly, it has been shown that αSyn can switch off the proteolytic cascade by downregulation of PKCδ expression. In dopaminergic cells, αSyn by deactivation of nuclear factor-κB reduces transcription of PKCδ. Therefore, αSyn can be considered to be a neuroprotective protein in dopaminergic cells.[88]

αSyn Function	Target	Mechanism	Result
Suppression of apoptosis[62]	Protein Kinase C	Deactivation of NFκB	Neuroprotection
Regulation of glucose levels[63–66]	G-protein-coupled-receptor The pancreatic β-cell KAPT channel	Increase tissue glucose uptake Inhibition of insulin secretion	Inhibition of type 2 diabetes Susceptibility to diabetes
Modulation of calmodulin activity[65]	CaM	Conversion of Cam from an inhibitor to an activator	Modulation of G-protein-coupled receptor kinase
Chaperone activity[67–72]	Presynaptic membranes Heat shock proteins	Maintenance of SNARE structure during assembly Helping proteins to obtain correct conformations	SNARE-complex activity Efficient neurotransmitter release
Maintenance of PUFA levels[73]	Acyl-coA synthetase	Modulations of lipid synthesis	Synthesis of brain vital fatty acids
Antioxidation[74–76]	Cytochrome c oxidase JNK-interacting protein	Prevention of Caspases activation Inhibition of JNK pathway	Neuroprotection
Neuronal differentation[77–79]	Rab3a	Activation of ERK/MAPK pathway	Transcription of genes
Regulation of dopamine biosynthesis[80,81]	Protein phosphatase 2A	Inhibition of tyrosine hydroxylase	Regulation of dopamine levels

Table 1. Alpha-Synuclein functions

Regulation of glucose levels

Apart from neurons, αSyn has also been identified in many other cell types, especially those involved in secretory processes. αSyn decreases insulin secretion as a consequence of interaction with insulin-containing secretory granules. αSyn interaction with KATP channels of insulin-secretory granules leads to the inhibition of insulin secretion triggered by glucose stimulation. These findings suggest a role for αSyn in diabetes that, like other degenerative disorders such as PD, is caused by a problem in the modulation of secretory processes.[89] Moreover, it has been shown that in type 2 diabetes (T2Ds), an amyloidogenic protein deposits in pancreatic β-cells and these patients are most likely to develop Parkinson's Disease (PD) as αSyn may combine to amyloid fibrils and form irreversible damaging complexes in dopaminergic cells.[90] On the other hand, in a recent study, αSyn is shown to increase tissue glucose uptake and thus diminish insulin resistance and possibly T2D. This study shows that in both humans and mice, higher levels of serum αSyn are directly associated with glucose metabolism.[91] It seems that αSyn can facilitate the entrance of glucose into adipose tissues and skeletal muscle through a G-protein-coupled receptor known as LPAR2-CD90.

Modulation of calmodulin activity

Calcium-modulated protein, also known as calmodulin (CaM), is a messenger protein that can be activated through binding to Ca^{2+} ions and triggers various mechanisms such as those involved in short- and long-term memory. It has been shown that both wild-type (WT) and mutant αSyn can interact with CaM not only in vitro but also in vivo. This interaction, which is dependent on calcium ions, causes αSyn fibrillization. Therefore, calcium ions can modulate αSyn function by inducing an interaction between αSyn and CaM. Moreover, CaM has an inhibitory effect on G-protein-coupled receptor kinase 5 (GRK5) in the absence of α-syn. On the other

hand, CaM stimulates GRK5 activity in the presence of αSyn. Taken together, αSyn by controlling the conversion of CaM from an inhibitor to an activator, and vice versa, is involved in the modulation of GRK indirectly.[92]

Promotion of sensitive factor attachment protein receptor-complex assembly *in vivo* and *in vitro*

Neurotransmitters are secreted several times from presynaptic vesicles within 1 min. The sequential secretion pathway of the neurotransmitter is strongly related to the organized activity of membrane fusion proteins. Assembly and disassembly of the N-ethylmaleimide – sensitive factor attachment protein receptor (SNARE) complex is one of the reactions, which has to be repeated for each single neurotransmitter release cycle. However, the assembly and disassembly of SNARE proteins are accompanied by the formation of intermediate SNARE protein structures that are unfolded and vulnerable to degeneration. αSyn, by its chaperone activity, is involved in the maintenance of SNARE structure during these assembly/disassembly cycles. Specifically, the direct interaction of αSyn with the SNARE -protein synaptobrevin-2/vesicle-associated membrane protein 2 causes the inhibition of SNARE complex assembly. Thus, αSyn dysfunction may lead to neurological problems because its deficiency reduces SNARE complex assembly.[93] During the SNARE complex assembly, unfolded cytosolic αSyn monomers bind to presynaptic membranes and form a complex of α-helically folded αSyn homomers, that is, chaperones assembly of SNARE complex and lead to neuroprotection in presynaptic terminals.[94] Moreover, large oligomers of α αSyn unlike monomers are harmful, and bind to an N-terminal domain of a specific SNARE protein called synaptobrevin-2 and prevent assembly of SNARE complex leading to neurodegeneration.[95]

Acting as a molecular chaperone

αSyn is considered to be a chaperone protein because it contains regions that are homologous with 14-3-3 proteins that interact with many cellular proteins. 14-3-3 proteins are members of the cytoplasmic chaperone family that phosphorylate the binding site of their targets, including PKC, Bcl-2-associated death promoter (BAD), and Extracellular signal-regulated kinases (ERK). It has been shown that αSyn can also bind to the targets of 14-3-3. In addition, overexpression of αSyn under thermal and chemical conditions that prevent aggregation of target proteins is another reason for suggesting αSyn as a chaperone. αSyn chaperone activity is dependent on both its *N*- and *C*-terminal regions. The *N*-terminal domain is responsible for αSyn interaction with substrate proteins, leading to the formation of a large complex while the *C*-terminal domain is responsible for the solubilization of that complex.[96] The HSPs are also a family of chaperone proteins that are expressed in response to cellular stresses. HSPs are involved in stabilizing proteins to obtain correct conformations, refolding of incorrect protein structures, and degradation of misfolded proteins. It has been shown that αSyn is part of a chaperone complex containing Hsc70/Hsp70 and two co-chaperones that are responsible for efficient neurotransmitter release.[97] The functional link between αSyn and HSPs is also examined in an experiment that the csp gene was deleted in knockout (KO) mice. CSPαas an HSP is recruited into the outer membrane of presynaptic vesicles and plays role in neurotransmitter release. Deletion of this protein is associated with the reduction of αSyn levels and lethal neurodegeneration. Interestingly, CSPα KO mice can be rescued from death if human WT-αSyn was overexpressed showing how αSyn can recover a chaperone activity.[98]

Maintenance of polyunsaturated fatty acids levels

The brain as the second main source of lipid content after adipose tissue is enriched in two polyunsaturated fatty acids (PUFAs), arachidonic acid and docosahexaenoic acid, which constitute about 20% of the brain fatty acids. Acyl-co A synthetase (ACSL) by adding acyl groups to a fatty acid backbone synthesizes these fatty acids from other available fatty acid stocks. The ACSL6 isoform that incorporates arachidonic acid into phospholipids is modulated by αSyn. Therefore, αSyn may be involved in the presentation of substrates to ACSL and consequently, in control of the brain's PUFAs levels.[99] Acting as an antioxidant and preventing oxidation of unsaturated lipids in vesicles Oxidative stress in dopaminergic neurons could initiate the pathological damage leading to PD. This damage is triggered by the oxidation of unsaturated phospholipids that consequently damage both cellular and intracellular membranes. The sensitivity of dopaminergic neurons to such damage is caused by the oxidative metabolism of dopamine within these cells. Therefore, dopaminergic cell membranes that are rich in unsaturated fatty acids are more vulnerable to this oxidation and damage. The monomeric form of αSyn by interaction with lipid membranes can protect lipids from oxidation, but the fibrillar form of αSyn does not have this capability. Therefore, it seems that monomeric αSyn could act as an antioxidant that plays an important role in dopaminergic neurons to protect them against oxidative damage.[100] Another study suggests that maybe αSyn is not an antioxidant but can prevent apoptosis by binding to cytochrome C oxidase in the mitochondrial membrane and inhibits the release of cytochrome c from mitochondria to cytosol. Consequently, caspases cannot be activated and thus cannot trigger apoptosis.[101] Moreover, hydrogen peroxide cannot damage αSyn expressing neural cells while it is toxic in control cells. Hydrogen peroxide in the absence of αSyn activates c-Jun N-terminal kinase (JNK), a member of mitogen-activated protein kinase (MAPK) family that promotes apoptosis under

oxidative stress condition. αSyn by activation of JNK-interacting protein/ islet-brain (JIP-1b/IB1) as an inhibitor of JNK pathway may protect cells from injury.[102] Neuronal differentiation As αSyn is both functionally and structurally homologous with chaperone protein 14-3-3[103], it can interact not only with 14-3-3 itself but also with its ligands, such as the kinase suppressor of Ras. Therefore, αSyn is considered to be involved in different cellular functions via activation of Ras. The activated form of Ras can activate a chain of events including the ERK/MAPK pathway that is involved in sending a growth factor signal from the cell receptor to transcription factors in the nucleus.[104] Moreover, αSyn binds to the membrane via interaction by Ras-related GTPase Rab3a. This molecular association is evidenced using antibody against Rab3a that dissociates bound αSyn from the membrane signifying that Rab3a is involved in stabilizing αSyn on synaptosomes.[105]

Regulation of dopamine biosynthesis

αSyn as a down regulator of tyrosine hydroxylase (TH) activity can modulate the production of dopamine and control its cellular levels. Therefore, αSyn-reduced expression or αSyn aggregation leads to increased dopamine synthesis, leading to oxidative stress caused by dopamine metabolism. The inhibitory effect of αSyn on TH activity is not direct and is dependent on the interaction between αSyn and protein phosphatase 2A (PP2A). This αSyn PP2A interaction activates PP2A phosphatase function, leading to dephosphorylation of TH-Ser 40 residue, and therefore TH inhibition. Both αSyn overexpression and mutations have been shown to upregulate the inhibitory effect of αSyn on TH and dopamine levels, leading to the downregulation of dopamine synthesis and release.[106] On the other hand, it has been shown that overexpression of αSyn increases activity of src, a member of the nonreceptor tyrosine kinases family, leading to hyperphosphorylation of proteins

and neurodegeneration. Scr can phosphorylate PP2A as a substrate at Tyr 307 and consequently inhibit its phosphates activity. [107]

Modulating vesicle trafficking

The synaptic vesicle formation pathway starts with the curvature of the membrane into a bud with the help of coat proteins such as clathrin which act as a spherical frame. This process is followed by the targeting of vesicles to a specific secretory point with the help of SNARE proteins. In this pathway, αSyn binds to the curved membrane selectively to modulate vesicle trafficking in synapses.[108] αSyn possibly reduces both the amount and the speed of vesicle recycling from synapses to the presynaptic area. This reduction in vesicular dynamics is important for synaptic homeostasis as the absence of αSyn disturbs; this equilibrium by increased vesicle trafficking.[109] This modulating role of αSyn is because of its specific structure. The 11 residue repeats of αSyn in the presence of liposomes can fold to a membrane binding helix that is divided by a mid-unstructured fragment.[110] αSyn can detect the vesicle pool as it has an affinity for lipid bilayers. This means that αSyn is more likely to be present at high levels in vesicle pools containing lots of small liposomes than in other parts of the cell since it can sense the membrane curvature of the vesicles.[111]

3.3 αSyn structure

αSyn is a small acidic protein with three domains namely *N*-terminal lipid-binding α-helix, amyloid-binding central domain (NAC), and *C*-terminal acidic tail (Figure 5).

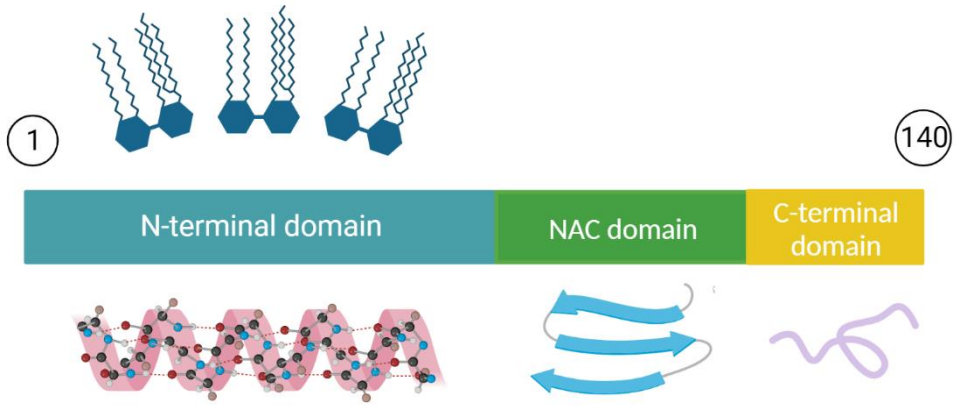

Figure 5. αSyn domains. The N-terminal domain is thought to bind to lipids and membranes and upon interaction it adopts an α-helical conformation. The NAC domain is the non-amyloid component. The C-terminal domain is rather not structured.

αSyn can be present as an α-helix structure in association with phospholipids or an unfolded conformation in the cytosol, suggesting that it plays specific roles in different cellular locations based on its dynamic structure.[112] The *N*-terminal domain of αSyn (residues 1–60) is a positively charged region, including seven series of 11-AA repeats. Each 11-AA repeat contains a highly conserved KTKEGV hexameric motif that is also present in the α-helical domain of apolipoproteins. Moreover, the ability of αSyn to disrupt lipid bilayers is related to these repeat sequences. These repeats, via their ability to induce αSyn helical structure and subsequently reduce the tendency of αSyn to form β-structures, are important in αSyn-lipid interactions.[113] The core region of αSyn (residues 61–95), also known as NAC, is involved in fibril formation and aggregation[114] as it can to form cross β-structures.[115] The *C*-terminal domain of αSyn (residues 96–140) is an acidic tail of 43-AA residues, containing 10 Glu and 5 Asp residues. Structurally, the *C*-terminal domain of αSyn is present in a random coil structure due to its low hydrophobicity and high net negative charge. *In vitro* studies have revealed that αSyn aggregation can be induced

by reduction of pH which neutralizes these negative charges.[116,117] An interaction between the C-terminal domain and the NAC region of αSyn is thought to be responsible for the inhibition of αSyn aggregation. Moreover, in the presence of $Al^{3+,}$ the *C*-terminal domain of αSyn binds to this metal ion and thus the disrupted inhibitory effect of the *C*-terminal on NAC leads to αSyn aggregation.[118] The phosphorylation of residue serine 129 is important in the inhibitory property of the *C*-terminal region as dephosphorylation of serine 129 causes αSyn aggregation.[119] Moreover, the *C*-terminal of αSyn is homologous with a small heat shock proteins (HSPs), suggesting a protective role for αSyn in keeping proteins out of the degradation process.[120]

Under normal conditions, native αSyn exists in a dynamic equilibrium between unfolded monomers and α-helically folded tetramers with a low propensity to aggregation.[121] The decline of the tetramer: monomer ratio and the consequent increase in the level of αSyn unfolded monomers favour its aggregation.[122]

3.4 Alpha-Synuclein and Parkinson's Disease

Parkinson's Disease (PD) is the second most common neurodegenerative disorder after Alzheimer's disease. Currently, PD affects 1%–2% of people over the age of 60 years, rising to 4% at age 80 years. PD is mainly characterized by the progressive loss of dopaminergic neurons of the substantia nigra that project to the striatum. [123] The deficiency of dopamine in the striatum leads to the development of the classic motor symptoms of PD, including bradykinesia, resting tremor, muscular rigidity, and postural instability. In addition to motor symptomatology, nonmotor manifestations, such as autonomic dysfunction, olfactory impairment, mood disorders (i.e., depression and anxiety), cognitive deficits, or sleep disturbances are also frequently present in PD. Most of these symptoms appear even before the motor symptoms and have a serious impact on the quality of life of patients.[124,125]

Because the PD motor symptoms emerge when the striatal dopamine levels have decreased by 60%–80%,[126] the study of PD non-motor symptoms is important to identify early biomarkers as well as targets to develop disease modifying therapies that slow or prevent the progression of neurodegeneration.

The neuropathological hallmark of PD is the abnormal accumulation and aggregation of αSyn in the form of Lewy bodies and Lewy neurites.[123] It is well established that pathological aggregation of αSyn is a common feature of several neurodegenerative diseases including PD, dementia with Lewy bodies (DLB) and multiple system atrophy (MSA), which are collectively referred to as synucleinopathies.[127]

αSyn is a protein with remarkable conformational plasticity since it can adopt a wide range of structural conformations.[128,129] Each αSyn conformation displays distinct properties in terms of neurotoxicity, stability and seeding and propagation ability. It has been proposed that the existence of structurally distinct αSyn assemblies or αSyn "strains" may contribute to explaining the clinical-pathological heterogeneity among synucleinopathies and help to develop strain-specific medications.[130–132]

Overexpressed monomeric WT-αSyn has been shown to inhibit vesicle endocytosis and impair neurotransmission. AS has been suggested to cause PD by disrupting the synthesis, storage, recycling, reuptake, and efflux of dopamine.[133] Increased levels of αSyn have also been found to reduce theactive tyrosine hydroxylase (TH) enzyme that is involved in the production of dopamine by stabilizing TH in its inactive form. αSyn overexpression was found to attenuate vesicular monoamine transporter 2 (VMAT2) activity. Thus, the dopamine is stored in synaptic vesicles via VMAT2 after its production to reduce the oxidative damage from its metabolites. Increased cytosol concentration of dopamine due to the reduction of VMAT2 activity by αSyn

has been proposed as a possible neurotoxic pathway in PD.[134] Dopamine transporter (DAT) has been associated with dopamine trafficking, but whether it increases or decreases DAT levels is still a debate because of evidence supporting both sides.[135] DAT knock-out mice showed high extracellular dopamine levels and low intraneuronal dopamine concentration; thus, DAT is important for neurotransmission and its activity (especially decreased dopamine uptake as well as increased dopamine clearance and efflux) upon disruption by αSyn can cause PD. Most of these proposed functions of αSyn rely on its membrane binding capacity.[136–141]

3.5. α-Synuclein mutations and their effects?

αSyn is a protein involved in PD, not only as the main component of Lewy bodies, but because of its several mutations observed in PD patients. It is well known that mutations can change the phenotype, having several effects on the structure of a protein. The most significant Parkinson's Disease-linked mutation can be observed in Table 2. Understanding how PD mutations affect αSyn structure and its functions is thus essential for gaining a profound understanding of the protein itself and for developing more effective pharmacological strategies.

Name	Sequence
A30P	^{22}TKQGVAEAPGKTKEGVLYV^{42}
A53T	^{43}KTKEGVVHGVTTVA**EKTKEQV**^{63}
E46K	^{43}KTKKGVVHGVATVA**EKTKEQV**^{63}
H50Q	^{43}KTKEGVVQGVATVA**EKTKEQV**^{63}
G51D	^{43}KTKEGVVHDVATVA**EKTKEQV**^{63}

Table 2. Most significant Parkinson's Disease-linked mutations.

A53T, A30P, and E46K Mutations

In 1997, Polymeropoulos *et al*.[142] identified the A53T mutation in the αSyn gene in Italian kindred and in three unrelated families of Greek origin with autosomal dominant inheritance for the PD phenotype.[143] A year after, Krüger *et al*.[144] reported the A30P mutation in the αSyn gene.[144] A third mutation, namely E46K, was identified in 2004.[145] During the years, it has been highlighted that mutations could impact both the free state of αSyn and its aggregated form. In this context, studies were performed using different techniques such as NMR spectroscopy, CD, and FTIR. Initial CD studies on WT αSyn and the first two identified mutations, A30P and A53T, showed that the three proteins lack a preferred conformation in solution.[146–148] However, in 2001, by conducting NMR studies, Bussell and Eliezer reported, that the mutation A30P strongly attenuates the helical propensity of the *N*-terminus. They observed indeed a positive C_α secondary shift, indicative of a significant preference for helical secondary structure in the WT 18–31 sequence, which was absent in mutant A30P. Conversely, A53T mutation leaves this region unperturbed, exerting a more modest and local influence on structural propensity. [149] In particular, the A53T mutant exhibited a slightly enhanced local preference for extended, β-sheet-like conformations around the site of the mutation. Other NMR studies on the WT, A30P and A53T, revealed a similar β-sheet-rich core region spanning residues 38–94 in the sequence of the two mutants, whereas the C-terminus remained flexible and unfolded in both cases.[150] McLean et al. investigated the αSyn long-range interactions by fluorescence resonance energy transfer (FRET). They reported, for both the WT and mutant A53T, a weak interaction between the N-terminal and C-terminal regions, whereas for mutant A30P they observed a statistical increase in the magnitude of FRET signal, indicating a closer vicinity between the N- and C- terminal regions.[151] In 2007, Fredenburg *et al*. reported a similar random coil secondary structure for both E46K and WT αSyn

when free in solution, as highlighted by CD experiments. [152] In 2009, Rospigliosi et al. studied the effect of mutation E46K on the long-range interactions by paramagnetic relaxation NMR(PRE) and residual dipolar coupling (RDC) measurements. Surprisingly, no decrease in long-range contacts was detected in the mutant E46K with respect to the WT. Furthermore, an increased interaction between the *C*-terminal tail, the NAC and the *N*-terminal regions was observed. The same experiments on A30P and A53T did not indicate any changes in the long-range structure. In the same work, the authors observed a slight increase in local helix propensity in the area immediately adjacent to the mutation of mutant E46K, by calculating its C_α chemical shifts deviations in comparison to the deviations of the random coil ones. [153] Kumar et al. used Molecular Dynamics (MD) to analyse the mutations A30P, A53T and E46K in water under explicit solvent conditions. These mutants showed variations, more specifically their RMSD scores were 0.529, 0.534, and 0.486 respectively, in their secondary structure compared to WT micelle-bound αSyn (PDB ID 1XQ8) simulated in sodium dodecyl sulphate (SDS). The secondary structure of A53T recorded in this study was similar to that determined by quenched hydrogen/ deuterium exchange NMR spectroscopy which states that five β-strands appear in the amyloid state of αSyn.[154,155] Passing from the last decade to the current one, computational techniques started being more intensively employed to shed light on the structures of the WT and the mutants. In 2011, Balesh *et al*.[156] performed classical MD and annealing MD (AMD) simulations and reported similar helical and β-sheet contents for the WT and A53T mutant-type αSyn proteins.[156] At the same time, A53T presented a more compact structure. In 2013, Coskuner and Wise-Scira performed all-atom replica exchange molecular dynamics (REMD) simulations on the full-length monomeric WT and A53T mutant-type αSyn proteins in aqueous solution utilizing implicit and explicit water models.[157] From these results, they observed that the helical content is minimally affected by the mutation

A53T except for a few residues in the *N*-terminal and *C*-terminal regions. Additionally, in contrast, to previous computational works[155] they reported an increase in the β-sheet formation close to the mutation site in the N-terminal region.[157] In the same year, a similar MD study was published on mutant A30P by Wise-Scira et al., reporting that the mutation has local as well as long-range effects on the protein structure. More specifically, the helical content of region 18–31 is less prominent in mutant A30P than in the WT protein. The β-sheet structure abundance decreases in the N-terminal region upon mutation A30P of the WT αSyn, whereas the NAC and *C*-terminal regions possess larger tendencies for β-sheet structure formation. Long-range intramolecular protein interactions are less abundant upon mutation A30P, especially between the NAC and *C*-terminal regions, leading to a less compact and less stable structure with respect to the WT.[158]

Recently Discovered Mutations

In 2013, a fourth mutation, namely H50Q, was identified.[159,160] Far-UV CD studies demonstrated that also the H50Q variant is a primarily unfolded protein in aqueous buffers.[161–163] Also, Chi et al. (2014), by using heteronuclear single quantum coherence (HSQC) NMR observed that the chemical shifts of most residues between the WT and H50Q were unperturbed, although the *C*-terminal region of H50Q is more flexible than that of the WT.[161] On the contrary, Ghosh et al. noticed chemical shift perturbations between WT αSyn and H50Q, by conducting the same experiments. In fact, they observed quite significant chemical shift perturbations in the mutation area and in the *C*-terminal region.[164] In 2014, a fifth mutation, G51D, was discovered.[160,165] Fares et al. performed CD experiments where the WT and G51D proteins exhibited the same random coil secondary structure. The 1 H, 15N-HSQC studies confirmed the lack of a preferred conformation for both proteins, while the analysis of the secondary structure propensity via C_α secondary shifts

deviations showed no significant loss or gain of secondary structure compared to the WT. Furthermore, it was observed that the mutation G51D also does not significantly perturb transient long-range contacts between *N*-and *C*-termini.[166] In the same year, mutation A53E was identified in a Finnish family.[167] Ghosh et al. performed NMR studies with the WT, A53T, and A53E αSyn. Their data showed approximately similar spectra of the WT, A53T, and A53E with relatively narrow dispersions in the proton dimension for all proteins, characteristic for unfolded structures. The chemical shift differences, however, suggest perturbation of chemical shifts for residues surrounding the A53E mutation site, as already observed for the other mutants. Significant chemical shift changes were also observed for the residues at the extreme C-terminus of αSyn. In contrast to chemical shift perturbation data, the secondary structural propensity did not show any major alteration due to mutation A53E or A53T.[164]

3.6. α-Synuclein, microtubules and tubulin

The first evidence of a link between αSyn and microtubule cytoskeleton dates to the beginning of this millennium, when αSyn was found to co-immunoprecipitate with α- and β-tubulin in zebra finch and murine forebrains.[73] Even though there are some research groups that have tried to investigate in detail this finding[168], there is still not enough information in order to produce a valid conclusion.

The key features regarding the MT organization and homeostasis in neurons are polarity, stability, and interaction with specific MAPs that make MTs unique for achieving the extraordinary morphological, mechanical, and functional complexity of the neuron. In addition, the stability of MTs marks out neuronal compartments as stabilized and dynamic MTs are differentially present in axons, dendrites, and synapses where they both shape MT arrays and control MT dependent functions.[4,169] Pivotal role for regulation of MT polarity, stability, and their

dependent intraneuronal processes are both post-translational modifications of tubulin and the activity of a plethora of microtubule-associated proteins.[170] In this context, understanding which is the role of αSyn as a partner of tubulin and how it impacts on neuronal microtubules is challenging.

3.6.1. 1 α-Synuclein and tubulin: a controversial interaction

Various investigators have detected an interaction of αSyn with tubulin[171,172], but the effects reported on tubulin polymerization are conflicting, with others reporting enhanced[173,174], and others reduced[172,175]tubulin polymerization as a result of αSyn overexpression.

The idea of possibly direct interaction between αSyn and tubulin/microtubules in neurons was first suggested by Payton *et al*.[73], and then developed thanks to the work of other teams. The connection between αSyn and different isoforms of tubulins was additionally supported by quantitative proteomics in rat MES cells.[176] More experimental evidence coming from mouse and rat nervous system[177,178]and in post-mortem human brain.[177] In detail, αSyn co-localizes and is in close proximity to α-tubulin in murine and human brain as revealed by confocal and electron microscopy analysis.[177] Next, focusing on MTs, αSyn binding to in vitro assembled MTs has been revealed.[178] However, although the above-described evidence strongly suggests the direct interaction of αSyn with tubulin, further data are required to consolidate the hypothesis that αSyn is a true MAP, namely a protein able to bind tubulin or MTs and regulate their behaviour. Certainly, at least the direct binding between αSyn and β-III tubulin has been demonstrated *in vitro* using two human proteins purified from E. coli, thus suggesting that indirect binding, from other proteins, could be excluded.[179] However, it is important to consider that proteins purified from E. coli are completely undressed from all those post

translational modifications which are known to exert a fundamental role in the regulation of tubulin functions and interactions. [170]

For solving the open question and get an insight into the molecular basis of the potential direct interaction between αSyn and tubulin, it is crucial to further investigate such interaction with the aid of advanced analytical approaches and tubulin purified by mammalian cells or organs. With this knowledge, the formation of a complex between αSyn and soluble tubulin has been demonstrated by native mass spectrometer/nano-electrospray ionization and NMR diffusion measurements approaches[75], and by surface plasmon resonance.[178] On the other hand, crystal structures of the αSyn-tubulin complex have yet to be acquired due to the intrinsically unstructured nature of αSyn that makes the formation of a stable complex highly improbable. From the available literature, different groups propose distinct regions of αSyn to be involved in its interaction with tubulin/MTs mainly *N*-terminal region[75], NAC region[172], or *C*-terminal region[173]. Vast differences in proposed regions of interest suggest that the αSyn α-synuclein sequence could be involved in such interactions.

Trying to dissect whether and how αSyn interplay with tubulin/MTs contributes to neuronal dysfunction and, ultimately, to neurodegeneration, two major issues must be assessed: the maintenance/loss of their interaction, both direct and mediated by common partners, and the impact on microtubule system behaviour and related function.

The first hypothesis could be that that alteration of the interaction between αSyn and tubulin could be directly linked to a pathogenic process. *In vitro* data obtained through different approaches indicate that mutations related to Parkinson's disease compromise the ability of αSyn to interact with tubulin/MTs. In fact, A30P and E46K mutations completely suppressed the binding affinity of the protein to tubulin, as

well as affecting microtubule assembly.[178] Also, A30P, A46K, and A53T αSyn variants exhibit changes in folding as they do not undergo tubulin-induced folding.[75] Furthermore, we pointed out that all the suggested putative microtubule binding domains on αSyn overlap with regions that are involved in its self-aggregation[168] being located as previously mentioned, in the central region able to acquire β-sheet structures[75,172], or located in the *C* terminal region.[173] Interestingly, *C*-terminal region seems to interact with the *N*-terminal region of αSyn in order to protect the aggregation-prone NAC domain, relevant towards the formation of compact aggregation-resistant monomeric structures.[180,181] On the basis that αSyn binding to MTs leads to acquisition of α-helices structures in physiological condition[75] and considering the high structural flexibility of αSyn and its predisposition to aggregate when the NAC domain is available, its proper interaction with its physiological partners, and therefore also with tubulins, can be required to avoid αSyn fold rearrangements that lead to self-aggregation. A second branch of evidence stems from studies on Tubulin Polymerization Promoting Protein (TPPP/p25), a brain-specific protein involved in the regulation of dynamics and stability of the MT system and capable of inducing MT bundling.[182] Pathologically, TPPP/p25α binds αSyn at its *C*-terminus region and forms αSyn oligomers/aggregates in neurons and oligodendrocytes in Parkinson's disease and multiple system atrophy, respectively.[183] The physiological role, if any, resulting from the interaction of TPPP/p25α with αSyn is still unknown as this complex has been detected exclusively at pathological conditions where defects in regulating MTs are also observed. Thus, the role played by TPPP/p25α could be attributable to it being a common partner for both αSyn and MTs. A third branch of evidence links the interplay between αSyn and tubulin with neurodegeneration. This has been suggested following studies on neuronal functions that rely on a healthy microtubule system. The physiological outcome of the αSyn interplay with tubulin/MTs includes the regulation of

microtubule behaviour in terms of assembly kinetics and dynamics, as well as axonal transport.

3.6.1.2. Impact on microtubule dynamics

Right from the beginning, it has been demonstrated that αSyn influences tubulin assembly kinetics both promoting[171,173,178] and inhibiting microtubule formation.[172] Subsequently, a more detailed view of such behaviour suggests that αSyn i) acts as a dynamase, due to its ability to regulate both MT nucleation and catastrophe in cell free systems; ii) increases MT growth rate in cells; and iii) colocalizes with tyrosinated α-tubulin, which is associated with the most dynamic MTs, in human neurons derived from embryonic stem cells expressing endogenous levels of αSyn itself.[75] Moving to the context of synucleinopathies, the interference of αSyn with tubulin assembly kinetics and dynamics has the potential to be a key player in the pathogenesis. MT assembly is reduced by A30P, A53T or E46K variants when compared to wild-type protein in cell free systems,[173,178] and in cells.[184]

4. Results and Discussion

The main goal of this work was to obtain insight into the questionable interaction between αSyn and tubulin/microtubules. Hence, a number of peptides, that were native and mutated sequences of αSyn, were synthesized and were used as molecular 'tools' for the conduction of *in vitro* experiments. The secondary structure of the peptides was characterized in order to have a better idea of their possible activities during the *in vitro* experiments. Microscale Thermophoresis (MST) and the tubulin polymerization assay were employed using these peptides, in conditions which were approximate to the physiological ones. Finally, a library of conformationally stable peptides was synthesized to obtain α-helically stable peptides.

4.1 Microwave-assisted Peptide Synthesis of αSyn domains

αSyn displays striking structural and functional similarities with the tubulin-interacting protein stathmin. Both of them are intrinsically disordered proteins of about 14-15 kDa, capable of adopting α-helix conformation upon interaction with binding partners.[185,186] Furthermore, αSyn, stathmin and RB3-SLD, interact all with the tubulin $\alpha_2\beta_2$ tetramer and promote MT catastrophes. Thus, we got inspired by the exploration of sequence similarities between αSyn and the members of the stathmin family to identify putative MTs binding domains that Cartelli *et al*. performed.[75] Pairwise alignment of WT-αSyn to stathmin showed about 20% identical residues and over 50% conservative substitutions. Two possible tubulin-interacting domains have been proposed for αSyn but the pathological point mutations, which impair the tubulin binding, are outside the suggested regions.[172,173] Therefore, searching for a tubulin-related physiological relevance for the region including the mutations, we decided to align two 21-residue stretches surrounding the residues 30 or 53 in the αSyn polypeptide chain. Interestingly, the fragment centered around αSyn residue 53, in which four of the five PD-linked point

mutations are clustered[187], aligned to one of the functionally relevant regions of the stathmin family (Figure 6, blue lines), namely the tubulin-binding domains.[188]

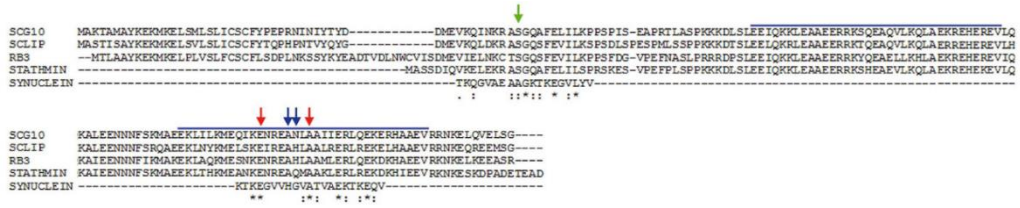

Figure 6. αSyn displays sequence similarities with stathmin. Multiple alignment of αSyn with four members of stathmin family was performed by ClustalW. Blue lines delimitate the domains of stathmin family involved in tubulin binding. Arrows mark the sites of αSyn pathological mutations: Ala30 (green arrow), the conserved Glu46 and Ala53 (red arrows), His50 and Gly51 (blue arrows). Asterisks mark invariant positions, while dots and colons highlight semi-conservative and conservative substitutions, respectively.

This region displays multiple invariant residues (Figure 6 asterisks), including the sites of the αSyn pathological mutations A53T and E46K (Figure 6, red arrows), besides several other conservative or semi-conservative substitutions (Figure 6, colons and dots, respectively). As the two domains reported in Figure 6, showed good conservation, they were anchored and aligned the other stretches of αSyn to the remaining regions of the stathmin-family. These regions display a very poor conservation and, thus, this result reinforces the idea that the region around the pathological mutations might be important for binding to tubulin and that its point mutations likely compromise αSyn/tubulin interaction. αSyn and stathmin share physicochemical and functional properties, and the good alignment of the fragment 43–63 of αSyn with a functionally relevant region of stathmins strongly indicates that αSyn and proteins belonging to the stathmin-family may be involved in some biological processes, such as the regulation of MT cytoskeleton. Therefore, we selected five regions in total to synthesize:

Region	Sequence
WT1	^{22}TKQGVAEAAGKTKEGVLYV^{42}
WT2	^{43}KTKEGVVHGVATVAEKTKEQV^{63}
NAC	^{60}KEQVTNVGGAVVTGVTAVAQKTVEGAGSI^{88}
C1	^{96}KKDQLGK^{102}
C2	^{131}EGYQDYEPEA^{140}

Table 3. αSyn regions selected to by synthesized.

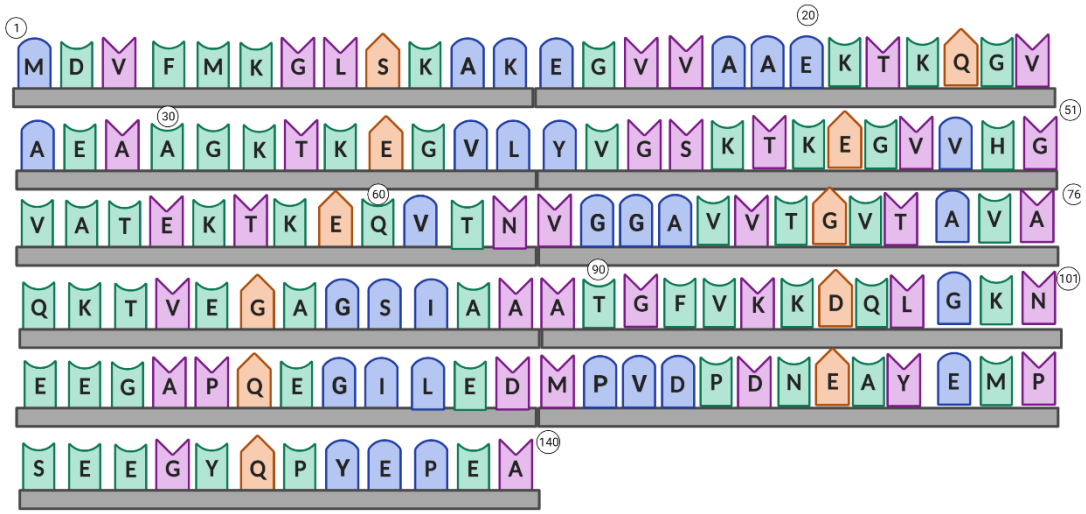

Figure 7. αSyn amino acid sequence.

In order to define the length of these sequences, we got inspired by the recent work of Cartelli *et al.*[189]

All the peptides synthesized can be observed in **Table 4**.

Name of peptide	Sequence	Mass	Purity
WT1(22-40)	TKQGVAEAAGKTKEGVLYV	28 mg	98%
Scrambled WT1(22-40)	AYKEVTVKVLGEAGAKQGT	30.7 mg	98%
A30P	TKQGVAEAPGKTKEGVLYV	30 mg	99%
Scrambled A30P	VLKETEKQAYVTGVPGAKG	10.2 mg	98%
WT2 (43-63)	KTKEGVVHGVATVA**EKTKEQV**	18 mg	91%
Scrambled WT2(43-63)	TQTVKKAAEVVEKVVTHKGEG	8 mg	98%
A53T	KTKEGVVHGVTTVA**EKTKEQV**	10 mg	92%
Scrambled A53T	VTTKVKQKKVETEVGAGHEVT	7 mg	90%
E46K	KTKKGVVHGVATVA**EKTKEQV**	3 mg	99%
Scrambled E46K	AKTKEKVKEGTGTVAVQKVHV	10 mg	99%
H50Q	KTKEGVVQGVATVA**EKTKEQV**	5.3 mg	95%
Scrambled H50Q	TAEVTKVGEVKKQKTQVAGVE	30.5 mg	95%
G51D	KTKEGVVHDVATVA**EKTKEQV**	6.5 mg	92%
Scrambled G51D	VEVEQKKQAKVVETTKAGTVG	7.3 mg	98%
NAC (60-88)	KEQVTNVGGAVVTGVTAVAQKTVEGAGSI	65 mg	90%
Scrambled NAC (60-88)	AAQNQVTSVKGVGEEVKITGGVAVAGTV	80 mg	90%
C1 (96-102)	KKDQLGK	17.3 mg	98%
Scrambled C1(96-102)	DKLKGKQ	13 mg	95%
C2 (131-140)	EGYQDYEPEA	34.3 mg	98%
Scrambled C2 (131-140)	QEEPGAYYDE	7.3 mg	95%

Table 4. αSyn peptides synthesized

In order to identify the “hot spot” of αSyn and tubulin interaction, we selected different domains to be synthesized by microwave assisted SPPS originating from the native αSyn sequence (Figure 7).

We also decided to employ the synthesis of the scrambled version for each peptide. Scrambled libraries are constructed through permutation of the original peptide sequence. They are typically used as:

1. Negative controls to show that a specific sequence rather than the amino acid composition is critical for activity; or
2. A tool for finding new leads by creating a random screening library.

We used them as negative controls on the assays that we performed.

All the peptides were synthesized by microwave-assisted solid phase peptide synthesis.

4.1.1 A brief overview of solid phase peptide synthesis SPPS

Bruce Merrifield developed solid phase peptide synthesis (SPPS) in 1963; this involves a solid support where the peptide is elongated, and excess reagents and by-products are removed through simple filtration after every reaction step (incorporating α-amino acid and deprotection).[190,191]

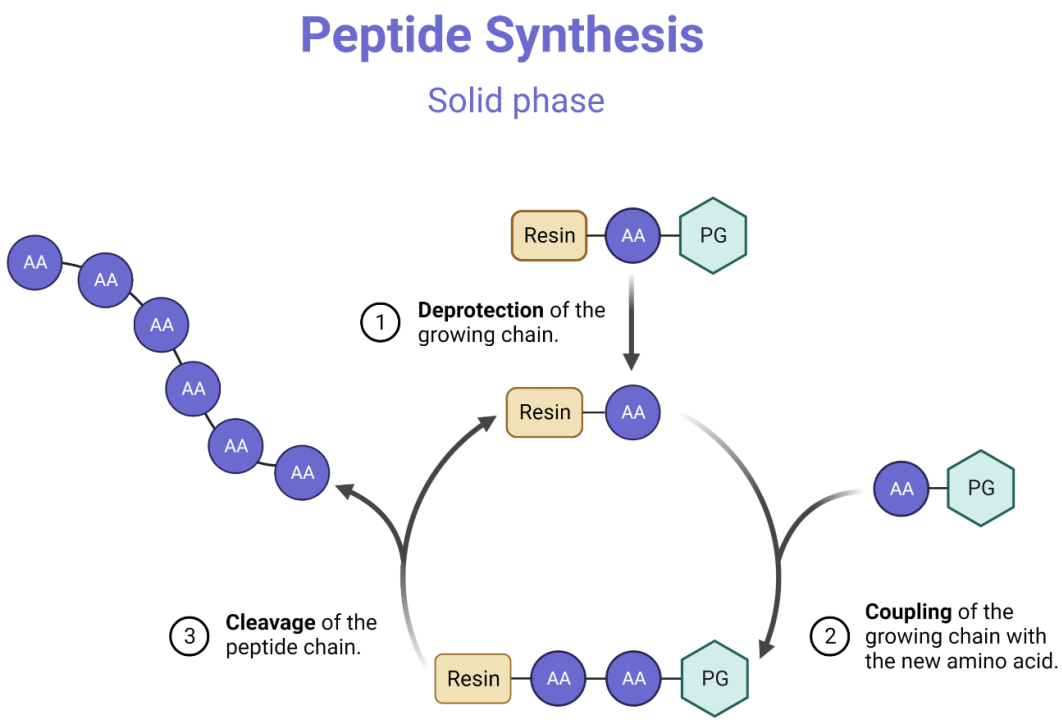

Figure 8. Solid-phase peptide synthesis. A repeated cycle of deprotection/coupling is followed.

SPPS involves the successive addition of protected amino acid derivatives to a growing peptide chain immobilized on a solid phase, including deprotection and washing steps to remove unreacted groups and also side products. The N-protected C-terminal amino-acid residue is anchored via its carboxyl group to a hydroxyl (or chloro) or amino resin to yield respectively an ester- or amide- linked peptide that will ultimately produce a C-terminal acid or a C-terminal amide peptide. After loading the first amino acid, the desired peptide sequence is assembled in a linear fashion from the C-terminus to the N-terminus (the C→N strategy) (Figure 8). Since its invention, SPPS has been a well-established and utilized method for convenient and rapid preparation of various peptides.[192] Although SPPS is typically used to synthesize peptides of approximately 30 amino acids in length, the peptide yield gradually decreases with repeated condensation reactions. As a result, the synthesis of longer peptides by SPPS is difficult. Furthermore, quite often intramolecular aggregations occur during the synthesis resulting in inaccessibility of the reagents to the reactive terminal of the elongating peptide. These problems can be only partially addressed with the use of more reactive coupling reagents, double coupling, excessive amount of reagents, and low-loading or highly distensible solid supports.

Microwave irradiation was reported to have several advantages over conventional SPPS, including a reduction in the reaction time, improved reaction efficiency, and

Figure 9. Liberty Blue automated synthesizer

suppression of inter- and intramolecular aggregations.[193] Microwave-assisted peptide synthesis has, hence, become one of the most useful tools for peptide chemists for the synthesis of difficult, as well as routine peptide sequences. In the early 1990s, Yu and co-workers[194] first reported the synthesis of short heptapeptides by using microwave-assisted SPPS in a kitchen microwave oven. At the conclusion of their communication letter, they envisioned that "the development of a convenient method for preparation of peptide fragment will be very useful for the synthesis of big peptides." When exposed to microwave irradiation, polar molecules or ions in a liquid solution will rotate in an attempt to follow the electric or magnetic field. The polar molecules have time to align with the field but not to follow exactly the oscillating field. During the peptide synthesis there are many polar molecules and ions present that can rapidly be heated by microwave energy including polar solvents (i.e., DMF or NMP or even water), the peptide backbone which contains the highly polar peptide bond, the N-terminal amine group, bases for the coupling and deprotection reactions, polar/ionic activators, and cleavage acids. All of them are amenable to microwave heating, accelerating reaction kinetics. Furthermore, the resulting raised temperature disrupts on-resin chain aggregation due to intra- and interchain association and allows for easier access to the growing end of the peptide chain, making efficient the synthesis of "difficult" and long peptidic sequences.[195]

4.1.2 Synthetical overview of αSyn domains

The peptide synthesis was carried out on a polymeric, swellable but insoluble support material (resin) of divinylbenzene cross-linked polystyrene, modified with Fmoc-Rink amide aminomethyl for the anchoring of the first amino acid (Fmoc-Rink amide AM resin, 100-200 mesh, 0.7 mmol/g) was used.

The automated synthesis was carried out using the Liberty Blue™ Automated Microwave Peptide Synthesizer (CEM) according to the Fmoc/*t*Bu strategy. All amino

acids (aa) were N-terminally Fmoc-protected, while the side chains of trifunctional aa were protected with orthogonal, acid labile groups. Even with the auxilium of the microwaves, we faced some difficulties with the synthesis, in particular for *N-terminal* peptides. The coupling of all the amino acids that are part of the amphipathic repeated motif of αSyn **KTKEQV** was quite challenging. A double coupling cycle was equipped to certify the adequate coupling of Val to Gln, Gln to Glu, Glu to Lys, Lys to Thr and Thr to Lys (Figure 9). However, even after following this strategy, at least one deletion was present at all crudes synthesized. Hence, for peptides WT2, H50Q, G51D, E46K and A53T a very efficient purification method had to be employed.

We first analysed via HPLC the crude peptides to obtain the initial % purity. The initial purities for peptides **WT2, E46K, H50Q, G51D** and **A53T** can be seen in **Table 5**.

Name	Sequence	Gradient	Crude purity
WT2	KTKEGVVHGVATVA**EKTKEQV**	15-85% solvent B	45%
E46K	KTK**K**GVVHGVATVA**EKTKEQV**	15-85% solvent B	40%
A53T	KTKEGVVHGV**T**TVA**EKTKEQV**	15-85% solvent B	50%
H50Q	KTKEGVV**Q**GVATVA**EKTKEQV**	15-85% solvent B	55%
G51D	KTKEGVVH**D**VATVA**EKTKEQV**	15-85% solvent B	35%

Table 5. Purities of crude peptides WT2, E46K, A53T, H50Q and G51D from analytical chromatograms.

Consequently, we run various trials of aliquots of the peptides in different eluents to verify which one is the most effective for the most efficient separation of the peaks. The crude peptides have a medium to good water solubility, so the starting gradient was always 15% ACN. We, then, tried four different methods that can be observed in Table 6:

Eluents	Duration	Flow rate
15-80% solvent B	30 minutes	10mL/min
15-70% solvent B	30 minutes	10mL/min
15-60% solvent B	30 minutes	10mL/min
15-50% solvent B	30 minutes	10mL/min

Table 6. Different purification methods tried to obtain the pure peptides. The eluents were composed as solvent A: water/trifluoroacetic acid 100: 0.1 and solvent B: acetonitrile/trifluoroacetic acid 100 :0.1.

Finally, the best separation of the peaks, to obtain the pure peptide with a purity of 90%, was the fourth method, which was also employed for their final purification.

In the case of the NAC peptide that is quite hydrophobic, small batches of the peptide, 15mg at a time, were dissolved in DMSO and the peptide was obtained pure after purification using a 35-75% solvent B (solvent A: water/trifluoroacetic acid 100: 0.1; solvent B: acetonitrile/trifluoroacetic acid 100 :0.1) over 40 min at a flow rate of 10 mL/min.

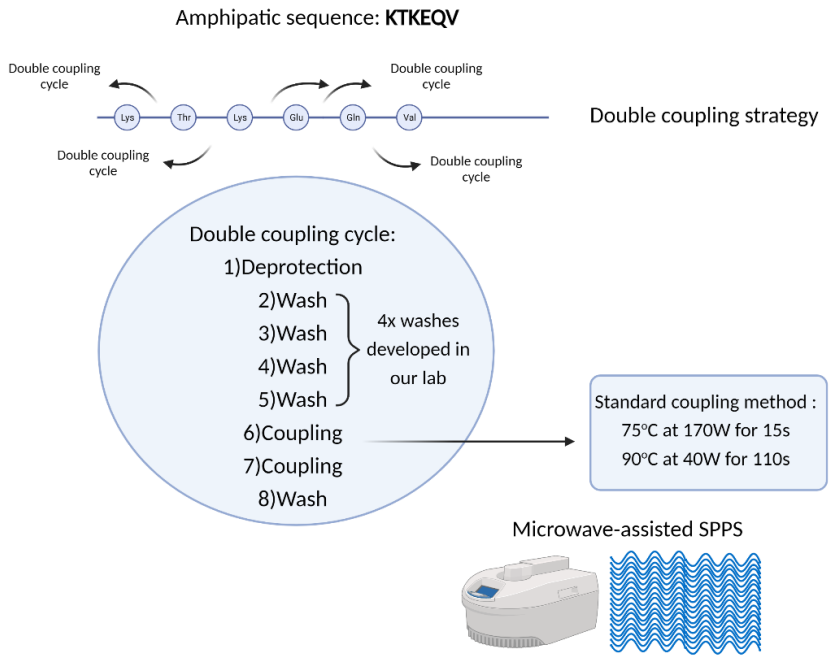

*Figure 10. Amphipathic sequence **KTKEQV** synthetic strategy.*

4.2 Conformational characterization of α-Synuclein domains

The fundamental structural features of αSyn have not yet been elucidated. The main hurdle to thoroughly understanding its behaviour is its intrinsically disordered nature and high susceptibility to the environment. αSyn, indeed, tends to acquire diverse transient and dynamic conformations depending on the presence of different biological and physico-chemical factors. As a consequence, we decided to analyse the synthesized domains in solution using circular dichroism and on solid state by ATR FT-IR.

4.2.1. Circular Dichroism experiments

Circular dichroism (CD) spectroscopy is a powerful method in structural biology that has been used to examine proteins, polypeptides, and peptide structures since the 1960s. CD signals only arise where absorption of radiation occurs, and thus spectral bands are easily assigned to distinct structural features of a molecule. An advantage of the CD technique in studies of proteins is that complementary structural information can be obtained from a number of spectral regions. In proteins, the chromophores of interest include the peptide bond (absorption below 240 nm), aromatic amino acid side chains (absorption in the range 260 to 320 nm) and disulphide bonds (weak broad absorption bands centred around 260 nm). When the chromophores of the amides of the polypeptide backbone of proteins are aligned in arrays, their optical transitions are shifted or split into multiple transitions as a result of 'exciton' interactions. The result is that different structural elements have characteristic CD spectra (Figure 10 B). For example, α-helical proteins have negative bands at 222 nm and 208 nm and a positive band at 193 nm (R). Proteins with well-defined antiparallel b-pleated sheets (β-helices) have negative bands at 218 nm and positive bands at 195 [196]nm, whereas disordered proteins have very low ellipticity above 210 nm and negative bands near 195 nm. The collagens are a unique class of proteins, which have three chains that wrap together in a triple helix.

Each strand has a conformation resembling that of poly-L-proline in an extended helical conformation in which all of the bonds are trans to each other (poly-L-proline II). Charged polypeptides, such as poly-L-glutamate or poly-L-lysine at neutral pH (originally thought to be in random coil conformation), have a similar extended poly-L-proline II-like conformation. The spectra of some representative proteins, with widely varying conformations, are shown in Figure 11 B.

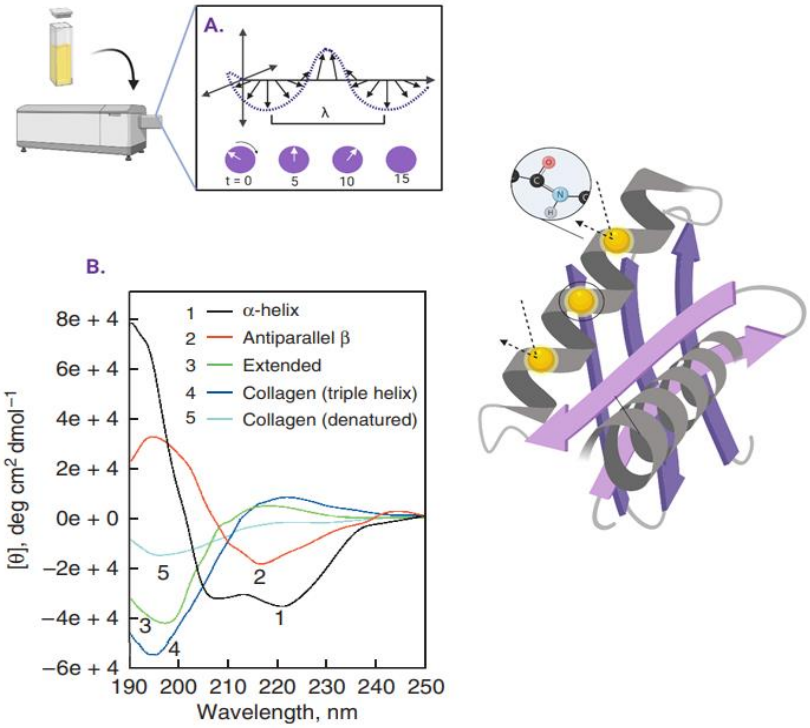

Figure 11. Sample is analysed using circularly polarized light (A). Light interacts with peptide bond and is refracted based on associated structure (B) Typical CD graphs for α-helix, antiparallel β-sheet, extended, collagen (triple helix) and collagen (denatured).

Consequently, analyses have been developed to deconvolute the various contributions arising from the different types of secondary structures present in a single molecule, thereby providing information on the overall structure of that protein.

Results from CD thermal experiments are usually presented by plotting the molar or the mean residue ellipticities at corresponding wavelengths versus the temperature.

The CD experiments on αSyn domains were performed in four different conditions:

a) In 100% Trifluoroethanol

b) In 100% NaH_2PO_4 - Na_2HPO_4 buffer at pH=7

c) In 100% MES Buffer at pH=6

d) In 100% NaH_2PO_4 -Na_2HPO_4 buffer at pH=8.

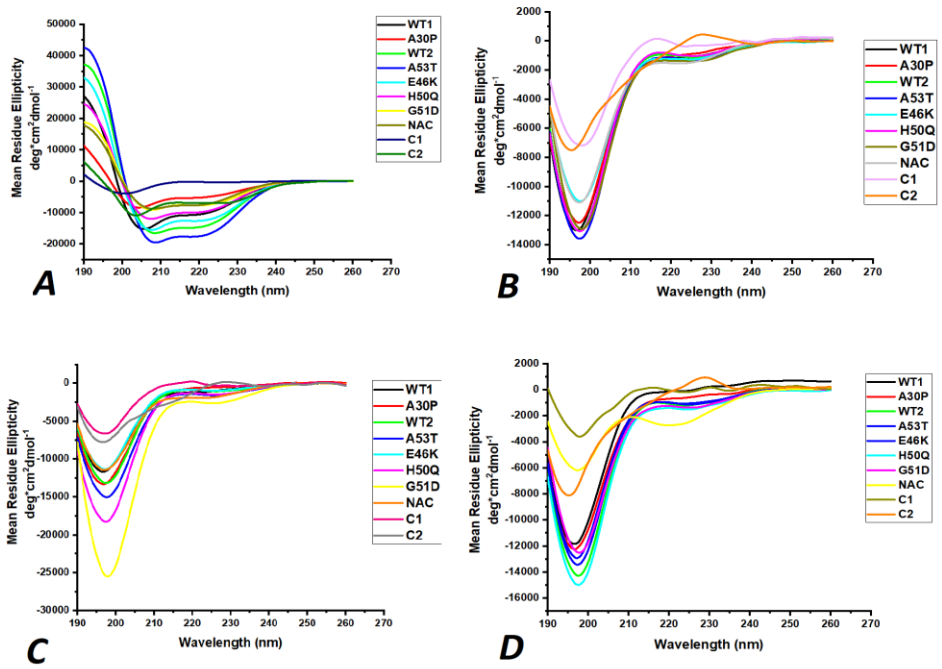

*Figure 12. CD data from all αSyn peptides in various pH conditions. **A**) All peptides at C=100 μM in 100% TFE. **B**) All peptides at C=100 μM in NaH_2PO_4 - Na_2HPO_4 buffer at pH=7. **C**) All peptides at C=100 μM in MES Buffer at pH=6. **D**) All peptides at C=100 μM in NaH_2PO4 -Na_2HPO_4 buffer at pH=8.*

A variety of conditions was chosen in order to ascertain the effect of the environment and of the pH on αSyn conformation. For most of the peptides, in

	$_{3\text{-}10}$helix	α-helix	anti parallel β-sheet	parallel β-sheet	β-turn	random
WT1	4,8%	10,5%	17,5%	8,8%	18,7	39,6%
A30P	0,5%	4,2%	27%	8,3%	12,2%	47,9%
WT2	6,6%	14%	-	8,3%	4,1%	67%
A53T	26,2%	25,7	-	6,1%	0,2%	41,7%
E46K	0,6%	12,3%	15,4%	8,9%	12,3%	45%
H50Q	7,5%	7,1%	20%	7,4%	13,6%	44,2%
G51D	1,6%	4%	38,4%	9,3%	14,6%	32,1%
NAC	3,2%	4,3%	33,4%	8%	9,5%	41,7%
C1	0,2%	2,6%	26,7%	13,5%	18,5%	38,5%
C2	1,2%	5,8%	21,9%	5,5%	5,8%	59,7%

Table 6. Percentages of secondary structure for each peptide at a concentration of 100 µM and in 100% TFE calculated on Dichroweb with the CONTIN algorithm.

various pH conditions, no preferred structure could be observed but when the peptides were measured in trifluoroethanol, a very intense alpha helical tendency was present (Figure 12). Analyses have been developed to deconvolute the various contributions arising from the different types of secondary structures present in a single molecule, thereby providing information on the overall structure of the peptide. The analyses were performed on the Dichroweb website using the CONTIN algorithm[197] for peptides in 100% TFE and 100% in NaH_2PO_4 -Na_2HPO_4 buffer at pH=7. The results of these analyses can be observed in **Table 6 and 7**.

	3-10helix	α-helix	anti parallel β-sheet	parallel β-sheet	β-turn	random
WT1	0,5%	3,1%	25,6%	13,1%%	18,7	39,6%
A30P	0,3%	3,1%	25,2%	12,9%	17,2%	41,3%
WT2	0,4%	3,3%	25,2%	13,2%	17,5%	40,4%%
A53T	0,4%	3,6%	25%	12,9%	17,1%	41,1%
E46K	0,4%	3,4%	24,9%	12,8%	17,1%	41,3%
H50Q	0,4%	3,2%	25,3%	13,2%	17,5%	40,3%
G51D	0,4%	3,6%	24,2%	12,5%	16,7%	42,6%
NAC	0,4%	3,5%	25,2%	12,7%	17%	41%
C1	0,2%	2,6%	26,9%	13,9%	18,9%	37,2%
C2	0,3%	2,9%	26,8%	13,4%	17,5%	39,2%

Table 7. Percentages of secondary structure for each peptide at a concentration of 100 uM and in 100% NaH_2PO_4 - Na_2HPO_4 buffer at pH=7 calculated on Dichroweb with the CONTIN algorithm.

4.2.2. Effects of the point mutations on the WT sequences in 100% TFE

αSyn is, as mentioned earlier, involved in PD, not only as the main component of Lewy bodies, but because of its several mutations observed in PD patients. It is well known that mutations can change the phenotype, having several effects on the structure of a protein. Understanding which are the effects of the point mutations on the secondary structure of αSyn are important for various reasons. The mutants A30P, E46K, H50Q, G51D, and A53T are considered some of the most potent of known mutations leading to PD and all of them are located in *N*-terminal domain of αSyn (Figure 13). Interestingly, despite all of these single amino acid changes leading to an early onset of PD, each provides very different effects on the αSyn aggregation rate and the oligomers that become populated. All mutations must therefore lead to either an increase in the aggregation rate, or a change in the oligomeric state or conformation that is populated upon aggregation, as well as a decrease in the normal tetramer: monomer ratios that facilitates these changes. Hence, the importance of the consolidation of how the structure and function of αSyn are influenced by these mutations is straightforward.

Having studied how much the secondary structure of the WT and PD-linked mutations is affected by different buffers, we then decided to investigate whether the mutated sequences having just one amino acid substituted would maintain their conformation or not. We could observe that in 100% TFE the A30P mutant in comparison to WT1 undergoes a transition, that according to our calculations equals to a total of 6,3% loss of α-helical conformation and an 8,3% increase of random coil conformation.

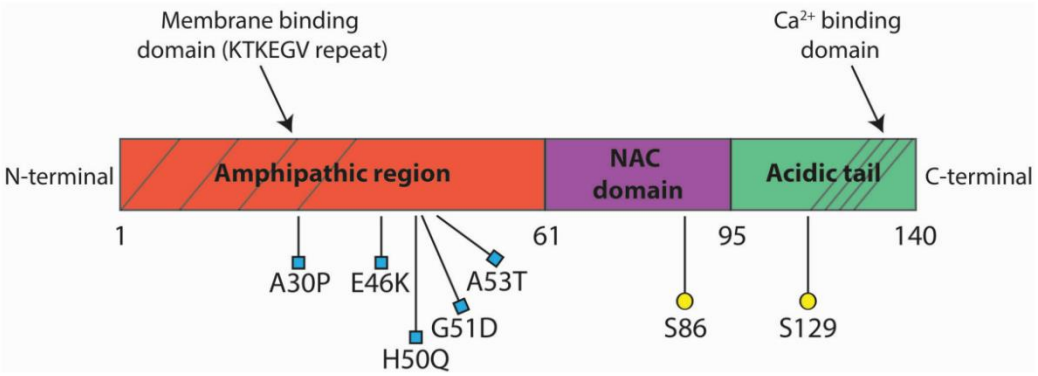

Figure 13. αSyn structure. Most of PD-linked mutants are located in the N-terminal.

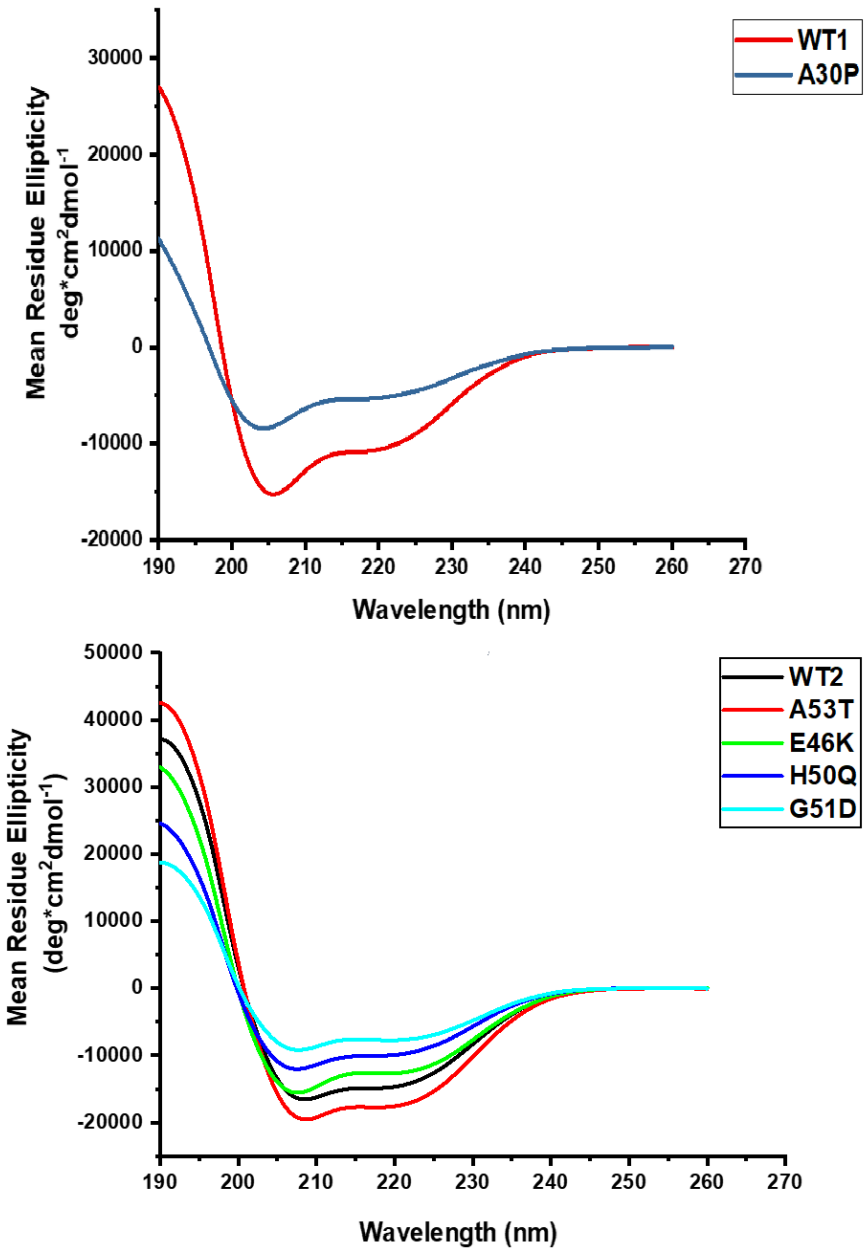

Figure 14. CD data from WT1 and A30P at a concentration of C=100 µM in 100% TFE (above) and CD data from WT2, A53T, E46K, H50Q and G51D at a concentration of C=100 µM in 100% TFE (bottom).

As for WT2 and the mutated sequences A53T, E46K, H50Q and G51D the results can be seen in **Table 8**.

Mutation	$_{3\text{-}10}$helix	α-helix	anti-parallel β-sheet	parallel β-sheet	β-turn	random
WT2→A53T	19,6% increase	11,7% increase	0%	2,2% loss	3,9% loss	25,3% loss
WT2→E46K	6% loss	1,7% loss	15,4% increase	0,6% increase	8,2% increase	2,2% loss
WT2→H50Q	0,9% increase	6,9% loss	20% increase	0,9% loss	9,5% increase	22,8% loss
WT2→G51D	5% loss	10% loss	38,4% increase	1% increase	10,5% increase	39% loss

Table 8. Percentual transition of secondary structure for mutants A53T, E46K, H50Q and G51D compared to WT2 at a concentration of 100 μM and in 100% TFE calculated from data obtained on Dichroweb with the CONTIN algorithm.

We conducted the calculation of the percentages of secondary structure for each peptide at a concentration of 100 μM and in 100% TFE calculated on Dichroweb with the CONTIN algorithm[197] and therefore we obtained insight into the various differences regarding secondary structure due to the mutations. The general trend is the increase in **anti-parallel β-sheet content** and the loss of **random coil content**.

4.2.3. Attenuated Total Reflectance-Fourier Transform Infrared (ATR-FTIR) spectroscopy of αSyn peptides

A large number of studies that included theoretical calculations and spectral methods have found that amides have some resonance structures,4 for example, the form of enol. The absorption spectrum bands of amide infrared radiation (IR), amide I (1600−1800 cm^{-1}), amide II (1470−1570 cm^{-1}), amide III (1250−1350 cm^{-1}), and amide A (3300−3500 cm^{-1}), are peaks of infrared characterization of amide. A protein peptide bond is an amide group. The amide A band (about 3500 cm^{-1}) and

amide B (about 3100 cm^{-1}) originate from a Fermi resonance between the first overtone of amide II and the N-H stretching vibration. Amide I and amide II bands are two major bands of the protein infrared spectrum. The amide I band (between 1600 and 1700 cm^{-1}) is mainly associated with the C=O stretching vibration (70-85%) and is directly related to the backbone conformation. Amide II results from the N-H bending vibration (40-60%) and from the C-N stretching vibration (18-40%). This band is conformationally sensitive. Amides III and IV are very complex bands resulting from a mixture of several coordinate displacements. The out-of-plane motions are found in amide V, VI and VIII. A protein structure is determined by using amide I, II, III, and A IR absorption peaks (Figure 16). [198] IR spectroscopy remains extremely useful as a tool to assess the structure of the large majority of the proteins that cannot be studied by X-ray crystallography and NMR.

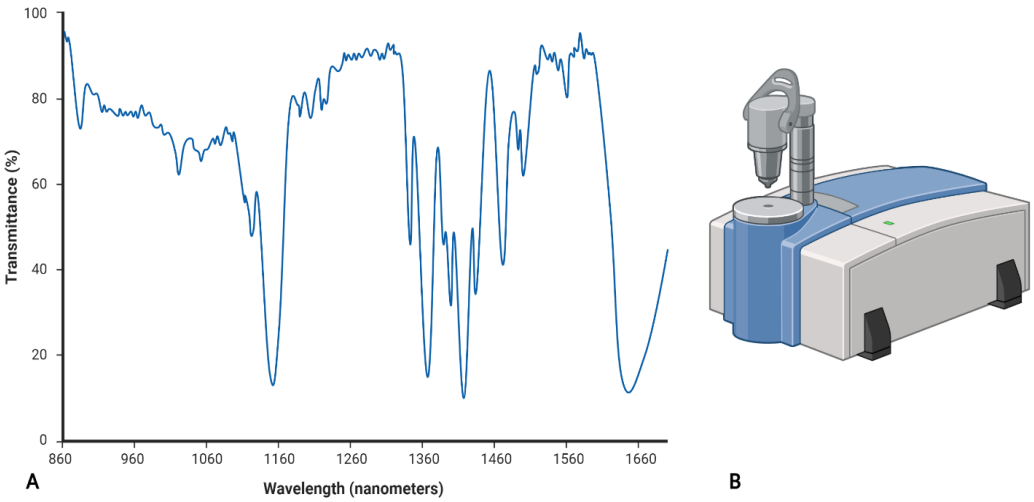

*Figure 15. **A** IR typical graph that plot % Transmittance and wavenumber **B** The instrument where few mg of the product is placed.*

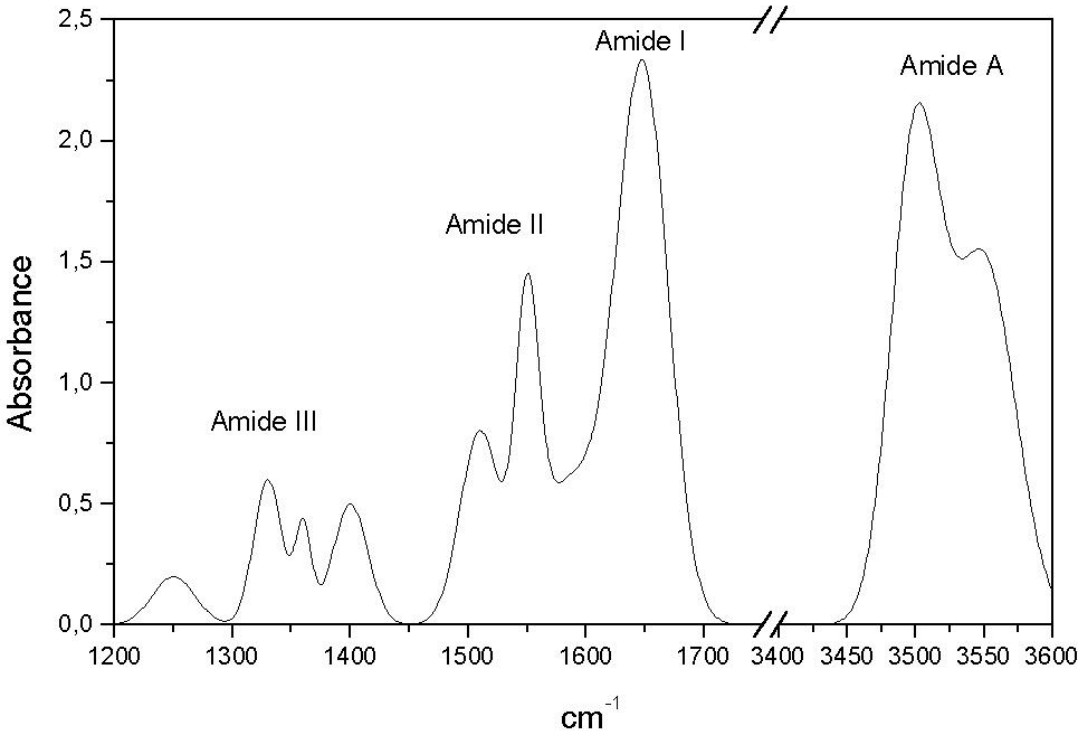

Figure 16. Characteristic peaks of amide I, amide II, amide III and amide A.

Attenuated total reflection Fourier transform infrared spectroscopy (ATR-FTIR) is one of the most powerful methods for recording IR spectra of biological materials in general, and for biological membranes in particular. Nowadays, the ATR-FTIR measurement is extremely convenient and easy as the sample is placed onto the ATR crystal and pressed down using the swivel press to ensure optimal contact between the sample and the crystal (Figure 9 B). After the measurement, the sample can then be recollected, ideal for peptides synthesized with low yields. The software on the computer plots the % Transmittance and the wavelength (Figure 9 A).[199]

ATR-FTIR spectroscopy is increasingly becoming an important method to determine the secondary structure of peptides and proteins. Among the spectral regions arising out of coupled and uncoupled stretching and bending modes of amide bonds, amide I and amide III spectral bands have been found to be the most

sensitive to variations in secondary structure folding. Amide I spectral region (1700–1600 cm^{-1}), although most commonly used primarily because of its strong signal, suffers from several limitations.

To further characterize the secondary structure of the peptides, we performed the ATR-FTIR analysis on the solid state. In Table 9, the most common secondary structures are reported along with their corresponding band assignment in water.

Secondary structure	Band Assignment in H_2O
α-helix	1648-1654cm^{-1}
β-sheet	1623-1641cm^{-1}
(high frequency component)	1674-1695cm^{-1}
Random	1642-1657cm^{-1}
Coils	1662-1686cm^{-1}

Table 9. Band assignments in water for secondary structures of proteins/peptides.

All the peptides revealed the typical bands of the amide bond (see Sup) and, the deconvolution of the amide I band highlighted that they adopt a mixture of conformations. In **Table 10**, we have reported the different conformations found after the deconvolution and their percentages for each peptide.

	β-sheet	$_{3\text{-}10}$helix	β-turn	α-helix	random
WT1	45%	55%	-	-	-
A30P	66,5%	-	34,5	-	-
WT2	42%	58%	-	-	-
A53T	52%	-	48%	-	-
E46K	53%	21%	25%	-	-
H50Q	30%	-	-	70%	-
G51D	42%	-	53%	5%	-
NAC	22%	-	-	-	78%
C1	-	0,7%	-	99,3%	-
C2	19%	-	-	-	81%

Table 10. Percentages of secondary structure for each peptide at the solid state calculated with OriginPro.

Hence, we compared these results with CD data to have a more complete idea of the secondary structure of the peptides. All of the peptides with a concentration of C=100 μM and in 100% NaH_2PO_4 - Na_2HPO_4 buffer at pH=7, adopted basically a random coil structure, which means they were unstructured. Diversly, in the solid state that the ATR-FTIR was conducted, from our deconvolution calculations, it can be deduced that they are a mix of conformations with a prevalence of the β-sheet structure in most of them. The two *C*-terminal peptides were an exception to this trend, mainly because of their short length and as it can be seen in **Table 6**, they were either α-helical or unstructured.

Finally, after having conducted a thorough characterization of the αSyn peptides' secondary structure using CD and AFT-IR, we could observe their disordered nature, being sequences that derive from αSyn, which is known as being an intrinsically disordered protein. In 100% TFE, the peptides showed a variability of conformations, which also included a good percentage of α-helical portion. When measured in 100% NaH_2PO_4 - Na_2HPO_4 buffer at pH=7, they all presented a complete loss of their α-helical tendency and were shown to obtain a mixture of β-sheet richer structures and random coil conformation. The increase in β-sheet content is also understandable because αSyn is an aggregation-prone protein. On the other hand, in the solid state, most of them presented high percentages of β-sheet content.

5.Investigation on the effects of α-Synuclein domains on Tubulin polymerization and binding

Peptides selected from 5 regions of αSyn were synthesized successfully using microwave-Assisted SPPS. The peptides were selected and synthesized as probes for studying, initially, whether there really is an interaction between them and tubulin. Secondly, the peptides were supposed to also provide information on the 'hot spot' of the interaction, since we hoped to receive valuable insight if one of them seemed to interact better. For these reasons, we chose two kinds of experiments. The first experiment conducted, was MicroScale Thermophoresis and it was supposed to provide thermodynamical information for the interaction, also measuring the dissociation constant K_D. The second experiment was the so-called 'Tubulin polymerization assay', which is based on the fact that light is scattered by microtubules to an extent that is proportional to the concentration of microtubule polymer. The tubulin polymerization assay provided information on the kinetics on the tubulin. Both of these experiments were conducted with the full-length αSyn and the mutants available in our collaborator's laboratory (Prof. Graziella Cappelletti laboratory in Biosciences, Unimi) and the peptides.

5.1 MicroScale Thermophoresis

Microscale thermophoresis is an immobilization-free technique for quantifying biomolecular interactions.[200] It measures the movement of molecules within a temperature gradient which induces changes in molecular properties of the studied molecules in terms of charge, size, hydration shell or conformation.[201] The MST technique is based on the directional movement of molecules along a temperature gradient. From a theoretical point of view, the directed movement of particles was originally described in 1856.[202] Thermophoresis equations and mathematical background have been previously described in princeps publications. [201,203]From a practical point of view, the MST instrument records fluorescence of the sample with

a focal infrared (IR) laser during and after the laser is turned on. Since the phenomenon of thermophoresis is diffusion limited, measurements are made within 30 s. The fluorescence traces contain different information on the binding event. The initial fluorescence has to be constant for every sample. Turning the IR-laser on results in a change in fluorescence intensity, called T-jump. This event relates to the temperature-dependent variation of fluorescence. The motion induces a concentration gradient of the fluorescent molecules. In the end, fluorescence intensity reaches a steady state where thermal diffusion is countered by mass diffusion.[201] When the laser is turned off, back diffusion occurs, led by mass diffusion.[201] Affinity is quantified by monitoring the change in normalized fluorescence called F_{norm} as a function of the concentration of the binding partner.[201] The K_D model used by MST describes a 1:1 stoichiometry interaction according to the law of mass action and allows to derive a formula for the fraction bound in case of a binding event.[201] The fraction bound is defined by the Kd and the concentration of the target molecule and depends on the ligand concentration.[203]

The technique is extremely sensitive to any change in molecular properties, allowing precise analysis of binding events within a few microliters of solution for almost any molecule, such as protein-binding small molecules or ligands binding to liposomes or enzyme substrates. Since MST is a solution-based method, it avoids surface artifacts and immobilization protocols. MST is not restricted by the molecular weight ratio of partners involved in the binding like DLS and does not require a size change like SPR.[204] Besides the phenomenon of thermophoresis, the shape of the MST response is also influenced by the temperature-related intensity change (TRIC).[204]TRIC is detected just after the IR laser is turned on, whereas thermophoresis is most noticeable at the later stage of signal collection.

MST relies on the two effects, which are closely linked together.[205] An illustration of the technology is presented in Figure 17.

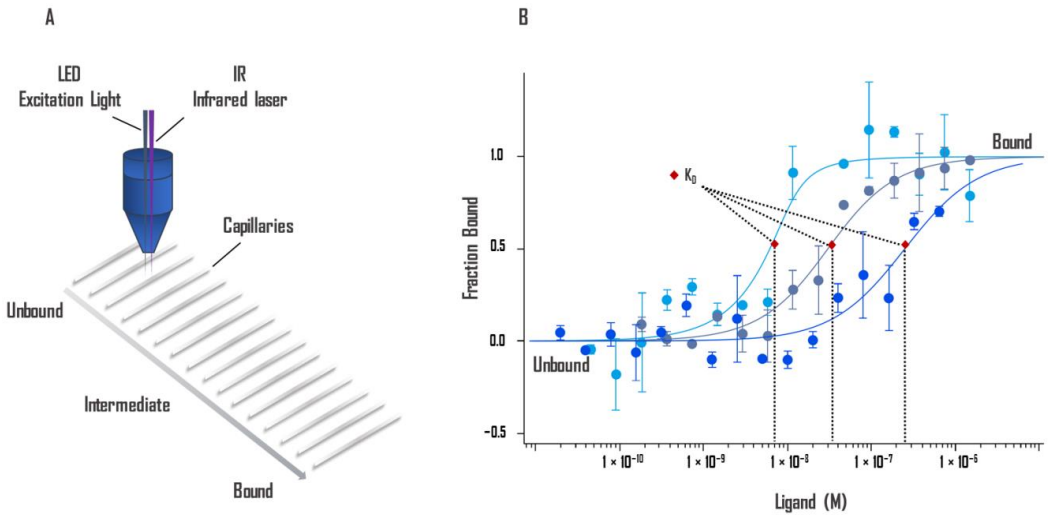

Figure 17. A. Schematic representation of the optical system. Fluorescent molecules in the 16 capillaries are excited and the fluorescence detected by the same objective. An IR laser heats up locally, and thermophoresis of the fluorescent molecules across the temperature gradient is detected. B. The intensity of fluorescence changes due to the movement of molecules away from the heated area differs when the ligand is bound. A binding curve can be established from difference of thermophoresis between the fluorescent molecules of both unbound and bound states against the ligand concentration. Binding constants K_d can be derived from binding curves. Graphs are represented as fraction bound against ligand concentration. Data represent three independent experiments and were fitted to a Kd binding model assuming a 1:1 binding stoichiometry.

MST was performed to measure the binding affinity between tubulin and αSyn and the mutated isoforms A53T and E46K. Tubulin was labelled with Red-NHS second generation kit at the lysines and during the assay it was used at a final concentration of 50nM. Lyophilized αSyn was resuspended using MST buffer and was used in the assay in serial dilutions, starting from 242 µM up to 15.6 µM. Higher concentration of αSyn weren't tested since it could lead to aggregation of both proteins. The parameters of the experiment can be observed in Table 11.

Protein	Buffer	Concentration
Tubulin	MST	50nM
WT-αSyn	MST	242 µM up to 15.6 µM
E46K	MST	242 µM up to 15.6 µM
A53T	MST	242 µM up to 15.6 µM

Table 11. MST experiment performed with tubulin and WT αSyn, E46K and A53T with specific concentrations all in MST buffer.

αSyn WT kD was found to be 20 µM, A53T instead was observed to increase the affinity for tubulin, and the E46K reduced the affinity. A30P showed no affinity at all (not shown here).

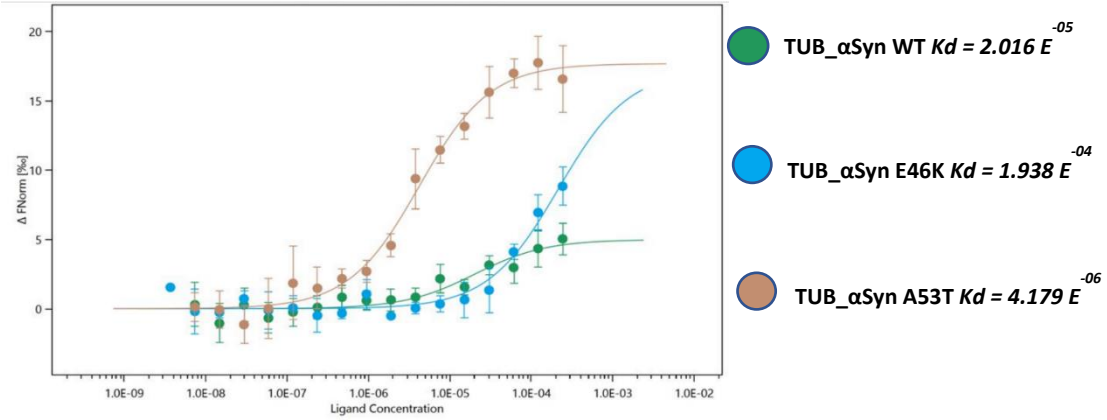

Graph 1. Binding of WT αsyn, E46K and A53T against tubulin using MST. Binding of all three proteins to labelled tubulin resulted in a clear response in fluorescence signal, dependent on the concentration of the αSyn proteins. Graphs are represented as ΔFnorm [‰] against ligand concentration. Data represent three independent experiments and were fitted to a K_d binding model assuming a 1:1 binding stoichiometry.

MST was also performed with peptides using a different approach to evaluate the possibility of later conducting the experiment with serial dilutions mainly because of the small molecular weight of the peptides compared to that of the long proteins.

In this experiment, peptides were dissolved using MST buffer at a final concentration equal to 500 µM during the assay. The assay conducted to investigate

whether there in an interaction between tubulin and the αSyn peptides was conducted on the 'Screening Mode' which allowed us to have a rough idea of whether there is not an interaction. If there was an interaction, we would then also conduct the 'Binding Affinity' experiment. The procedure of an Binding Affinity experiment can be observed in Figure 18.

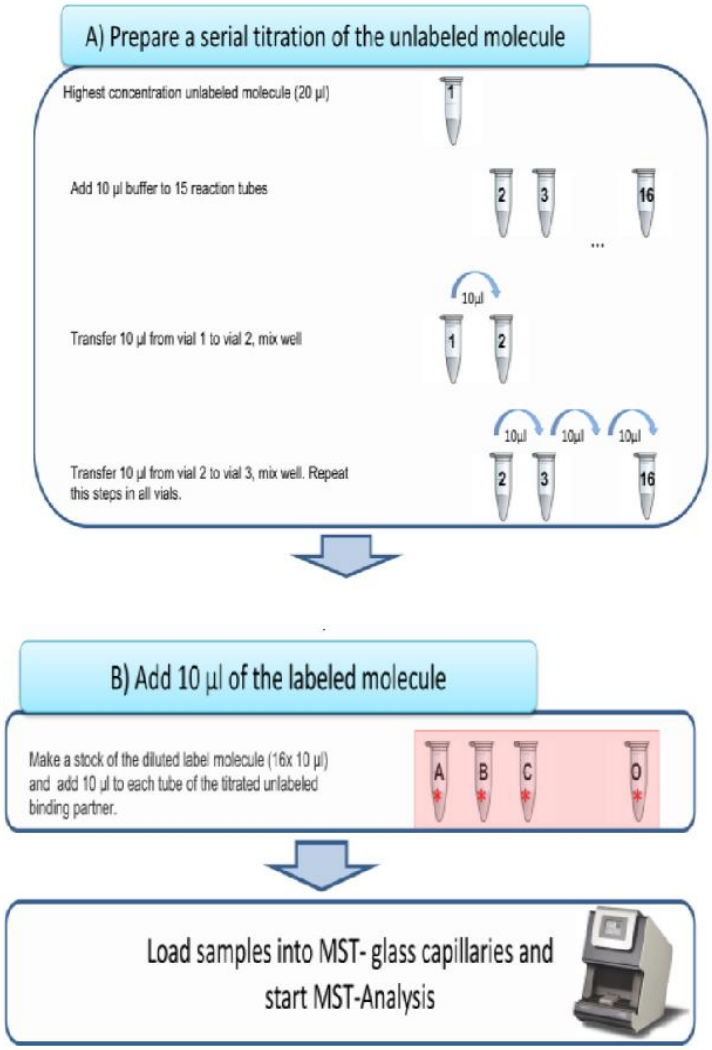

Figure 18. A schematic overview how to prepare a MST-Experiment.

Unfortunately, from our experiments we did not detect an interaction between tubulin and the peptides. However, we did face a number of difficulties during the experiment.

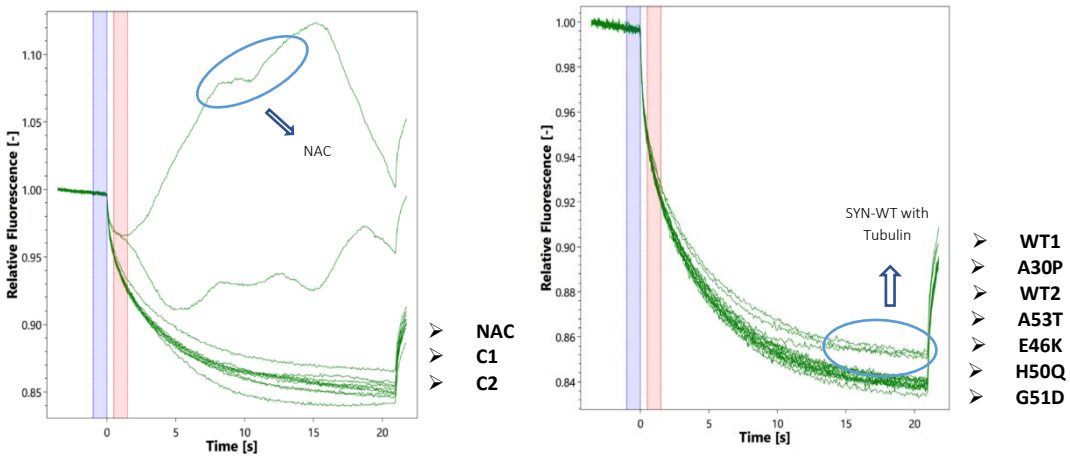

Graph 2. Graphs are represented as Relative F [‰] against time. Data represent three independent experiments and were fitted to a K_d binding model assuming a 1:1 binding stoichiometry.

Tubulin is a quite difficult protein to work with, as after only a few hours in any buffer that doesn't contain Mg^{+2} it tends to aggregate. Its aggregation then caused a phenomenon known as 'Aggregation-Caused Quenching', which practically means that tubulin was not fluorescent anymore, and hence, we were not able to use it anymore for the experiment. In addition, some of the αSyn peptides, in the concentration that we wanted to use them during the assay, tended to aggregate, as can also be seen in graph 2. However, the peptides compared to tubulin are quite smaller in molecular weight and this could also have influenced the fact that we did not see any binding.

Finally, taking into consideration all the difficulties faced during these experiments and the results we had for the peptides we concluded that MST is not an appropriate technique to be used in order to study the interaction of αSyn protein domains with tubulin.

Peptide	Buffer	Concentration
WT1	MST	500 µM
A30P	MST	500 µM
WT2	MST	500 µM
A53T	MST	500 µM
E46K	MST	500 µM
H50Q	MST	500 µM
G51D	MST	500 µM
NAC	MST	500 µM
C1	MST	500 µM
C2	MST	500 µM

Table 12. MST experiment performed with tubulin and αSyn peptides with specific concentrations all in MST buffer.

5.2 Tubulin Polymerization Assay

The analysis of MT dynamics in cells has been elucidated thanks to in vitro studies on MT polymerization. Purified tubulin deriving from porcine or bovine brains, indeed is able to polymerize in vitro into MTs when incubated in the presence of an appropriate buffer containing glycerol, GTP and Mg^{2+}.[206] In such conditions, it is possible to follow the increase in absorbance over time of a solution in which tubulin is incubated at 37 °C in this kind of buffer, thus obtaining quantitative data regarding the kinetics of the reaction assembling MTs. These assays are particularly useful in order to demonstrate the effects of MT-stabilizing or de-stabilizing additives.[207] Tubulin polymerization assay data are plotted in characteristic sigmoidal curves representing the different phases of in vitro MT assembly, which can be resumed in three main points: nucleation phase, elongation phase and a steady phase (Figure 19).

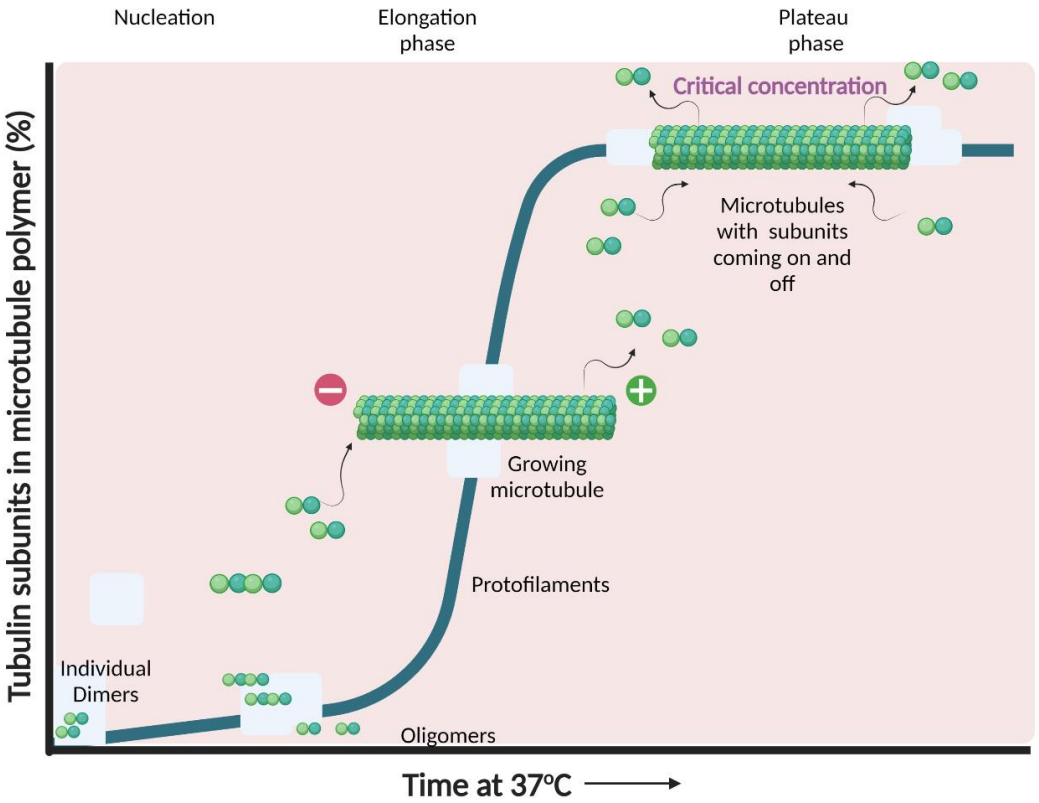

Figure 19. Tubulin polymerization can be monitored in vitro at 37 °C as absorbance increase over time (x axis) as an indication of MT polymer concentration in solution (y axis). The 3 main phases involved in MT polymerization are represented: nucleation phase (lag phase), in which a stable and polymerization-competent nucleus is formed by the gathering of tubulin dimers; elongation phase, in which tubulin dimers rapidly add onto MT ends and steady state phase (plateau), in which MT polymers are in equilibrium with a fixed critical concentration of tubulin dimers are represented: nucleation phase (lag phase), in which a stable and polymerization-competent nucleus is formed by the gathering of tubulin dimers; elongation phase, in which tubulin dimers rapidly add onto MT ends and steady state phase (plateau), in which MT polymers are in equilibrium with a fixed critical concentration of tubulin dimers.

The nucleation phase is a highly cooperative process, in which several thermodynamically unfavoured tubulin assembly intermediates have to be assessed in order to obtain the so called "critical nucleus", defined as: "the first stable oligomer whose growth is thermodynamically more favourable than its disassembly".[208] In summary, the critical nucleus represents the rate limiting step of in vitro MT nucleation. Once a certain size, in terms of tubulin monomers, of this polymerization-competent nucleus is reached, the elongation phase can take place, since the thermodynamic barrier has been surpassed. During this phase, tubulin

monomers rapidly polymerize by consecutive addition of tubulin subunits onto MT's ends. This phase continues until it is compensated by the release of monomers at MT ends, and, at that point, the steady state phase is reached, when the addition and the release of monomers at MT ends are in a sort of equilibrium.[209] An important point at the basis of this kind of studies, is that there is a linear relationship between absorbance increment and MTs mass concentration.[210]Therefore, all the data coming from in vitro tubulin polymerization assays can be analysed in terms of kinetic parameters, representative of each of the mentioned phases.

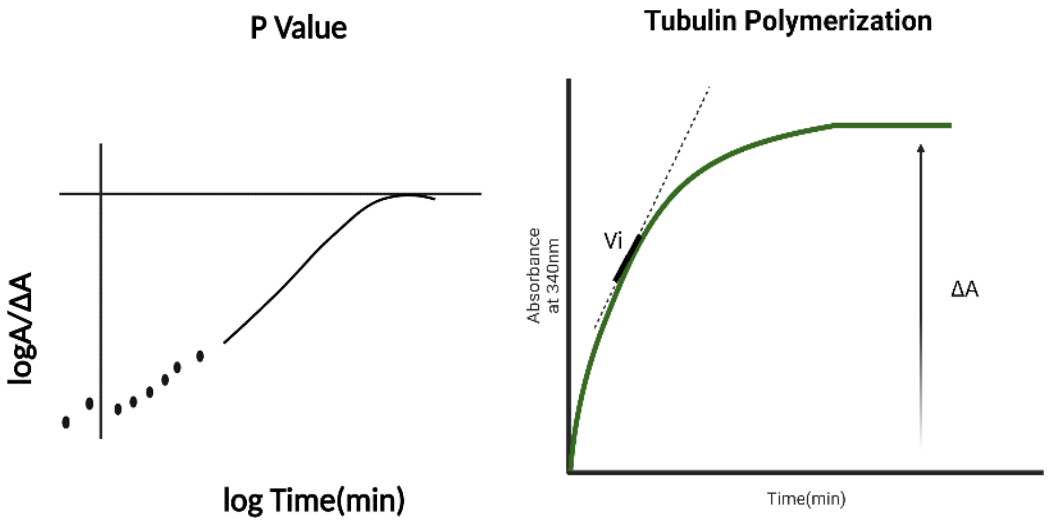

Figure 20. Graphical representation of the three main kinetic parameters relative to tubulin polymerization. On the right, the parameters associated to the elongation phase (Vi) and to the absorbance plateau reached during tubulin polymerization (DA) are shown. On the left, the P value is shown on a logarithmic scale.

To study the interplay between αSyn peptides and MTs, we investigated the impact of αSyn peptides on tubulin polymerization. We evaluated the effects of WT1 and WT2, being the native sequences of αSyn, and E46K, A53T, A30P, H50Q and G51D, which are their Parkinson's disease linked counterparts, on MT polymerization. To do this, we performed tubulin polymerization kinetics, an in vitro assay that allows to follow spectrophotometrically the formation of MTs from tubulin, since this

polymerization causes an increase in absorbance over time. To verify if the peptides affect tubulin polymerization, we performed tubulin kinetics in presence of tubulin alone (control) or in presence of tubulin together with the peptides (ratio 4:1), and we compared the obtained results. Importantly, before inducing MT polymerization, we pre-incubated each sample 10 minutes at 20 °C in the thermomixer: this is a very important step in order to observe the effect exerted by WT-αSyn on MT polymerization, since this window of time is required to allow the folding of αSyn and its concomitant interaction with tubulin[189]. After pre-incubation, kinetic tubulin assembly buffer containing GTP was added in order to begin MT polymerization and the reaction was monitored for 2 hours through a microplate reader. Then, we analysed in detail the three parameters that allow to better understand a-Synuclein effects on tubulin polymerization: i) ΔA, a parameter used to indicate MT mass (Figure 20), ii) Vi, a parameter describing the elongation rate of tubulin polymerization (Figure 20), and iii) the P value, a parameter describing the nucleation phase (Figure 20).

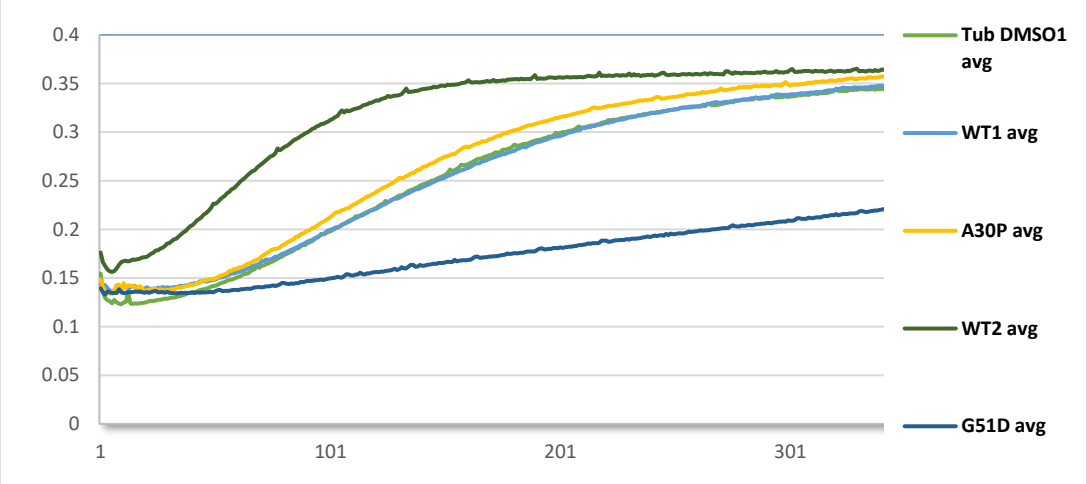

Figure 21. Effect of peptides WT2, A53T, WT1 and E46K on the polymerization of tubulin with tubulin on its own. G51D seems to have a clear effect on the polymerization.

	Tub+ DMSO1 %	Tub+ WT1	Tub+ A30P	Tub +W T2	Tub+ A53T	Tub+ E46K	Tub+ H50Q	Tub+ G51D
ΔA	0.3113	0.1678	0.197 6	0.3 158	0.2843	0.3138	0.2139	0.102
Vi (ΔA/min)	0.0121	0.0091	0.010 8	0.0 115	0.0094	0.0101	0.0038	0.0006
P value	1.0542	1.0879	1.163 8	1.1 239	1.0711	1.0823	2.5029	2.4975

Table 13. ΔA, Vi and P value calculated for peptides WT1, A30P, WT2, A53T, E46K, H50Q and G51D.

From these preliminary results, we could observe that peptide WT1 was shown to the affect Vi parameter (Figure 21), meaning that it is able to decrease the elongation rate of tubulin polymerization. We found no significant changes in the P value (Table 13), an important parameter evaluating the nucleation rate of tubulin, which was shown to significantly decrease in presence of WT αSyn. [75]The decrease in the P value indicates a boost in the nucleation phase, whereas an increase means a worsening in obtaining a stable and competent nucleus for beginning the polymerization of MTs. We observe a slight but not significant reduction of this parameter. While WT2, that is also native αSyn sequence, was not shown to affect the parameters of interest. Parkinson's disease linked mutations were also shown to induce MT polymerization but to a different extent compared to control (Figure 21). The A30P mutant was found to decrease slight the ΔA compared to control, but no significant data were obtained for Vi nor for P value, thus our data pointed towards a tendency in decreasing microtubular mass by A30P mutant (Figure 21 and Table 13). The A53T mutant, instead, was found to not alter most kinetic parameters considered. The E46K mutant impacted tubulin assembly decreasing slight the Vi parameter. The H50Q mutant peptide seemed to affect both ΔA and Vi, thus decreasing the polymerization of tubulin. The most significant effect, however, was observed for G51D mutant, which decreased both ΔA and Vi values, showing a very important decrease in the polymerization of tubulin. These data

indicate that pathological mutations in as well as the WT form are related to specific effects on tubulin polymerization. Almost all αSyn peptides decrease the total MT mass but they have different effects on the elongation rate and on the nucleation of in vitro assembled MTs. Interestingly, the G51D mutant peptide has been shown to affect especially the Vi and ΔA in contrast with the other forms of αSyn investigated.

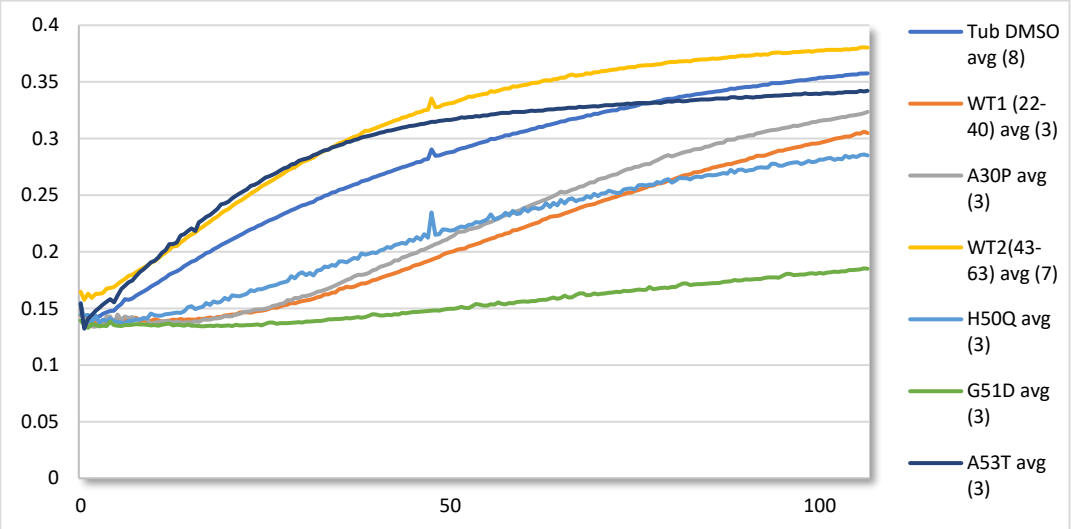

Figure 22 Effect of peptides WT2, A53T, WT1, H50Q and E46K on the polymerization of tubulin with tubulin on its own. G51D has a clear effect on the polymerization.

5.3 *In vivo* studies of the αSyn peptides to study their interaction with tubulin.

Based on the promising results showing that αSyn peptides G51D and H50Q impacts on the polymerization on tubulin, we decided to investigate the effect of these peptides in a human neuroblastoma cell model.

5.3.1 MW SPPS of αSyn peptides capped with carboxyfluorescein

To study the cellular effects of the peptides, an additional modification was introduced at the peptides: labeling with 5(6)-carboxyfluorescein (CF) (Figure 23).

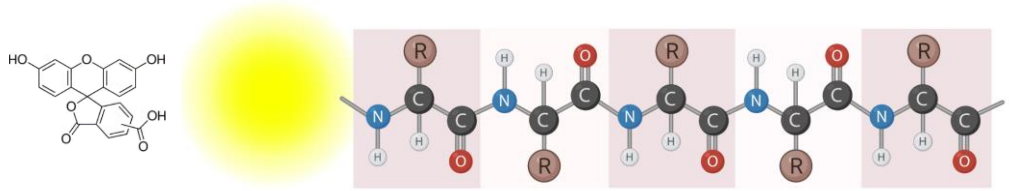

Figure 23. CF structure used to label a peptide.

The peptides were synthesized with good yields using MW-SPPS. The peptides obtained can be seen in Table 14.

Name of peptide	Sequence	Mass	Purity
WT 2-CF	CF-KTKEGVVHGVATVAEKTKEQV-NH_2	5 mg	98%
H50Q-CF	CF-KTKEGVVHDVATVAEKTKEQV-NH_2	6 mg	98%
G51D-CF	CF-KTKEGVVQGVATVAEKTKEQV-NH_2	4 mg	99%

Table 14. Peptides labelled with CF.

5.3.2 Analysis of the impact of αSyn labelled peptides on microtubule network in human neuroblastoma cells.

First, viability assay was assessed by 3-(4,5-dimethylthiazol-2-yl)-2,5-diphenyltetrazolium bromide (MTT) assay in undifferentiated naïve cells cultured for 24 h and then exposed to peptides or vehicle for 24 h. As shown in Figure 24, the viability of SK-N-SH cells significantly decreases upon treatment with 10 and 100 μM of peptides when compared to vehicle. Thus, we decided to investigate the

impact on microtubule network of peptides at the concentration of 1 μM, which does not affect cell viability.

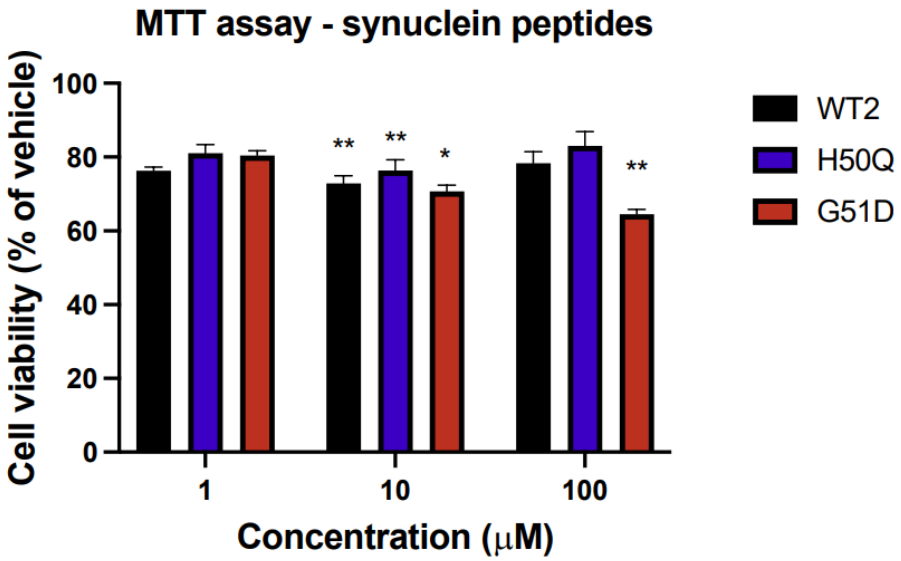

*Figure 24. The effect of wild type (WT2), H50Q and G51D peptide on cell viability by MTT assay. Naïve SKN-SH neuroblastoma cells were treated with peptides ranging from 1 to 100 μM for 24h. Data are the mean ± SD of triplicate measurements. ** p <0.01.*

We checked for the effect of peptides on microtubule network in terms of distribution and level of total α-tubulin and tyrosinated tubulin in undifferentiated naïve cells (Figure 25).

The staining for total tubulin reveals that the network of microtubules changes in cells incubated with the peptides suggesting that their effect mimics that induced by overexpression of αSyn. In addition, the staining for tyrosinated tubulin is remarkably affected by the peptides and its redistribution is evident inside the cytoplasm. Our results indicate these peptides as potential tools for interfering with the arrangement of microtubules and mimicking the effect of αSyn on microtubule system.

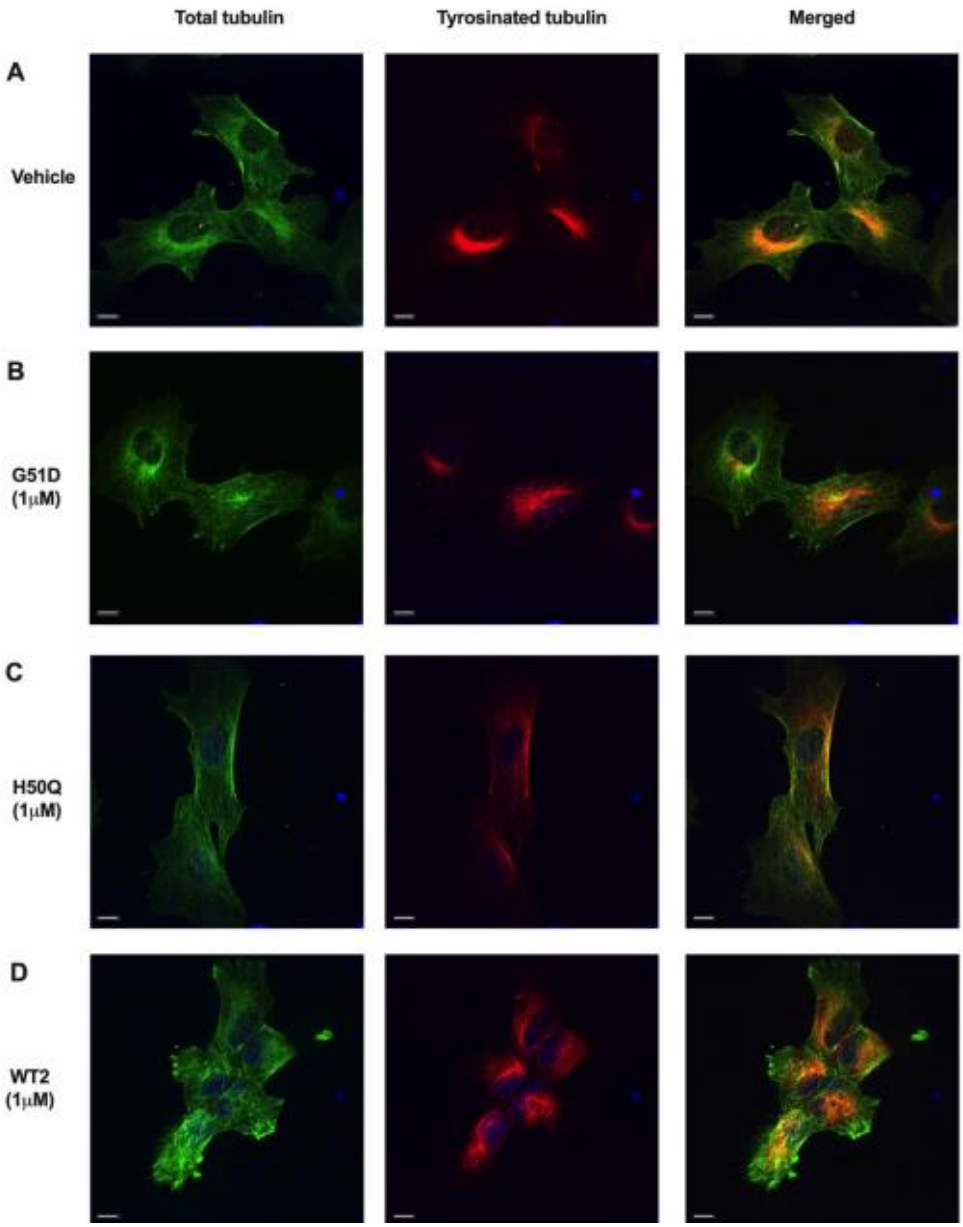

Figure 25. Confocal images of undifferentiated naïve SK-N-SH cells incubated with 1 μM WT2, G51D, and H50Q peptides for 24 h. Staining for total tubulin (green), tyrosinated tubulin (red), and nuclei (blue) is shown. Scale bar, 10 μm

6. Synthesis of α-Synuclein peptidomimetics

Based on the structural analysis that we conducted for the peptides, more specifically from our CD experiments, we found that the WT2 sequence in aqueous buffer pH 7 is unstructured, so we hypothesized that probably a more stable conformation would help us to decipher better the interaction of the peptides with tubulin. Moreover, WT2 mutants, H50Q and G51D, were shown to influence the polymerization of tubulin. Therefore, we decided to focus on the WT2 sequence of the αSyn peptides synthesized and attempt to stabilize a stable conformation by various strategies. One of the most employed strategies to stabilize the secondary structures of peptides is the synthesis of stapled peptides.

Taking into consideration numerous works published already on peptide stapling and a recently published review on stapling strategies[78] we decided to employ a conventional strategy of stapling, the lactam bond formation, since our WT2 sequence is equipped natively with lysines and glutamic acids. On the other hand, we thought of trying a rather forgotten stapling pattern, the glutamic acid to glutamic acid one, since again our sequence is rich in glutamic acids. First, we synthesized a shorter sequence of the WT2 from T_{54} to V_{63} on resin.

$$T_{54}V_{55}A_{56}\mathbf{EKT}_{59}\mathbf{KE}_{61}\mathbf{QV_{63}}$$

6.1 Stapled Peptides

Stapled peptides primarily refer to olefin/alkene-braced peptides. More generally, peptide stapling refers to the concept of cross-linking either side chain to side chain or side chain to terminus of the anchoring amino acids, thereby forming preorganized stable conformations with a reduced entropic penalty. There are 3.6 residues per turn in α-helices, or 3.613-helices, and the residues are aligned on the same face of the helix at positions i, i+4, i+7, and i+11 (one, two, and three turns, respectively). Among these positions, i, i +4 and i, i+7 are the most common stapling positions for crosslinking one and two helical turns, respectively; i, i+3 is also available in some special cases for a single turn (Figure 26). Both natural and nonnatural amino acids have been successfully used as anchoring residues for peptide stapling. One of the most established peptide stapling strategies, "hydrocarbon stapling", which uses Grubbs metathesis catalysts8 to tether the side chains of two nonnatural amino acids in the solid phase at the i, i+4 or i, i+7 positions, was first described by Verdine and coworkers.[78] Early stapling strategies entailed the use of natural amino acids for side chain-to-side chain cross-linking, such as lactam formation between Lys and Glu/Asp residues,10 and various bis-thioether tethers between two Cys residues.[78]

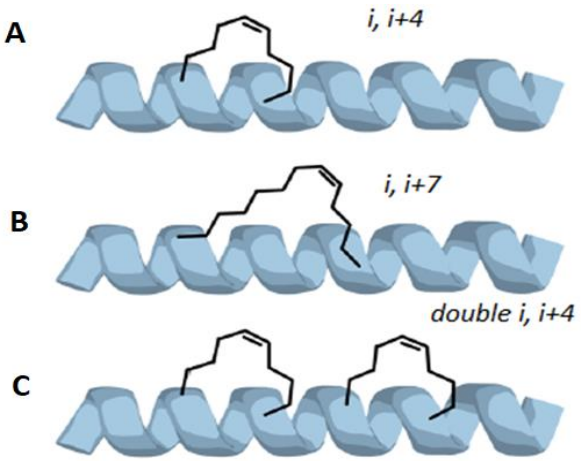

Figure 26. Most common stapling positions. Example of i, i + 4 (A), i, i + 7 (B) and double i, i + 4 (C) stapling.

6.2 Lys-Glu Stapling via Lactamization

6.2.1 A brief overview of the Lys-Asp/Glu Stapling via Lactamization

The first peptide stapling strategy was based on the formation of a lactam bridge between the endogenous residues Lys (bearing an amino group) and either Asp or Glu (each bearing a carboxyl group). It has been shown from extended research work[78] that Lys (7.2%), Glu (5.8%), and Asp (5.9%) have high frequency, but the multiple selective amine and carboxylic protection and deprotection steps in peptide synthesis enable the preparation of site-specific lactam cyclization and even multiple lactam-stapled peptides. The solid-phase cyclization approach to lactam stapled peptides is preferred over in-solution stapling because the target stapled peptides can be obtained via one-step cleavage with global deprotection followed by a single purification.[78] For lactam formation in Fmoc/*t*-butyl SPPS, at least three commercially available amino acids paired with selective side chain protecting groups are available. The Lys(Alloc)/Glu (OAll)/Asp(OAll) protecting groups can be subjected to standard TFA cleavage or low TFA cleavage from resins with good yield, and the only disadvantage is that the alloc and allyl ester protecting groups must be removed by restrictive Pd_0-catalyzed hydrolysis.

6.2.2 Synthesis of stapled αSyn peptides using the Lys-Glu Stapling via Lactamization

To begin with, we tried **one stapling by substituting V_{55} and T_{59}** with Fmoc-Glu (Oallyl)- OH and Fmoc- Lys(Alloc)- OH.

We then tried one stapling by replacing **E_{57}** and **E_{61}** with Fmoc-Glu(Oallyl)- OH and Fmoc- Lys(Alloc)- OH to try the formation of a lactam and also with the Glu-Glu stapling.

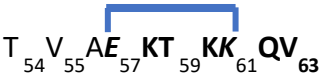

In order to compare the stapled peptides with their linear counterparts, we also synthesized KPM6.

Hence, we have synthesized the peptides summarized in Table 15.

Name of peptide	Sequence	Mass	Purity
KPM1	H-TEAEKKKEQV-NH_2 	18mg	98%
KPM2	H- KTKEGVVHGVATVAEKTKKQV-NH_2 	5 mg	98%
KPM3	H-KTKEGEVHGKATVAEKTKEQV-NH_2 	10 mg	99%
KPM6	H-TEAEKKKEQV-NH_2	40 mg	98%
KPM8	H-TVAEKTKKQV-NH_2 	7mg	98%

Table 15. Stapled αSyn peptides synthesized

The synthesis of KPM1, KPM2, KPM3 and KPM8 can be seen in Scheme 1.

The overall synthesis of the stapled peptides was developed readily since microwave-assisted synthesis was employed. The substitution of V_{55} and T_{59} which are both part of the amphipathic repeated motif of αSyn, **KTKEQV,** which as reported in 4.2.1 was very difficult, decreased the synthetic difficulty. Even though, valine was substituted by a glutamic acid and threonine by a lysine, which both are quite bulky amino acids, no coupling had to be performed twice.

The selective deprotection of the orthogonal protecting group, -allyl and -allyloxycarbonyl was performed successfully by employing $Pd(PPh_3)_4$ and $PhSiH_3$ in

a palladium-catalysed reaction. Moreover, the lactam bond was formed using a mixture of HoBt and HBTU and DIPEA as a base overnight. After the cleavage and precipitation which was performed with standard protocols, the peptides were to be purified.

The crude lactam peptides presented an overall mediocre initial purity (Table 16).

Name	Sequence	Initial purity
KPM1	H-TEAEKKKEQV-NH_2 	63%
KPM2	H- KTKEGVVHGVATVAEKTKKQV-NH_2 	68%
KPM3	H-KTKEGEVHGKATVAEKTKEQV-NH_2 	52%
KPM8	H-TVAEKTKKQV-NH_2 	59%

Table 16. Initial purity of stapled αSyn peptides

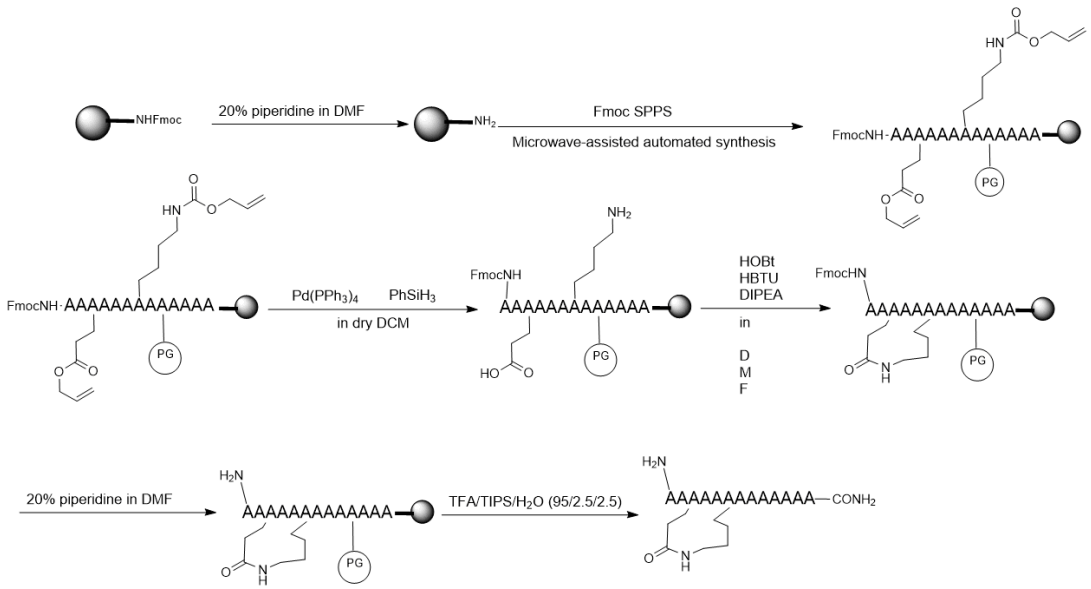

Scheme 1. Summary of the synthetical strategy of KPM1, KPM2, KPM3 and KPM8

6.2.3 Conformational characterization of lactam-bond containing peptides

6.2.3.1 Circular Dichroism of lactam-bond containing peptides

Once the synthesis was completed, in order to investigate if the stapling of the linear peptides had been successful, we conducted CD experiments.

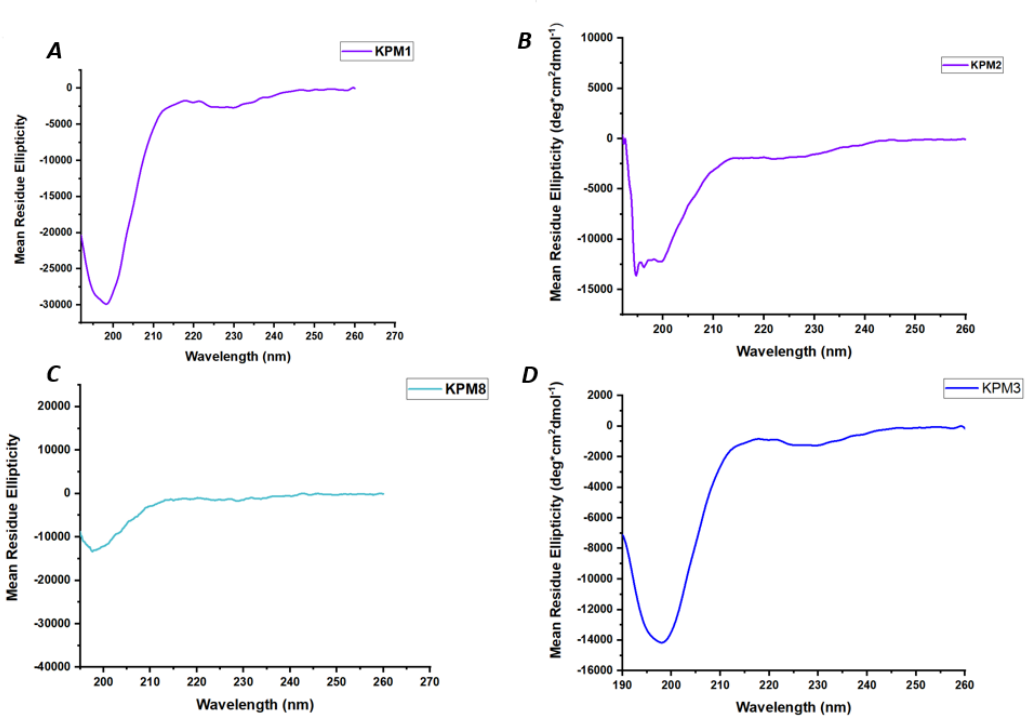

Figure 27. CD data from all stapled αSyn peptides at C=100 µM in NaH_2PO_4 - Na_2HPO_4 buffer at pH=7. ***A****) KPM1 peptide* ***B)*** *KPM2 peptide* ***C)*** *KPM3 peptide* ***D)*** *KPM8 peptide*

As mentioned before, analyses have been developed to deconvolute the various contributions arising from the different types of secondary structures present in a single molecule, thereby providing information on the overall structure of the peptide. The analyses were performed on the Dichroweb website using the CONTIN algorithm for peptides in 100% in NaH_2PO_4 -Na_2HPO_4 buffer at pH=7. The results of these analyses can be observed in **Table 17**.

	$_{3\text{-}10}$helix	α-helix	anti-parallel β-sheet	parallel β-sheet	β-turn	random
KPM1	31,5%	33,6%	0%	34,8%	0%	0%
KPM2	5,9%	1,9%	30,7%	9,9%	9,2%	42,4%
KPM3	35,3%	2,4%	16,9%	10,4%	3,2%	37,4%
KPM6	1,4%	4,5%	22,4%	10,8%	13,2%	47,6%
KPM8	18%	5,2%	21%	9,6%	11,4%	51%

Table 17. Percentages of secondary structure for each peptide at a concentration of 100uM and in 100% NaH_2PO_4 - Na_2HPO_4 buffer at pH=7 calculated on Dichroweb with the CONTIN algorithm.

In order to understand how sufficient, the stapling was, we calculated the percentual difference of every conformation for each peptide with the results we obtained from the CONTIN algorithm. The results of these calculations can be observed in the Table 18.

Stapling	$_{3\text{-}10}$helix	α-helix	anti-parallel β-sheet	parallel β-sheet	β-turn	random
KPM6 →KPM1	30,1% increase	29,1% increase	22,4% loss	24% loss	13,2% increase	47,6% loss
KPM6 →KPM8	16,6% increase	0,7% increase	1,4% loss	1,2% loss	1,8% loss	3,4% increase
WT2 →KPM2	5,5% increase	1,4% loss	5,5% loss	3,3% loss	8,3% loss	2,2% loss
WT2 →KPM3	34,9% increase	0,9% loss	8,3% loss	2,8% loss	14,3% loss	3% loss

Table 18. Percentual transition of secondary structure for stapled peptides KPM1 and KPM8 compared to KPM6 and KPM2 and KPM3 compared to WT2 at a concentration of 100 µM and in 100% % NaH_2PO_4 - Na_2HPO_4 buffer at pH=7 calculated from data obtained on Dichroweb with the CONTIN algorithm.

The stapling of the short WT2 sequence and the full-length WT2 sequence seemed to have partially worked. Indeed, peptides **KPM1** and **KPM3** seem to have a changed secondary structure compared to their linear counterparts **KPM6** and **WT2**. For KPM1 there is an 30% increase in $_{3\text{-}10}$helix content and a 29% increase in α-helix content, which both result in a 47,6% total loss of random structure. As for KPM3, good results were obtained as well. An increase of 34,9% of $_{3\text{-}10}$helix content was observed for KPM3 compared to WT2. However, when a stapling is really successful

the overall yield of the change in the secondary structure should be about 60-70%. In conclusion, the Lys-Glu stapling via lactamization that we afforded was not totally successful.

6.2.3.2 ATR-FTIR spectroscopy of lactam-bond containing peptides

To further characterize the secondary structure of the peptides, we performed the ATR-FTIR analysis. All the peptides in the solid state revealed the typical bands of the amide bond (see attachment) and, the deconvolution of the amide I band highlighted that they adopt a mixture of conformations. In **Table 19**, we have reported the different conformations found after the deconvolution and their percentages for each peptide.

	β-sheet	$_{3\text{-}10}$helix	β-turn	α-helix	random
KPM1	-	45,4%	-	-	54,6%
KPM2	45%	55%	-	-	-
KPM3	7%	38%	-	32%	23%
KPM6	-	21%	-	-	79%
KPM8	14%	23%	-	-	63%

Table 19. Percentages of secondary structure for each peptide at the solid state calculated with OriginPro.

6.3 αSyn stapled peptides: Glu-Glu stapling

This part of my PhD started in Paris, during my secondment, and was interrupted due to health issues at the end of April 2022. Then, I took a break from the PhD for one month and went back to Milan where I started working in June 2022.

During the period spent at Universitè Paris Saclay, the main focus of the work was to obtain a novel linker in order to attempt a stapling strategy.

6.3.1 Glu-Glu via Lactamization or bis-Hydrazidation: a general overview

Similar to Lys-Lys anchoring paired residues, Glu-Glu partners also served as the initializing residues for yielding bis-lactam staples through double amide formation. An early experiment was performed by Phelan and co-workers[211] using Boc-SPPS, Ally and Fm ester-protected Glu residues were sequentially assembled at i, i+7 position on resin, and the Fm group was then easily removed by 20% piperidine in DMF and amidated with an appropriate diaminoalkane. In the next cycle, Allyl deprotection and amide coupling afforded the resin-bound stapled peptide, which was released by HF cleavage and underwent HPLC purification.[211] (Phelan et al 1997) In this case, α,ω-diaminoalkane was used as the functional cross-linker to react with the side chain carboxylates of i, i+7 Glu-Glu residues in solid phase. The resulting stapled peptide showed increased helicity compared to the linear counterpart and thiolysine cross-linked peptide.

6.3.2 Synthesis of the novel diaza linker

It is clear that from recent works published on glutamic acid to glutamic acid stapling, a functional linker is necessary in order to unite the two carboxylates. Moreover, in the laboratory of Prof. Ongeri, that is the co-supervisor of the present work, aza amino acids are used quite often. Aza amino acids are natural amino acids in which the C_α is replaced by nitrogen. The introduction of one aza-amino acid in peptides, in order to afford the so-called aza-peptides, has shown significant success in providing biologically active peptides.[212] They also have been demonstrated to induce turn conformations in peptides by spectroscopic, crystallographic, as well as computational studies.[212]

Therefore, a diaza linker was chose to be synthesized and the overall synthesis can be observed in Scheme 2.

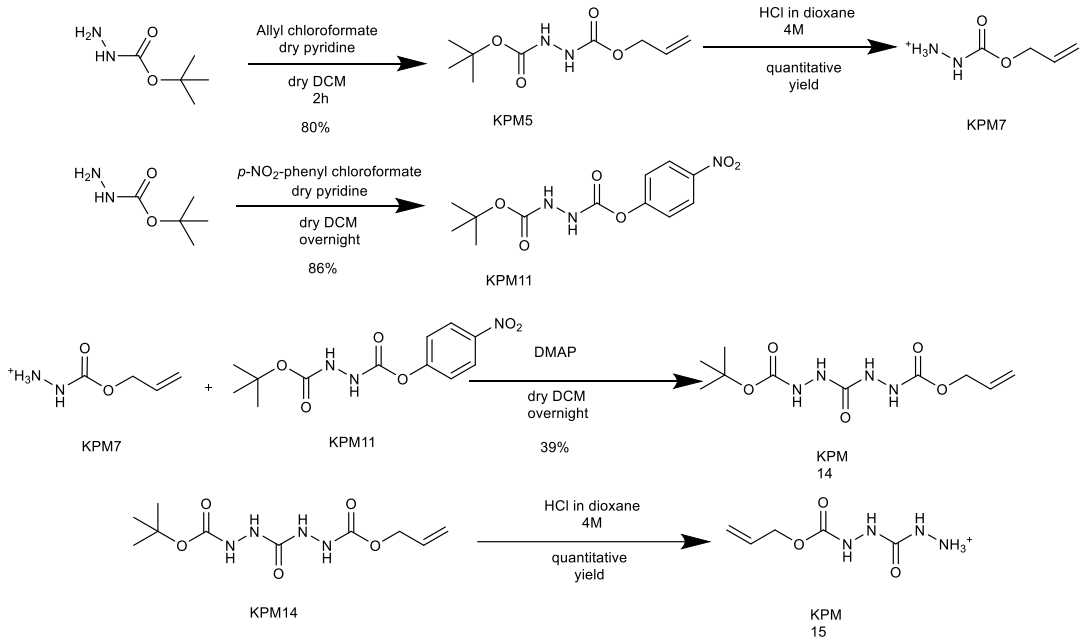

Scheme 2. Overall synthesis to afford final diaza linker.

To obtain final compound KPM14, we started with the synthesis of KPM5 by protecting with the -alloc group *tert*-butyl carbazate using 1.1 eq of allyl chloroformate and 1.2 eq of dry pyridine in dry DCM. Then, to obtain KPM7 we cleaved the *tert*-butoxycarbonyl protecting group using 10 eq of 4.0 M HCl in dioxane. After, for the synthesis of KPM11 we activated *tert*-butyl carbazate using 1.1 eq of nitrophenyl chloroformate and 3 eq of dry pyridine in dry DCM. Later, for product KPM12 we performed the coupling between KPM7 and KPM11 using 1 eq of DMAP in dry DCM. Finally, we afforded compound KPM14 by cleaving the *tert*-butoxycarbonyl group using 10 eq of 4.0 M HCl in dioxane.

The next step was to couple KPM14 with the Fmoc- Glu- OtBu (Scheme 3) in order to obtain our modified amino acid to attach on resin and test the new coupling strategy. We attempted various couplings using different coupling reagents that are summarized in Table 20. We obtained the best results by using HCTU and DIPEA.

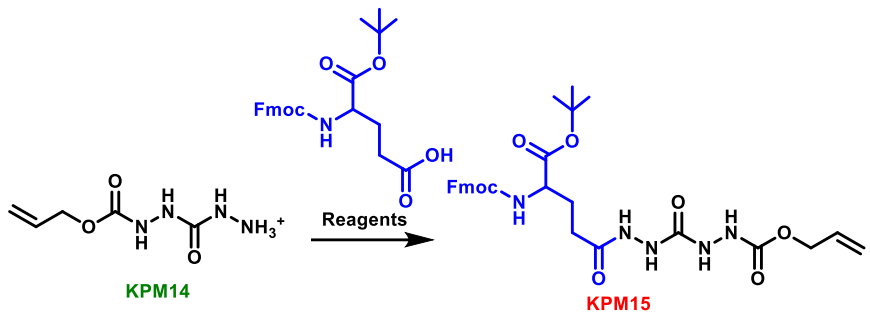

Scheme 3. Coupling reaction of Fmoc-Glu-OtBu with the Alloc-NH-NH-CO-NH-NH$_2$ moiety

Reagents	Procedure	Equivalents	Yield
HCTU HoBt DIPEA	Left overnight in DCM with the addition of 0.25 eq next morning	1.1 1.1 3	31%
HCTU HoBt DIPEA	Left over weekend in DCM	1.1 1.1 3	25%
DEPBT DIPEA	Left for 5h	1.2 2	25%
COMU Oxyma DIPEA	Left overnight in DCM	1.1 1.1 3	29%
EDC Oxyma Collidine	Left overnight in DCM	1.2 1.2 5	24%
BTC DIPEA	Left for 5 h	0.4 2	29%

Table 20 Coupling reaction attempts of Fmoc-Glu-OtBu with the Alloc-NH-NH-CO-NH-NH$_2$ moiety

After obtaining the Fmoc-Glu (CONH-NH-CO-NH-NH-Alloc)-OtBu we performed the final reaction which was the deprotection of the tertbutyl group from the carboxylic acid. The reaction can be seen in the Scheme 4.

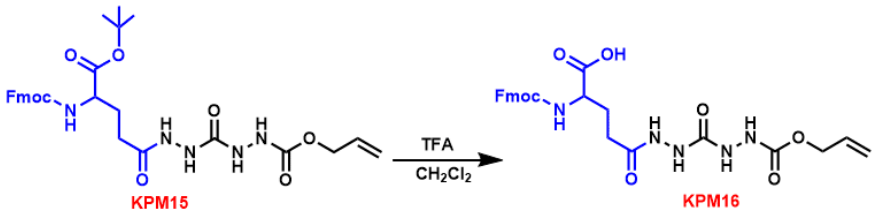

Scheme 4. Deprotection reaction of Fmoc-Glu(CONH-NH-CO-NH-NH-Alloc)-OtBu using TFA.

6.2.3 Synthesis of stapled αSyn peptide using the Glu-Glu Stapling-KPM30

As soon as compound **KPM16** was successfully purified, it was coupled on resin in the correct position.

The synthetical strategy that was decided can be in Scheme 5.

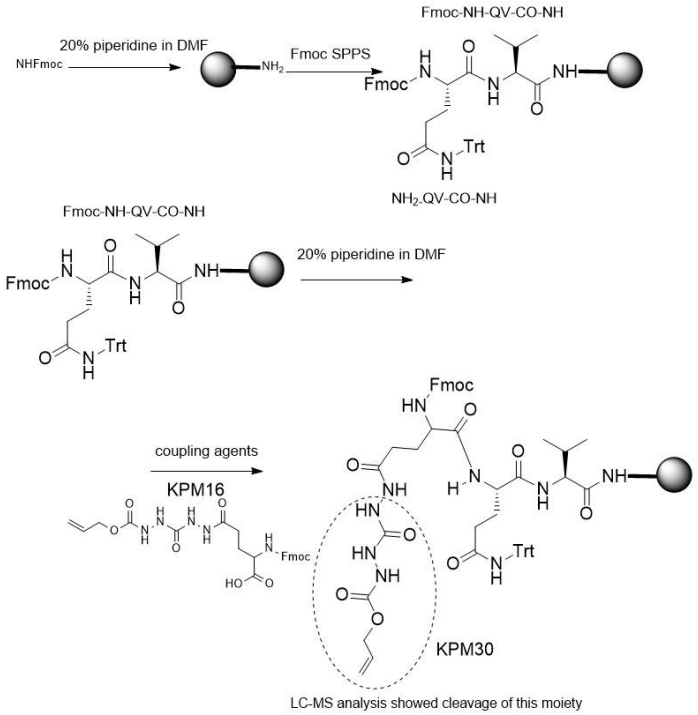

Scheme 5. Synthetical strategy of stapled peptide KPM30 containing the Fmoc-Glu (CONH-NH-CO-NH-NH-Alloc)-OH

First, we performed the manual SPPS of KPM30 by coupling the first two amino acids of the sequence. Then, the coupling of the Fmoc-Glu(CONH-NH-CO-NH-NH-Alloc)-OH with glutamine was attempted. A mini cleavage was performed to assess the coupling. Via LC-MS, we could detect a very small percentage of the amino acid coupled. Various couplings were attempted later but our final conclusion was that our linker is probably cleaved during the mini cleavage since we have to use a high percentage of TFA.

For future experiments, different cleaving conditions could be employed, such as cleavage cocktails containing a minimum quantity of TFA.

Chapter II

7. Tau protein

7.1. Structure of Normal Brain Tau

A single gene, MAPT, which lies on human chromosome 17, encodes Tau. The microtubule-associated protein Tau is held inside the axons of the nerve cells that bind tubulin and help in its polymerization and adjustment into microtubules. The Tau primary transcript is over 100 kb long and located at band location 17q21 on the long arm of chromosome 17. The Tau protein can be subdivided into an amino-terminal (*N*-terminal) domain that projects from the surface of the microtubule and the microtubule-binding carboxy-terminal (*C*-terminal). Tau binds to microtubules through repetitive regions in the *C*-terminus (Figure 28). The *N*-terminal domain, which is also referred to as the projection domain, may interact with other cytoskeletal components and plasma membranes. Between the projection domain and the microtubule-binding domain lies a basic proline-rich region. A single Tau

gene contains 16 exons, which are transcribed into nuclear RNA and produce multiple Tau messenger RNAs (mRNAs) after alternative splicing. The translation of these mRNAs generates different Tau isoforms. Since exons 4A, 6, and 8 are not transcribed in humans, the Tau primary transcript has 13 exons. Exon 1 is transcribed but not translated and is part of the promoter. Apart from these, exons 1, 4, 5, 7, 9, 11, 12, and 13 are referred to as constitutive exons, while exons 2, 3, and 10 are spliced. Exon 14 can be present on mRNA, but it does not undergo translation while exon 3 is never found without the presence of exon 2. Subsequently, six different combinations are possible when these three exons (2, 3, 10) are spliced differently. The Tau primary transcript produces six mRNAs in the human brain, each of which is translated into one of the six CNS Tau isoforms. The repeat domains (R1–R4) encoded by exons 9–12 are the repetitive regions. Six molecular isoforms ranging from 352 to 441 amino acids are produced in adult human brains. The six isoforms in human Tau are dependent on the presence or absence of 29 or 58 amino acid N-terminal insertions and a C-terminal region with three (3R) or four (4R) microtubule-binding repeats of 31 or 32 amino acids. 2N4R is the longest isoform of human Tau, composed of 441 amino acids. All six Tau isoforms are extremely hydrophilic and heat-stable. During the foetal stages, only one Tau isoform is present, with no N-terminal inserts and three C-terminal repeats, while six isoforms (with one or two N-terminal inserts and three or four C-terminal repeats) are expressed during adulthood. Except for 2N3R, calculated isoelectric points (pI) (8.2–9.4) suggest that Tau isoforms are mostly basic proteins. The presence of three or four repeats (3R or 4R, respectively) in the Tau microtubule-binding domain is the distinguishing factor among tauopathies in biochemical protein isoform profiles. Tau tangles in AD are comprised of an equimolar amount of 3R and 4R isoforms. 4R tau pathology is seen in CDB, PSP, and a few variants of FTDP-17 (and related MAPT mutations). Pick's disease is characterized by 3R Tau

pathology, and changes in normal Tau isoform levels contribute to the disease's pathogenesis. Tau is an intrinsically disordered protein and thus exhibits little tendency to aggregate structurally. Various post-translational modifications are known to affect Tau aggregation, for instance, phosphorylation, a common feature of AD, leads to Tau aggregation. Experiments have proven that Tau aggregation is critical for toxicity induced by Tau. Tau aggregation not only reduces functional soluble Tau levels but also interferes with axonal transport and ultimately leading to neurodegeneration. Overexpression of Tau protein leads to the disappearance of neurites mitochondria in differentiated N2a cells. It affects mitochondrial distribution to peripheral cell compartments, the endoplasmic reticulum thins out and stops encircling the cell periphery, retards cell development and dramatically alters the distribution of various organelles which are known to be transported by microtubule-dependent motor proteins. In order to study Tau-Tau interaction in cells, a variety of fluorescent protein methods, including fluorescence resonance energy transfer (FRET) and bimolecular fluorescence complementation (BiFC) have been developed. FRET includes energy transfer from a donor fluorophore (CFP) to an acceptor fluorophore (YFP). In the study conducted by Wanjoo and Gail, full-length Tau and caspase-cleaved Tau were labelled, respectively, with CFP and YFP and then co-expressed in HEK293 cells. This study demonstrates for the first time by measuring FRET intensity, the levels of Tau aggregation can be quantified in living cells. Further, to reduce the size of fluorescence protein tagging, BiFC was applied to detect and quantitate Tau aggregation in living cells. This technique includes the formation of a fluorescent complex when two proteins fused to non-fluorescent constituents of fluorescent protein interact with each other. To measure Tau aggregation in mammalian cells, split green fluorescent protein (GFP), complementation assay was developed. GFP is separated into two soluble and spontaneously associating fragments, GFP11 and GFP1–10; both together result in

GFP folding and the formation of fluorescently active GFP. Full-length Tau protein is directly fused to GFP11, which results in a decrease in accessibility of this part of GFP and shows a loss of fluorescence in cells. Even though phosphorylation is essential for the physiological functioning of Tau, but hyperphosphorylation decreases its biological activity. Tau hyperphosphorylation might weaken the affinity of tau for microtubules, leading to instability and disassembly of microtubules and promoting self-aggregation of Tau into oligomers and other aggregates. [213]

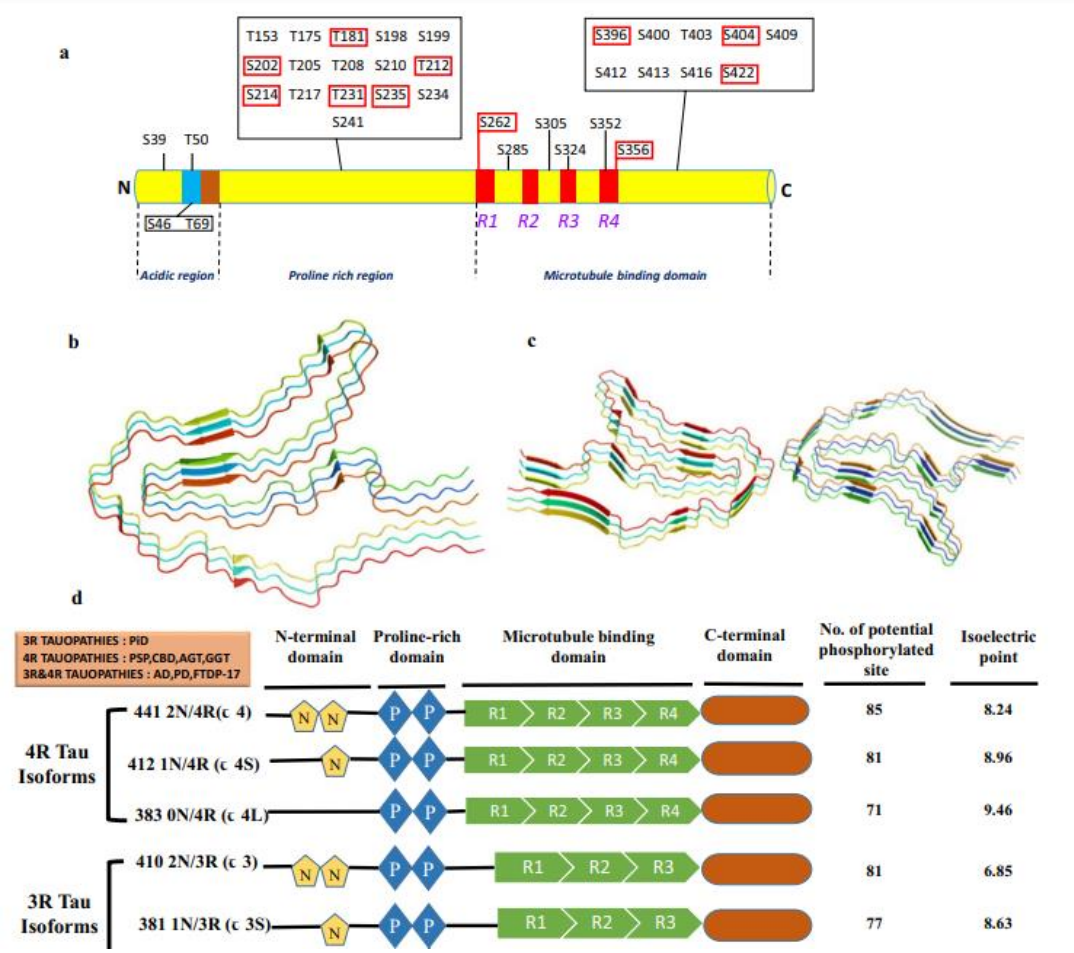

Figure 28. Tau protein.

7.1.1. Tau in Neurodegenerative Diseases

The chances of developing neurodegenerative diseases such as AD and Parkinson's disease (PD) increase dramatically with age. In numerous other neurodegenerative disorders, irregular filamentous Tau deposits have been identified as pathological characteristic features, including AD, FTDP-17, Pick's disease, PSP, CBD, and AGD. The expression and aggregation of Tau in the human brain depend on many cellular factors ranging from post-translational modifications like phosphorylation, nitrosylation, glycosylation, glycation, and acetylation, proteolytic cleavage, and chaperones as binding partners which induce indirect modifications. Key factors controlling the expression of Tau at DNA and RNA levels are repeated motifs, DNA haplotypes, CpG islands and their methylation, untranslated regions (UTR) in the mRNA, and splicing patterns.

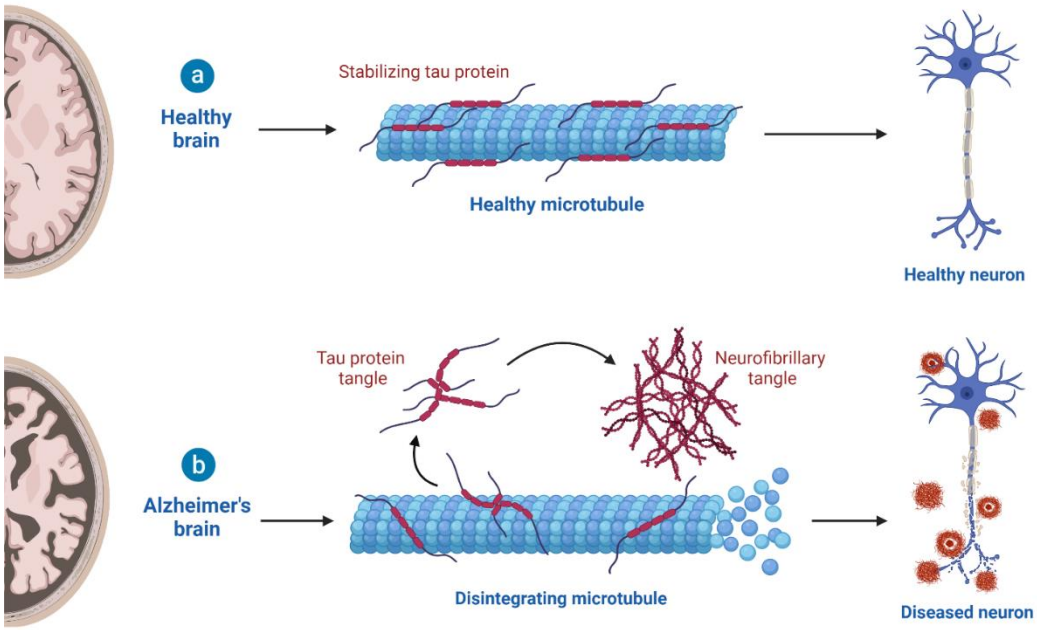

Figure 29. a In healthy neuron, tau binds and stabilizes microtubules promoting axonal stability and synaptic vesicles transport. Tau proteins bind to microtubules through repetitive regions of C-terminus. The N-terminal part refers to as the projection domain since it projects from the microtubule surface where it may interact with other cytoskeletal elements and plasma membrane. b Tau dissociates from microtubules, leading to their destabilization. Abnormally phosphorylated tau lesion causes death of neuron cells, resulting in irreversible and progressive neurodegeneration

muscles, and testis, and there are some reports which state the presence of Tau in pathological peripheral tissues also. In mouse models, Tau overexpression leads to resemblance to early-stage AD and other neurodegenerative diseases. There are several reports, which have described the antibody presence for hyperphosphorylated Tau in AD. Two such antibodies include CBTAU-7.1 and CBTAU-22.1 with the capability to bind to proline-rich region and C-terminal region of Tau, respectively, and are able to detect pathological form of Tau in brain tissues in post-mortem condition. CBTAU-22.1 even has the capability to detect neurofibrillary changes.

Phosphorylation has also been associated with the spread of AD. Further, hyperphosphorylation hinders the degradation of Tau by ubiquitin–proteasome system. Abnormal Tau phosphorylation reduces the chances of interaction of Tau with its partners, thus altering Tau properties. Abnormally hyperphosphorylated Tau loses its biological activity and disassociates from microtubules, further polymerize into neurofibrillary tangles and paired helical filaments, which are apparently inert and restrict its binding to tubulin, causing cell death. AD P-Tau sequesters microtubule-associated Tau proteins MAP1 and MAP2, which further facilitate the disruption of microtubules. Hyperphosphorylation is also responsible for the redistribution of Tau from axons to somatodendritic compartments and results in impaired synaptic functions. Affinity purification-mass spectrometry confirmed 75 proteins in NFTs specifically bound to phosphorylated Tau; most of these were involved in protein ubiquitination pathway and phagosome maturation. There are 85 potential phosphorylation sites on the longest Tau isoform (441 amino acids long) characterized using phospho-dependent Tau antibodies, phospho-peptide mapping, mass spectrometry (MS), or nuclear magnetic resonance (NMR). Several phosphorylation sites have been found to regulate microtubule (MT)-

binding and assembly activity of Tau and are also involved in the development, morphogenesis, and maintenance of axons in neurons[213].

7.1.2. Tau as a MAP

Tau binds to the C-terminal tail of tubulin, a structure that is on the MT exterior, although it seems likely that there are also additional binding sites, perhaps including inside the MT. This exterior binding is required for Tau's roles in MT spacing and motor regulation. Recent biochemical data have shown that Tau also binds to unpolymerized tubulin, which creates an additional complication in understanding the mechanism of how Tau regulates MT dynamics. Other aspects of Tau–MT interactions are less certain. For example, there is still a debate about the geometry of Tau–MT interactions: do the MT-binding repeats of Tau bind laterally across or longitudinally along MT protofilaments, or can both types of binding occur? In addition, it is clear that Tau binding occurs along the length of MTs (i.e., it is not end-specific), but it is unclear why this occurs. One explanation for this binding behaviour is that Tau is insensitive to the nucleotide state of the polymer. Alternatively, Tau might prefer to bind to the guanosine diphosphate (GDP) lattice, which is present everywhere except at the MT tip. Finally, it is not clear how Tau might interact with, cooperate with, or antagonize the elements of the MT plus-end tracking protein (+TIP) network, a set of proteins that is generally believed to be the "master regulator" of MT dynamics. To establish the mechanism by which Tau stabilizes MTs, we need to understand Tau's binding geometry, but resolving this question has been challenging because Tau is largely "invisible" by standard electron microscopy methods [24]. Cryo-EM combined with helical image analysis led Al-Bassam et al. to conclude that Tau binds primarily along the MT protofilament ridges, that is, longitudinally. In contrast, Santarella et al. showed that Tau can stabilize tubulin sheets; these data, together with other data, led them to suggest that Tau can bind both longitudinally (along) and laterally (across) protofilaments.

However, Schaap et al. used atomic-force-microscopy-based imaging and measurements of radial elasticity of Tau–MT complexes to again conclude that Tau binds mainly along protofilaments. In addition, recent isothermal titration calorimetry studies by Tsvetkov and colleagues also led the authors to conclude that Tau binds primarily along protofilaments. However, the interpretation of their data is complicated by the recent demonstration that Tau binds to unpolymerized tubulin.[214]

7.2. Results and Discussion

7.2.1. Synthesis of Tau deriving peptides

The mechanistic details of the interaction of full-length Tau with tubulin and MTs have remained elusive for many years, and several controversial models have been proposed. Early studies identified both, the four repeating peptides in the C-terminal half of the protein Tau, known as the microtubule binding repeats R1-R4, and intramolecular interactions with their flanking proline rich regions to promote the interaction with stabilized MTs.[215–218] The location of the Tau binding site along and across protofilaments was first revealed by cryo-EM studies at low resolution.[219,220] However, co-assembly experiments with Tau and tubulin dimers also suggested the existence of an interaction site at the lumen of MTs, comprising a Tau binding site close to the taxane site. [221] It was further shown by NMR spectroscopy that functional fragments of Tau remain highly dynamic upon binding with high affinity to tubulin dimers.[222] Recently, single-particle cryo-EM models of synthetic Tau-repeats bound to MTs revealed for the first time a detailed picture of Tau-tubulin interactions along the crest of protofilaments.[223]Subsequently, Inaba and co-workers described the binding of a Tau-derived peptide (2N) to or near to the taxane-site at the luminal surface of MTs, which recently attracted our attention.[224]

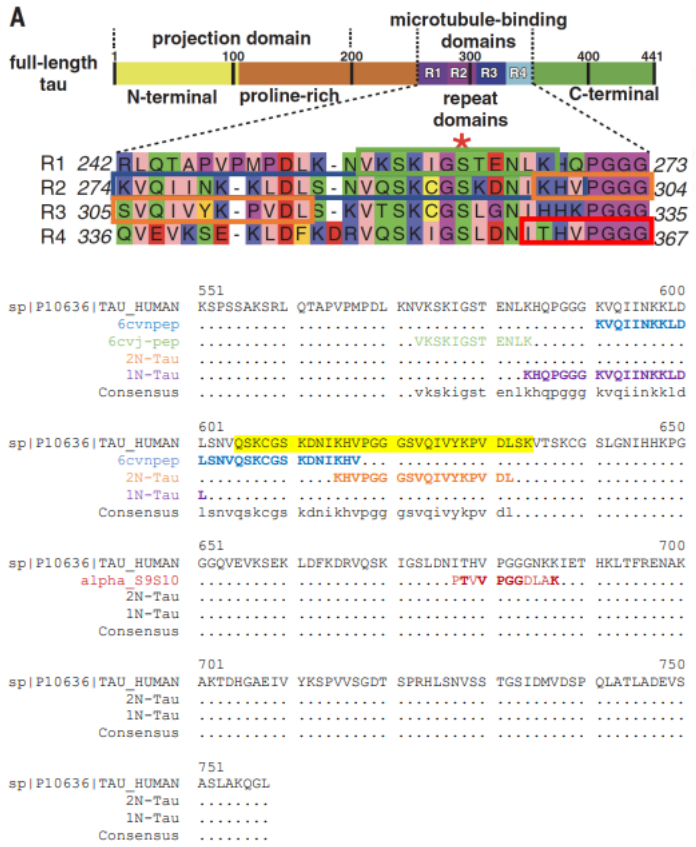

Figure 30. Tau protein with its various domains. The sequence of the 2N peptide is highlighted in yellow.

The sequence of 2N only partially overlaps with the seven C-terminal residues of the synthetic R2x4 Tau repeats described by Kellogg and co-workers, of which the last four residues were not visible in the cryo-EM maps. The Tau-derived peptide 2N was employed in a series of soaking and co-crystallization experiments by X-ray crystallography by our co-workers in PSI, Switzerland. To date, they did not detect binding of the peptide to tubulin, which might have been hampered by crystal contacts in our crystal systems. Hence, more experiments are needed.

Confirmation of binding to or close to the taxane site would open a new playground to design new tools to study the mechanism of action of Tau and to perturb MTs in neurons.

Name of peptide	Sequence	MW	Mass	Purity
Tau1	H-QSKCGSKDNIK-NH_2	1206.38 g/mol	21,3mg	>98%
Tau2	H-QSKCGSKDNIKHVPGGGSVQIVYKPVDLSK-NH_2	3168.63 g/mol	12mg	>98%

Table 21. Tau deriving peptides

We, therefore, synthesized two Tau-deriving peptides to use them as molecular tools to detect their binding site on tubulin (Table 21). Microwave-assisted automated peptide synthesis was exploited using the Fmoc/*t*Bu protection group strategy at a Rink amide resin with a loading capacity of 0.7 mmol/g on a Liberty Blue synthesizer using a scale of 0.1 mmol per peptide. The amino acids concentration was equal to 0.2M in DMF.

DIC and Oxyma were used as coupling reagents (0.5 in DMF and 1M in DMF) while for the deprotection 20% Piperidine in DMF was used. For Lys, Thr, Glu, Gly, Val, Ala, Gln and Asp couplings were performed at 75 °C using 170 W for 15 seconds and then at 90 °C using 40 W for 110 seconds. While for His, since it is susceptible to epimerization at elevated temperatures, couplings are performed at 25 °C at 0W for 120 seconds and then at 50 °C using 50W for 480 seconds. Deprotection was performed at 75 °C using 155 W for 15 seconds and then at 90 °C using 50 W for 50 seconds.

The peptides Tau1 and Tau2 were successfully synthesized and purified. Finally, they were sent at the PSI in Switzerland, where our co-workers will conduct further experiments to investigate whether there is an interaction with tubulin.

9. Conclusions

A number of αSyn peptides were synthesized as investigative tools over αSyn/Tub-Microtubules interaction. MW-SPPS was used to afford a library of 20 peptides, containing WT, mutated and scrambled sequences (Table 4). Their conformation was characterized by CD and AFT-IR. The peptides were unstructured, so we were interested in exploring whether it was possible to try to stabilize a secondary conformation to obtain our 'molecular tools' with an enhanced feature. Hence, a library of stapled peptides was prepared and characterized conformationally. Additionally, as a complementary synthesis, we inspected two Tau-deriving peptides, which are both undergoing *in vitro* experiments to study their possible interaction tubulin in the laboratory of our collaborator Andrea Prota in PSI, Switzerland. Moreover, *in vitro* experiments were set up to obtain information about the interaction between the full-length proteins and the peptides. MST was employed to obtain thermodynamic details and the polymerization of tubulin was monitored in the presence of the peptides to obtain a kinetic information and see if the peptides influence the polymerization. The study of the effects of the peptides on the polymerization of tubulin was fruitful since two mutants were able to decrease the polymerization. Finally, we studied the effect of the peptides also in cells, where a different distribution of the microtubules network was observed in presence of the peptides.

In the future, a more accurate technique should be exploited for the study of the interaction of αSyn and tubulin. NMR studies could provide deeper understanding of the two proteins in solution. However, αSyn is, as stated earlier, an intrinsically disorder protein, thus physiological conditions should be maintained in order to obtain a clear indication of their interaction.

Material and Methods

10.Materials

10.1 Chemicals and consumables

All reagents, solvents and consumables were purchased from the companies IRIS Biotech GmbH, Sigma-Aldrich, VWR BDH, Fluorochem, and their purity fulfilled at least the specifications for synthesis quality.

10.2 Methods

10.2.1 Synthesis of linear MW-SPPS

Using MW-SPPS the following peptides were synthesized: WT1, A30, WT2, A53T, E46K, H50Q, G51D, NAC, C1, C2, WT1_scr, A30P_scr, WT2_scr, A53T_scr, E46K_scr, H50Q_scr, G51D_scr, NAC_scr, C1_scr, C2_scr, KPM6, Tau1, Tau2, WT2_CF, G51D_CF and H50Q_CF. After the synthesis, the peptides were transferred into a reactor. Each peptide was cleaved off the resin and precipitated.

10.2.1.1 Automated Solid Phase Peptide Synthesis

The peptide synthesis was carried out on a polymeric, swellable but insoluble support material (resin) of divinylbenzene cross-linked polystyrene, modified with Fmoc-Rink amide aminomethyl for the anchoring of the first amino acid (Fmoc-Rink amide AM resin, 100-200 mesh, 0.7 mmol/g) was used. The automated synthesis was carried out on a 0.1mmol scale using the Liberty Blue™ Automated Microwave Peptide Synthesizer (CEM) according to the Fmoc/*t*Bu strategy. All amino acids (aa) were N-terminally Fmoc-protected, while the side chains of trifunctional aa were protected with orthogonal, acid labile groups. The following side chain protecting groups were used: Trityl (Trt) for Asn, His, and Gln; *tert*-Butyl (*t*Bu) for Asp and Glu and tert-butyloxycarbonyl (Boc) for Lys. For the selective protection of side chains also the allyl group was used for Fmoc-Glu(OAllyl)-OH and the allyloxycarbonyl

group was used for Fmoc-Lys(Alloc)-OH. During the automated synthesis, the resin was first pre-swollen for 30 min in 1 mL of DMF, the solvent was the filtered off and afterwards the Fmoc-protecting group on the resin was cleaved with a 20% (v/v) piperidine solution in DMF in 2 steps: 80 °C, 200W, 30s, ΔT=2 °C; 90 °C, 50W, 70s, ΔT=1 °C. After the deprotection, the resin was washed 4 times with 5 mL DMF each. The aa were dissolved to 0.2 M in DMF. For the coupling the dissolved aa, DIC (0.25 M) and Oxyma Pure (0.5 M) were transferred into the reaction vessel and the coupling was performed in 2 steps: : 75 °C, 170W, 15s, ΔT=2 °C; 90 °C, 30W, 70s, ΔT=1 °C. For some aa the coupling was pre-set from the method to be conducted twice to improve the yield. The deprotection/coupling cycle is repeated until the last aa of the sequences is coupled.

The final Fmoc protecting group is cleaved as previously described. Once the syntheses were finished, the resin was transferred into a syringe equipped with a filter, washed 5 times with DMF, 5 times with DCM and 3 times with Et_2O. Finally, the resin was dried under compressed air.

10.2.1.2 Full cleavage

To obtain the deprotected crude peptide cleaved off the resin, initially scavengers (250 µL H_2O, 250 µL TIPS) and after 2.5 mL of TFA were added to the dry resin in the reactor. The reaction was left shaking for 3 h and then the reaction solution was filtered through the Teflon frit from the syringe into a 50 mL centrifuge tube containing 30 mL of ice-cold Et_2O. Subsequently, the solution was centrifuged off (4 °C, 6500rpm, 20 min), the supernatant was discarded, and the peptide was washed 3 times with ice-cold Et_2O. The peptide was dried under compressed air. For ESI-MS analysis, 1 mg of the peptide was dissolved in MeOH. For analytical HPLC, 0.5 mg of the peptide was dissolved with 400 µL of H_2O/A.

10.2.2 Synthesis of stapled peptides

10.2.2.1 MW-Assisted SPPS

First peptides KPM1, KPM2, KPM3 and KPM8 were synthesized using MW-Assisted SPPS as described before. Then the resin was transferred in a reactor to perform the two reactions of orthogonal protecting groups cleavage and lactamization. The final Fmoc protecting group was cleaved. Finally, the peptides were cleaved off the resin and precipitated.

10.2.2.2 Allyl and allyloxycarbonyl cleavage

The resin was initially swollen in dry DCM under nitrogen for at least 1 h. The solvent was removed and $Pd(PPh_3)_4$ (0.5 eq) and PhH_3Si (24 eq) dissolved in 2 mL of dry DCM were added to the reactor and left shaking for 45 minutes . The deprotection reaction was repeated twice. A Kaiser test was performed to ensure the completeness of the reaction.

10.2.2.3 Lactam-bond formation reaction

The resin was initially swollen in DMF for 30 minutes. HBTU (6 eq), HOBT (6 eq) and DIPEA (12 eq) were added to the reactor dissolved in the maximum amount of DMF to avoid intermolecular coupling and to ensure intramolecular cyclization of the peptide.

10.2.2.4 Fmoc-cleavage

The resin was initially pre-swollen for at least 30 minutes in 5 mL of DMF. After removing the solvent, 4 mL of 20% piperidine were added and left 5 minutes shaking at rt; the solution was filtered and additional 4 mL of 20% piperidine were added and left 20 minutes shaking. The resin was either washed 5 times with DMF to

continue the manual synthesis or washed 5 times with DMF, 5 times with DCM, 3 times with Et_2O and dried under compressed air.

10.2.2.5 Full cleavage

To obtain the deprotected crude stapled peptide cleaved off the resin, initially scavengers (250 µL H_2O, 250 µL TIPS) and after 2.5 mL of TFA were added to the dry resin in the reactor. The reaction was left shaking for 3 h and then the reaction solution was filtered through the Teflon frit from the syringe into a 50 mL centrifuge tube containing 30 mL of ice-cold Et_2O. Subsequently, the solution was centrifuged off (4 °C, 6500 rpm, 20 min), the supernatant was discarded, and the peptide was washed 3 times with ice-cold Et_2O. The peptide was dried under compressed air. For ESI-MS analysis, 1 mg of the peptide was dissolved in MeOH. For analytical HPLC, 0.5 mg of the peptide was dissolved with 400 µL of H_2O/ACN.

10.2.3.1 Manual coupling

The resin was initially pre-swollen for at least 30 minutes in 5 mL of DMF. Afterwards, the solvent was filtered off and the Fmoc-protected aa (5 eq) and Oxyma Pure (5 eq) were dissolved in 2 mL of DMF. DIC (5 eq) was added to the mixture which was subsequently loaded to the resin and left shaking for 2 h at rt. Alternatively, the coupling was carried out with HATU (2 eq) and DIPEA (2 eq) for 1 h at rt. The resin was then washed 5 times with DMF, 5 times with DCM, 3 times with Et_2O and dried under compressed air. To check the completeness of the coupling a Kaiser test was performed.

10.2.3.2 Kaiser Test

The Kaiser Test is used to detect any primary or secondary amine by a colorimetric reaction with ninhydrin. In peptide synthesis, it is useful as we can understand if a coupling or deprotection reaction is completed. Few dry resin beads were transferred in an 1.5 mL tube and 2 drops of each of the following reagents were added in this order:

- Reagent A: 1 g of ninhydrin in 20 mL of ethanol;
- Reagent B: 20 g of phenol in 5 mL of ethanol;
- Reagent C: 0.4mL of 1mM aqueous KCN colution in 20 mL in pyridine.

The reaction mixture was incubated for 5 minutes at 95 ^{o}C in a thermomixer. When the color of the solution or the resin beads was blue a presence of free amines was indicated, suggesting the incompleteness of the coupling reaction. On the contrary, a yellow color indicated the absence of free amino groups.

10.2.3.3 Sample cleavage

In order to ensure that the on-going manual synthesis is proceeding well, the peptide was cleaved from a small amount of resin and the all the acid-labile protective group were also removed. Few dry resin beads were transferred into a 1.5 mL tube. Initially, scavengers (2.5 µL H_2O, 2.5 µL TIPS) were added to the tube and then 95 µL of TFA were added. The reaction was left shaking for 3 h and the 1 mL of ice-cold Et_2O was added. The tube was stored for at least 15 minutes at -20^{o}C and subsequently centrifuged (4 ^{o}C, 15000 rpm, 20 min). The supernatant was discarded, and the precipitated peptide was washed at least 3 times with ice-cold Et_2O. The peptide was dried under compressed air and dissolved in 400 µl of H_2O/ACN. The in-solution peptide was transferred to a vial and further analysed.

10.2.4 Synthesis of novel linker

The synthetical strategy can be observed in Scheme 6.

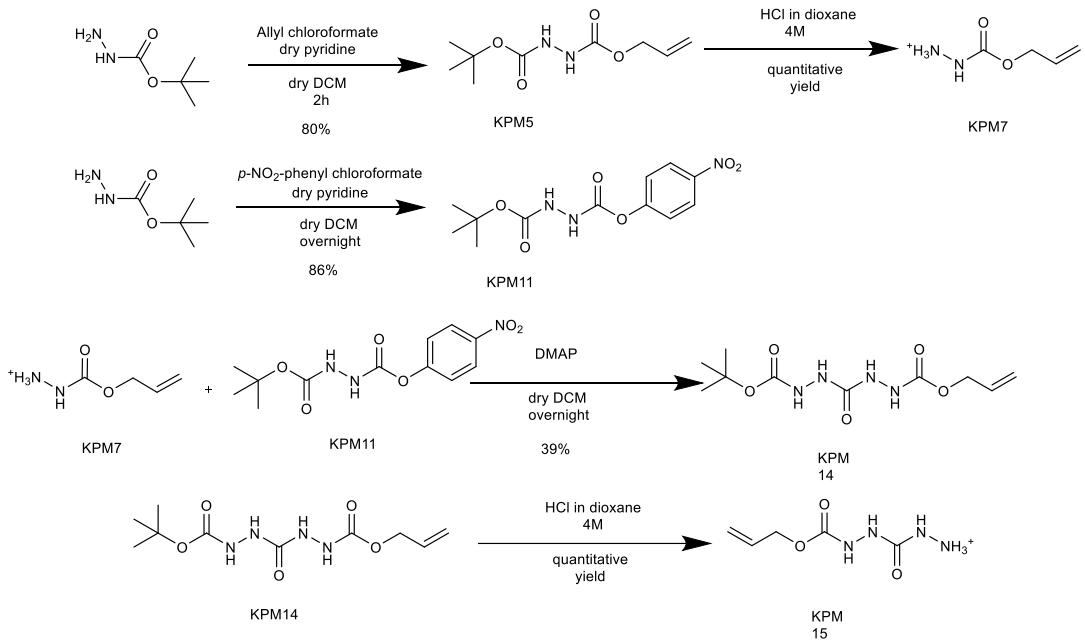

Scheme 6. Overall synthesis to afford final diaza linker.

10.2.4.1. Synthesis of compound KPM5

tert-butyl carbazate (2 g, 15.15 mmol, 1 eq) and dry pyridine (1.46 mL, 18.18 mmol, 1.2 eq) were dissolved in dry diethyl ether. The reaction was brought at 0°C and after 15 minutes, allyl chloroformate (1.17 mL, 16.66 mmol, 1.1 eq) was added dropwise. After the addition, the reaction was left stirring for 2 h. The completion of the reaction was followed by TLC (8:2/Hexane:EtOAc).

The reaction was then washed with 10% citric acid, distilled water, 10% K_2CO_3 and brine. The combined organics were dried over Na_2SO_4 and concentrated under reduced pressure. The crude product was purified by flash chromatography and eluted with 6:4/Hexane:EtOAc. The pure product, a white solid, was obtained with 65% yield.

^{1}H-NMR ($CDCl_3$): δ 1.47 (s, 9H), 4.62-4.63 (m, 1H), 4.64-4.65 (m, 1H), 5.21-5.26 (m, 1H), 5.29-5.36 (m, 1H), 5.84-5.97 (m, 1H), 6.31 (br s, 1H), 6.47 (br s, 1H).

10.2.4.2. Synthesis of compound KPM7

KPM5 (2g, 15.15 mmol, 1 eq) was directly dissolved in HCl 4M (37.875 mL, 151.5 mmol, 10 eq) and the reaction was left under stirring for 3 h. The reaction was followed by TLC (8:2/Hexane:EtOAc). The solution was concentrated under reduced pressure. The crude product was pure enough to continue the synthesis and was obtained with a quantitative yield.

^{1}H-NMR (MeOH-d_4): δ 4.60 (overlapped, 2H), 5.22 (d, J = 10 Hz, 1H), 5.33 (d, J = 17 Hz, 1H), 5.89-5.93 (m, 1H), 7.57 (s, 1H).

10.2.4.3. Synthesis of compound KPM11

tert-butyl carbazate(2 g, 15.15 mmol, 1 eq) and dry pyridine (4.8 mL, 45.45 mmol, 3 eq) were dissolved in dry DCM. The reaction was brought at 0^{o}C and after 15 minutes, *p*-nitro phenyl chloroformate (3.34 g, 16.66 mmol, 1.1 eq) dissolved in dry DCM was added dropwise to the reaction. The reaction was left stirring at 0 ^{o}C for 45 minutes and was, then, brought to rt and left under stirring overnight. The next morning the reaction was controlled by TLC (7:3/Hexane:EtOAc) and it was washed with 10% citric acid, distilled water, 10% K_2CO_3 and brine, being careful to be very fast and not adding a lot of solution due to the sensibility of the product to aqueous solutions. The organics were dried over Na_2SO_4 and concentrated under reduced pressure. The crude was used as it was for the next reaction. The crude obtained was a yellow oil and was afforded with a 96% yield.

^{1}H-NMR ($CDCl_3$): δ 1.90 (s, 9H), 6.47 (br s, 1H), 6.91 (br s, 1H), 7.35 (d, J = 9 Hz, 2H), 8.26 (d, J = 9 Hz, 2H).

10.2.4.4. Synthesis of compound KPM12

KPM7, KPM11 and dimethylaminopyridine were combined and dissolved in dry DCM in a round bottom flush and the reaction was left stirring overnight. The next

day, the completion of the reaction was verifired by TLC (7:3/Hexane:EtOAc). The reaction was washed with 10% citric acid, distilled water, 10% K_2CO_3 and brine. The organics were dried over Na_2SO_4 and concentrated under reduced pressure. The crude product was purified by flash chromatography and eluted with (1:1/Hexane:EtOAc). The pure product is a shining solid and was afforded with 36% yield.

^{1}H-NMR (D_2O): δ 1.48 (s, 9H), 4.61 (d, *J* = 5 HZ, 2H), 5.21 (d, *J* = 10 Hz, 1H), 5.35 (d, *J* = 17 Hz, 1H), 5.92-6.01 (m, 1H).

10.2.4.5. Synthesis of compound KPM14

KPM12 (2g, 15.15 mmol, 1 eq) was directly dissolved in HCl 4M (37.875 mL, 1515 mmol, 10 eq) and the reaction was left under stirring for 3 h. The reaction was followed by TLC (8:2/Hexane:EtOAc). The solution was concentrated under reduced pressure. The crude product was pure enough to continue the synthesis and was obtained with a quantitative yield.

^{1}H-NMR (DMSO-d_6): δ 4.54-4.64 (m, 2H), 5.22 (d, J = 10 Hz, 1H), 5.33 (d, J = 17 Hz,1H), 5.87-5.97 (m, 1H), 8.91 (s, 1H), 9.19 (br s, 1H), 9.44 (br s, 1H).

10.2.4.6. Synthesis of compound KPM15

KPM14(1g, 5.71 mmol, 1 eq) was dissolved in DCM and reagents were added (See Table 22). The pH was controlled carefully reassuring it did not become more than 8. The reaction mixture was usually left under stirring for different time periods (See Table 22). After, the completion of the reaction was verified by TLC (7:3/Hexane:EtOAc). The reaction was washed with 10% citric acid, distilled water, 10% K_2CO_3 and brine. The organics were dried over Na_2SO_4 and concentrated under reduced pressure. The crude product was purified by flash chromatography and

eluted with (1:9/Hexane:EtOAc). The pure product is a white solid and was afforded with yields varying for 24% to 31%.

^{1}H-NMR (DMSO-d6): δ 1.40 (s, 9H), 1.72-1.84 (m, 1H), 1.89-2.00 (m, 1H), 2.20 (t, J = 7 Hz, 2H), 3.87-3.96 (m, 1H), 4.19-4.32 (overlapped, m, 3H), 4.50-4.51 (m, 2H), 5.19 (d, J = 10 Hz, 1H), 5.32 (d, J = 17 Hz, 1H), 5.81-5.95 (m, 1H), 7.31-7.36 (m, 2H), 7.40-7.45 (m, 2H), 7.69-7.74 (m, 2H), 7.89-7.91 (m, 2H), 8.18 (br s, 1H), 8.25 (br s, 1H), 8.93 (br s, 1H), 9.51 (s, 1H).

Reagents	Procedure	Equivalents	Yield
HCTU HoBt DIPEA	Left overnight in DCM with the addition of 0.25 eq next morning	1.1 1.1 3	31%
HCTU HoBt DIPEA	Left over weekend in DCM	1.1 1.1 3	25%
DEPBT DIPEA	Left for 5h	1.2 2	25%
COMU Oxyma DIPEA	Left overnight in DCM	1.1 1.1 3	29%
EDC Oxyma Collidine	Left overnight in DCM	1.2 1.2 5	24%
BTC DIPEA	Left for 5 h	0.4 2	29%

Table 22 Coupling reaction attempts of Fmoc-Glu-OtBu with the Alloc-NH-NH-CO-NH-NH_2 moiety

10.2.4.6. Synthesis of compound KPM16

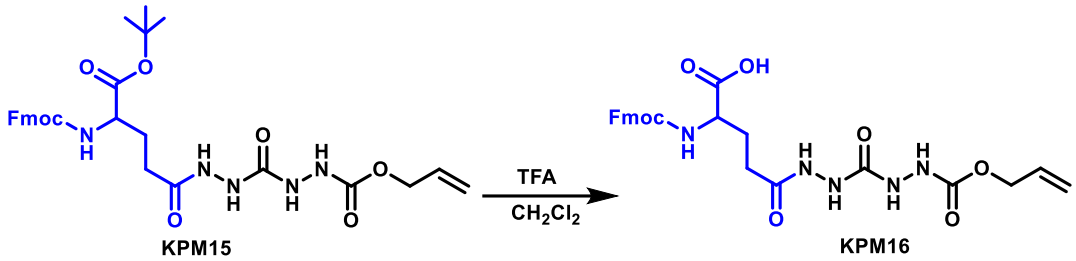

Scheme 7. Deprotection of KPM15 with TFA to obtain compound KPM16

KPM15 (2g, 1.9mmol, 1 eq) was directly dissolved in HCl 4M (37.875 mL, 19 mmol, 10 eq) and the reaction was left under stirring for 3 h. The reaction was followed by TLC (8:2/Hexane:EtOAc). The solution was concentrated under reduced pressure. The crude product was pure enough to continue the synthesis and was obtained with a quantitative yield.

^{1}H-NMR (DMSO-d_6): δ 1.76-1.87 (m, 1H), 1.94-2.07 (m, 1H), 2.21 (t, J = 7 Hz, 2H), 3.92-4.01 (m, 1H), 4.17-4.34 (overlapped, m, 3H), 4.50 (d, J = 5 Hz, 2H), 5.18 (d, J = 10 Hz, 1H), 5.31 (d, J = 17 Hz, 1H), 5.80-5.96 (m, 1H), 7.32-7.36 (m, 2H), 7.40-7.45 (m, 2H), 7.67-7.75 (m, 2H), 7.89-7.91 (m, 2H), 8.18 (br s, 1H), 8.26 (br s, 1H), 8.92 (br s, 1H),9.51 (s, 1H), 12.61 (br s, 1H).

10.2.4.7 Synthesis of peptide containing the diaza linker

KPM30 peptide was synthesized manually, and all the reactions attempted were performed at room temperature. After each coupling, the Kaiser Test was performed and a sample cleavage to verify the coupling or deprotection success.

10.2.5. Peptide analysis

All solvents and eluents used for the HPLC fulfilled the required purity with the specification “HPLC Gradient quality”.

10.2.5.1. Analytical HPLC

Each peptide was controlled during and at the end of the synthesis using reverse phase high-performance liquid chromatography. Samples of the peptides were prepared as described before. The linear gradient used was typically 10-70% B in A in 20 min with a flow rate of 0.8 mL / min (A: 0.1% TFA in water, B: 0.1% TFA in ACN). Samples were, thus, injected into a C18 analytical column and that then passed from the UV detector for the measurement of the absorbance at 205 and 220 nm. Chromatograms were obtained and further analysed.

10.2.5.2 Electrospray Ionization Mass Spectrometry

Samples of the peptides were prepared as described previously and a 10 uL of the peptide solution were diluted in MeOH and ionized in the mass spectrometer and the *m/z* values of the ions were detected.

10.2.6 Preparative HPLC

Crude peptides had to be purified after the cleavage, to remove any scavengers or to separate from other impurities. All the peptides were purified by semi-preparative reverse phase HPLC. Usually, 35 mg of each peptide were dissolved in (maximum) 5 mL of the starting gradient solution, that varied based on the hydrophobicity of the peptide. The dissolved peptide was then injected in the column manually and the elution was performed with a linear gradient, for most cases 10-50% B in A (A: 0.1% TFA in water, B: 0.1% TFA in ACN) in 20 or 30 minutes at a flow rate of 20 mL/min. The absorbance was detected at 220 nm and the various peaks were separated into plastic tubes. After the analysis by analytical HPLC and ESI-MS, the fractions of interest were concentrated and lyophilized.

10.2.7 Secondary structural characterization of peptides

10.2.7.1 Circular dichroism spectroscopy

CD spectra were recorder from 260 nm to 180 nm at 25 ^{o}C using a Jasco J spectropolarimeter purged with N_2 gas. The peptides were measured in a concentration of 100 μM in 7 different conditions:

1) 100 % Trifluoroethanol (TFE) that is known to enhance the alpha-helical propensities of peptides-proteins.
2) 100% Phosphate Buffer (NaH_2PO_4 - Na_2HPO_4) at pH = 7.
3) 100% MES Buffer at pH = 6.
4) 100% Phosphate Buffer (NaH_2PO_4 - Na_2HPO_4) at pH = 8.
5) 50% TFE- 50% Buffer pH=7
6) 50% TFE- 50% Buffer pH= 6.
7) 50% TFE- 50% Buffer pH=8.

10.2.7.2. Attenuated Total Reflectance-Fourier Transform Infrared (ATR-FTIR) spectroscopy of peptides

FTIR spectroscopy measurements were made on a Perkin Elmer Spotlight 400 FT-IR spectrophotometer equipped with a diamond crystal attenuated total reflectance (ATR) accessory. All the sample were analysed at room temperature in the solid state. A total of 32 scans were performed for all measurements with a resolution of 4 cm^{-1} in the 4000-650 cm^{-1} spectral region. Data processing was performed using OriginPro software. The deconvolution of the spectra was done in the spectral region between 1550-1750 cm^{-1}, using the Fit Peaks (Pro) function.

10.2.8 Experiments to investigate the interaction between αSyn and Tubulin

10.2.8.1 Tubulin Polymerization Assay

Tubulin tends to spontaneously form microtubules in vitro when incubated in a solution in presence of GTP at 37 °C. Based on this, we performed tubulin polymerization kinetics taking advantages of a specific kinetic tubulin assembly buffer (composed by 0.1 M PIPES, 1 mM EGTA, 0.2 mM Tris,3 mM $MgCl_2$ pH=6.9, 0.1 mM GTP + 10% glycerol). The buffers used to prepare the samples were degassed to avoid bubbles formation. Importantly, in order to remove cold-stable fractions and eventual aggregates formed during their storage at -80 °C, tubulin aliquots were first ultra-centrifuged for 30 minutes at 158000 x g (Beckman + TLA, 100.3 rotor: 54000 rpm). Once centrifuged, the supernatant was retrieved, the protein concentration was determined with the Nanodrop (e = 115x103 M-1 cm-1, MW=100 kDa, l = 280 nm) and then, once the concentration of the batch was verified, kinetic samples were prepared.

To investigate peptides effects, we assembled:

• Samples: 25 µM tubulin + 100 µM α-Synuclein peptide in degassed assembly buffer+1% DMSO.

Each experiment consisted of 3 replicates of each sample.

Once assembled, samples were incubated for 10 minutes at room temperature in the thermomixer (Cartelli et al., 2016). After a gently mix, samples were transferred into the multiwell plate and polymerization reaction was initiated by placing the plate at 37 °C into the microplate reader. Polymerization kinetics were followed for 2 hours, checking the absorbance at 340 nm and maintaining a stable temperature of 37 °C during the entire run.

10.2.8.2 MicroScale Thermophoresis (MST)

MST was performed to measure the binding affinity between tubulin and αSyn and the mutated isoforms (A53T, E46K and A30P). Tubulin was labelled with Red-NHS second generation kit at the lysines which was purchased by NanoTemper and during the assay it was used at a final concentration of 50 nM. Lyophilized alpha synuclein was resuspended using MST buffer purchased by Nanotemper and was used in the assay in serial dilutions, starting from 242 µM up to 15.6 µM. Higher concentrations of α-Synuclein weren't tested since it could lead to aggregation of both proteins.

The peptides were tested using the "Binding check" assay. To conduct it, peptides were dissolved in MST buffer and used at 500 µM and labelled tubulin at 50 nM.

10.2.8.3 MTT assay in undifferentiated naïve cells

Human neuroblastoma SK-N-SH cells were grown in complete medium composed of DMEM low glucose, supplemented with 10% fetal bovine serum, 1% penicillin/ streptomycin, 1% L-glutamine, and 1% non-essential amino acids. Cells were maintained at 37 °C under a humidified atmosphere of 5% CO_2. The cell viability was tested by MTT (3-(4,5-dimethylthiazol2-yl)-2,5-diphenyl tetrazolium bromide) assay. Neuroblastoma cells were seeded into a 48-well plate (15000 cells/well) in complete medium. After 24 h, cells were treated with different concentrations (0.001–100 µM) of the compound of interest or with vehicle (1% DMSO). Treated and untreated cells were incubated for 24 h at 37° C under a humidified atmosphere of 5% CO_2. Next, 30 µL of MTT (5 mg/mL) was added to the cells and incubated for 3 h at 37° C under a humidified atmosphere of 5% CO_2. Afterward, formazan crystals were solubilized with acidified (0.1 M HCl) isopropanol containing 10% Triton X100. The optical density (OD) was determined at a wavelength of 570 nm using an Infinite 200Pro Tecan plate reader (Tecan Group Ltd.). Compounds were tested in triplicate.

The cell viability was expressed as the percentage (%) of viable cells relative to the vehicle (100%). All experimental data were shown as mean ± SD. Data were analyzed by a one-way nonparametric ANOVA Kruskal–Wallis test with Dunnett's correction for multiple comparison using Prism Software. The statistical significance was set at $p < 0.05$.

11. Abbreviations

αSyn: alpha-Synuclein

Ala: alanine

Alloc: allyloxycarbonyl

ATR-FTIR: attenuated total reflectance Fourier Transform infrared

CAMSAPs: calmodulin-regulated spectrin-associated proteins

CD: circular dichroism

DCM: dichloromethane

DIC: *N,N*-diisopropylcarbodiimide

DIPEA: *N,N*,N-diisopropylethylamine

DMAP: 4-dimethylaminopyridine

DMF: *N,N*-dimethylformamide

ESI-MS: electrospray ionization mass spectrometry

Gln: glutamine

Glu: glutamic acid

Gly: glycine

HBTU: 2-(1H-Benzotriazole-1-yl)-1,1,3,3-tetramethyluronium hexafluorophosphate

HOBt: hydroxybenzotriazole

Lys: lysine

MAP: microtubules associated protein

MST: microscale thermophoresis

MTs: microtubules

MTT: 3-(4,5-dimethylthiazol-2-yl)-2,5-diphenyltetrazolium bromide

MW: microwave

NMR: nuclear magnetic resonance

o.n.: over-night

Pd: palladium

RP-HPLC: reversed-phase high performance liquid chromatography

rt: room temperature

SPPS: solid phase peptide synthesis

TFA: trifluoroacetic acid

TFE: trifluoroethanol

TIPS: triisopropylsilane

Val: valine

12. Bibliography

1. Ilan Y. Microtubules as a Potential Platform for Energy Transfer in Biological Systems: A Target for Implementing Individualized, Dynamic Variability Patterns to Improve Organ Function. *Mol Cell Biochem* 2023;478(2):375–392, doi: 10.1007/s11010-022-04513-1.

2. Mitchison T, Kirschnert M. Cytoskeletal Dynamics and Nerve Growth. *Neuron* 1988;1(9):761-72. doi: 10.1016/0896-6273(88)90124-9.

3. Hahn I, Voelzmann A, Liew YT, Costa-Gomes B, Prokop A. The Model of Local Axon Homeostasis - Explaining the Role and Regulation of Microtubule Bundles in Axon Maintenance and Pathology. *Neural Development*, 2019, *14*, DOI: 10.1186/s13064-019-0134-0.

4. Baas PW, Rao AN, Matamoros AJ, Leo L. Stability Properties of Neuronal Microtubules. *Cytoskeleton*, 2016, *73*, 442–460, DOI: 10.1002/cm.21286.

5. Avila J, Dominguez J, Diaz-Nido' J. Regulation of Microtubule Dynamics by Microtubule-Associated Protein Expression and Phosphorylation during Neuronal Development, *Int. J. Dev. Biol.* 1994, 38 : 13-25

6. Grenningloh G, Soehrman S, Bondallaz P, Ruchti E, Cadas H. Role of the Microtubule Destabilizing Proteins SCG10 and Stathmin in Neuronal Growth. *Journal of Neurobiology*, 2004, *58*, 60–69, DOI: 10.1002/neu.10279.

7. Yu W, Qiang L, Solowska JM, Karabay A, Korulu S, Baas PW. The Microtubule-Severing Proteins Spastin and Katanin Participate Differently in the Formation of Axonal Branches. *Mol Biol Cell* 2008;19:1485–1498, DOI: 10.1091/mbc.E07-09.

8. Van De Willige D, Hoogenraad CC, Akhmanova A. Microtubule Plus-End Tracking Proteins in Neuronal Development. *Cellular and Molecular Life Sciences*, 2016, *73*, 2053–2077, DOI: 10.1007/s00018-016-2168-3.

9. Tim Mitchison and March Kirschner Cytoskeletal Dynamics and Nerve Growth, *Neuron* 1988, vol 1, 761-772

10. Desai A, Mitchison TJ. MICROTUBULE POLYMERIZATION DYNAMICS, *Annu. Rev. Cell Dev. Biol* 1997, Vol. 13, 83-117

11. Downing KH. STRUCTURAL BASIS FOR THE INTERACTION OF TUBULIN WITH PROTEINS AND DRUGS THAT AFFECT MICROTUBULE DYNAMICS, *Annu. Rev. Cell Dev. Biol.* 2000, 16:89–111

12. Hanukoglu I. Proteopedia: Rossmann Fold: A Beta-Alpha-Beta Fold at Dinucleotide Binding Sites. *Biochemistry and Molecular Biology Education* 2015;43(3):206–209, DOI: 10.1002/bmb.20849.

13. Nogales E, Wang HW. Structural Mechanisms Underlying Nucleotide-Dependent Self-Assembly of Tubulin and Its Relatives. *Current Opinion in Structural Biology*, 2006, *16*, 221–229, DOI: 10.1016/j.sbi.2006.03.005.

14. Caplow M, Ruhlen RL, Shanks J, Caplow M. *The Free Energy for Hydrolysis of a Microtubule-Bound Nucleotide Tripllosphate Is Near Zero: All of the Free Energy for Hydrolysis Is Stored in the Microtubule Lattice*, Vol. 127. 1994.

15. Nogales E, Zhang R. Visualizing Microtubule Structural Transitions and Interactions with Associated Proteins. *Current Opinion in Structural Biology*, 2016, *37*, 90–96, DOI: 10.1016/j.sbi.2015.12.009.

16. Akhmanova A, Steinmetz MO. Tracking the Ends: A Dynamic Protein Network Controls the Fate of Microtubule Tips. *Nature Reviews Molecular Cell Biology*, 2008, *9*, 309–322, DOI: 10.1038/nrm2369.

17. Jiang K, Hua S, Mohan R, Grigoriev I, Yau KW, Liu Q, Katrukha EA, Altelaar AFM, Heck AJR, Hoogenraad CC, Akhmanova A. Microtubule Minus-End Stabilization by Polymerization-Driven CAMSAP Deposition. *Dev Cell* 2014;28(3):295–309, DOI: 10.1016/j.devcel.2014.01.001.

18. Janke C, Bulinski JC. Post-Translational Regulation of the Microtubule Cytoskeleton: Mechanisms and Functions. *Nature Reviews Molecular Cell Biology*, 2011, *12*, 773–786, DOI: 10.1038/nrm3227.

19. Janke C. The Tubulin Code: Molecular Components, Readout Mechanisms, Functions. *Journal of Cell Biology* 2014;206(4):461–472, DOI: 10.1083/jcb.201406055.

20. Hirokawa N, Noda Y, Tanaka Y, Niwa S. Kinesin Superfamily Motor Proteins and Intracellular Transport. *Nature Reviews Molecular Cell Biology*, 2009, *10*, 682–696, DOI: 10.1038/nrm2774.

21. Bhabha G, Johnson GT, Schroeder CM, Vale RD. How Dynein Moves Along Microtubules. *Trends in Biochemical Sciences*, 2016, *41*, 94–105, DOI: 10.1016/j.tibs.2015.11.004.

22. Roostalu J, Surrey T. Microtubule Nucleation: Beyond the Template. *Nature Reviews Molecular Cell Biology*, 2017, *18*, 702–710, DOI: 10.1038/nrm.2017.75.

23. Goto A, Wang YL, Kabuta T, Setsuie R, Osaka H, Sawa A, Ishiura S, Wada K. Proteomic and Histochemical Analysis of Proteins Involved in the Dying-Back-Type of Axonal Degeneration in the Gracile Axonal Dystrophy (Gad) Mouse. *Neurochem Int* 2009;54(5–6):330–338, DOI: 10.1016/j.neuint.2008.12.012.

24. Dadon-Nachum M, Melamed E, Offen D. The “Dying-Back” Phenomenon of Motor Neurons in ALS. *Journal of Molecular Neuroscience*, 2011, *43*, 470–477, DOI: 10.1007/s12031-010-9467-1.

25. Skovronsky DM, Lee VMY, Trojanowski JQ. Neurodegenerative Diseases: New Concepts of Pathogenesis and Their Therapeutic Implications. *Annual Review of Pathology*, 2006, *1*, 151–170, DOI: 10.1146/annurev.pathol.1.110304.100113.

26. Glass CK, Saijo K, Winner B, Marchetto MC, Gage FH. Mechanisms Underlying Inflammation in Neurodegeneration. *Cell*, 2010, *140*, 918–934, DOI: 10.1016/j.cell.2010.02.016.

27. Arnold SE, Toledo JB, Appleby DH, Xie SX, Wang LS, Baek Y, Wolk DA, Lee EB, Miller BL, Lee VMY, Trojanowski JQ. Comparative Survey of the Topographical Distribution of Signature Molecular Lesions in Major Neurodegenerative Diseases. *Journal of Comparative Neurology* 2013;521(18):4339–4355, DOI: 10.1002/cne.23430.

28. Baird FJ. Microtubule Defects and Neurodegeneration. *J Genet Syndr Gene Ther* 2013;04(11), DOI: 10.4172/2157-7412.1000203.

29. Takalo M, Salminen A, Soininen H, Hiltunen M, Haapasalo A. *Protein Aggregation and Degradation Mechanisms in Neurodegenerative Diseases*, Vol. 2. 2013.

30. Paschen W, Mengesdorf T. Endoplasmic Reticulum Stress Response and Neurodegeneration. *Cell Calcium* 2005;38(3-4 SPEC. ISS.):409–415, DOI: 10.1016/j.ceca.2005.06.019.

31. Ischiropoulos H, Beckman JS. Oxidative Stress and Nitration in Neurodegeneration: Cause, Effect, or Association? *Journal of Clinical Investigation*, 2003, *111*, 163–169, DOI: 10.1172/JCI200317638.

32. Goedert M, Jakes R. Mutations Causing Neurodegenerative Tauopathies. *Biochimica et Biophysica Acta - Molecular Basis of Disease*, 2005, *1739*, 240–250, DOI: 10.1016/j.bbadis.2004.08.007.

33. De Vos KJ, Grierson AJ, Ackerley S, Miller CCJ. Role of Axonal Transport in Neurodegenerative Diseases. *Annual Review of Neuroscience*, 2008, *31*, 151–173, DOI: 10.1146/annurev.neuro.31.061307.090711.

34. Franker MAM, Hoogenraad CC. Microtubule-Based Transport -Basic Mechanisms, Traffic Rules and Role in Neurological Pathogenesis. *J Cell Sci* 2013;126(11):2319–2329, DOI: 10.1242/jcs.115030.

35. Hinckelmann MV, Zala D, Saudou F. Releasing the Brake: Restoring Fast Axonal Transport in Neurodegenerative Disorders. *Trends in Cell Biology*, 2013, *23*, 634–643, DOI: 10.1016/j.tcb.2013.08.007.

36. Millecamps S, Julien JP. Axonal Transport Deficits and Neurodegenerative Diseases. *Nature Reviews Neuroscience*, 2013, *14*, 161–176, DOI: 10.1038/nrn3380.

37. Beharry C, Cohen LS, Di J, Ibrahim K, Briffa-Mirabella S, Alonso ADC. Tau-Induced Neurodegeneration: Mechanisms and Targets. *Neuroscience Bulletin*, 2014, *30*, 346–358, DOI: 10.1007/s12264-013-1414-z.

38. Encalada SE, Goldstein LSB. Biophysical Challenges to Axonal Transport: Motor-Cargo Deficiencies and Neurodegeneration. *Annu Rev Biophys* 2014;43(1):141–169, DOI: 10.1146/annurev-biophys-051013-022746.

39. Craig AM, Banker G. NEURONAL POLARITY, *Annu. Rev. Neurosci.* 1994, 17:267-310

40. Witte H, Neukirchen D, Bradke F. Microtubule Stabilization Specifies Initial Neuronal Polarization. *Journal of Cell Biology* 2008;180(3):619–632, DOI: 10.1083/jcb.200707042.

41. Jacobs JR, Stevens JK. *Changes in the Organization of the Neuritic Cytoskeleton during Nerve Growth Factor-Activated Differentiation of PC12 Cells: A Serial Electron Microscopic Study of the Development and Control of Neurite Shape*.

42. Jaworski J, Kapitein LC, Gouveia SM, Dortland BR, Wulf PS, Grigoriev I, Camera P, Spangler SA, Di Stefano P, Demmers J, Krugers H, Defilippi P, Akhmanova A, Hoogenraad CC. Dynamic Microtubules Regulate Dendritic Spine Morphology and Synaptic Plasticity. *Neuron* 2009;61(1):85–100, DOI: 10.1016/j.neuron.2008.11.013.

43. Liu G, Dwyer T. Microtubule Dynamics in Axon Guidance. *Neuroscience Bulletin*, 2014, *30*, 569–583, DOI: 10.1007/s12264-014-1444-6.

44. Janmey PA. The Cytoskeleton and Cell Signaling: Component Localization and Mechanical Coupling, *Physiological Reviews* 1998, Vol. 78. 1998.

45. Bounoutas A, Kratz J, Emtage L, Ma C, Nguyen KC, Chalfie M. Microtubule Depolymerization in Caenorhabditis Elegans Touch Receptor Neurons Reduces Gene Expression through a P38 MAPK Pathway. *Proc Natl Acad Sci U S A* 2011;108(10):3982–3987, DOI: 10.1073/pnas.1101360108.

46. Dent EW, Baas PW. Microtubules in Neurons as Information Carriers. *Journal of Neurochemistry*, 2014, *129*, 235–239, DOI: 10.1111/jnc.12621.

47. McNally FJ, Roll-Mecak A. Microtubule-Severing Enzymes: From Cellular Functions to Molecular Mechanism. *Journal of Cell Biology*, 2018, *217*, 4057–4069, DOI: 10.1083/jcb.201612104.

48. Akhmanova A, Steinmetz MO. Control of Microtubule Organization and Dynamics: Two Ends in the Limelight. *Nature Reviews Molecular Cell Biology*, 2015, *16*, 711–726, DOI: 10.1038/nrm4084.

49. Teng J, Takei Y, Harada A, Nakata T, Chen J, Hirokawa N. Synergistic Effects of MAP2 and MAP1B Knockout in Neuronal Migration, Dendritic Outgrowth, and Microtubule Organization. *Journal of Cell Biology* 2001;155(1):65–76, DOI: 10.1083/jcb.200106025.

50. Walters GB, Gustafsson O, Sveinbjornsson G, Eiriksdottir VK, Agustsdottir AB, Jonsdottir GA, Steinberg S, Gunnarsson AF, Magnusson MI, Unnsteinsdottir U, Lee AL, Jonasdottir A, Sigurdsson A, Jonasdottir A, Skuladottir A, Jonsson L, Nawaz MS, Sulem P, Frigge M, Ingason A, Love A, Norddhal GL, Zervas M, Gudbjartsson DF, Ulfarsson MO, Saemundsen E, Stefansson H, Stefansson K. MAP1B Mutations Cause Intellectual Disability and Extensive White Matter Deficit. *Nat Commun* 2018;9(1), DOI: 10.1038/s41467-018-05595-6.

51. Harada A, Teng J, Takei Y, Oguchi K, Hirokawa N. MAP2 Is Required for Dendrite Elongation, PKA Anchoring in Dendrites, and Proper PKA Signal Transduction. *Journal of Cell Biology* 2002;158(3):541–549, DOI: 10.1083/jcb.200110134.

52. Biswas S, Kalil K. The Microtubule-Associated Protein Tau Mediates the Organization of Microtubules and Their Dynamic Exploration of Actin-Rich Lamellipodia and Filopodia of Cortical Growth Cones. *Journal of Neuroscience* 2018;38(2):291–307, DOI: 10.1523/JNEUROSCI.2281-17.2017.

53. Caceres A, Kosik K.S, Inhibition of neurite polarity by tau antisense oligonucleotides in primary cerebellar neurons, *Nature* 1990, vol 343 : 461-63

54. Sapir T, Frotscher M, Levy T, Mandelkow EM, Reiner O. Tau's Role in the Developing Brain: Implications for Intellectual Disability. *Hum Mol Genet* 2012;21(8):1681–1692, DOI: 10.1093/hmg/ddr603.

55. Liu G, Thangavel R, Rysted J, Kim Y, Francis MB, Adams E, Lin Z, Taugher RJ, Wemmie JA, Usachev YM, Lee G. Loss of Tau and Fyn Reduces Compensatory Effects of MAP2 for Tau and Reveals a Fyn-Independent Effect of Tau on Calcium. *J Neurosci Res* 2019;97(11):1393–1413, DOI: 10.1002/jnr.24517.

56. Ma QL, Zuo X, Yang F, Ubeda OJ, Gant DJ, Alaverdyan M, Kiosea NC, Nazari S, Chen PP, Nothias F, Chan P, Teng E, Frautschy SA, Cole GM. Loss of MAP Function Leads to Hippocampal Synapse Loss and Deficits in the Morris Water Maze with Aging. *Journal of Neuroscience* 2014;34(21):7124–7136, DOI: 10.1523/JNEUROSCI.3439-13.2014.

57. Castillo-Carranza DL, Gerson JE, Sengupta U, Guerrero-Muñoz MJ, Lasagna-Reeves CA, Kayed R. Specific Targeting of Tau Oligomers in Htau Mice Prevents Cognitive

Impairment and Tau Toxicity Following Injection with Brain-Derived Tau Oligomeric Seeds. *Journal of Alzheimer's Disease* 2014;40(S1), DOI: 10.3233/JAD-132477.

58. Swanson E, Breckenridge L, McMahon L, Som S, McConnell I, Bloom GS. Extracellular Tau Oligomers Induce Invasion of Endogenous Tau into the Somatodendritic Compartment and Axonal Transport Dysfunction. *Journal of Alzheimer's Disease* 2017;58(3):803–820, DOI: 10.3233/JAD-170168.

59. A Ash PE, Lei S, Shattuck J, Boudeau S, Carlomagno Y, Medalla M, Mashimo BL, Socorro G, A Al-Mohanna LF, Jiang L, Öztürk MM, Knobel M, Ivanov P, Petrucelli L, Wegmann S, Kanaan NM, Wolozin B. TIA1 Potentiates Tau Phase Separation and Promotes Generation of Toxic Oligomeric Tau., DOI: 10.1073/pnas.2014188118/-/DCSupplemental.

60. Usenovic M, Niroomand S, Drolet RE, Yao L, Gaspar RC, Hatcher NG, Schachter J, Renger JJ, Parmentier-Batteur S. Internalized Tau Oligomers Cause Neurodegeneration by Inducing Accumulation of Pathogenic Tau in Human Neurons Derived from Induced Pluripotent Stem Cells. *Journal of Neuroscience* 2015;35(42):14234–14250, DOI: 10.1523/JNEUROSCI.1523-15.2015.

61. Fiock KL, Smith JD, Crary JF, Hefti MM. β-Amyloid and Tau Pathology in the Aging Feline Brain. *Journal of Comparative Neurology* 2020;528(1):108–113, DOI: 10.1002/cne.24741.

62. Schultz C, Hubbard GB, Rüb U, Braak E, Braak H. *Age-Related Progression of Tau Pathology in Brains of Baboons*. *Neurobiol Aging* 2000 Nov-Dec;21(6):905-12. doi: 10.1016/s0197-4580(00)00176-7.

63. Lemere CA, Beierschmitt A, Iglesias M, Spooner ET, Bloom JK, Leverone JF, Zheng JB, Seabrook TJ, Louard D, Li D, Selkoe DJ, Palmour RM, Ervin FR. Alzheimer's Disease Aβ Vaccine Reduces Central Nervous System Aβ Levels in a Non-Human Primate, the Caribbean Vervet. *American Journal of Pathology* 2004;165(1):283–297, DOI: 10.1016/S0002-9440(10)63296-8.

64. Elfenbein H.A., Beauprè M., Lèvesque M, Hess U., Toward a dialect theory: cultural differences in the expression and recognition of posed facial expressions. *Emotion* 2007;7(1):131-146. doi: 10.1037/1528-3542.7.1.131.

65. Rosen RF, Farberg AS, Gearing M, Dooyema J, Long PM, Anderson DC, Davis-Turak J, Coppola G, Geschwind DH, Paré JF, Duong TQ, Hopkins WD, Preuss TM, Walker LC. Tauopathy with Paired Helical Filaments in an Aged Chimpanzee. *Journal of Comparative Neurology* 2008;509(3):259–270, DOI: 10.1002/cne.21744.

66. Perez SE, Raghanti MA, Hof PR, Kramer L, Ikonomovic MD, Lacor PN, Erwin JM, Sherwood CC, Mufson EJ. Alzheimer's Disease Pathology in the Neocortex and

Hippocampus of the Western Lowland Gorilla (Gorilla Gorilla Gorilla). *Journal of Comparative Neurology* 2013;521(18):4318–4338, DOI: 10.1002/cne.23428.

67. Banik A, Brown RE, Bamburg J, Lahiri DK, Khurana D, Friedland RP, Chen W, Ding Y, Mudher A, Padjen AL, Mukaetova-Ladinska E, Ihara M, Srivastava S, Srivastava MVP, Masters CL, Kalaria RN, Anand A. Translation of Pre-Clinical Studies into Successful Clinical Trials for Alzheimer's Disease: What Are the Roadblocks and How Can They Be Overcome? *Journal of Alzheimer's Disease*, 2015, *47*, 815–843, DOI: 10.3233/JAD-150136.

68. Drummond E, Wisniewski T. Alzheimer's Disease: Experimental Models and Reality. *Acta Neuropathologica*, 2017, *133*, 155–175, DOI: 10.1007/s00401-016-1662-x.

69. Head E, Moffat K, Das P, Sarsoza F, Poon WW, Landsberg G, Cotman CW, Murphy MP. β-Amyloid Deposition and Tau Phosphorylation in Clinically Characterized Aged Cats. *Neurobiol Aging* 2005;26(5):749–763, DOI: 10.1016/j.neurobiolaging.2004.06.015.

70. Gunn-Moore DA, McVee J, Bradshaw JM, Pearson GR, Head E, Gunn-Moore FJ. Ageing Changes in Cat Brains Demonstrated by β-Amyloid and AT8-Immunoreactive Phosphorylated Tau Deposits. *J Feline Med Surg* 2006;8(4):234–242, DOI: 10.1016/j.jfms.2006.01.003.

71. Chambers JK, Tokuda T, Uchida K, Ishii R, Tatebe H, Takahashi E, Tomiyama T, Une Y, Nakayama H. The Domestic Cat as a Natural Animal Model of Alzheimer's Disease. *Acta Neuropathol Commun* 2015;3:78, DOI: 10.1186/s40478-015-0258-3.

72. Barbier P, Zejneli O, Martinho M, Lasorsa A, Belle V, Smet-Nocca C, Tsvetkov PO, Devred F, Landrieu I. Role of Tau as a Microtubule-Associated Protein: Structural and Functional Aspects. *Frontiers in Aging Neuroscience*, 2019, *10*, DOI: 10.3389/fnagi.2019.00204.

73. Payton JE, Perrin RJ, Clayton DF, George JM. *Protein-Protein Interactions of Alpha-Synuclein in Brain Homogenates and Transfected Cells*, Vol. 95. 2001.

74. Mazzetti S, Calogero AM, Pezzoli G, Cappelletti G. Cross-Talk between α-Synuclein and the Microtubule Cytoskeleton in Neurodegeneration. *Exp Neurol* 2023;359, DOI: 10.1016/j.expneurol.2022.114251.

75. Cartelli D, Aliverti A, Barbiroli A, Santambrogio C, Ragg EM, Casagrande FVM, Cantele F, Beltramone S, Marangon J, De Gregorio C, Pandini V, Emanuele M, Chieregatti E, Pieraccini S, Holmqvist S, Bubacco L, Roybon L, Pezzoli G, Grandori R, Arnal I, Cappelletti G. α-Synuclein Is a Novel Microtubule Dynamase. *Sci Rep* 2016;6, DOI: 10.1038/srep33289.

76. Calogero AM, Mazzetti S, Pezzoli G, Cappelletti G. Neuronal Microtubules and Proteins Linked to Parkinson's Disease: A Relevant Interaction? *Biological Chemistry*, 2019, *400*, 1099–1112, DOI: 10.1515/hsz-2019-0142.

77. Inaba H, Yamamoto T, Kabir AMR, Kakugo A, Sada K, Matsuura K. Molecular Encapsulation Inside Microtubules Based on Tau-Derived Peptides. *Chemistry - A European Journal* 2018;24(56):14958–14967, DOI: 10.1002/chem.201802617.

78. Li X, Chen S, Zhang WD, Hu HG. Stapled Helical Peptides Bearing Different Anchoring Residues. *Chemical Reviews*, 2020, *120*, 10079–10144, DOI: 10.1021/acs.chemrev.0c00532.

79. Lavedan C., The Synuclein Family. *Genome Res* 1998;8(9):871-80. doi: 10.1101/gr.8.9.871.

80. Clayton DF, George JM. Synucleins in Synaptic Plasticity and Neurodegenerative Disorders, *J Neurosci Res* 1999;58(1):120-9. Vol. 58. 1999.

81. Maroteaux L, Campanelli JT, Scheller RH. Synuclein: A Neuron-Specific Protein Localized to the Nucleus and Presynaptic Nerve Terminal, *J Neurosci* 1988;8(8):2804-15. doi: 10.1523/JNEUROSCI.08-08-02804.1988.

82. Tobe T, Nakajo S, Tanaka A, Mitoya A, Omata K, Nakaya K, Tomita M, Asuharu Nakamura Y. Cloning and Characterization of the CDNA Encoding a Novel Brain-Specific 14-KDa Protein. *J Neurochem* 1992 ;59(5):1624-9. doi: 10.1111/j.1471-4159.1992.tb10991.x.

83. Ueda K, Fukushima H, Masliah E, Xia YU, Iwai A, Yoshimoto M, Otero DAC, Kondo J, Ihara Y, Saitoh T. *Molecular* Cloning of CDNA Encoding an Unrecognized Component of Amyloid in Alzheimer Disease (Neurodegeneration/Chaperone/Amyloid P/A4 Protein/Neuritic Plaque*), Proc Natl Acad Sci* 1993 1;90(23):11282-6.

84. Bayer A.T., Alpha-Synuclein accumulates in Lewy bodies in Parkinson's disease and dementia with Lewy bodies but not in Alzheimer's disease beta-amyloid plaque cores, *Neurosci Lett* 1999;266(3):213-6. doi: 10.1016/s0304-3940(99)00311-0.

85. Jakes R, Spillantini MG, Goedert M. Identification of Two Distinct Synucleins from Human Brain, *FEBS Lett* 1994;345(1):27-32.

86. Ji H., Liu Y.E., Jia T., Wang M., Liu J., Xiao G., Joseph B.K., Rosen C., Shi Y. E., Identification of a breast cancer-specific gene, BCSG1, by direct differential cDNA sequencing. *Cancer Res* 1997;57(4):759-64.

87. Buchman VL, Hunter HJA, Pinõ LGP, Thompson J, Privalova EM, Ninkina NN, Davies AM. Persyn, a Member of the Synuclein Family, Has a Distinct Pattern of Expression in the Developing Nervous System. *J Neurosci* 1998;18(22):9335-41. doi: 10.1523/JNEUROSCI.18-22-09335.1998.

88. Jin H, Kanthasamy A, Ghosh A, Yang Y, Anantharam V, Kanthasamy AG. α-Synuclein Negatively Regulates Protein Kinase Cδ Expression to Suppress Apoptosis in Dopaminergic Neurons by Reducing P300 Histone Acetyltransferase Activity. *Journal of Neuroscience* 2011;31(6):2035–2051, DOI: 10.1523/JNEUROSCI.5634-10.2011.

89. Geng X, Lou H, Wang J, Li L, Swanson AL, Sun M, Beers-Stolz D, Watkins S, Perez RG, Drain P. α-Synuclein Binds the KATP Channel at Insulin-Secretory Granules and Inhibits Insulin Secretion. *Am J Physiol Endocrinol Metab* 2011;300(2), DOI: 10.1152/ajpendo.00262.2010.

90. Sharma SK, Chorell E, Steneberg P, Vernersson-Lindahl E, Edlund H, Wittung-Stafshede P. Insulin-Degrading Enzyme Prevents α-Synuclein Fibril Formation in a Nonproteolytical Manner. *Sci Rep* 2015;5, DOI: 10.1038/srep12531.

91. Rodriguez-Araujo G, Nakagami H, Takami Y, Katsuya T, Akasaka H, Saitoh S, Shimamoto K, Morishita R, Rakugi H, Kaneda Y. Low Alpha-Synuclein Levels in the Blood Are Associated with Insulin Resistance. *Sci Rep* 2015;5, DOI: 10.1038/srep12081.

92. Martinez J, Moeller I, Erdjument-Bromage H, Tempst P, Lauring B. Parkinson's Disease-Associated α-Synuclein Is a Calmodulin Substrate. *Journal of Biological Chemistry* 2003;278(19):17379–17387, DOI: 10.1074/jbc.M209020200.

93. Burré J, Sharma M, Tsetsenis T, Buchman V, Etherton MR, Südhof TC. *A-Synuclein Promotes SNARE-Complex Assembly in Vivo and in Vitro*.

94. Burré J, Sharma M, Südhof TC. α-Synuclein Assembles into Higher-Order Multimers upon Membrane Binding to Promote SNARE Complex Formation. *Proc Natl Acad Sci U S A* 2014;111(40):E4274–E4283, DOI: 10.1073/pnas.1416598111.

95. Choi BK, Choi MG, Kim JY, Yang Y, Lai Y, Kweon DH, Lee NK, Shin YK. Large α-Synuclein Oligomers Inhibit Neuronal SNARE-Mediated Vesicle Docking. *Proc Natl Acad Sci U S A* 2013;110(10):4087–4092, DOI: 10.1073/pnas.1218424110.

96. Sang MP, Han YJ, Kim TD, Jeon HP, Yang CH, Kim J. Distinct Roles of the N-Terminal-Binding Domain and the C-Terminal-Solubilizing Domain of α-Synuclein, a Molecular Chaperone. *Journal of Biological Chemistry* 2002;277(32):28512–28520, DOI: 10.1074/jbc.M111971200.

97. Witt SN. Molecular Chaperones, α-Synuclein, and Neurodegeneration. *Molecular neurobiology*, 2013, *47*, 552–560, DOI: 10.1007/s12035-012-8325-2.

98. Chandra S, Gallardo G, Fernández-Chacón R, Schlüter OM, Südhof TC. α-Synuclein Cooperates with CSPα in Preventing Neurodegeneration. *Cell* 2005;123(3):383–396, DOI: 10.1016/j.cell.2005.09.028.

99. Ruipérez V, Darios F, Davletov B. Alpha-Synuclein, Lipids and Parkinson's Disease. *Progress in Lipid Research*, 2010, *49*, 420–428, DOI: 10.1016/j.plipres.2010.05.004.

100. Zhu M, Qin ZJ, Hu D, Munishkina LA, Fink AL. α-Synuclein Can Function as an Antioxidant Preventing Oxidation of Unsaturated Lipid in Vesicles. *Biochemistry* 2006;45(26):8135–8142, DOI: 10.1021/bi052584t.

101. Latchoumycandane C, Anantharam V, Kitazawa M, Yang Y, Kanthasamy A, Kanthasamy AG. Protein Kinase Cδ Is a Key Downstream Mediator of Manganese-Induced Apoptosis in Dopaminergic Neuronal Cells. *Journal of Pharmacology and Experimental Therapeutics* 2005;313(1):46–55, DOI: 10.1124/jpet.104.078469.

102. Hashimoto M, Hsu LJ, Rockenstein E, Takenouchi T, Mallory M, Masliah E. α-Synuclein Protects against Oxidative Stress via Inactivation of the c-Jun N-Terminal Kinase Stress-Signaling Pathway in Neuronal Cells. *Journal of Biological Chemistry* 2002;277(13):11465–11472, DOI: 10.1074/jbc.M111428200.

103. Ostrerova N, Petrucelli L, Farrer M, Mehta N, Choi P, Hardy J, Wolozin B. Synuclein Shares Physical and Functional Homology with 14-3-3 Proteins. *J Neurosci* 1999;19(14):5782-91. doi: 10.1523/JNEUROSCI.19-14-05782.1999.

104. Fu H, Subramanian RR, Masters SC. 4-3-3 PROTEINS: Structure, Function, and Regulation. *Annu Rev Pharmacol Toxicol* 2000;40:617-47. doi: 10.1146/annurev.pharmtox.40.1.617.

105. Chen RHC, Wislet-Gendebien S, Samuel F, Visanji NP, Zhang G, Marsilio D, Langman T, Fraser PE, Tandon A. α-Synuclein Membrane Association Is Regulated by the Rab3a Recycling Machinery and Presynaptic Activity. *Journal of Biological Chemistry* 2013;288(11):7438–7449, DOI: 10.1074/jbc.M112.439497.

106. Peng XM, Tehranian R, Dietrich P, Stefanis L, Perez RG. α-Synuclein Activation of Protein Phosphatase 2A Reduces Tyrosine Hydroxylase Phosphorylation in Dopaminergic Cells. *J Cell Sci* 2005;118(15):3523–3530, DOI: 10.1242/jcs.02481.

107. Yang W, Wang X, Duan C, Lu L, Yang H. Alphα-Synuclein Overexpression Increases Phospho-Protein Phosphatase 2A Levels via Formation of Calmodulin/Src Complex. *Neurochem Int* 2013;63(3):180–194, DOI: 10.1016/j.neuint.2013.06.010.

108. Pranke IM, Morello V, Bigay J, Gibson K, Verbavatz JM, Antonny B, Jackson CL. α-Synuclein and ALPS Motifs Are Membrane Curvature Sensors Whose Contrasting Chemistry Mediates Selective Vesicle Binding. *Journal of Cell Biology* 2011;194(1):89–103, DOI: 10.1083/jcb.201011118.

109. Scott D, Roy S. α-Synuclein Inhibits Intersynaptic Vesicle Mobility and Maintains Recycling-Pool Homeostasis. *Journal of Neuroscience* 2012;32(30):10129–10135, DOI: 10.1523/JNEUROSCI.0535-12.2012.

110. Varkey J, Isas JM, Mizuno N, Jensen MB, Bhatia VK, Jao CC, Petrlova J, Voss JC, Stamou DG, Steven AC, Langen R. Membrane Curvature Induction and Tubulation Are Common Features of Synucleins and Apolipoproteins. *Journal of Biological Chemistry* 2010;285(42):32486–32493, DOI: 10.1074/jbc.M110.139576.

111. Drin G, Antonny B. Amphipathic Helices and Membrane Curvature. *FEBS Letters*, 2010, *584*, 1840–1847, DOI: 10.1016/j.febslet.2009.10.022.

112. Ahn BH, Rhim H, Shi Yeon Kim YMS, Lee MY, Choi JY, Wolozin B, Chang JS, Lee YH, Kwon TK, Chung KC, Yoon SH, Hahn SJ, Kim MS, Jo YH, Mina DS. α-Synuclein Interacts with Phospholipase D Isozymes and Inhibits Pervanadate-Induced Phospholipase d Activation in Human Embryonic Kidney-293 Cells. *Journal of Biological Chemistry* 2002;277(14):12334–12342, DOI: 10.1074/jbc.M110414200.

113. Sode K, Ochiai S, Kobayashi N, Usuzaka E. Effect of Reparation of Repeat Sequences in the Human α-Synuclein on Fibrillation Ability, *Int J Biol Sci.* 2007; 3(1): 1–7 doi: 10.7150/ijbs.3.1

114. Rajagopalan S, Andersen JK. Alpha Synuclein Aggregation: Is It the Toxic Gain of Function Responsible for Neurodegeneration in Parkinson's Disease?, *Mech Ageing Dev* 2001;122(14):1499-510. doi: 10.1016/s0047-6374(01)00283-4.

115. Rodriguez JA, Ivanova MI, Sawaya MR, Cascio D, Reyes FE, Shi D, Sangwan S, Guenther EL, Johnson LM, Zhang M, Jiang L, Arbing MA, Nannenga BL, Hattne J, Whitelegge J, Brewster AS, Messerschmidt M, Boutet S, Sauter NK, Gonen T, Eisenberg DS. Structure of the Toxic Core of α-Synuclein from Invisible Crystals. *Nature* 2015;525(7570):486–490, DOI: 10.1038/nature15368.

116. Ahn M, Kim SB, Kang M, Ryu Y, Doohun Kim T. Chaperone-like Activities of α-Synuclein: α-Synuclein Assists Enzyme Activities of Esterases. *Biochem Biophys Res Commun* 2006;346(4):1142–1149, DOI: 10.1016/j.bbrc.2006.05.213.

117. Hoyer W, Antony T, Cherny D, Heim G, Jovin TM, Subramaniam V. Dependence of α-Synuclein Aggregate Morphology on Solution Conditions. *J Mol Biol* 2002;322(2):383–393, DOI: 10.1016/S0022-2836(02)00775-1.

118. Ly T, Julian RR. Protein-Metal Interactions of Calmodulin and α-Synuclein Monitored by Selective Noncovalent Adduct Protein Probing Mass Spectrometry. *J Am Soc Mass Spectrom* 2008;19(11):1663–1672, DOI: 10.1016/j.jasms.2008.07.006.

119. Esposito A, Dohm CP, Kermer P, Bähr M, Wouters FS. α-Synuclein and Its Disease-Related Mutants Interact Differentially with the Microtubule Protein Tau and Associate with the Actin Cytoskeleton. *Neurobiol Dis* 2007;26(3):521–531, DOI: 10.1016/j.nbd.2007.01.014.

120. Kim TD, Choi E, Rhim H, Paik SR, Yang CH. α-Synuclein Has Structural and Functional Similarities to Small Heat Shock Proteins. *Biochem Biophys Res Commun* 2004;324(4):1352–1359, DOI: 10.1016/j.bbrc.2004.09.208.

121. Lashuel HA, Overk CR, Oueslati A, Masliah E. The Many Faces of α-Synuclein: From Structure and Toxicity to Therapeutic Target. *Nature Reviews Neuroscience*, 2013, *14*, 38–48, DOI: 10.1038/nrn3406.

122. Nuber S, Rajsombath M, Minakaki G, Winkler J, Müller CP, Ericsson M, Caldarone B, Dettmer U, Selkoe DJ. Abrogating Native α-Synuclein Tetramers in Mice Causes a L-DOPA-Responsive Motor Syndrome Closely Resembling Parkinson's Disease. *Neuron* 2018;100(1):75-90.e5, DOI: 10.1016/j.neuron.2018.09.014.

123. Xu L, Pu J. Alpha-Synuclein in Parkinson's Disease: From Pathogenetic Dysfunction to Potential Clinical Application. *Parkinson's Disease*, 2016, *2016*, DOI: 10.1155/2016/1720621.

124. Kalia L V., Lang AE. Parkinson's Disease. *The Lancet*, 2015, *386*, 896–912, DOI: 10.1016/S0140-6736(14)61393-3.

125. Schapira AHV, Chaudhuri KR, Jenner P. Non-Motor Features of Parkinson Disease. *Nature Reviews Neuroscience*, 2017, *18*, 435–450, DOI: 10.1038/nrn.2017.62.

126. Dauer W., Przedborski S., Parkinson's disease: mechanisms and models, *Neuron* 2003;39(6):889-909. doi: 10.1016/s0896-6273(03)00568-3.

127. Goedert M., Alpha Synuclein and Neurodegenerative Diseases. *Nat Rev Neurosci* 2001 ;2:492–501. https://doi.org/10.1038/35081564

128. Deleersnijder A, Gerard M, Debyser Z, Baekelandt V. The Remarkable Conformational Plasticity of Alpha-Synuclein: Blessing or Curse? *Trends in Molecular Medicine*, 2013, *19*, 368–377, DOI: 10.1016/j.molmed.2013.04.002.

129. Mehra S, Sahay S, Maji SK. α-Synuclein Misfolding and Aggregation: Implications in Parkinson's Disease Pathogenesis. *Biochimica et Biophysica Acta - Proteins and Proteomics*, 2019, *1867*, 890–908, DOI: 10.1016/j.bbapap.2019.03.001.

130. Melki R. Role of Different Alpha-Synuclein Strains in Synucleinopathies, Similarities with Other Neurodegenerative Diseases. *Journal of Parkinson's Disease*, 2015, *5*, 217–227, DOI: 10.3233/JPD-150543.

131. Peelaerts W, Bousset L, Van Der Perren A, Moskalyuk A, Pulizzi R, Giugliano M, Van Den Haute C, Melki R, Baekelandt V. α-Synuclein Strains Cause Distinct Synucleinopathies after Local and Systemic Administration. *Nature* 2015;522(7556):340–344, DOI: 10.1038/nature14547.

132. Candelise N, Schmitz M, Llorens F, Villar-Piqué A, Cramm M, Thom T, da Silva Correia SM, da Cunha JEG, Möbius W, Outeiro TF, Álvarez VG, Banchelli M, D'Andrea C, de Angelis M, Zafar S, Rabano A, Matteini P, Zerr I. Seeding Variability of Different Alpha Synuclein Strains in Synucleinopathies. *Ann Neurol* 2019;85(5):691–703, DOI: 10.1002/ana.25446.

133. Cook C, Stetler C, Petrucelli L. Disruption of Protein Quality Control in Parkinson's Disease. *Cold Spring Harb Perspect Med* 2012;2(5), DOI: 10.1101/cshperspect.a009423.

134. Alter SP, Lenzi GM, Bernstein AI, Miller GW. Vesicular Integrity in Parkinson's Disease. *Curr Neurol Neurosci Rep* 2013;13(7), DOI: 10.1007/s11910-013-0362-3.

135. Chen R, Gnegy F. Imaging photogenerated charge carriers on surfaces and interfaces of photocatalysts with surface photovoltage microscopy. *Chem. Soc. Rev*. 2018;47: 8238-8262 https://doi.org/10.1039/C8CS00320C

136. Butler B, Sambo D, Khoshbouei H. Alpha-Synuclein Modulates Dopamine Neurotransmission. *Journal of Chemical Neuroanatomy*, 2017, *83–84*, 41–49, DOI: 10.1016/j.jchemneu.2016.06.001.

137. Bendor JT, Logan TP, Edwards RH. The Function of α-Synuclein. *Neuron*, 2013, *79*, 1044–1066, DOI: 10.1016/j.neuron.2013.09.004.

138. Snead D, Eliezer D. Alpha-Synuclein Function and Dysfunction on Cellular Membranes. *Exp Neurobiol* 2014;23(4):292–313, DOI: 10.5607/en.2014.23.4.292.

139. Fusco G, Sanz-Hernandez M, De Simone A. Order and Disorder in the Physiological Membrane Binding of α-Synuclein. *Current Opinion in Structural Biology*, 2018, *48*, 49–57, DOI: 10.1016/j.sbi.2017.09.004.

140. Vargas KJ, Schrod N, Davis T, Fernandez-Busnadiego R, Taguchi Y V., Laugks U, Lucic V, Chandra SS. Synucleins Have Multiple Effects on Presynaptic Architecture. *Cell Rep* 2017;18(1):161–173, DOI: 10.1016/j.celrep.2016.12.023.

141. Eguchi K, Taoufiq Z, Thorn-Seshold O, Trauner D, Hasegawa M, Takahashi T. Wild-Type Monomeric α-Synuclein Can Impair Vesicle Endocytosis and Synaptic Fidelity via Tubulin Polymerization at the Calyx of Held. *Journal of Neuroscience* 2017;37(25):6043–6052, DOI: 10.1523/JNEUROSCI.0179-17.2017.

142. Polymeropoulos MH, Lavedan C, Leroy E, Ide SE, Dehejia A, Dutra A, Pike B, Root H, Rubenstein J, Boyer R, Stenroos ES, Chandrasekharappa S, Athanassiadou A, Papapetropoulos T, Johnson WG, Lazzarini AM, Duvoisin RC, Di Iorio G, Golbe LI, Nussbaum RL. Mutation in the α-Synuclein Gene Identified in Families with Parkinson's Disease. *Science (1979)* 1997;276(5321):2045–2047, DOI: 10.1126/science.276.5321.2045.

143. Kruger R., Kuhn W., Muller T., Woitalla D., Gaeber M., Kosel S., Przuntek H., Epplen J. T., Schols L., Riess O, Ala30Pro mutation in the gene encoding α-synuclein in Parkinson's disease, *Nature Genetics* 1998;18:106-108

144. Zarranz JJ, Alegre J, Gómez-Esteban JC, Lezcano E, Ros R, Ampuero I, Vidal L, Hoenicka J, Rodriguez O, Atarés B, Llorens V, Gomez Tortosa E, Del Ser T, Muñoz DG, De Yebenes JG. *The New Mutation, E46K, of-Synuclein Causes Parkinson and Lewy Body Dementia*, Vol. 55. 2004.

145. Conway K.A., Harper J.D., Lansbury P.T., *Nat Med.* 1998 Nov;4(11):1318-20. doi: 10.1038/3311.

146. Narhi L, Wood SJ, Steavenson S, Jiang Y, Wu GM, Anafi D, Kaufman SA, Martin F, Sitney K, Denis P, Louis J-C, Wypych J, Biere AL, Citron M. Both Familial Parkinson's Disease Mutations Accelerate-Synuclein Aggregation. *J Biol Chem* 1999;274(14):9843-6. doi: 10.1074/jbc.274.14.9843.

147. Serpell LC, Berriman J, Jakes R, Goedert M, Crowther RA., Fiber Diffraction of Synthetic-Synuclein Filaments Shows Amyloid-like Cross-Conformation. *Proc Natl Acad Sci U S A* 2000;97(9):4897-902. doi: 10.1073/pnas.97.9.4897.

148. Bussell R, Eliezer D. Residual Structure and Dynamics in Parkinson's Disease-Associated Mutants of α-Synuclein. *Journal of Biological Chemistry* 2001;276(49):45996–46003, DOI: 10.1074/jbc.M106777200.

149. Heise H, Hoyer W, Becker S, Andronesi OC, Riedel D, Baldus M. Molecular-Level Secondary Structure, Polymorphism, and Dynamics of Full-Length-Synuclein Fibrils Studied by Solid-State NMR, *Proc Natl Acad Sci U S A* 2005;102(44):15871-6. doi: 10.1073/pnas.0506109102.

150. Mclean PJ, Kawamata H, Ribich S, Hyman BT., Membrane Association and Protein Conformation Of-Synuclein in Intact Neurons. *J Biol Chem* 2000;275(12):8812-6. doi: 10.1074/jbc.275.12.8812.

151. Fredenburg RA, Rospigliosi C, Meray RK, Kessler JC, Lashuel HA, Eliezer D, Lansbury PT. The Impact of the E46K Mutation on the Properties of α-Synuclein in Its Monomelic and Oligomeric States. *Biochemistry* 2007;46(24):7107–7118, DOI: 10.1021/bi7000246.

152. Rospigliosi CC, McClendon S, Schmid AW, Ramlall TF, Barré P, Lashuel HA, Eliezer D. E46K Parkinson's-Linked Mutation Enhances C-Terminal-to-N-Terminal Contacts in α-Synuclein. *J Mol Biol* 2009;388(5):1022–1032, DOI: 10.1016/j.jmb.2009.03.065.

153. Vilar M, Chou H-T, Lü Hrs † T, Maji SK, Riek-Loher D, Verel R, Manning G, Stahlberg H, Riek R. The Fold Of-Synuclein Fibrils. *Proc Natl Acad Sci U S A* 2008;105(25):8637-42. doi: 10.1073/pnas.0712179105

154. Kumar S, Sarkar A, Sundar D. Controlling Aggregation Propensity in A53T Mutant of Alpha-Synuclein Causing Parkinson's Disease. *Biochem Biophys Res Commun* 2009;387(2):305–309, DOI: 10.1016/j.bbrc.2009.07.008.

155. Balesh D, Ramjan Z, Floriano WB. Unfolded Annealing Molecular Dynamics Conformers for Wild-Type and Disease-Associated Variants of Alpha-Synuclein Show No Propensity for Beta-Sheetformation. *Journal of Biophysical Chemistry* 2011;02(02):124–134, DOI: 10.4236/jbpc.2011.22015.

156. Coskuner O, Wise-Scira O. Structures and Free Energy Landscapes of the A53T Mutant-Type α-Synuclein Protein and Impact of A53T Mutation on the Structures of the Wild-Type α-Synuclein Protein with Dynamics. *ACS Chem Neurosci* 2013;4(7):1101–1113, DOI: 10.1021/cn400041j.

157. Wise-Scira O, Aloglu AK, Dunn A, Sakallioglu IT, Coskuner O. Structures and Free Energy Landscapes of the Wild-Type and A30P Mutant-Type α-Synuclein Proteins with Dynamics. *ACS Chem Neurosci* 2013;4(3):486–497, DOI: 10.1021/cn300198q.

158. Appel-Cresswell S, Vilarino-Guell C, Encarnacion M, Sherman H, Yu I, Shah B, Weir D, Thompson C, Szu-Tu C, Trinh J, Aasly JO, Rajput A, Rajput AH, Jon Stoessl A, Farrer MJ. Alpha-Synuclein p.H50Q, a Novel Pathogenic Mutation for Parkinson's Disease. *Movement Disorders* 2013;28(6):811–813, DOI: 10.1002/mds.25421.

159. Kiely AP, Asi YT, Kara E, Limousin P, Ling H, Lewis P, Proukakis C, Quinn N, Lees AJ, Hardy J, Revesz T, Houlden H, Holton JL. A-Synucleinopathy Associated with G51D SNCA Mutation: A Link between Parkinson's Disease and Multiple System Atrophy? *Acta Neuropathol* 2013;125(5):753–769, DOI: 10.1007/s00401-013-1096-7.

160. Chi YC, Armstrong GS, Jones DNM, Eisenmesser EZ, Liu CW. Residue Histidine 50 Plays a Key Role in Protecting α-Synuclein from Aggregation at Physiological PH. *Journal of Biological Chemistry* 2014;289(22):15474–15481, DOI: 10.1074/jbc.M113.544049.

161. Ghosh D, Mondal M, Mohite GM, Singh PK, Ranjan P, Anoop A, Ghosh S, Jha NN, Kumar A, Maji SK. The Parkinson's Disease-Associated H50Q Mutation Accelerates α-Synuclein Aggregation in Vitro. *Biochemistry* 2013;52(40):6925–6927, DOI: 10.1021/bi400999d.

162. Khalaf O, Fauvet B, Oueslati A, Dikiy I, Mahul-Mellier AL, Ruggeri FS, Mbefo MK, Vercruysse F, Dietler G, Lee SJ, Eliezer D, Lashuel HA. The H50Q Mutation Enhances Aα-Synuclein Aggregation, Secretion, and Toxicity. *Journal of Biological Chemistry* 2014;289(32):21856–21876, DOI: 10.1074/jbc.M114.553297.

163. Ghosh D, Mondal M, Mohite GM, Singh PK, Ranjan P, Anoop A, Ghosh S, Jha NN, Kumar A, Maji SK. The Parkinson's Disease-Associated H50Q Mutation Accelerates α-

Synuclein Aggregation in Vitro. *Biochemistry* 2013;52(40):6925–6927, DOI: 10.1021/bi400999d.

164. Lesage S, Anheim M, Letournel F, Bousset L, Honoré A, Rozas N, Pieri L, Madiona K, Dürr A, Melki R, Verny C, Brice A. G51D α-Synuclein Mutation Causes a Novel Parkinsonian-Pyramidal Syndrome. *Ann Neurol* 2013;73(4):459–471, DOI: 10.1002/ana.23894.

165. Fares MB, Ait-Bouziad N, Dikiy I, Mbefo MK, Jovičić A, Kiely A, Holton JL, Lee SJ, Gitler AD, Eliezer D, Lashuel HA. The Novel Parkinson's Disease Linked Mutation G51D Attenuates in Vitro Aggregation and Membrane Binding of α-Synuclein, and Enhances Its Secretion and Nuclear Localization in Cells. *Hum Mol Genet* 2014;23(17):4491–4509, DOI: 10.1093/hmg/ddu165.

166. Pasanen P, Myllykangas L, Siitonen M, Raunio A, Kaakkola S, Lyytinen J, Tienari PJ, Pöyhönen M, Paetau A. A Novel α-Synuclein Mutation A53E Associated with Atypical Multiple System Atrophy and Parkinson's Disease-Type Pathology. *Neurobiol Aging* 2014;35(9):2180.e1-2180.e5, DOI: 10.1016/j.neurobiolaging.2014.03.024.

167. Calogero AM, Mazzetti S, Pezzoli G, Cappelletti G. Neuronal Microtubules and Proteins Linked to Parkinson's Disease: A Relevant Interaction? *Biological Chemistry*, 2019, *400*, 1099–1112, DOI: 10.1515/hsz-2019-0142.

168. Waites C, Qu X, Bartolini F. The Synaptic Life of Microtubules. *Current Opinion in Neurobiology*, 2021, *69*, 113–123, DOI: 10.1016/j.conb.2021.03.004.

169. Janke C, Magiera MM. The Tubulin Code and Its Role in Controlling Microtubule Properties and Functions. *Nature Reviews Molecular Cell Biology*, 2020, *21*, 307–326, DOI: 10.1038/s41580-020-0214-3.

170. Alim MA, Hossain MS, Arima K, Takeda K, Izumiyama Y, Nakamura M, Kaji H, Shinoda T, Hisanaga S, Uéda K. Tubulin Seeds α-Synuclein Fibril Formation. *Journal of Biological Chemistry* 2002;277(3):2112–2117, DOI: 10.1074/jbc.M102981200.

171. Zhou RM, Huang YX, Li XL, Chen C, Shi Q, Wang GR, Tian C, Wang ZY, Jing YY, Gao C, Dong XP. Molecular Interaction of α-Synuclein with Tubulin Influences on the Polymerization of Microtubule in Vitro and Structure of Microtubule in Cells. *Mol Biol Rep* 2010;37(7):3183–3192, DOI: 10.1007/s11033-009-9899-2.

172. Alim MA, Ma Q-L, Takeda K, Aizawa T, Matsubara M, Nakamura M, Asada A, Saito T, Kaji H, Yoshii M, Hisanaga S, Uéda K. *Demonstration of a Role for α-Synuclein as a Functional Microtubule-Associated Protein*, Vol. 6. IOS Press, 2004.

173. Lin X, Parisiadou L, Gu XL, Wang L, Shim H, Sun L, Xie C, Long CX, Yang WJ, Ding J, Chen ZZ, Gallant PE, Tao-Cheng JH, Rudow G, Troncoso JC, Liu Z, Li Z, Cai H. Leucine-Rich Repeat Kinase 2 Regulates the Progression of Neuropathology Induced by Parkinson's-

Disease-Related Mutant α-Synuclein. *Neuron* 2009;64(6):807–827, DOI: 10.1016/j.neuron.2009.11.006.

174. Lee HJ, Khoshaghideh F, Lee S, Lee SJ. Impairment of Microtubule-Dependent Trafficking by Overexpression of α-Synuclein. *European Journal of Neuroscience* 2006;24(11):3153–3162, DOI: 10.1111/j.1460-9568.2006.05210.x.

175. Zhou Y, Gu G, Goodlett DR, Zhang T, Pan C, Montine TJ, Montine KS, Aebersold RH, Zhang J. Analysis of α-Synuclein-Associated Proteins by Quantitative Proteomics. *Journal of Biological Chemistry* 2004;279(37):39155–39164, DOI: 10.1074/jbc.M405456200.

176. Amadeo A, Pizzi S, Comincini A, Modena D, Calogero AM, Madaschi L, Faustini G, Rolando C, Bellucci A, Pezzoli G, Mazzetti S, Cappelletti G. The Association between α-Synuclein and α-Tubulin in Brain Synapses. *Int J Mol Sci* 2021;22(17), DOI: 10.3390/ijms22179153.

177. Toba S, Jin M, Yamada M, Kumamoto K, Matsumoto S, Yasunaga T, Fukunaga Y, Miyazawa A, Fujita S, Itoh K, Fushiki S, Kojima H, Wanibuchi H, Arai Y, Nagai T, Hirotsune S. Alpha-Synuclein Facilitates to Form Short Unconventional Microtubules That Have a Unique Function in the Axonal Transport. *Sci Rep* 2017;7(1), DOI: 10.1038/s41598-017-15575-3.

178. Suzuki Y, Jin C, Iwase T, Yazawa I. β-III Tubulin Fragments Inhibit α-Synuclein Accumulation in Models of Multiple System Atrophy. *Journal of Biological Chemistry* 2014;289(35):24374–24382, DOI: 10.1074/jbc.M114.557215.

179. Bernadó P, Bertoncini CW, Griesinger C, Zweckstetter M, Blackledge M. Defining Long-Range Order and Local Disorder in Native α-Synuclein Using Residual Dipolar Couplings. *J Am Chem Soc* 2005;127(51):17968–17969, DOI: 10.1021/ja055538p.

180. Dedmon MM, Lindorff-Larsen K, Christodoulou J, Vendruscolo M, Dobson CM. Mapping Long-Range Interactions in α-Synuclein Using Spin-Label NMR and Ensemble Molecular Dynamics Simulations. *J Am Chem Soc* 2005;127(2):476–477, DOI: 10.1021/ja044834j.

181. Lehotzky A, Tirián L, Tökési N, Lénárt P, Szabó B, Kovács J, Ovádi J. Dynamic Targeting of Microtubules by TPPP/P25 Affects Cell Survival. *J Cell Sci* 2004;117(25):6249–6259, DOI: 10.1242/jcs.01550.

182. Oláh J, Lehotzky A, Szunyogh S, Szénási T, Orosz F, Ovádi J. Microtubule-Associated Proteins with Regulatory Functions by Day and Pathological Potency at Night. *Cells*, 2020, *9*, DOI: 10.3390/cells9020357.

183. Cartelli D, Cappelletti G. Microtubule Destabilization Paves the Way to Parkinson's Disease. *Molecular Neurobiology*, 2017, *54*, 6762–6774, DOI: 10.1007/s12035-016-0188-5.

184. Steinmetz MO. Structure and Thermodynamics of the Tubulin-Stathmin Interaction. *Journal of Structural Biology*, 2007, *158*, 137–147, DOI: 10.1016/j.jsb.2006.07.018.

185. Uversky VN. Neuropathology, Biochemistry, and Biophysics of α-Synuclein Aggregation. *Journal of Neurochemistry*, 2007, *103*, 17–37, DOI: 10.1111/j.1471-4159.2007.04764.x.

186. Kara E, Lewis PA, Ling H, Proukakis C, Houlden H, Hardy J. α-Synuclein Mutations Cluster around a Putative Protein Loop., *Neurosci Lett* 2013;546: 67–70, DOI: 10.2210/pdb1xq8/pdb.

187. Honnappa S, Cutting B, Jahnke W, Seelig J, Steinmetz MO. Thermodynamics of the Op18/Stathmin-Tubulin Interaction. *Journal of Biological Chemistry* 2003;278(40):38926–38934, DOI: 10.1074/jbc.M305546200.

188. Cartelli D, Aliverti A, Barbiroli A, Santambrogio C, Ragg EM, Casagrande FVM, Cantele F, Beltramone S, Marangon J, De Gregorio C, Pandini V, Emanuele M, Chieregatti E, Pieraccini S, Holmqvist S, Bubacco L, Roybon L, Pezzoli G, Grandori R, Arnal I, Cappelletti G. α-Synuclein Is a Novel Microtubule Dynamase. *Sci Rep* 2016;6, DOI: 10.1038/srep33289.

189. Mitchell AR. R. Bruce Merrifield and Solid-Phase Peptide Synthesis: A Historical Assessment*, Biopolymers* 2008;90(3):175-84. doi: 10.1002/bip.20925.

190. Kimmerlin T, Seebach D. "100 Years of Peptide Synthesis": Ligation Methods for Peptide and Protein Synthesis with Applications to β-Peptide Assemblies. *Journal of Peptide Research* 2005;65(2):229–260, DOI: 10.1111/j.1399-3011.2005.00214.x.

191. Merrifield R.B., Synthesis of a Tetrapeptide., *J. Am. Chem. Soc*. 1963 ;85, 14, 2149–2154

192. Pedersen SL, Tofteng AP, Malik L, Jensen KJ. Microwave Heating in Solid-Phase Peptide Synthesis. *Chem Soc Rev* 2012;41(5):1826–1844, DOI: 10.1039/c1cs15214a.

193. Motoyama J., Takabatake T., Takeshima K., Hui C.C., Ala30Pro mutation in the gene encoding a-synuclein in Parkinson's disease, *Nature Genetics* 1998;18: 106-108

194. Friligou I, Papadimitriou E, Gatos D, Matsoukas J, Tselios T. Microwave-Assisted Solid-Phase Peptide Synthesis of the 60-110 Domain of Human Pleiotrophin on 2-Chlorotrityl Resin. *Amino Acids* 2011;40(5):1431–1440, DOI: 10.1007/s00726-010-0753-6.

195. Greenfield NJ. Using Circular Dichroism Spectra to Estimate Protein Secondary Structure. *Nat Protoc* 2007;1(6):2876–2890, DOI: 10.1038/nprot.2006.202.

196. Sreerama N, Woody RW. Estimation of Protein Secondary Structure from Circular Dichroism Spectra: Comparison of CONTIN, SELCON, and CDSSTR Methods with an Expanded Reference Set. *Anal Biochem* 2000;287(2):252–260, DOI: 10.1006/abio.2000.4880.

197. Ji Y, Yang X, Ji Z, Zhu L, Ma N, Chen D, Jia X, Tang J, Cao Y. DFT-Calculated IR Spectrum Amide I, II, and III Band Contributions of N-Methylacetamide Fine Components. *ACS Omega* 2020;5(15):8572–8578, DOI: 10.1021/acsomega.9b04421.

198. Vigano C, Manciu L, Buyse F, Goormaghtigh E, Ruysschaert JM. Attenuated Total Reflection IR Spectroscopy as a Tool to Investigate the Structure, Orientation and Tertiary Structure Changes in Peptides and Membrane Proteins. *Biopolymers - Peptide Science Section*, 2000, *55*, 373–380, DOI: 10.1002/1097-0282(2000)55:5<373::AID-BIP1011>3.0.CO;2-U.

199. Wienken CJ, Baaske P, Rothbauer U, Braun D, Duhr S. Protein-Binding Assays in Biological Liquids Using Microscale Thermophoresis. *Nat Commun* 2010;1(7), DOI: 10.1038/ncomms1093.

200. Seidel SAI, Dijkman PM, Lea WA, van den Bogaart G, Jerabek-Willemsen M, Lazic A, Joseph JS, Srinivasan P, Baaske P, Simeonov A, Katritch I, Melo FA, Ladbury JE, Schreiber G, Watts A, Braun D, Duhr S. Microscale Thermophoresis Quantifies Biomolecular Interactions under Previously Challenging Conditions. *Methods*, 2013, *59*, 301–315, DOI: 10.1016/j.ymeth.2012.12.005.

201. Ludwig C. *Ludwig. Diffusion Zwischen Ungleich Erwärmten Orten Etc. S39 Diffusion Zwischen Ungleich Erwärmten Orten Gleich Zusammengesetzter Lösungen*.

202. Tso SC, Chen Q, Vishnivetskiy SA, Gurevich V V., Iverson TM, Brautigam CA. Using Two-Site Binding Models to Analyze Microscale Thermophoresis Data. *Anal Biochem* 2018;540–541:64–75, DOI: 10.1016/j.ab.2017.10.013.

203. López-Méndez B, Uebel S, Lundgren LP, Sedivy A. Microscale Thermophoresis and Additional Effects Measured in NanoTemper Monolith Instruments. *European Biophysics Journal* 2021;50(3–4):653–660, DOI: 10.1007/s00249-021-01529-1.

204. Nowak PM, Woźniakiewicz M. The Acid-Base/Deprotonation Equilibrium Can Be Studied with a MicroScale Thermophoresis (MST). *Molecules* 2022;27(3), DOI: 10.3390/molecules27030685.

205. Voter WA, Erickson HP. The Kinetics of Microtubule Assembly. Evidence for a Two-Stage Nucleation Mechanism. *Journal of Biological Chemistry* 1984;259(16):10430–10438, DOI: 10.1016/s0021-9258(18)90982-8.

206. Mirigian M, Mukherjee K, Bane SL, Sackett DL. Measurement of In Vitro Microtubule Polymerization by Turbidity and Fluorescence. In *Methods in Cell Biology*, Vol. 115. Academic Press Inc., 2013; 215–229, DOI: 10.1016/B978-0-12-407757-7.00014-1.

207. Roostalu J, Surrey T. Microtubule Nucleation: Beyond the Template. *Nature Reviews Molecular Cell Biology*, 2017, *18*, 702–710, DOI: 10.1038/nrm.2017.75.

208. Bonfils C, Bec N, Lacroix B, Harricane MC, Larroque C. Kinetic Analysis of Tubulin Assembly in the Presence of the Microtubule-Associated Protein TOGp. *Journal of Biological Chemistry* 2007;282(8):5570–5581, DOI: 10.1074/jbc.M605641200.

209. Chrambach T, Naughton A, Kamen MA;, Bartsch MD, Horio RG, De Klerk T, Kamen H, Dus MD, Flatmark KM, King H, Klingenberg TE, Ed M, New York NY, Keller RM, Pettigrew GW, Wuthrich K, Laemmli UK, Lemberg R, Barrett J, Cytochromes L, Mcdonald CC, Phillips WD, Legall J, Margoliash E, Schejter A, Nagel GW, Schachman HK, Redfield AG, Gupta RK; FR, Freer ST, Xuong NH, Alden RA, Kraut J, Sano S, Nanzyo N, Rimington C, Smith WR, Sybesma C, Kitchfield WJ, Dus K, Sutherland JC, Vickery LE, Klein MP, Weisen-Berg RC, Timasheff SN. *In Vitro Reconstitution of Calf Brain Microtubules: Effects of Solution Variables? The Effects of Solution Variables on the in Vitro Reconstitution of Calf Brain Tubulin, Purified by the Method Of*, Vol. 9. Academic Press.

210. Phelan JC, Skelton NJ, Braisted AC, Mcdowell RS. *A General Method for Constraining Short Peptides to an R-Helical Conformation*. 1997.

211. Tonali N, Correia I, Lesma J, Bernadat G, Ongeri S, Lequin O. Introducing Sequential Aza-Amino Acids Units Induces Repeated β-Turns and Helical Conformations in Peptides. *Org Biomol Chem* 2020;18(18):3452–3458, DOI: 10.1039/c9ob02654a.

212. Kaur P, Khera A, Alajangi HK, Sharma A, Jaiswal PK, Singh G, Barnwal RP. Role of Tau in Various Tauopathies, Treatment Approaches, and Emerging Role of Nanotechnology in Neurodegenerative Disorders. *Molecular Neurobiology*, 2023, *60*, 1690–1720, DOI: 10.1007/s12035-022-03164-z.

213. Duan AR, Jonasson EM, Alberico EO, Li C, Scripture JP, Miller RA, Alber MS, Goodson H V. Interactions between Tau and Different Conformations of Tubulin: Implications for Tau Function and Mechanism. *J Mol Biol* 2017;429(9):1424–1438, DOI: 10.1016/j.jmb.2017.03.018.

214. Butner KA, Kirschner MW. Tau Protein Binds to Microtubules through A Flexible Array of Distributed Weak Sites. *J Cell Biol* 1991, 115 (3): 717–730 https://doi.org/10.1083/jcb.115.3.717

215. Goode BL, Feinstein SC. Identification of a Novel Microtubule Binding and Assembly Domain in the Developmentally Regulated Inter-Repeat Region of Tau. *J Cell Biol* 1994, 124 (5): 769–782. https://doi.org/10.1083/jcb.124.5.769

216. Gustke N, Trinczek B, Biernat J, Mandelkow E-M, Mandelkow' E. Domains of T Protein and Interactions with Microtubules. *Biochemistry* 1994,16;33(32):9511-22. doi: 10.1021/bi00198a017.

217. Al-Bassam J, Ozer RS, Safer D, Halpain S, Milligan RA. MAP2 and Tau Bind Longitudinally along the Outer Ridges of Microtubule Protofilaments. *Journal of Cell Biology* 2002;157(7):1187–1196, DOI: 10.1083/jcb.200201048.

218. Santarella RA, Skiniotis G, Goldie KN, Tittmann P, Gross H, Mandelkow EM, Mandelkow E, Hoenger A. Surface-Decoration of Microtubules by Human Tau. *J Mol Biol* 2004;339(3):539–553, DOI: 10.1016/j.jmb.2004.04.008.

219. Kar S., Fan J., Smith J.M., Goedert M., Amos L.A., Repeat motifs of tau bind to the insides of microtubules in the absence of taxol. *The Embo Journal* 2003;(22):70-77, DOI: 10.1093/emboj/cdg001

220. Gigant B, Landrieu I, Fauquant C, Barbier P, Huvent I, Wieruszeski JM, Knossow M, Lippens G. Mechanism of Tau-Promoted Microtubule Assembly as Probed by NMR Spectroscopy. *J Am Chem Soc* 2014;136(36):12615–12623, DOI: 10.1021/ja504864m.

221. Kellogg EH, Hejab NMA, Poepsel S, Downing KH, DiMaio F, Nogales E. Near-Atomic Model of Microtubule-Tau Interactions. *Science (1979)* 2018;360(6394):1242–1246, DOI: 10.1126/science.aat1780.

222. Inaba H, Yamamoto T, Kabir AMR, Kakugo A, Sada K, Matsuura K. Molecular Encapsulation Inside Microtubules Based on Tau-Derived Peptides. *Chemistry - A European Journal* 2018;24(56):14958–14967, DOI: 10.1002/chem.201802617.

13. Supplementary data

13.1. Supplementary data: RP-HPLC chromatograms and MS-ESI analyses

- **WT1**

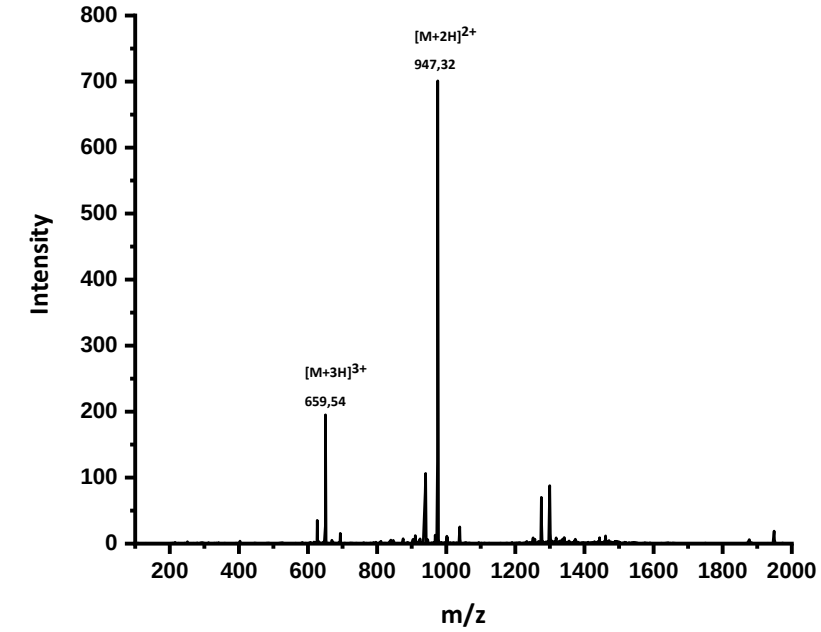

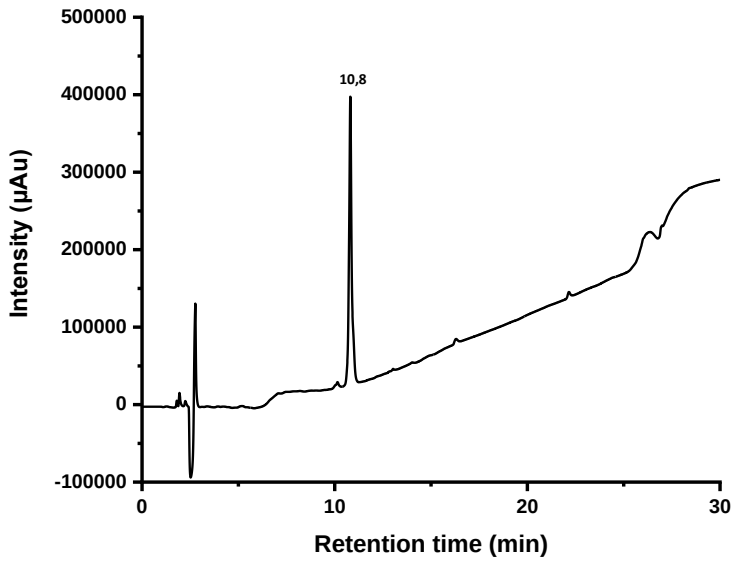

Figure 31. UV chromatogram and ESI-MS spectrum of WT1. Gradient: 15-60% of B in A in 20 min. 0.8 mL/min. A: 0.1% TFA in 100% H2O: B: 0.1% TFA in CH_3CN. The peaks signed correspond to: $[M+2H]^{2+}$ (947.32 m/z) and $[M+3H]^{3+}$ (659.54 m/z).

- **A30P**

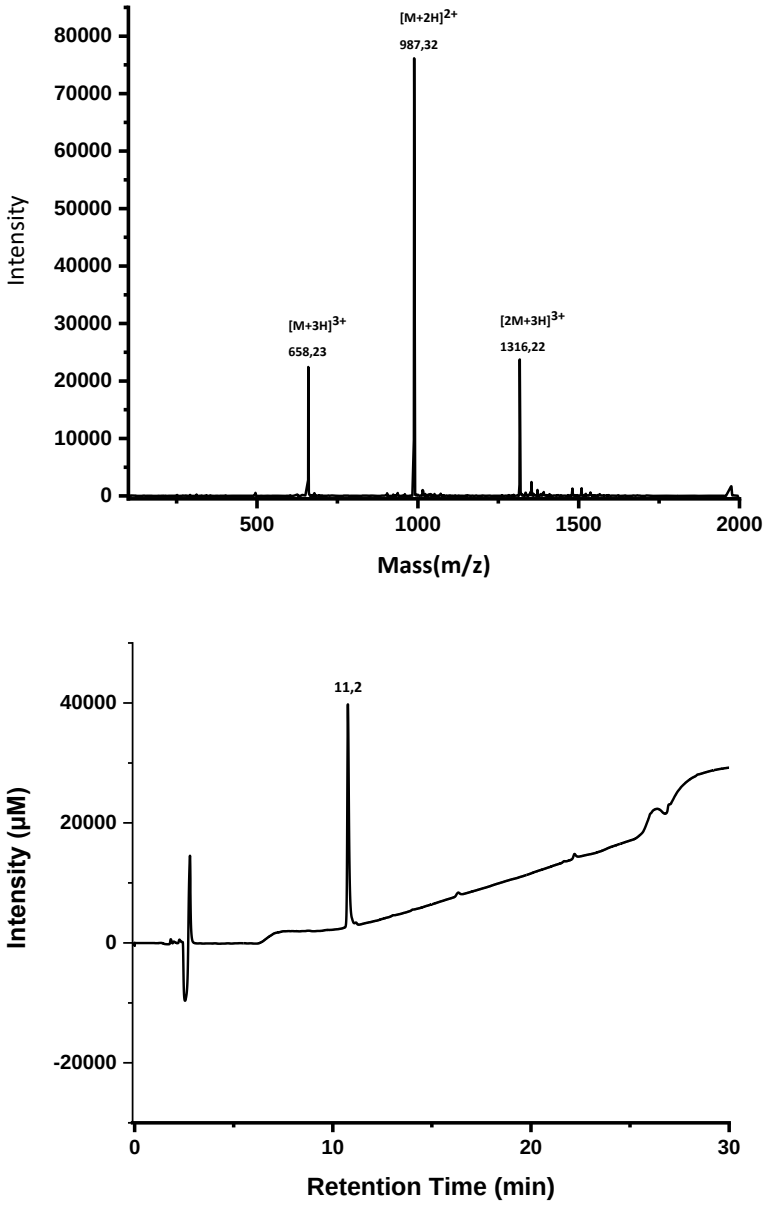

Figure 32. UV chromatogram and ESI-MS spectrum of A30P. Gradient: 15-60% of B in A in 20 min. 0.8 mL/min. A: 0.1% TFA in 100% H2O: B: 0.1% TFA in CH_3CN. The peaks signed correspond to: $[M+2H]^{2+}$ (987.32 m/z), $[M+3H]^{3+}$ (658.23 m/z) and $[2M+3H]^{3+}$ (1312.22 m/z)

- **WT2**

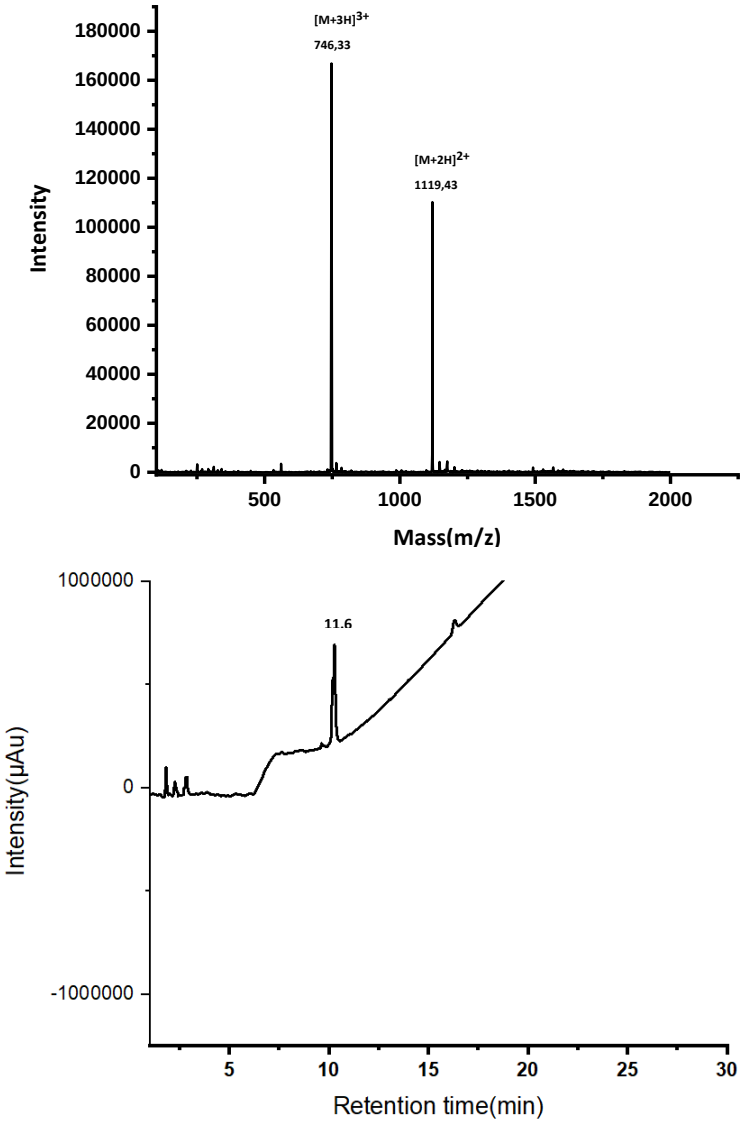

Figure 33. chromatogram and ESI-MS spectrum of WT2. Gradient: 15-60% of B in A in 20 min. 0.8 mL/min. A: 0.1% TFA in 100% H2O: B: 0.1% TFA in CH_3CN. The peaks signed correspond to: $[M+2H]^{2+}$ (1119,43 m/z) and $[M+3H]^{3+}$ (747.33 m/z)

- **WT2_scr**

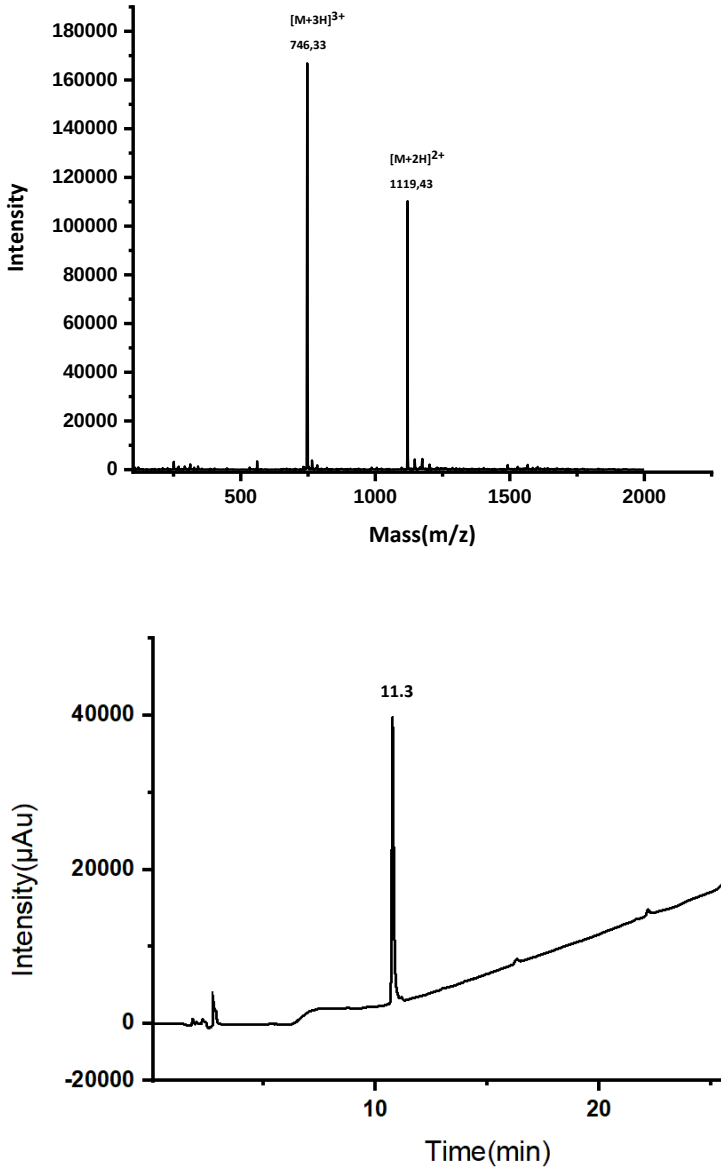

Figure 34. UV chromatogram and ESI-MS spectrum of WT2_scr. Gradient: 15-60% of B in A in 20 min. 0.8 mL/min. A: 0.1% TFA in 100% H2O: B: 0.1% TFA in CH_3CN. The peaks signed correspond to: $[M+2H]^{2+}$ (1119,43 m/z) and $[M+3H]^{3+}$ (747.33 m/z)

- **A53T**

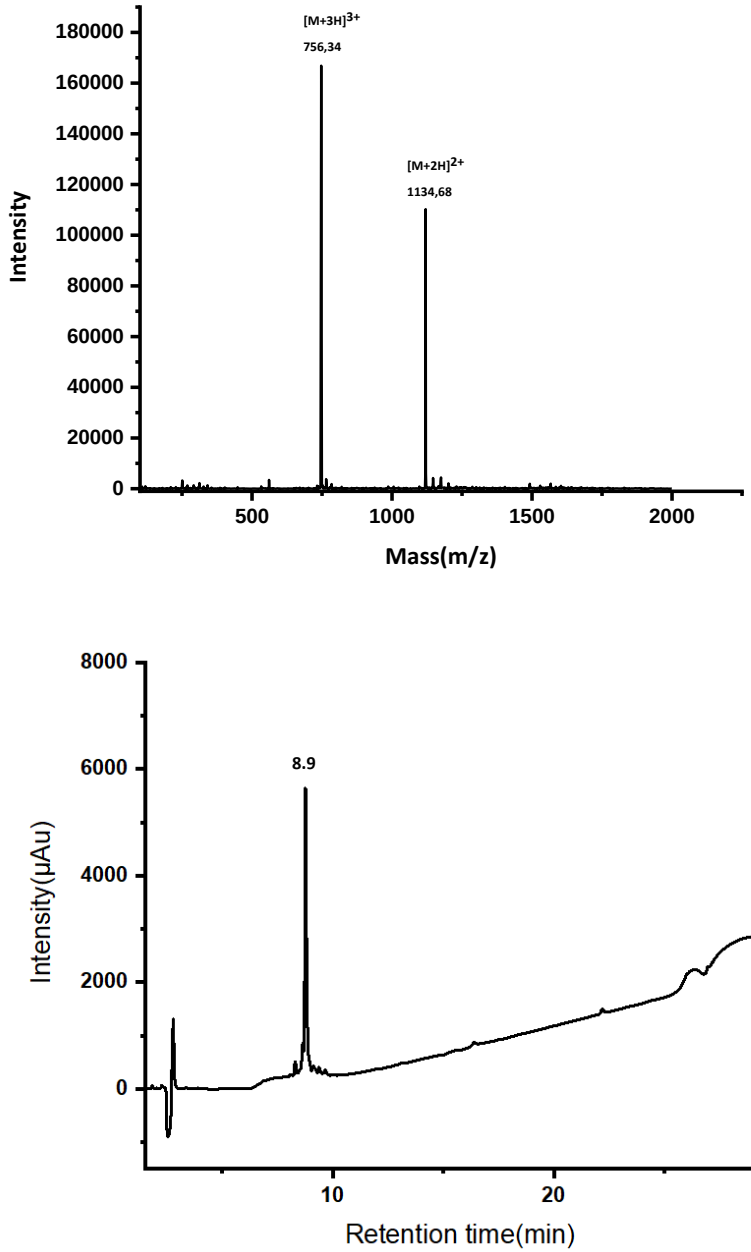

Figure 35. UV chromatogram and ESI-MS spectrum of A53T. Gradient: 05-60% of B in A in 20 min. 0.8 mL/min. A: 0.1% TFA in 100% H2O: B: 0.1% TFA in CH_3CN. The peaks signed correspond to: $[M+2H]^{2+}$ (1134,68 m/z) and $[M+3H]^{3+}$ (756.34 m/z)

- **A53T_scr**

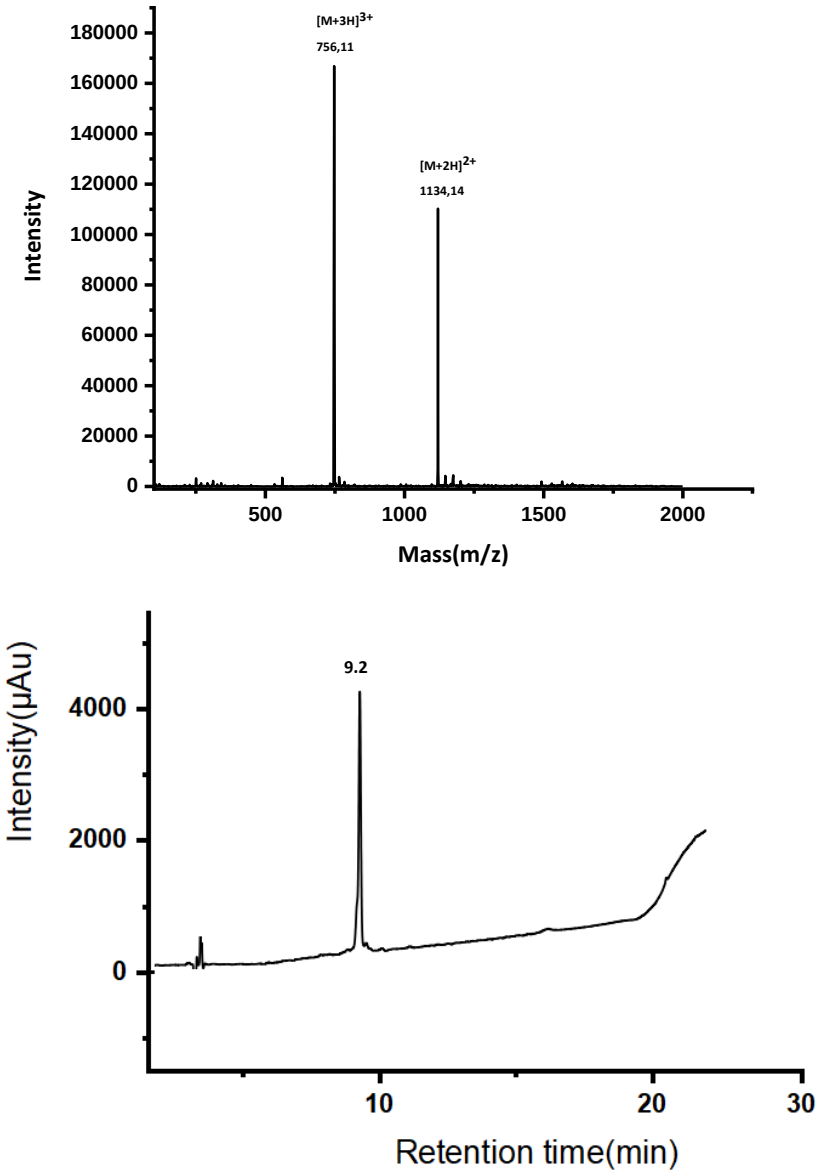

Figure 36. UV chromatogram and ESI-MS spectrum of A53T_scr. Gradient: 15-60% of B in A in 20 min. 0.8 mL/min. A: 0.1% TFA in 100% H2O: B: 0.1% TFA in CH_3CN. The peaks signed correspond to: $[M+2H]^{2+}$ (1134,14 m/z) and $[M+3H]^{3+}$ (756.11 m/z)

- **G51D**

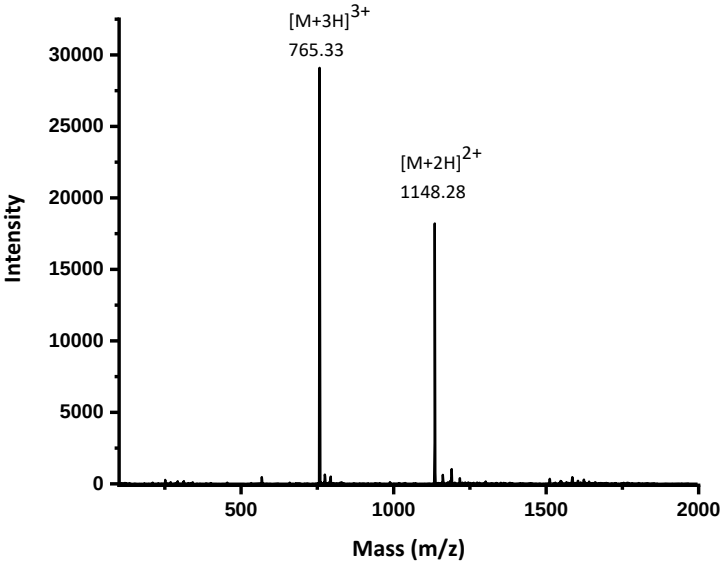

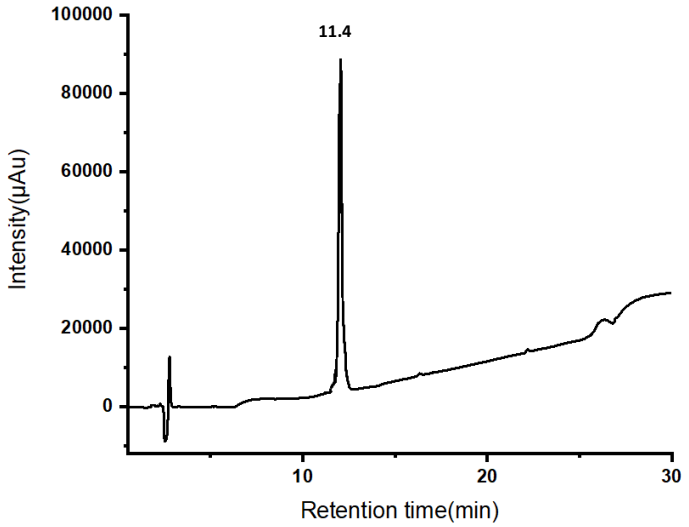

Figure 37. UV chromatogram and ESI-MS spectrum of G51D. Gradient: 15-60% of B in A in 20 min. 0.8 mL/min. A: 0.1% TFA in 100% H2O: B: 0.1% TFA in CH_3CN. The peaks signed correspond to: $[M+2H]^{2+}$ (1148,28 m/z) and $[M+3H]^{3+}$ (765.33 m/z)

- **G51D_scr**

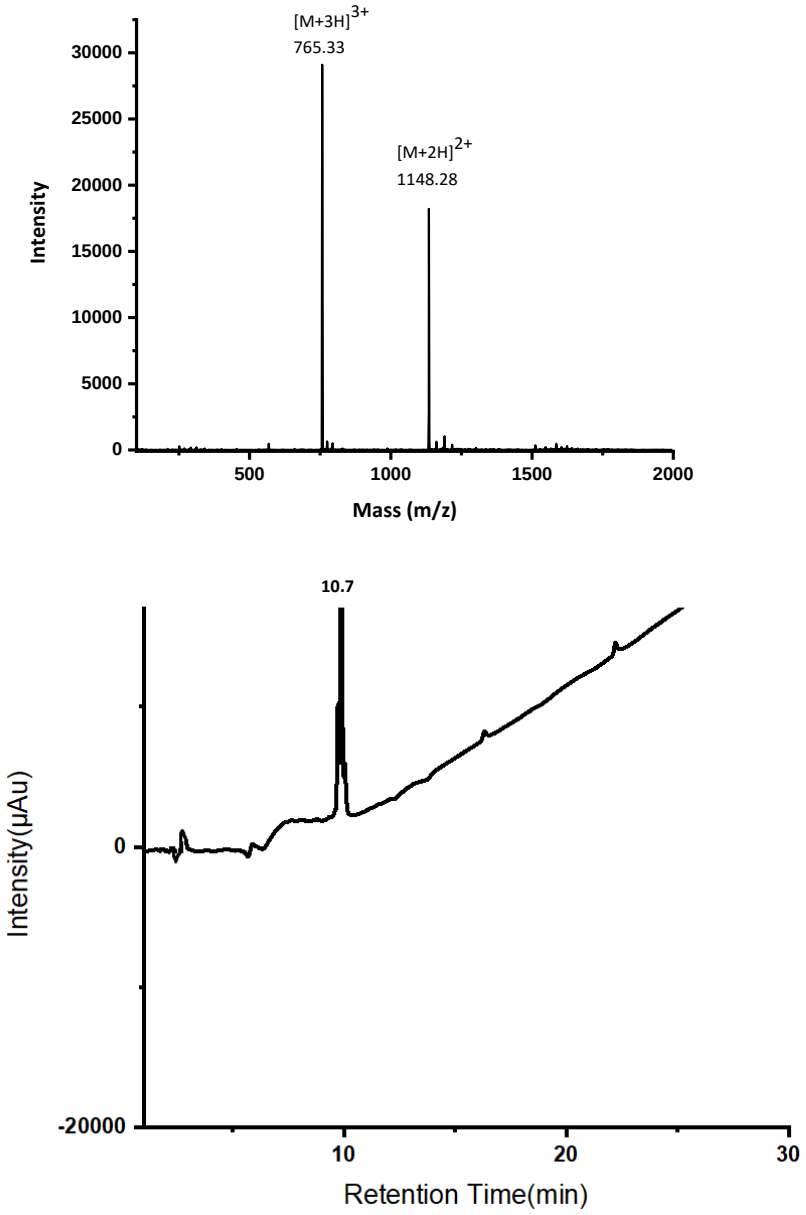

Figure 38. UV chromatogram and ESI-MS spectrum of G51D_scr. Gradient: 15-60% of B in A in 20 min. 0.8 mL/min. A: 0.1% TFA in 100% H2O: B: 0.1% TFA in CH_3CN. The peaks signed correspond to: $[M+2H]^{2+}$ (1148,28 m/z) and $[M+3H]^{3+}$ (765.33 m/z)

- **H50Q**

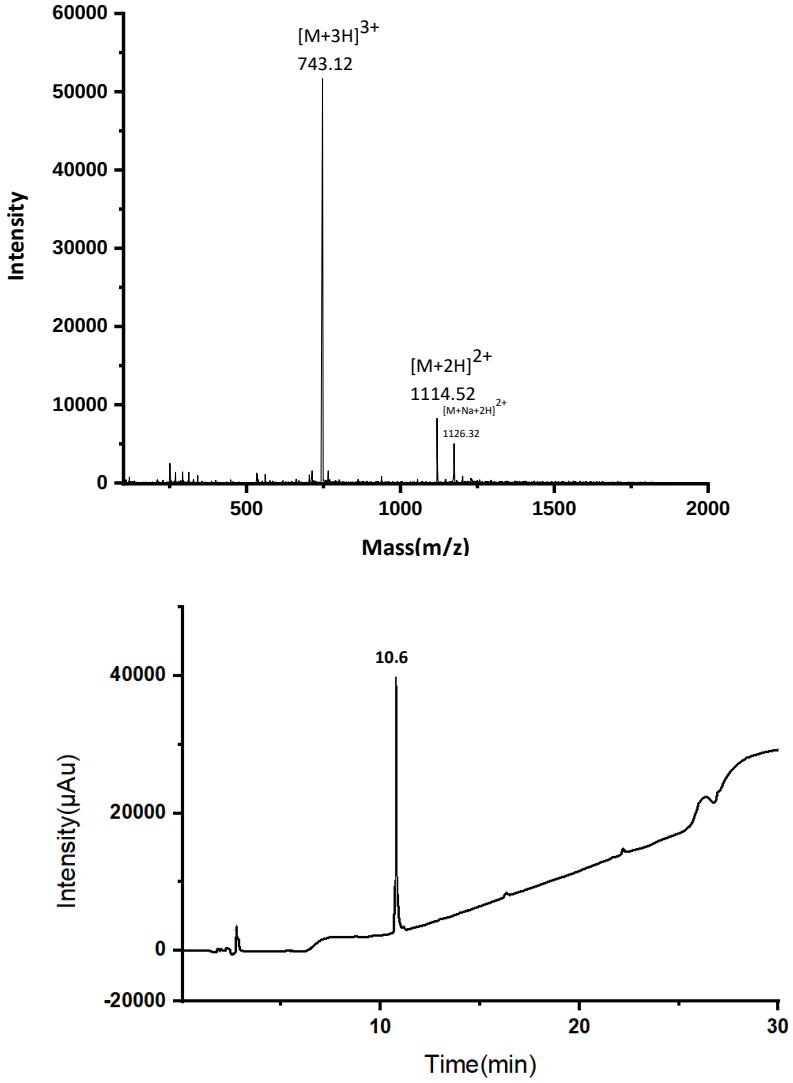

Figure 39. UV chromatogram and ESI-MS spectrum of H50Q. Gradient: 15-60% of B in A in 20 min. 0.8 mL/min. A: 0.1% TFA in 100% H2O: B: 0.1% TFA in CH_3CN. The peaks signed correspond to: $[M+2H]^{2+}$ (1114,52 m/z) and $[M+3H]^{3+}$ (743.12 m/z)

- H50Q_scr

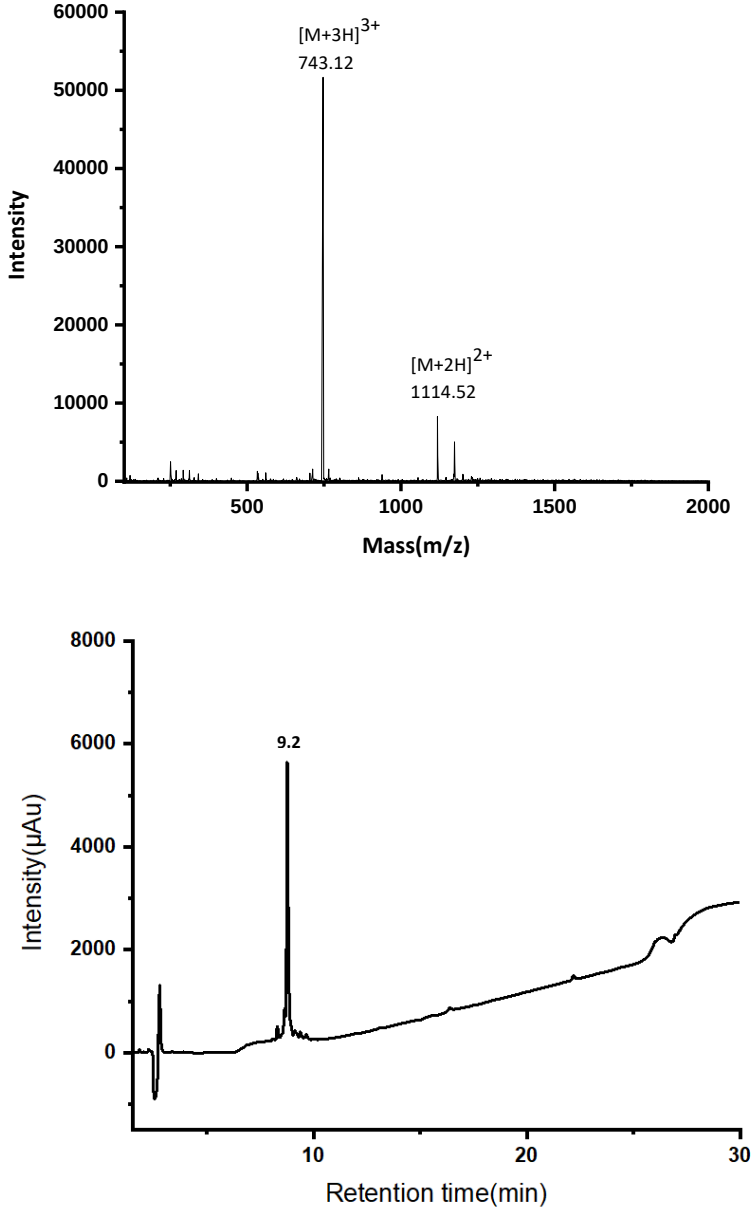

Figure 40. UV chromatogram and ESI-MS spectrum of H50Q_scr. Gradient: 15-60% of B in A in 20 min. 0.8 mL/min. A: 0.1% TFA in 100% H2O: B: 0.1% TFA in CH_3CN. The peaks signed correspond to: $[M+2H]^{2+}$ (1114,52 m/z) and $[M+3H]^{3+}$ (743.12 m/z)

- NAC

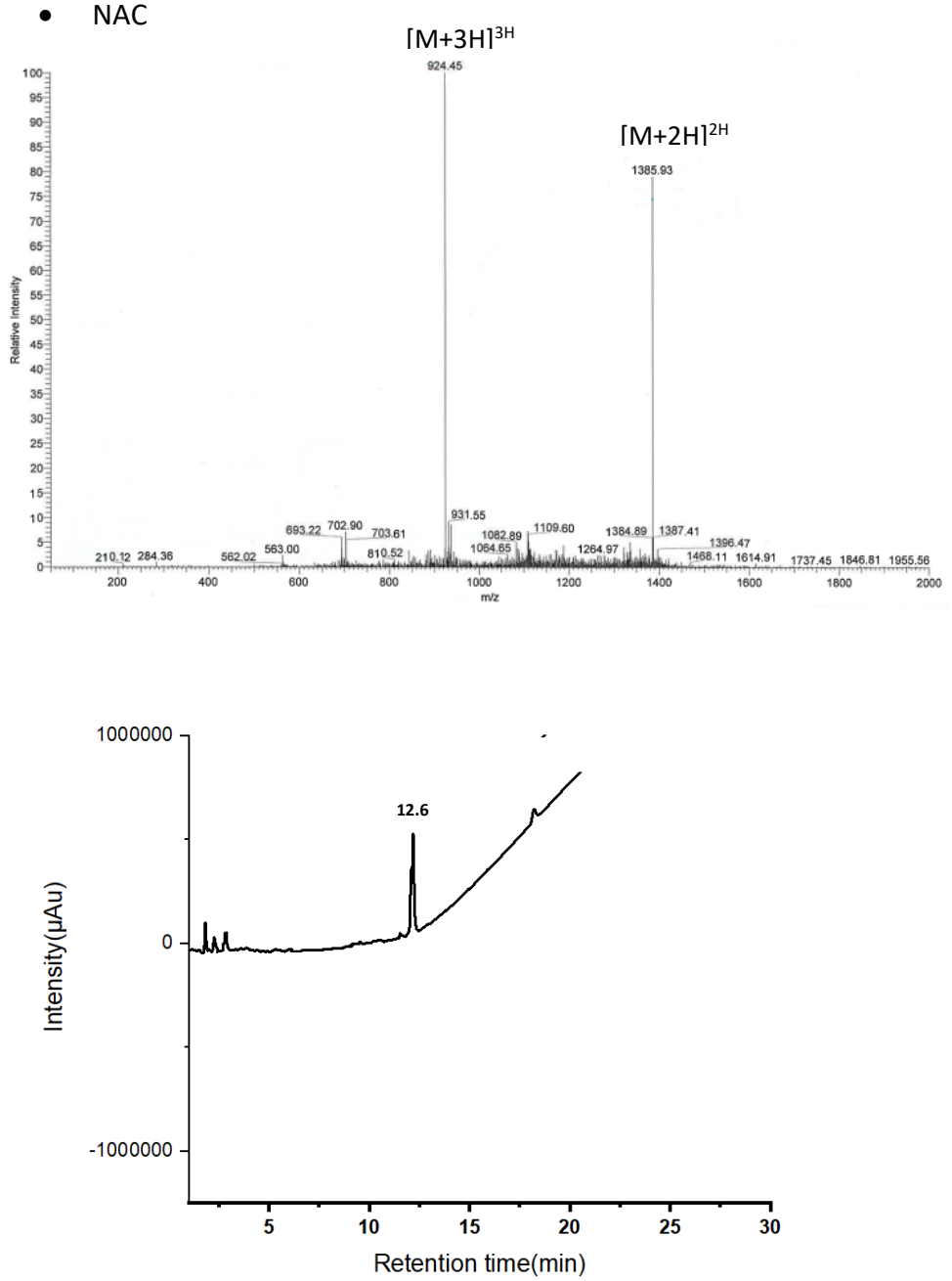

Figure 41. UV chromatogram and ESI-MS spectrum of NAC. Gradient: 15-60% of B in A in 20 min. 0.8 mL/min. A: 0.1% TFA in 100% H2O: B: 0.1% TFA in CH_3CN. The peaks signed correspond to: $[M+2H]^{2+}$ (1385,93 m/z) and $[M+3H]^{3+}$ (724.45 m/z)

- NAC_scr

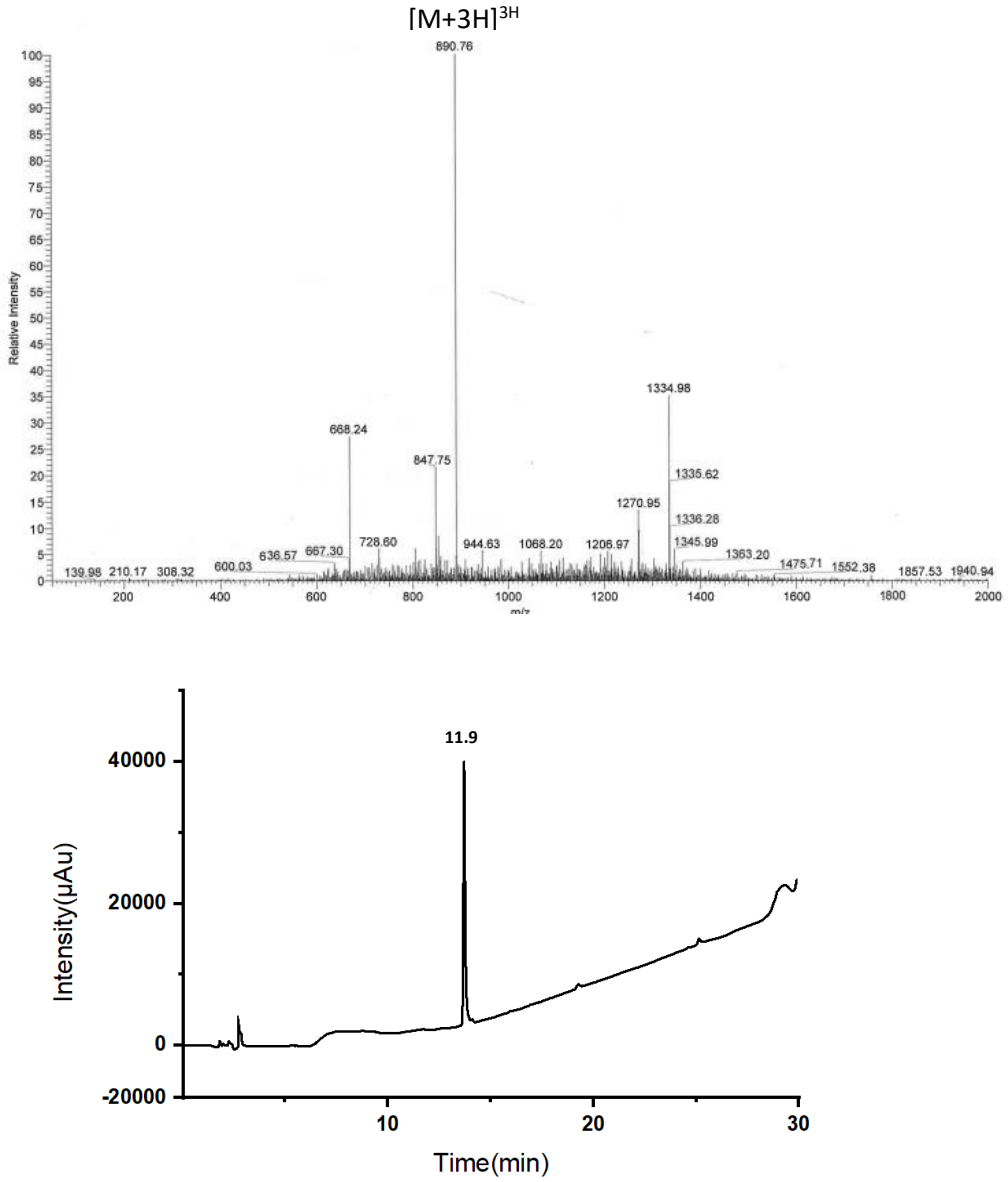

Figure 42. UV chromatogram and ESI-MS spectrum of NAC_scr. Gradient: 15-60% of B in A in 20 min. 0.8 mL/min. A: 0.1% TFA in 100% H2O: B: 0.1% TFA in CH_3CN. The peaks signed correspond to: $[M+3H]^{3+}$ (890.76 m/z)

- E46K_scr

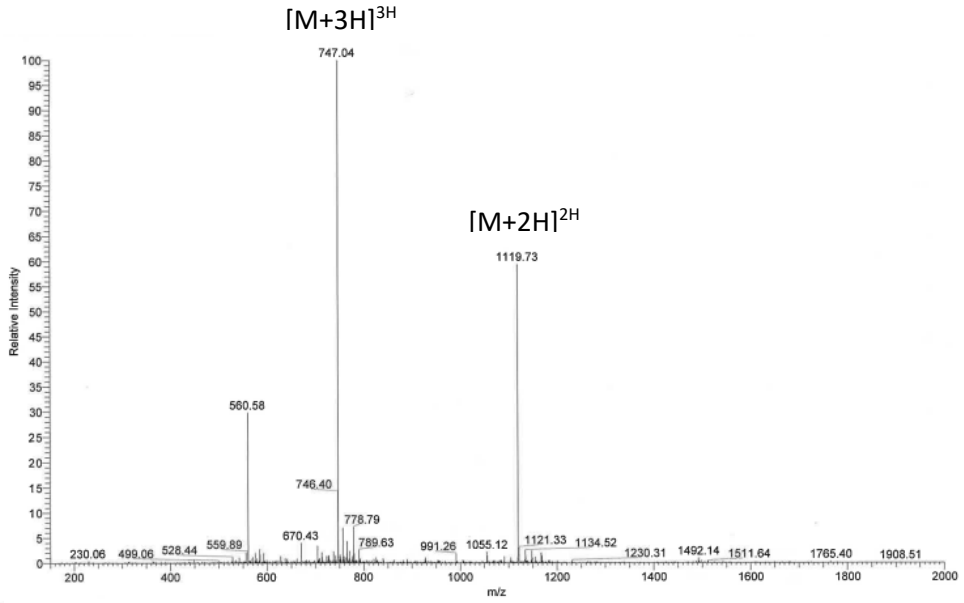

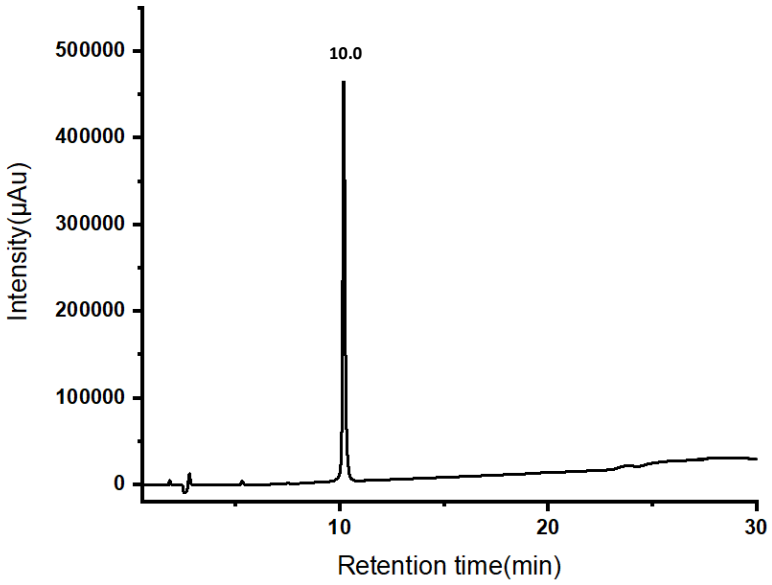

Figure 43. UV chromatogram and ESI-MS spectrum of E46K_scr. Gradient: 15-60% of B in A in 20 min. 0.8 mL/min. A: 0.1% TFA in 100% H2O: B: 0.1% TFA in CH_3CN. The peaks signed correspond to: $[M+2H]^{2+}$ (1119,73 m/z) and $[M+3H]^{3+}$ (747.04 m/z)

- A30P_scr

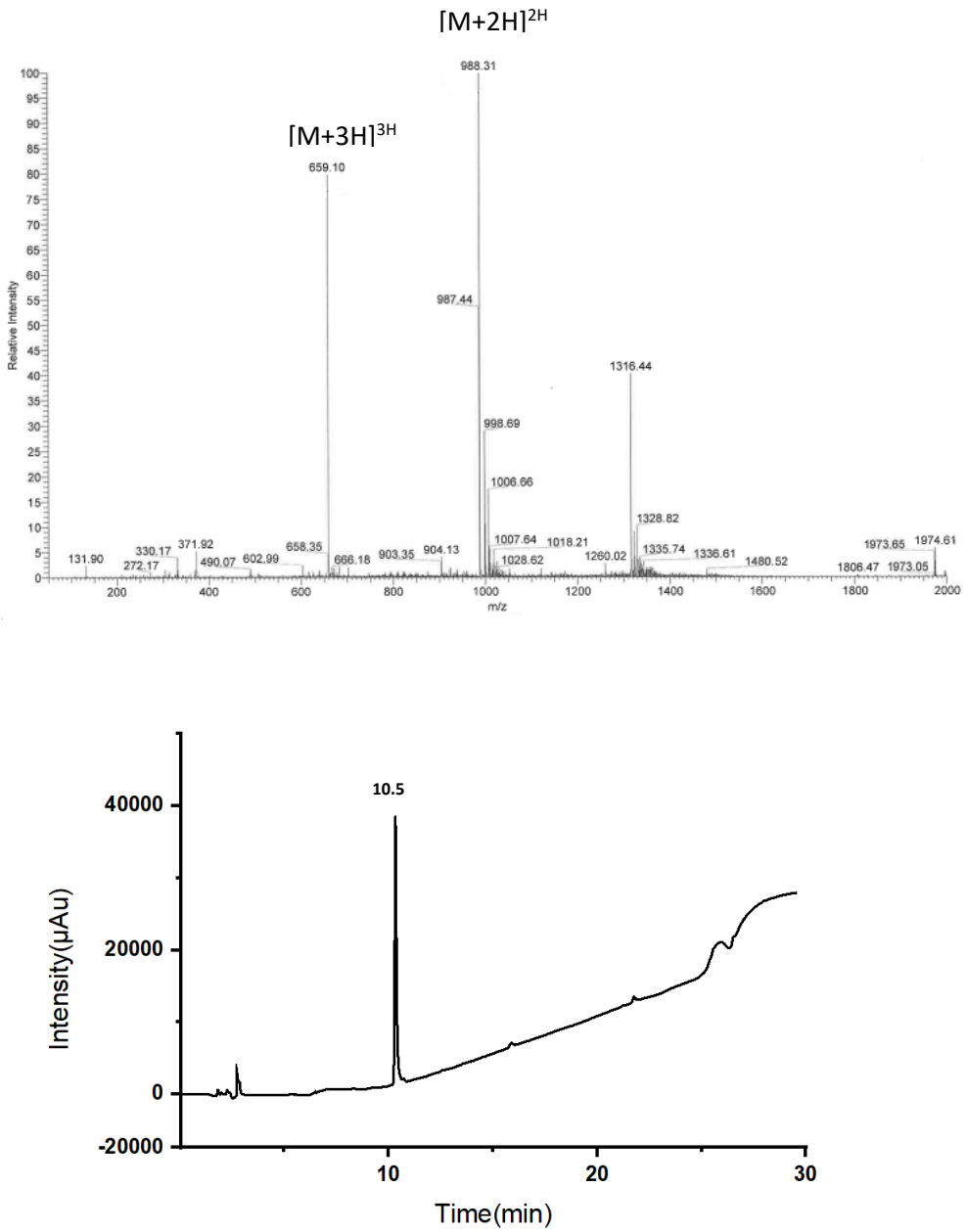

Figure 44. UV chromatogram and ESI-MS spectrum of A30P_scr. Gradient: 15-60% of B in A in 20 min. 0.8 mL/min. A: 0.1% TFA in 100% H2O: B: 0.1% TFA in CH_3CN. The peaks signed correspond to: $[M+2H]^{2+}$ (988,31 m/z) and $[M+3H]^{3+}$ (659.10 m/z)

- C1

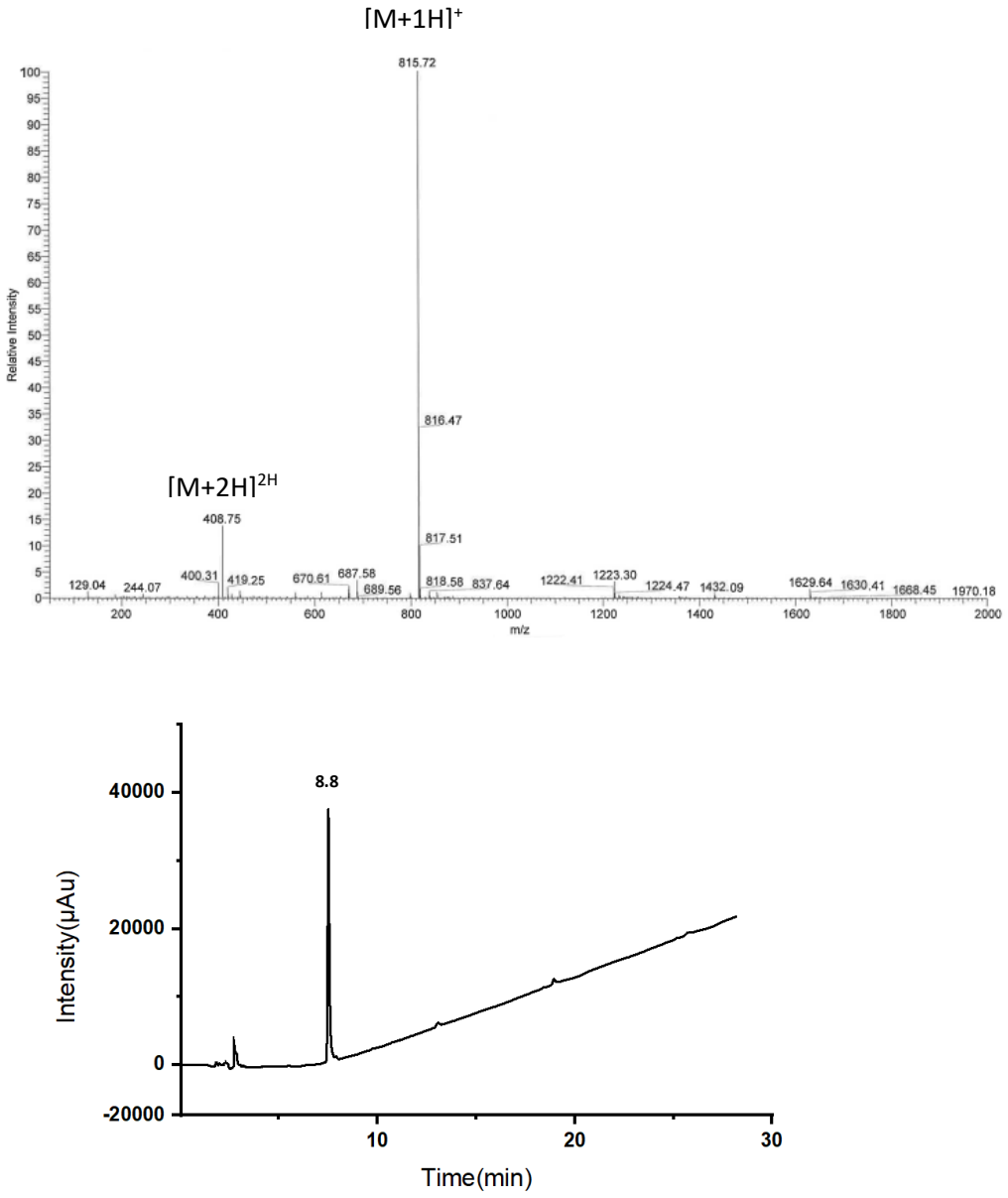

Figure 45. UV chromatogram and ESI-MS spectrum of C1. Gradient: 05-60% of B in A in 20 min. 0.8 mL/min. A: 0.1% TFA in 100% H2O: B: 0.1% TFA in CH_3CN. The peaks signed correspond to: $[M+1H]^+$ (815,72 m/z) and $[M+2H]^{2+}$ (408.75 m/z)

- C1_scr

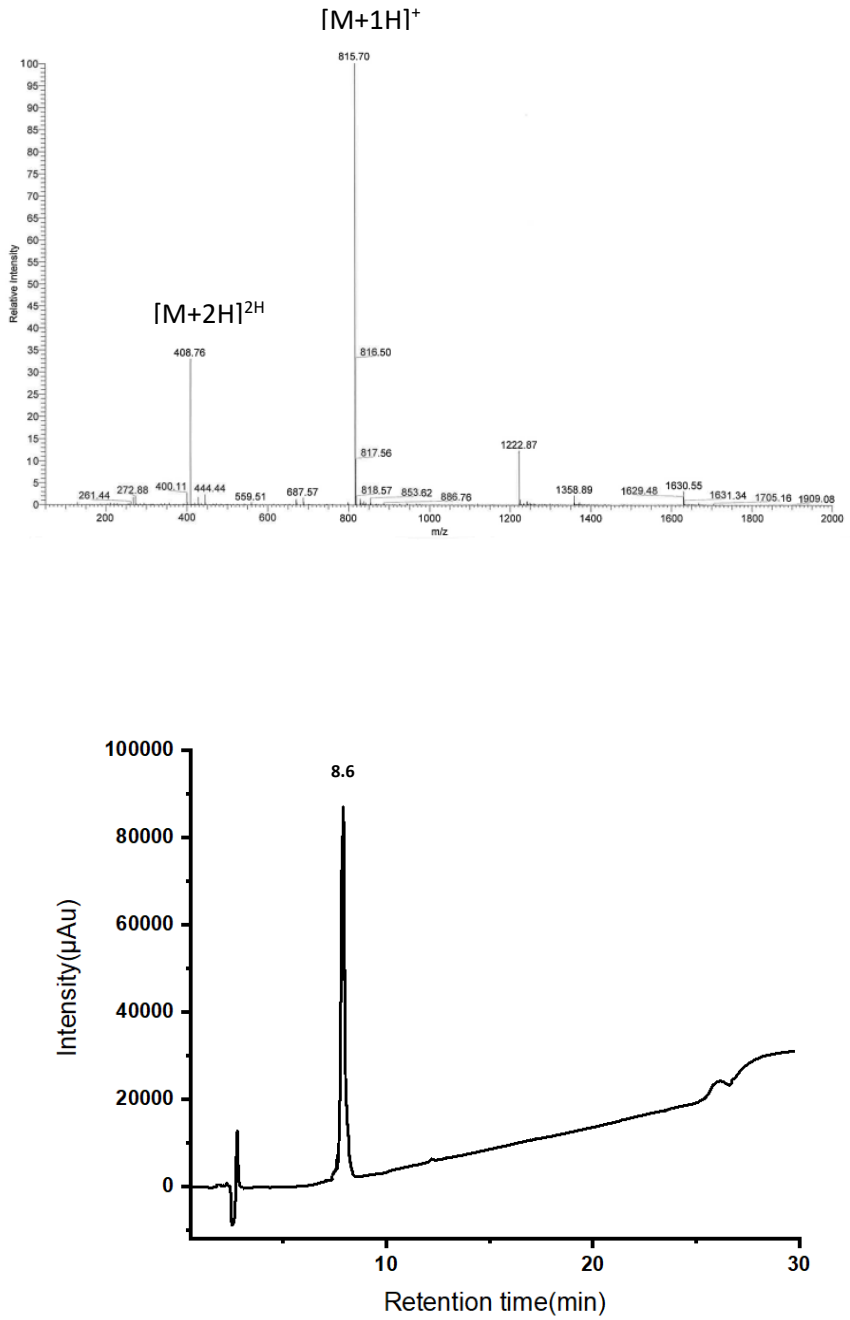

Figure 46. UV chromatogram and ESI-MS spectrum of C1_scr. Gradient: 05-60% of B in A in 20 min. 0.8 mL/min. A: 0.1% TFA in 100% H2O: B: 0.1% TFA in CH_3CN. The peaks signed correspond to: $[M+1H]^+$ (815,70 m/z) and $[M+2H]^{2+}$ (408.76 m/z)

- C2

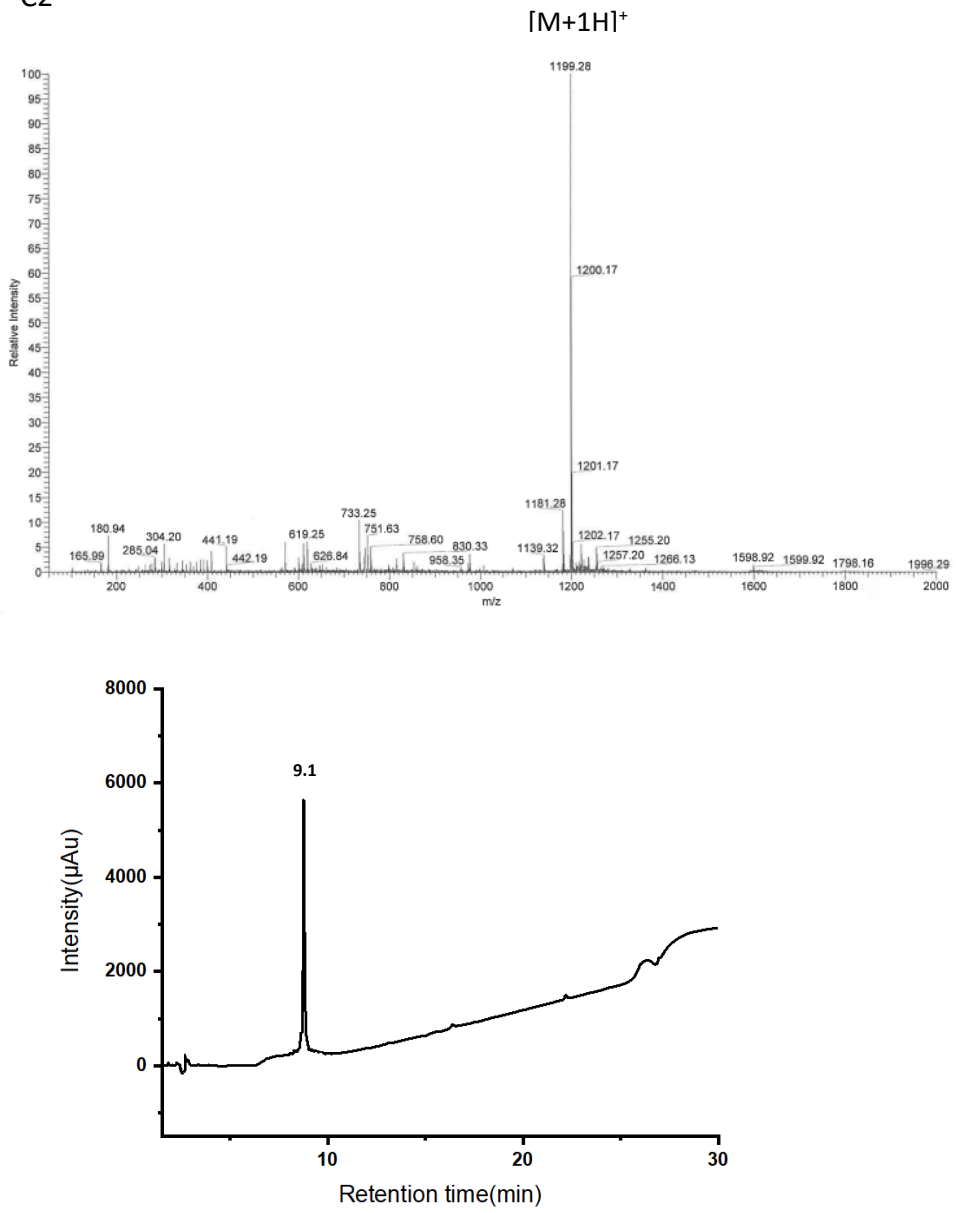

Figure 47. UV chromatogram and ESI-MS spectrum of C2. Gradient: 05-60% of B in A in 20 min. 0.8 mL/min. A: 0.1% TFA in 100% H2O: B: 0.1% TFA in CH_3CN. The peaks signed correspond to: $[M+1H]^+$ (1199,28 m/z)

- C2_scr

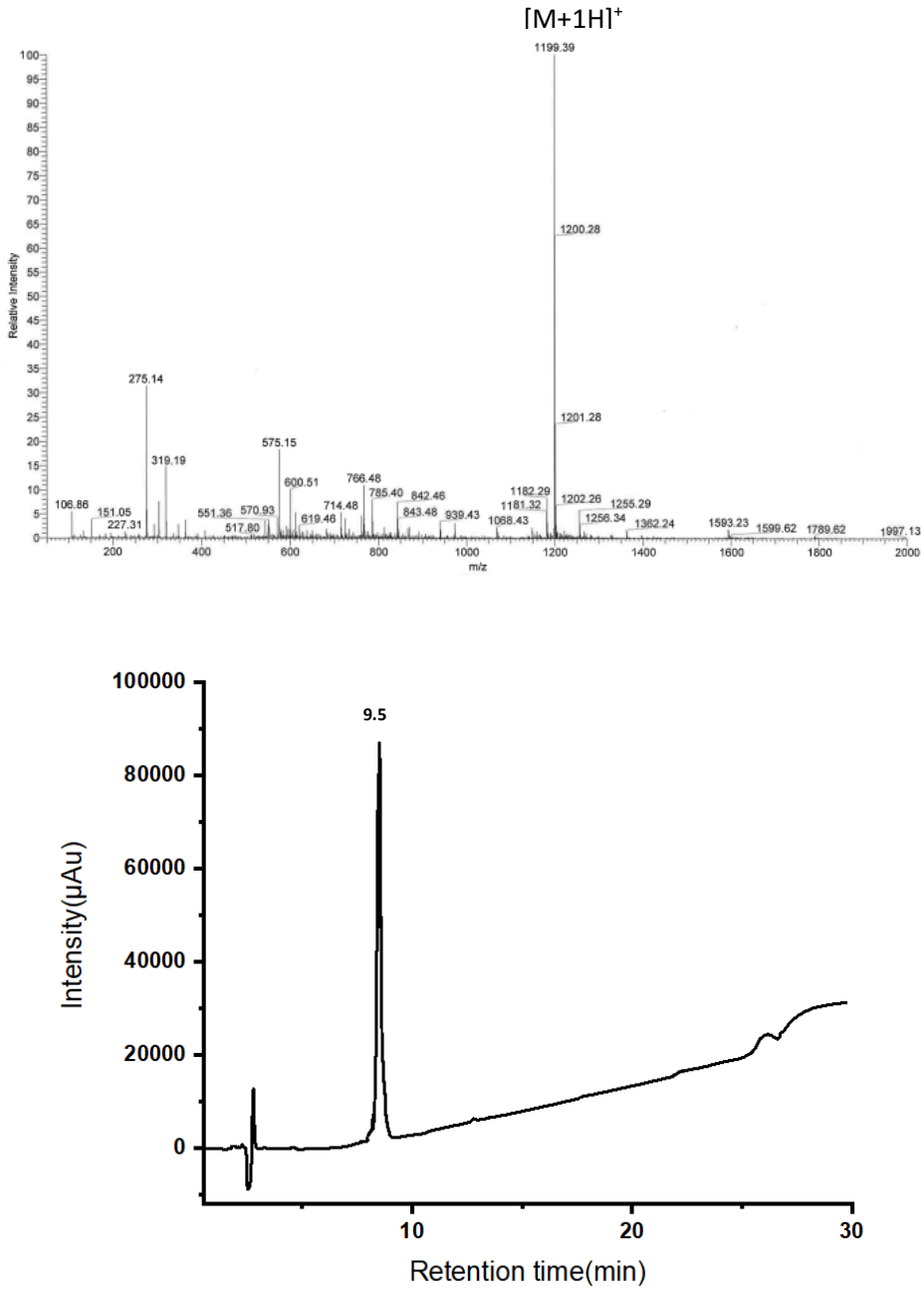

Figure 48. UV chromatogram and ESI-MS spectrum of C2_scr. Gradient: 05-60% of B in A in 20 min. 0.8 mL/min. A: 0.1% TFA in 100% H2O: B: 0.1% TFA in CH_3CN. The peaks signed correspond to: $[M+1H]^+$ (1199,39 m/z)

- **KPM1**

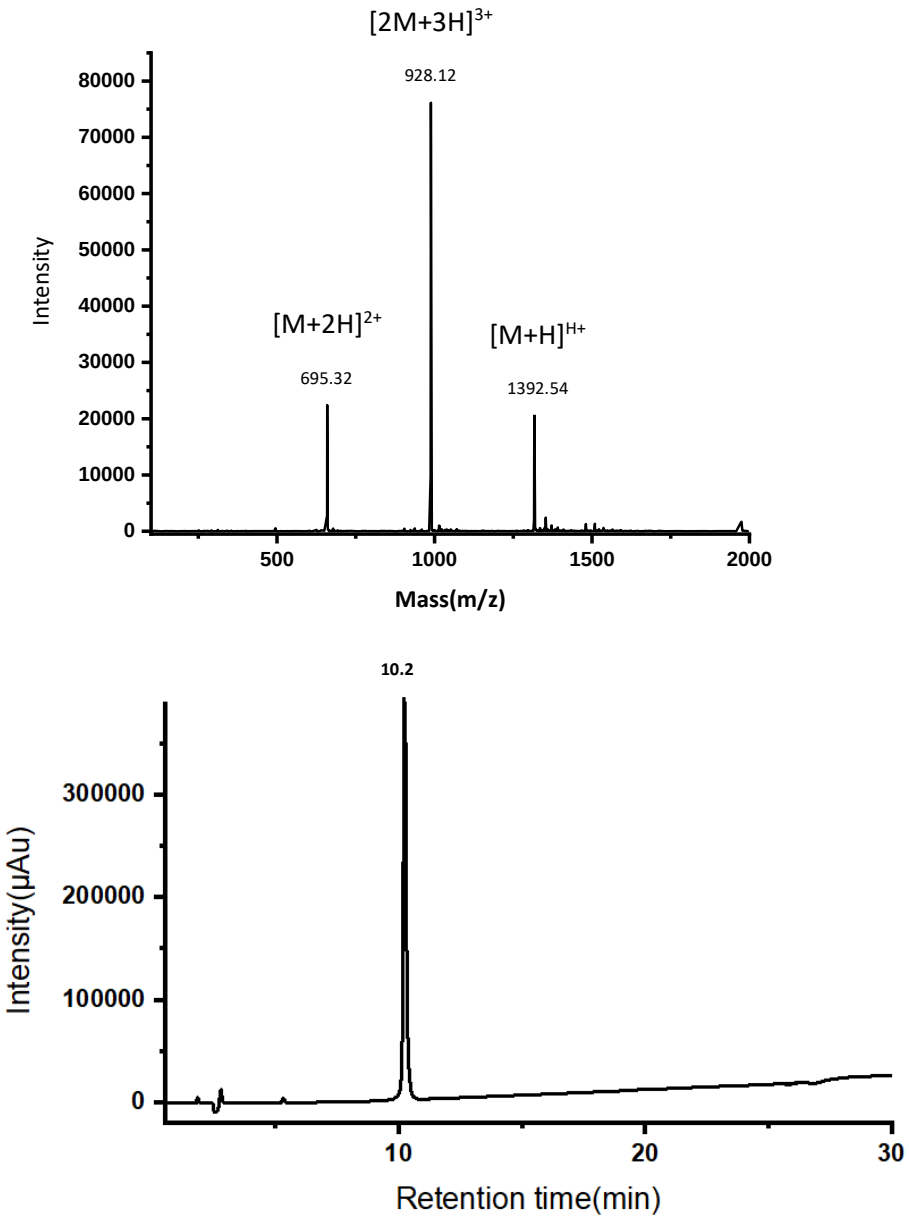

Figure 49. UV chromatogram and ESI-MS spectrum of KPM1. Gradient: 15-60% of B in A in 20 min. 0.8 mL/min. A: 0.1% TFA in 100% H2O: B: 0.1% TFA in CH_3CN. The peaks signed correspond to: $[M+2H]^{2+}$ (695,35 m/z), $[M+H]^{+}$ (1392,54 m/z) and $[2M+3H]^{3+}$ (928.12 m/z)

- **KPM3**

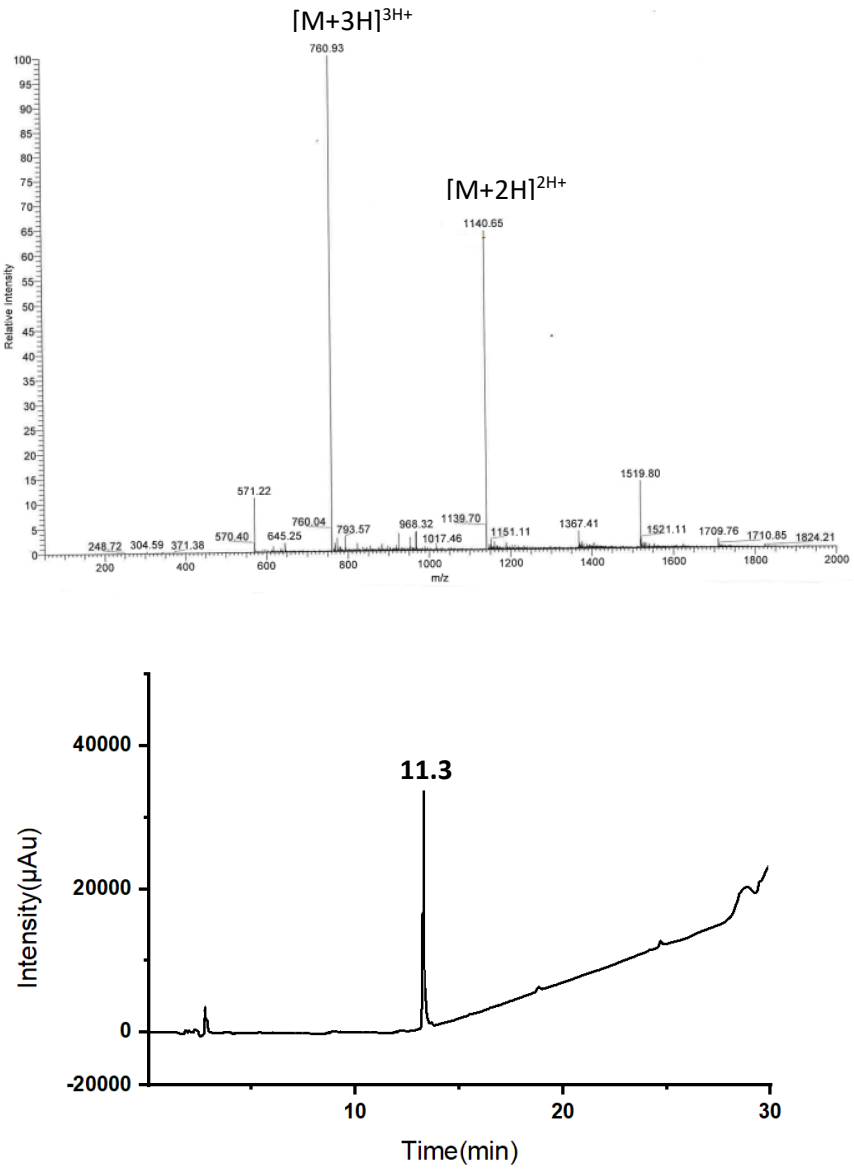

Figure 50. UV chromatogram and ESI-MS spectrum of KPM3. Gradient: 20-60% of B in A in 20 min. 0.8 mL/min. A: 0.1% TFA in 100% H2O: B: 0.1% TFA in CH_3CN. The peaks signed correspond to: $[M+2H]^{2+}$ (1140,65 m/z), $[M+3H]^{3+}$ (760,93 m/z)

- **KPM2**

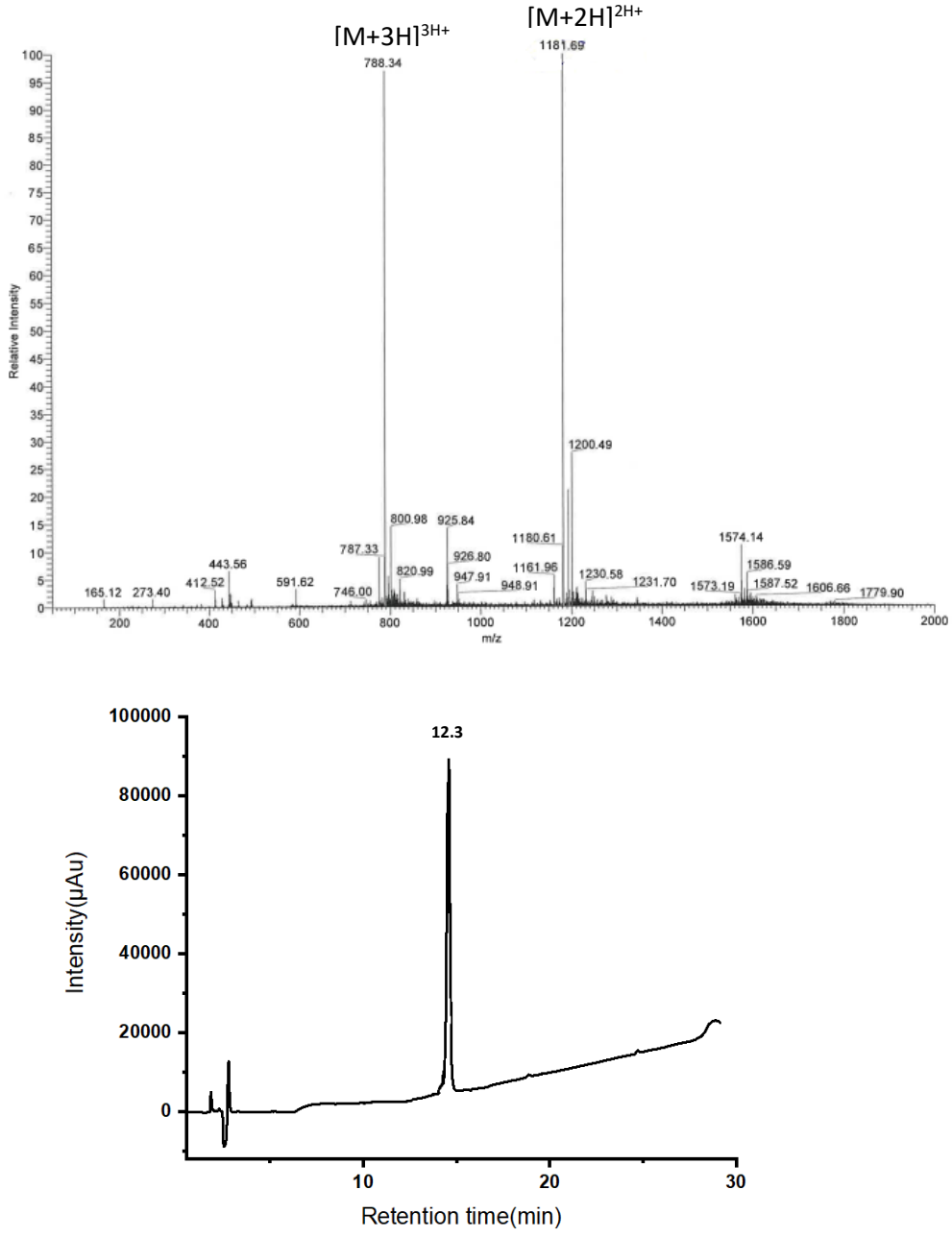

Figure 51. UV chromatogram and ESI-MS spectrum of KPM2. Gradient: 20-60% of B in A in 20 min. 0.8 mL/min. A: 0.1% TFA in 100% H2O: B: 0.1% TFA in CH_3CN. The peaks signed correspond to: $[M+2H]^{2+}$ (1181,69 m/z), $[M+3H]^{3+}$ (788,34 m/z)

- **KPM6**

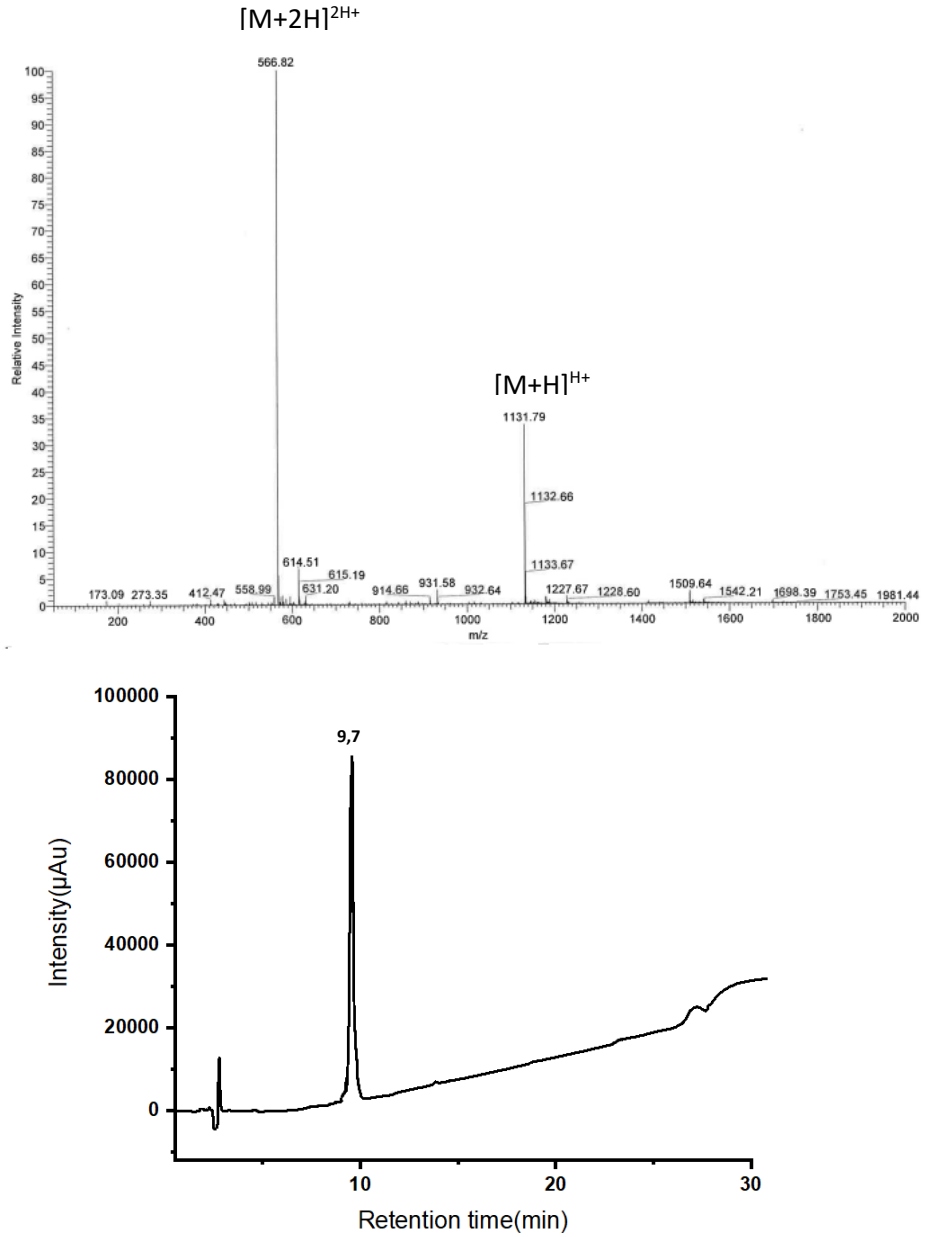

Figure 52. UV chromatogram and ESI-MS spectrum of KPM6. Gradient: 2-60% of B in A in 20 min. 0.8 mL/min. A: 0.1% TFA in 100% H2O: B: 0.1% TFA in CH_3CN. The peaks signed correspond to: $[M+H]^+$ (1131,79 m/z), $[M+2H]^{2+}$ (566,82 m/z)

- **KPM8**

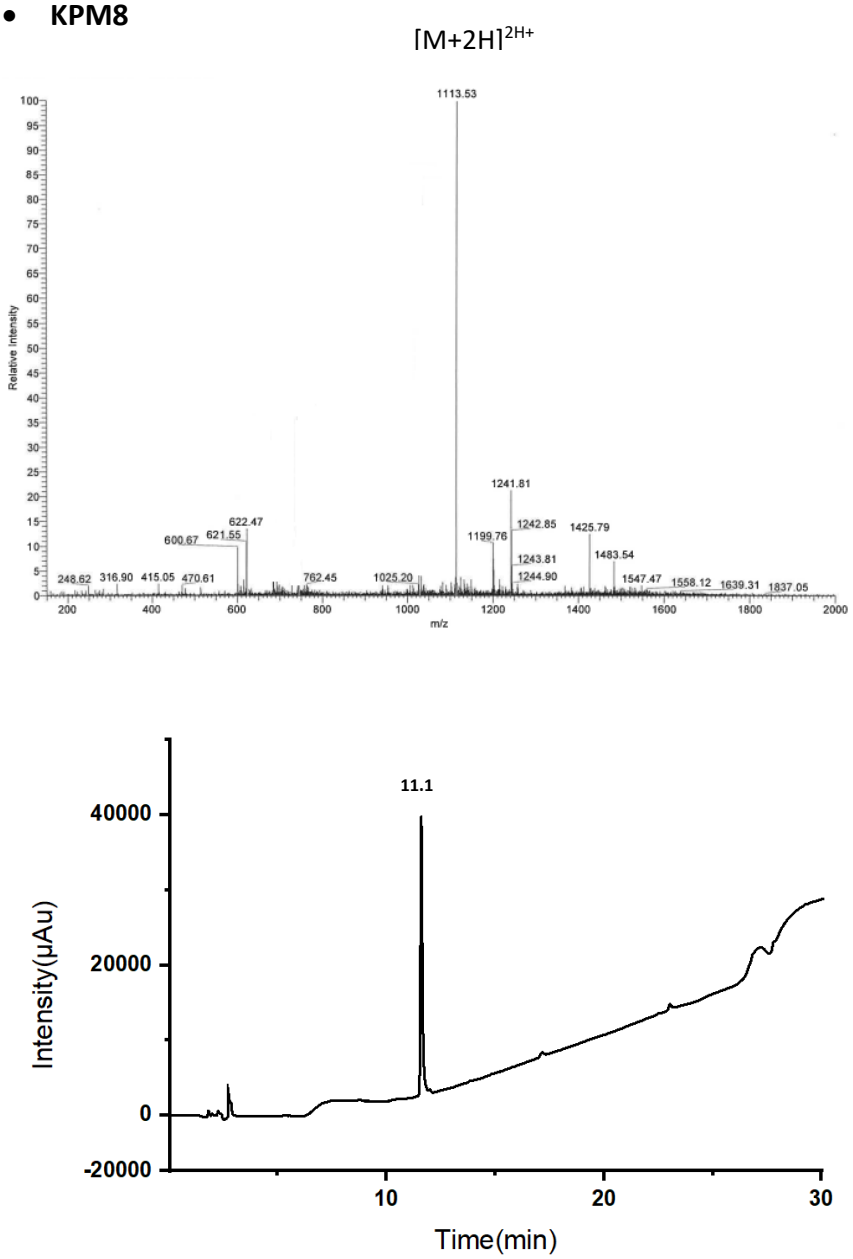

Figure 53. UV chromatogram and ESI-MS spectrum of KPM8. Gradient: 5-60% of B in A in 20 min. 0.8 mL/min. A: 0.1% TFA in 100% H2O: B: 0.1% TFA in CH_3CN. The peaks signed correspond to: $[M+2H]^{2+}$ (1113,53 m/z)

- **WT2_CF**

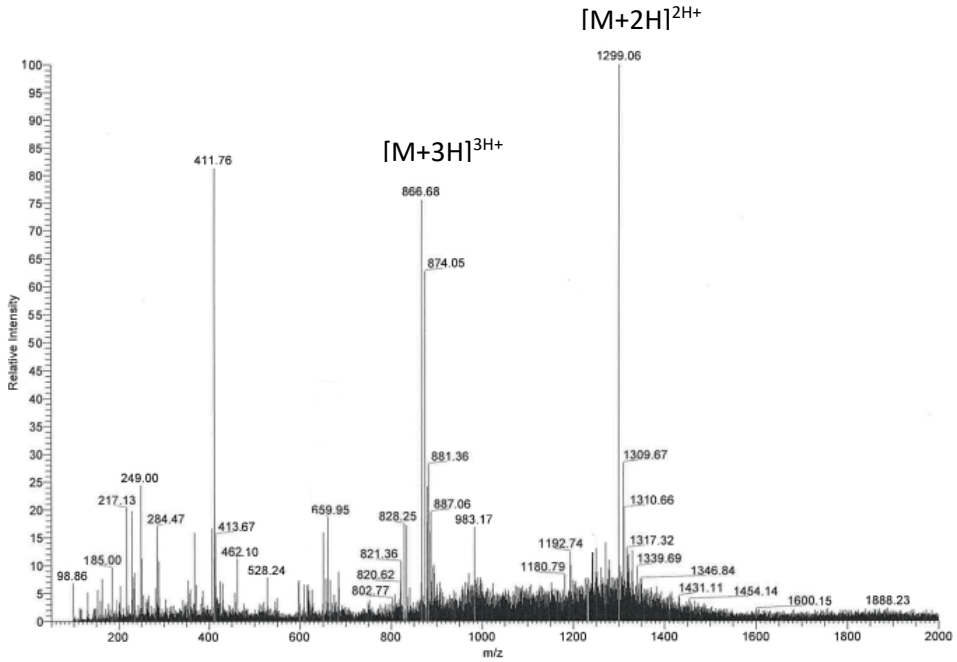

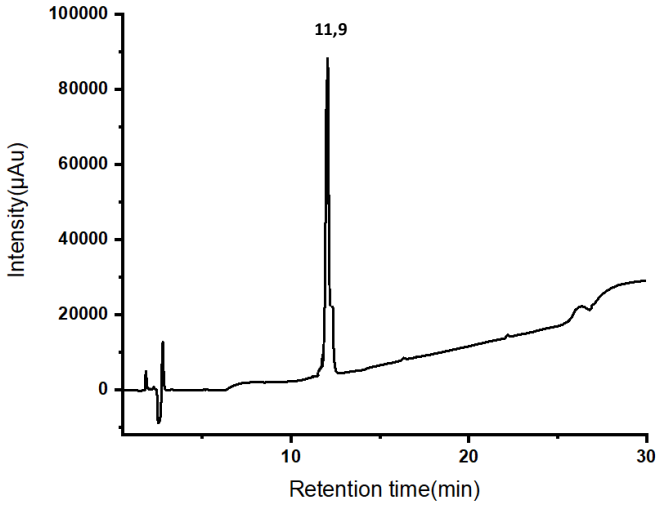

Figure 54. UV chromatogram and ESI-MS spectrum of WT2_CF. Gradient: 15-60% of B in A in 20 min. 0.8 mL/min. A: 0.1% TFA in 100% H2O: B: 0.1% TFA in CH_3CN. The peaks signed correspond to: $[M+2H]^{2+}$ (1299,06 m/z), $[M+3H]^{3+}$ (866,68 m/z)

- **H50Q_CF**

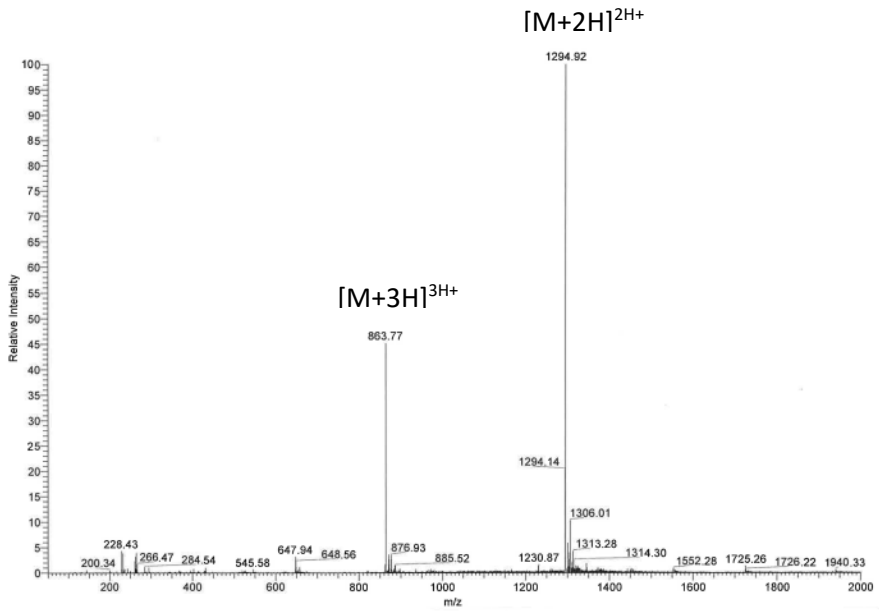

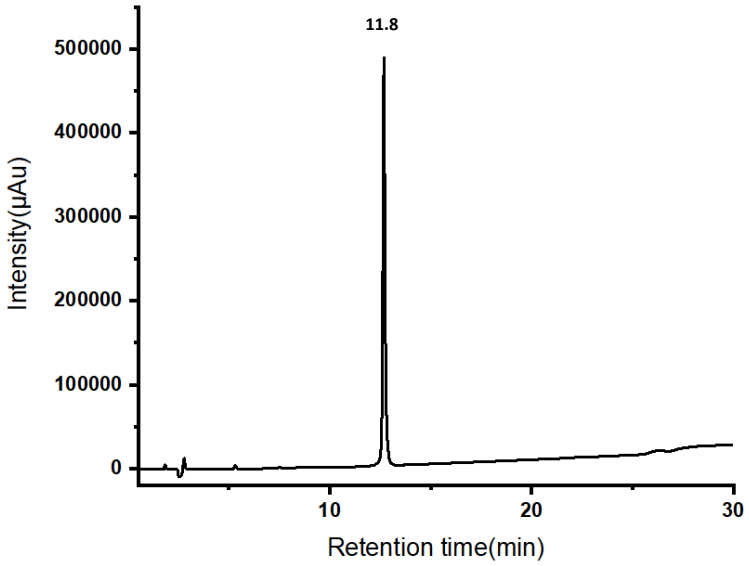

Figure 55. UV chromatogram and ESI-MS spectrum of WT2_CF. Gradient: 15-60% of B in A in 20 min. 0.8 mL/min. A: 0.1% TFA in 100% H2O: B: 0.1% TFA in CH_3CN. The peaks signed correspond to: $[M+2H]^{2+}$ (1294,92 m/z), $[M+3H]^{3+}$ (863,77 m/z)

- **G51D_CF**

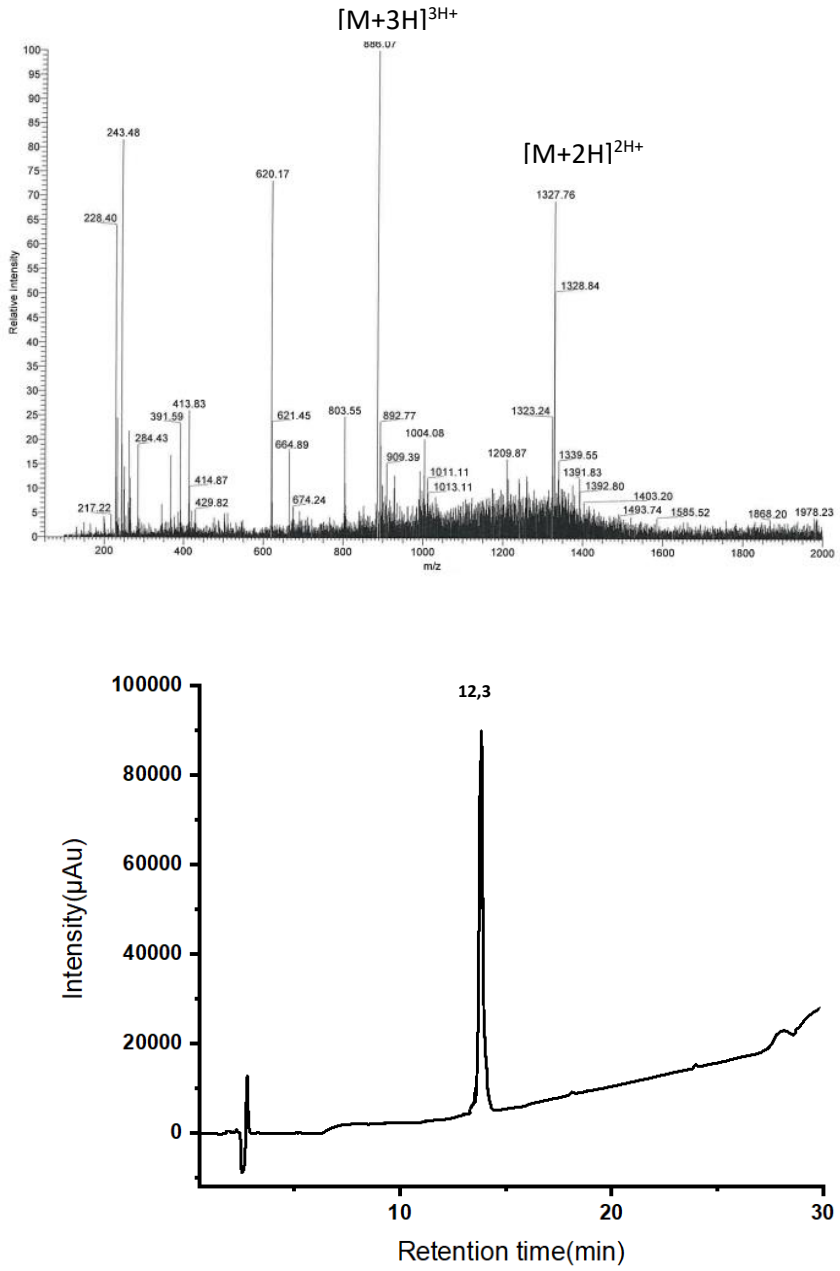

Figure 56. UV chromatogram and ESI-MS spectrum of G51D_CF. Gradient: 15-60% of B in A in 20 min. 0.8 mL/min. A: 0.1% TFA in 100% H2O: B: 0.1% TFA in CH_3CN. The peaks signed correspond to: $[M+2H]^{2+}$ (1327,76 m/z), $[M+3H]^{3+}$ (886,07 m/z)

- **Tau1**

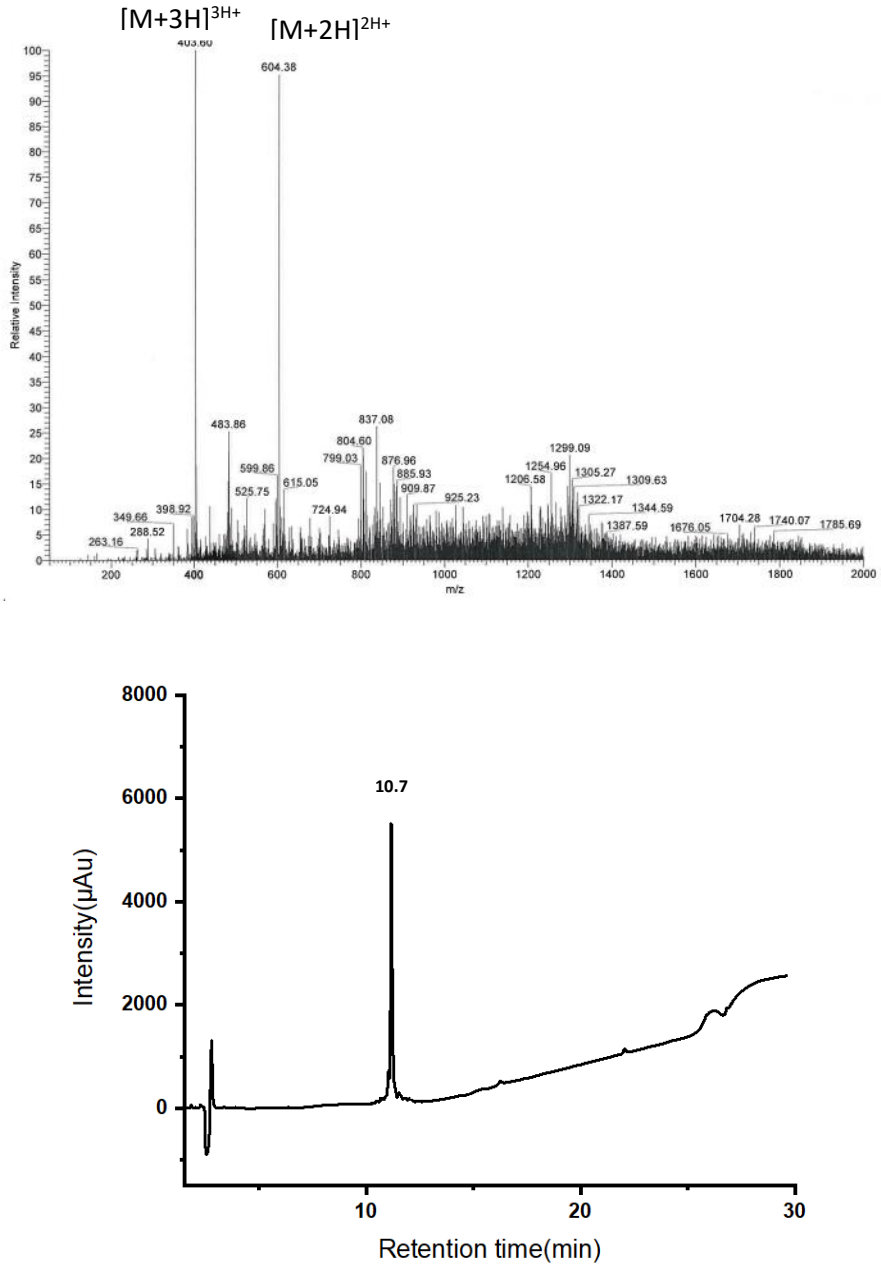

Figure 57. UV chromatogram and ESI-MS spectrum of Tau1. Gradient: 15-60% of B in A in 20 min. 0.8 mL/min. A: 0.1% TFA in 100% H2O: B: 0.1% TFA in CH_3CN. The peaks signed correspond to: $[M+2H]^{2+}$ (604,38 m/z), $[M+3H]^{3+}$ (403,60 m/z)

- **Tau2**

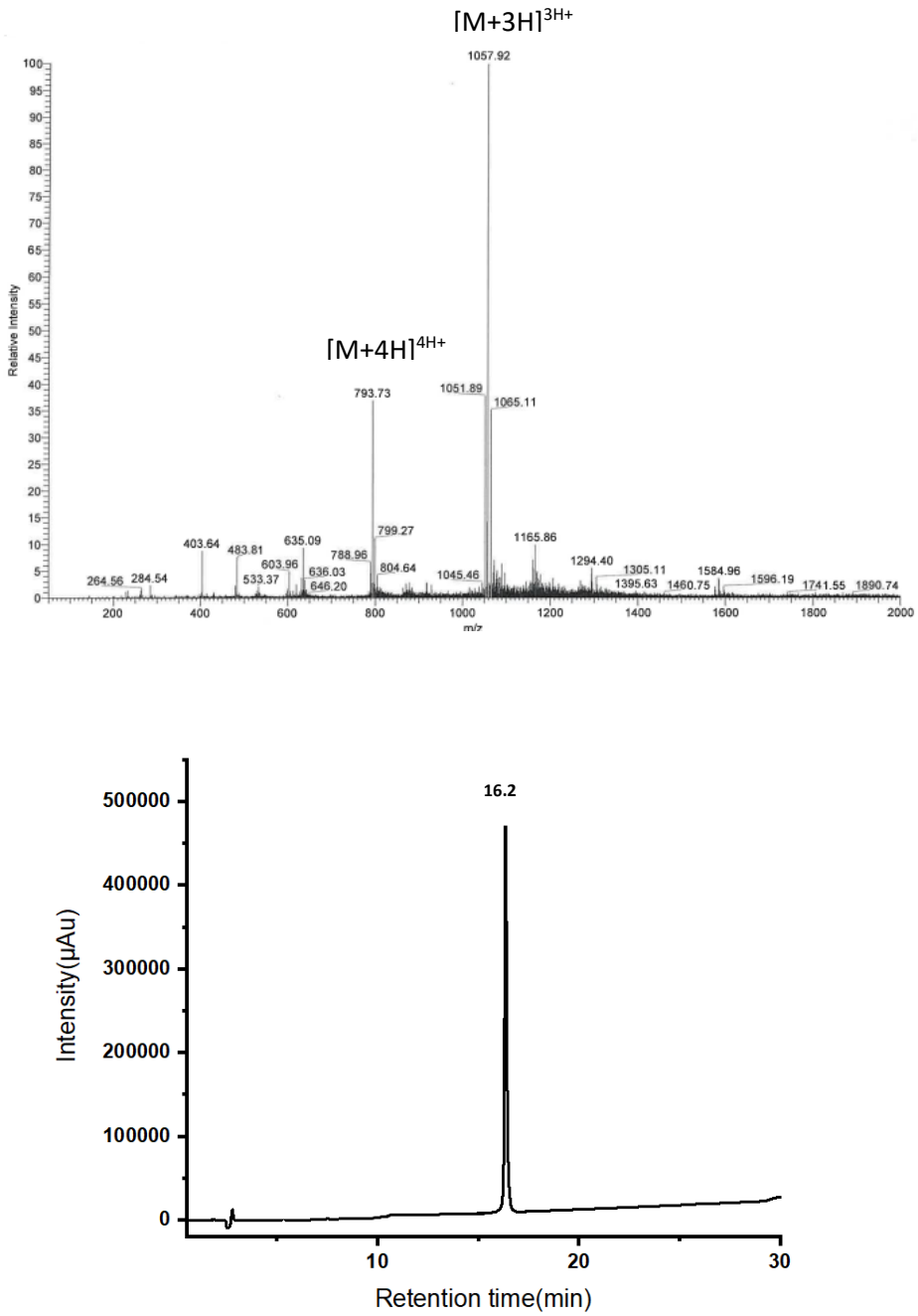

Figure 58. UV chromatogram and ESI-MS spectrum of Tau2. Gradient: 15-60% of B in A in 20 min. 0.8 mL/min. A: 0.1% TFA in 100% H2O: B: 0.1% TFA in CH_3CN. The peaks signed correspond to: $[M+3H]^{3+}$ (1057,92 m/z), $[M+4H]^{4+}$ (793,73 m/z)

13.2. Supplementary data: NMR spectra of compounds

The NMR spectroscopic experiments were carried out on a 300 MHz spectrometer

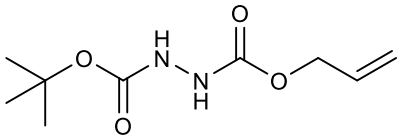

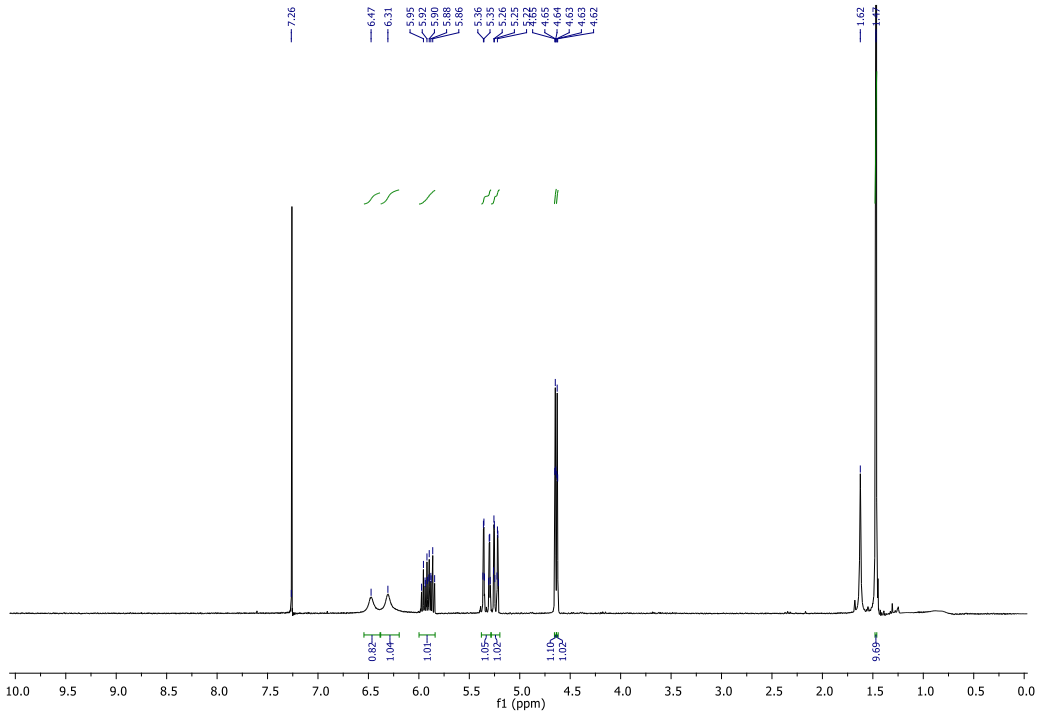

Figure 59. ^{1}H-NMR spectrum of KPM5 (300 MHz, $CDCl_3$)

^{1}H-NMR ($CDCl_3$): δ 1.47 (s, 9H), 4.62-4.63 (m, 1H), 4.64-4.65 (m, 1H), 5.21-5.26 (m, 1H), 5.29-5.36 (m, 1H), 5.84-5.97 (m, 1H), 6.31 (br s, 1H), 6.47 (br s, 1H).

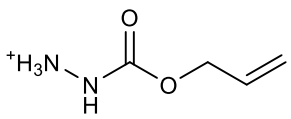

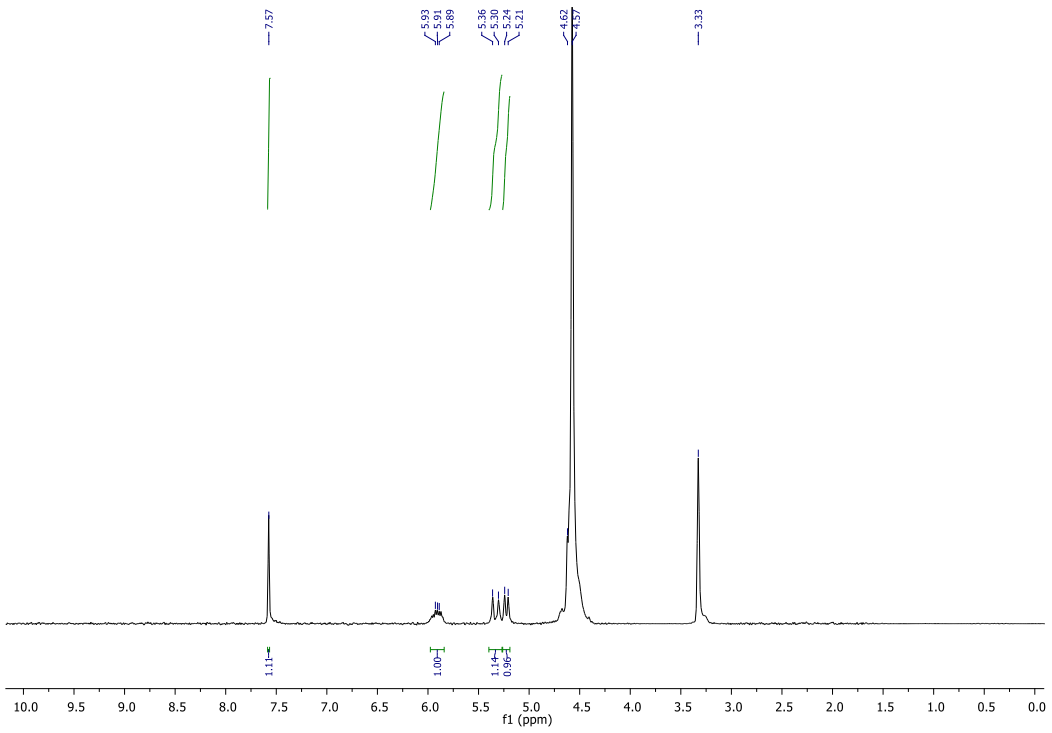

Figure 60. ^{1}H-NMR spectrum of KPM7 (300 MHz, MeOH-d_4,)

^{1}H-NMR (MeOH-d_4): δ 4.60 (overlapped, 2H), 5.22 (d, *J* = 10 Hz, 1H), 5.33 (d, *J* = 17 Hz, 1H), 5.89-5.93 (m, 1H), 7.57 (s, 1H).

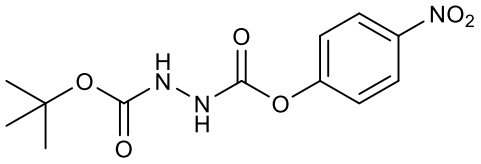

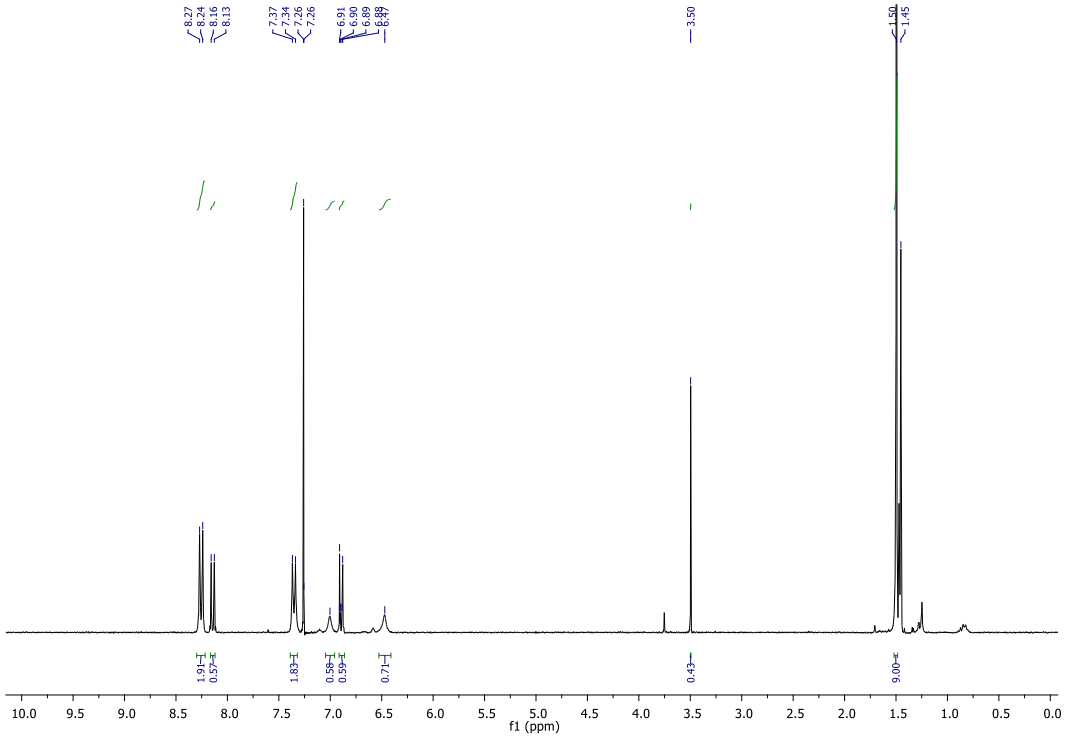

Figure 61. ^{1}H-NMR spectrum of KPM11 (300 MHz, $CDCl_3$,)

^{1}H-NMR ($CDCl_3$): δ 1.90 (s, 9H), 6.47 (br s, 1H), 6.91 (br s, 1H), 7.35 (d, *J* = 9 Hz, 2H), 8.26 (d, *J* = 9 Hz, 2H).

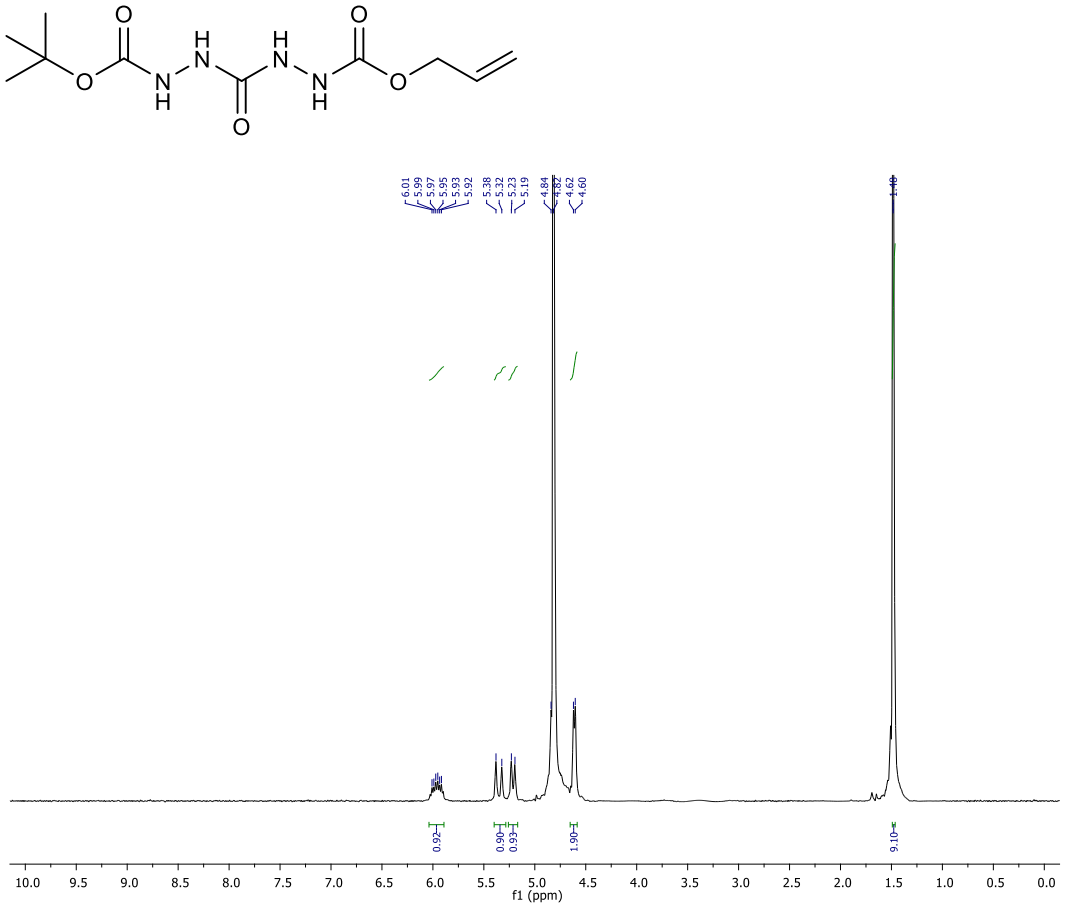

Figure 62. ^{1}H-NMR spectrum of KPM12 (300 MHz, D_2O)

^{1}H-NMR (D_2O): δ 1.48 (s, 9H), 4.61 (d, *J* = 5 HZ, 2H), 5.21 (d, *J* = 10 Hz, 1H), 5.35 (d, *J* = 17 Hz, 1H), 5.92-6.01 (m, 1H).

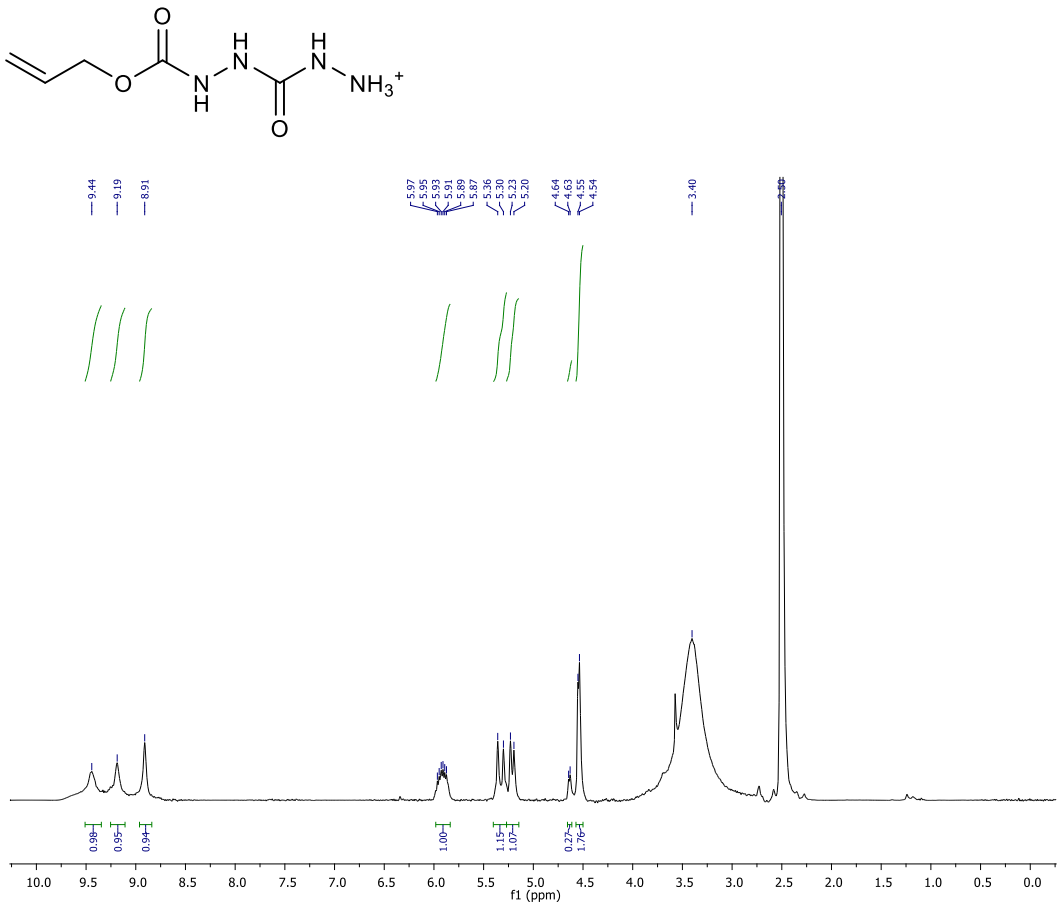

Figure 63. ^{1}H-NMR spectrum of KPM14 (300 MHz, DMSO-d_6)

^{1}H-NMR (DMSO-d_6): δ 4.54-4.64 (m, 2H), 5.22 (d, J = 10 Hz, 1H), 5.33 (d, J = 17 Hz, 1H), 5.87-5.97 (m, 1H), 8.91 (s, 1H), 9.19 (br s, 1H), 9.44 (br s, 1H).

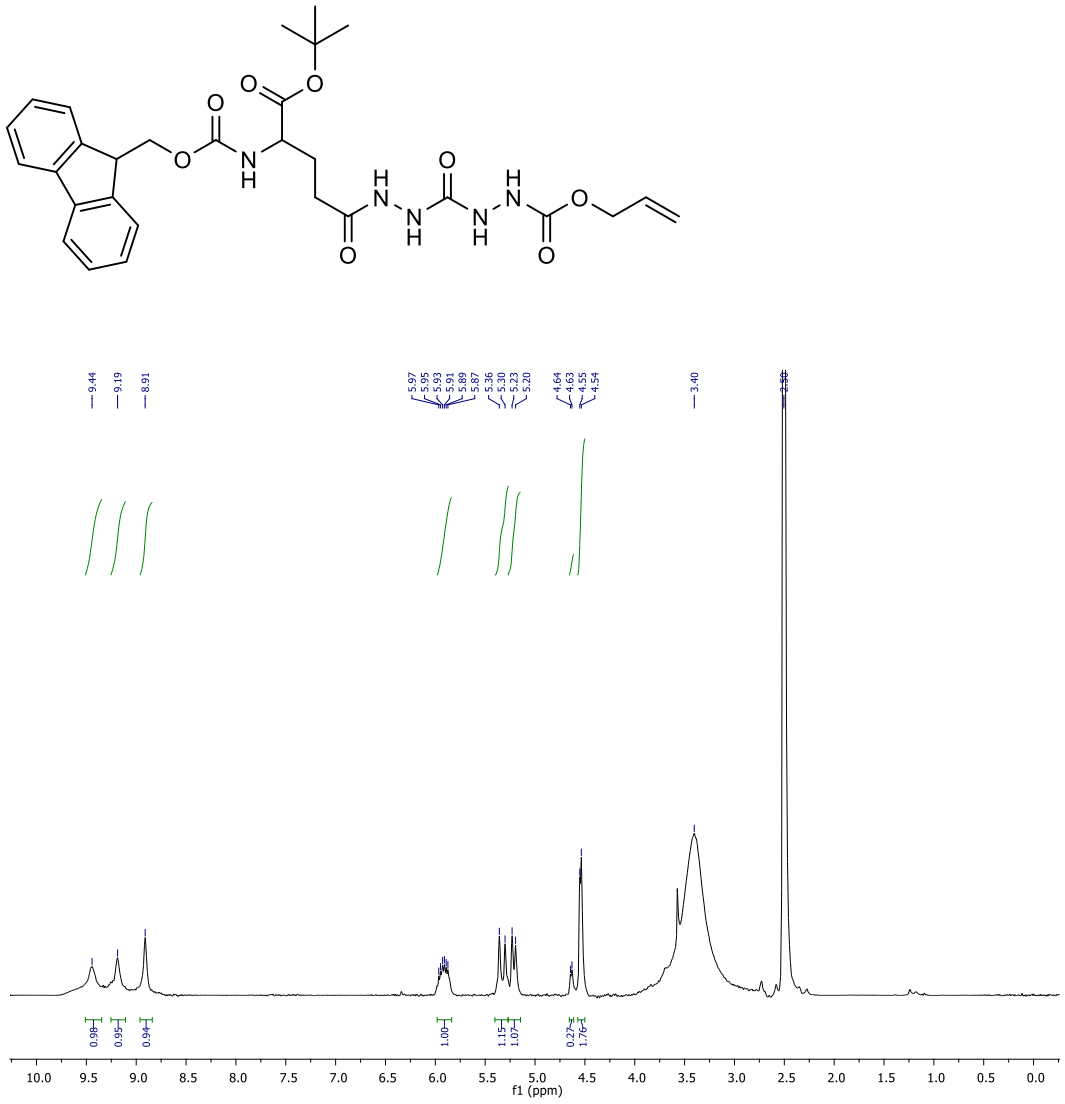

Figure 64. ^{1}H-NMR spectrum of KPM15 (300 MHz, DMSO-d_6)

^{1}H-NMR (DMSO-d_6): δ 1.40 (s, 9H), 1.72-1.84 (m, 1H), 1.89-2.00 (m, 1H), 2.20 (t, *J* = 7 Hz, 2H), 3.87-3.96 (m, 1H), 4.19-4.32 (overlapped, m, 3H), 4.50-4.51 (m, 2H), 5.19 (d, *J* = 10 Hz, 1H), 5.32 (d, *J* = 17 Hz, 1H), 5.81-5.95 (m, 1H),7.31-7.36 (m, 2H), 7.40-7.45 (m, 2H), 7.69-7.74 (m, 2H), 7.89-7.91 (m, 2H), 8.18 (br s, 1H), 8.25 (br s, 1H), 8.93 (br s, 1H), 9.51 (s, 1H).

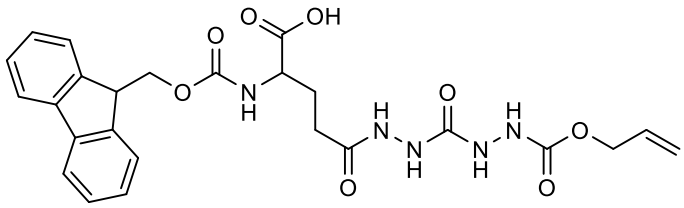

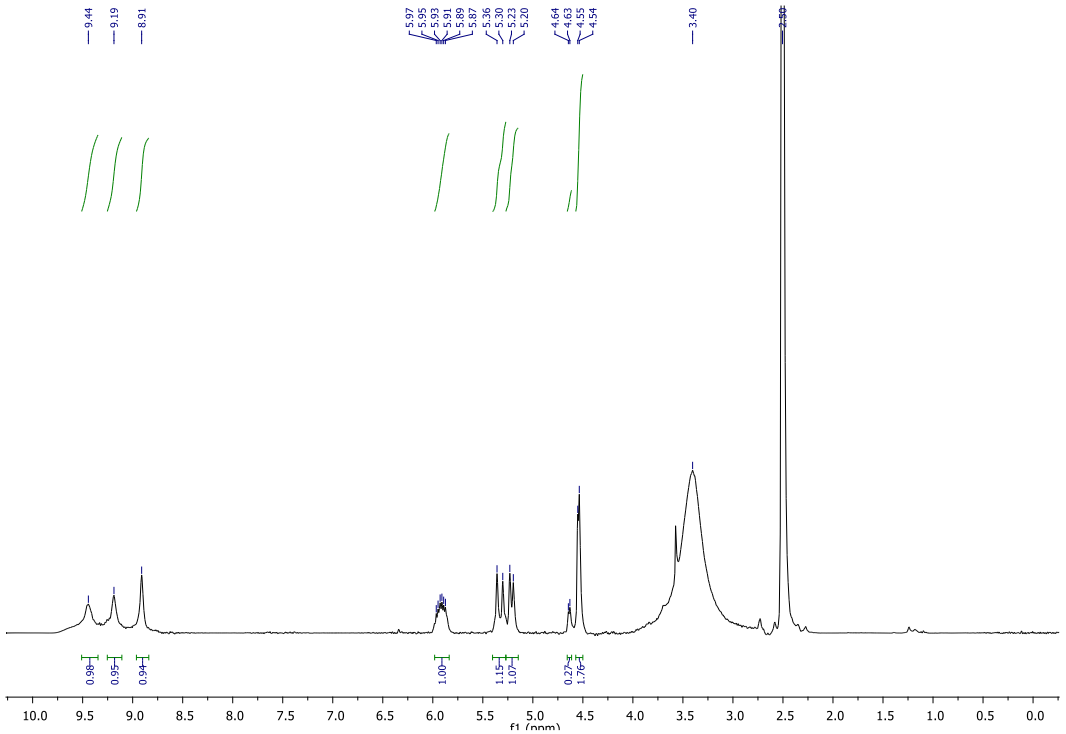

Figure 65. ^{1}H-NMR spectrum of KPM16 (300 MHz, DMSO-d_6)

^{1}H-NMR (DMSO-d_6): δ 1.76-1.87 (m, 1H), 1.94-2.07 (m, 1H), 2.21 (t, *J* = 7 Hz, 2H), 3.92-4.01 (m, 1H), 4.17-4.34 (overlapped, m, 3H), 4.50 (d, *J* = 5 Hz, 2H), 5.18 (d, *J* = 10 Hz, 1H), 5.31 (d, *J* = 17 Hz, 1H), 5.80-5.96 (m, 1H), 7.32-7.36 (m, 2H), 7.40-7.45 (m, 2H), 7.67-7.75 (m, 2H), 7.89-7.91 (m, 2H), 8.18 (br s, 1H), 8.26 (br s, 1H), 8.92 (br s, 1H),9.51 (s, 1H), 12.61 (br s, 1H).

13.3. Supplementary data: ATR-FTIR spectra

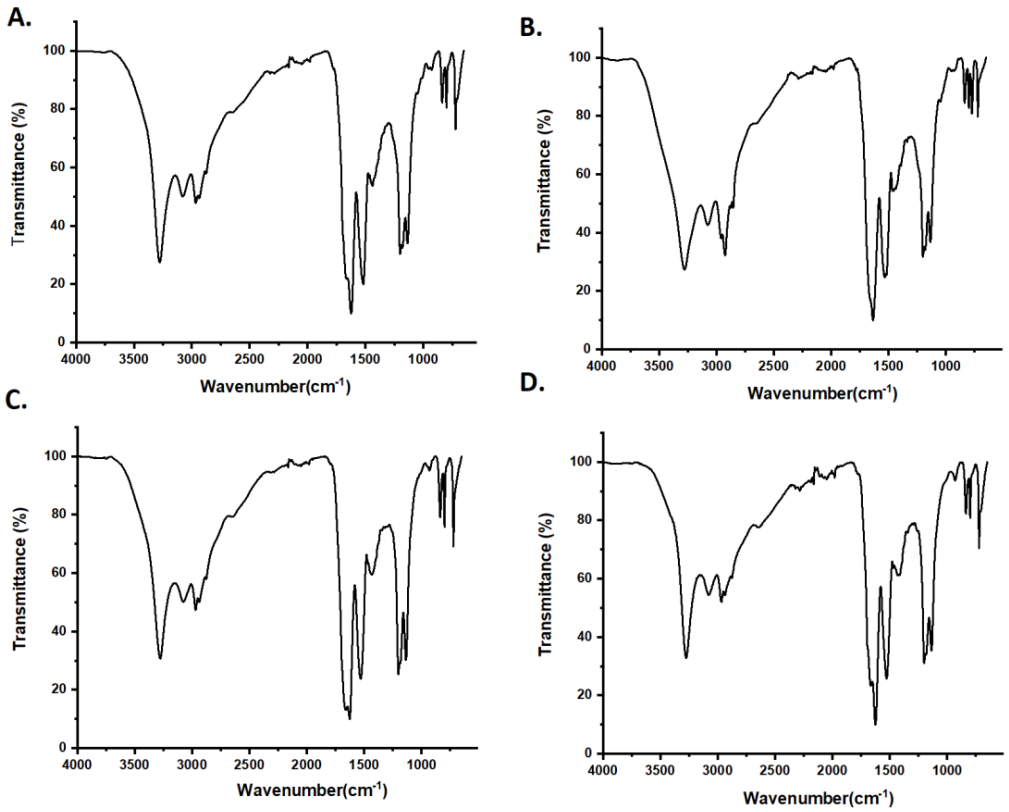

Figure 66. ATR-FTIR spectra of (A) WT1, (B) A30P, (C) WT2 and (D) A53T, acquired in the solid state.

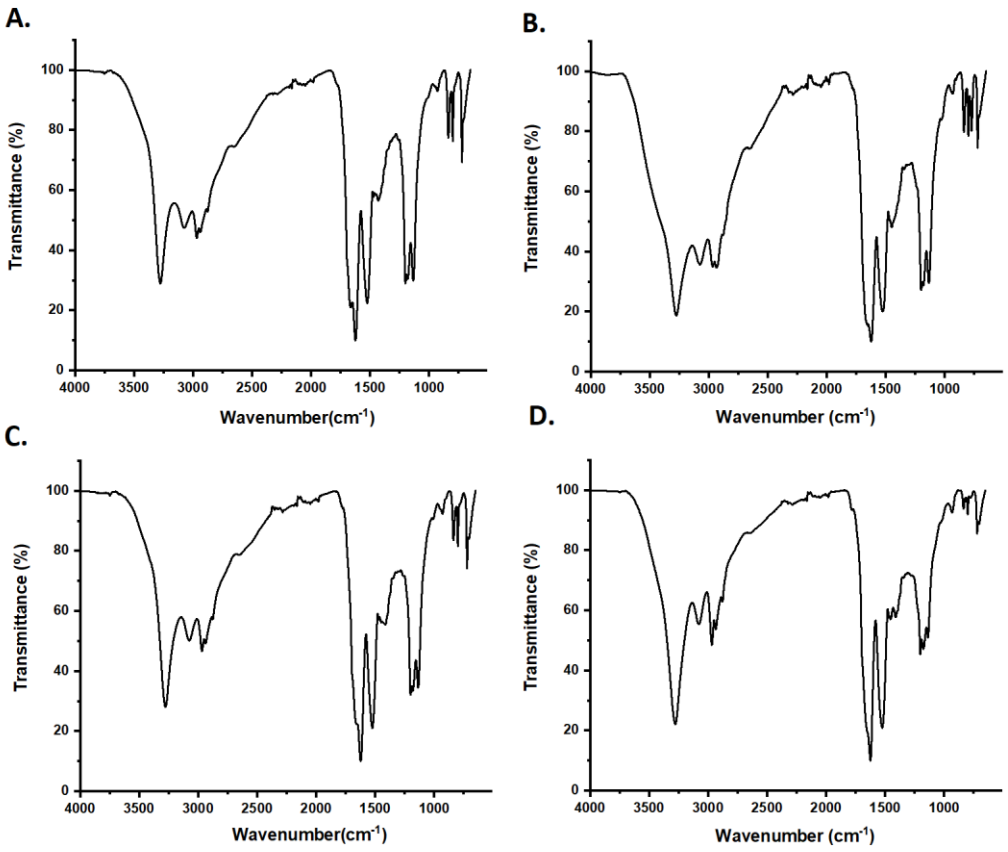

Figure 67. ATR-FTIR spectra of (A) E46K, (B) G51D, (C) H50Q and (D) NAC, acquired in the solid state.

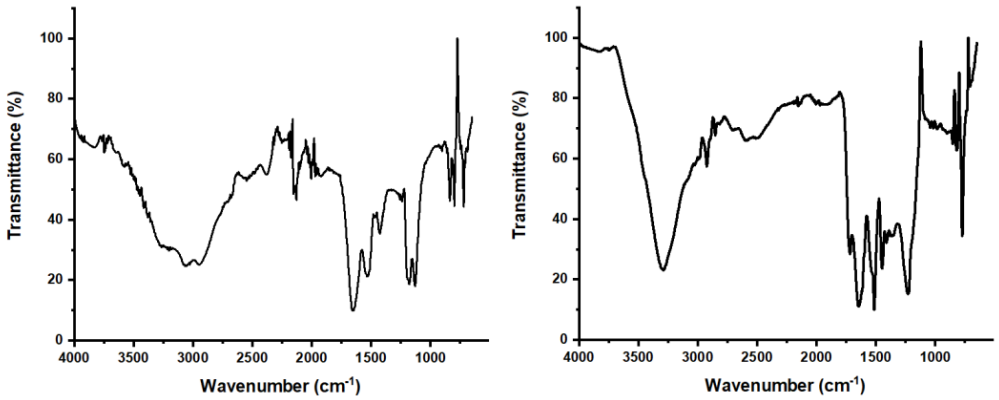

Figure 68. ATR-FTIR spectra of C1 (left) and C2 (right), acquired in the solid state.

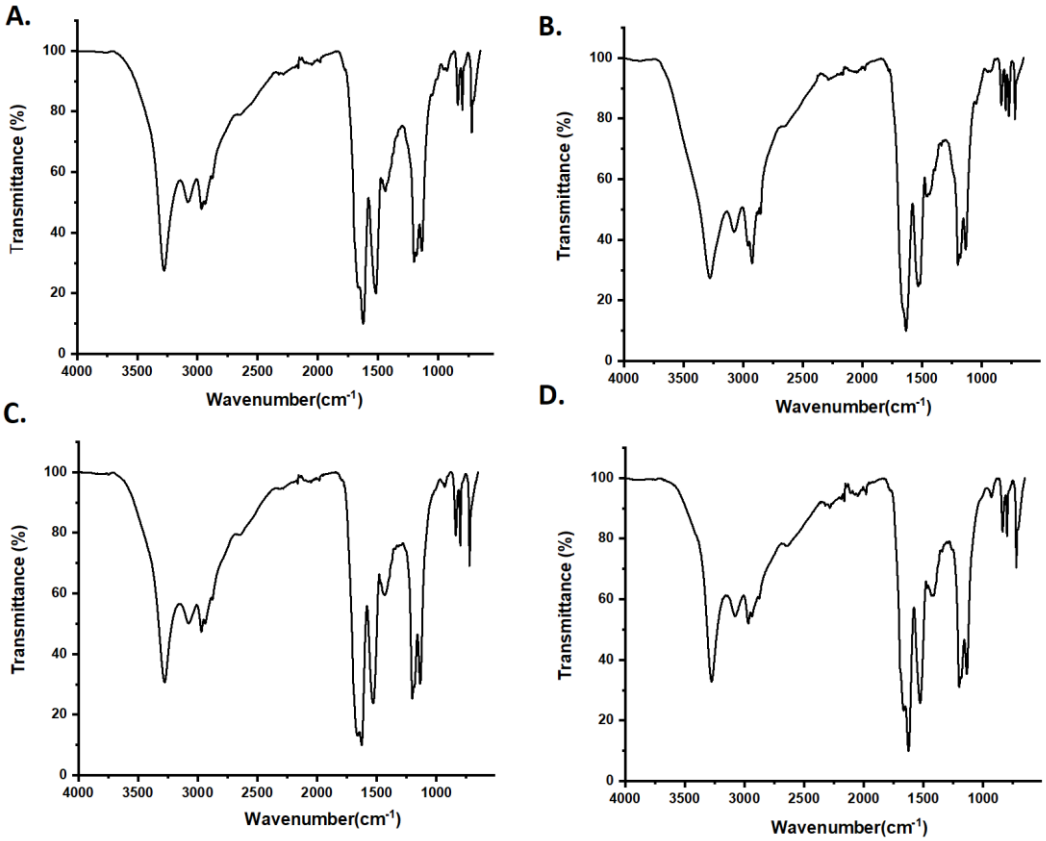

Figure 69. ATR-FTIR spectra of (A) WT1_scr, (B) A30P_scr, (C) WT2_scr and (D) A53T_scr, acquired in the solid state.

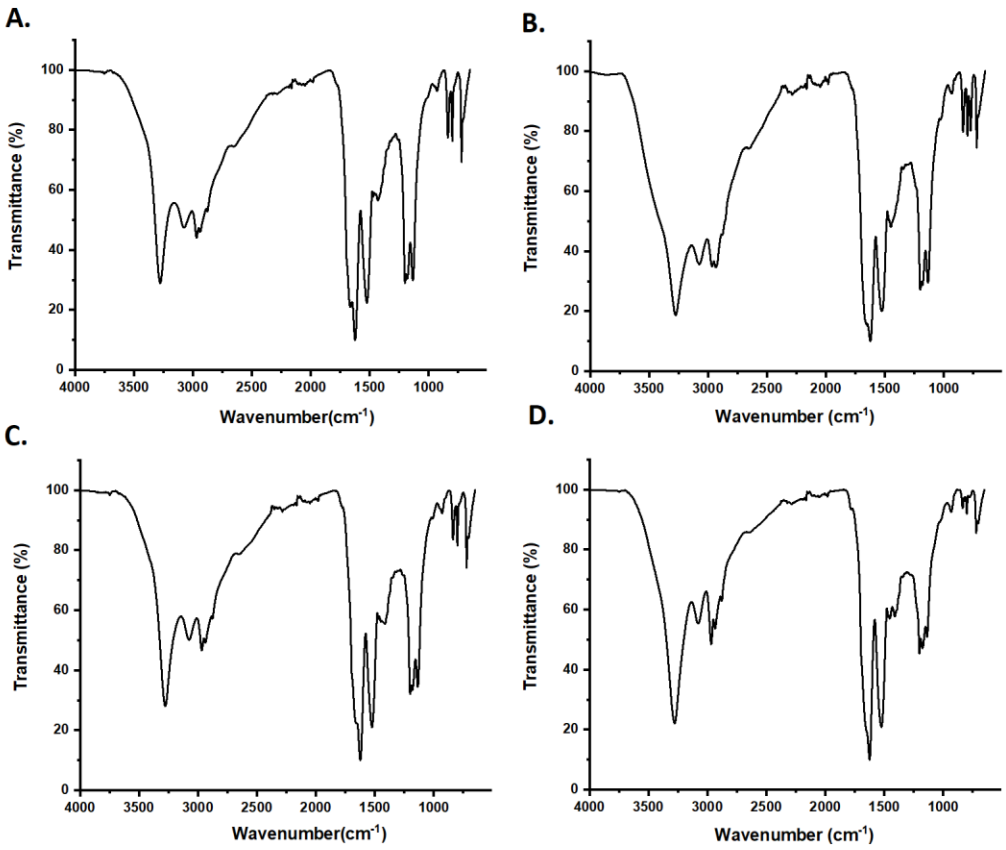

Figure 70. ATR-FTIR spectra of (A) H50Q_scr, (B) G51D_scr, (C) E46K_scr and (D) NAC_scr, acquired in the solid state.

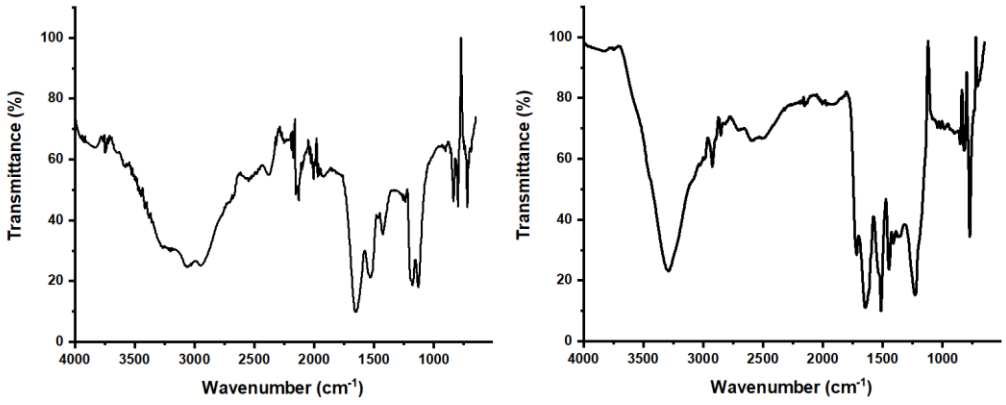

Figure 71. ATR-FTIR spectra of C1_scr (left) and C2_scr (right), acquired in the solid state.

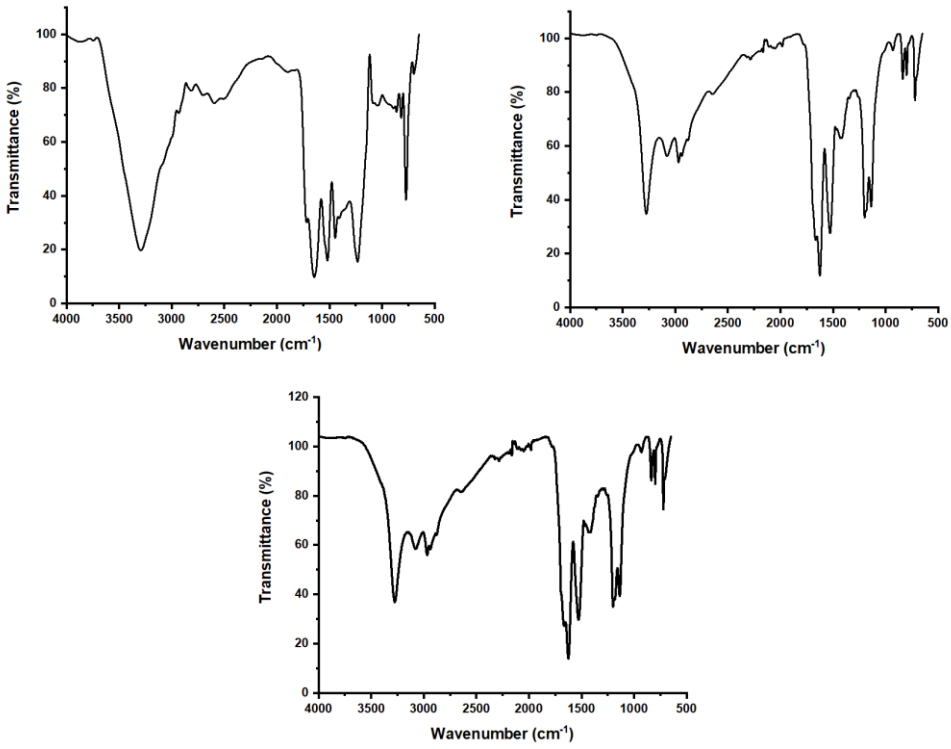

Figure 72. ATR-FTIR spectra of KPM1 (upper left), KPM2 (upper right) and KPM3(lower), acquired in the solid state.

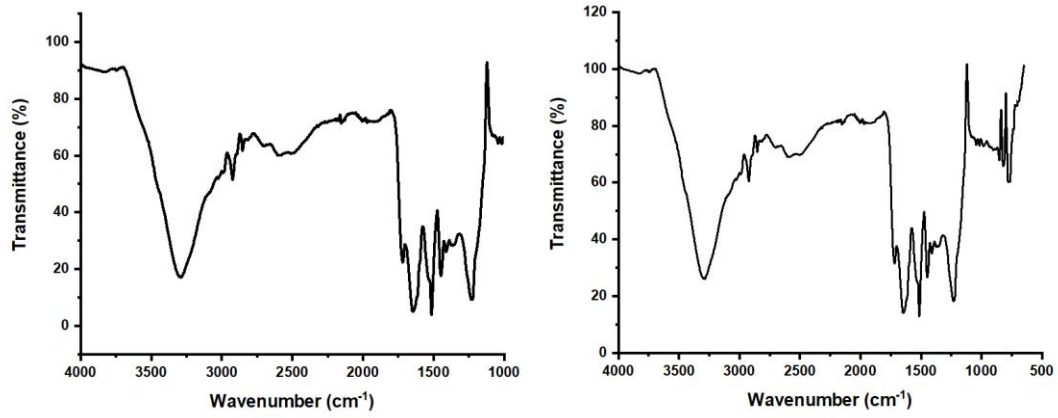

Figure 73. ATR-FTIR spectra of KPM6 (left) and KPM8 (right), acquired in the solid state.

14. ACKNOWLEDGEMENTS

At this part of my PhD thesis, I would like to express my gratitude to the people that helped me and supported me in these three years.

First, I would like to thank the TubinTrain network, our coordinator, Prof. Passarella for creating this and for including me. I would also like to thank Benedetta, for always being there and helping us with everything.

I would like to thank Prof. Sandrine, Nicolò and Julia, for accepting me in the group in Paris and for being there for some difficult time.

I would like to thank all my TubinTrain colleagues for being there and for sharing these three years with me. Annie, Josine, Helena, Zlata, Davide (or 'DL'), Nicolò (or 'NB'), Milo, Simone, Sai, Ahmed, Francesca, thank you for all the nice memories and interesting science discussions. In particular, I would like to thank the Milano girls, Zlatina, Helena and Josine for sharing the first months of the PhD and the Covid-19 period. Also, I would like to thank from my heart, sweet and caring Simone, for teaching me how to work with proteins, for all the cigarettes that we shared, all the beers and all for supporting me and my crying, grazie amico.

Avendo passato però ormai quattro anni in Italia, ci tengo a ringraziare tutte le persone che mi hanno aiutato e sostenuto in italiano.

Innanzitutto, vorrei ringraziare la mia tutor, Sara Pellegrino, che tutti chiamano Sara, ma che per me sarà sempre la Prof. Grazie di cuore per tutti i tuoi insegnamenti che mi hanno fatto crescere e diventare la persona che sono oggi. Grazie per tutti i consigli e per avermi tranquillizzato prima di ogni presentazione. Grazie per tutte le volte che mi hai ricordato che sono brava e per avermi apprezzato dal primo giorno.

Grazie alle altre due 'peptidare', Lucia (ovvero la spani) ed Elisa (ovvero la bionda/mima), per tutti i momenti che abbiamo condiviso. Elisa, grazie per avermi fatto vedere il duomo più bello dell'Italia, per avermi insegnato l'italiano, per tutte le sigarette che abbiamo fumato insieme, per tutte le volte che io piangevo e tu mi abbracciavi cercando di tranquillizzarmi. Lucia, la mia spani, non so neanche da dove cominciare. Sei la collega migliore che abbia mai avuto, una delle persone più belle che abbia mai conosciuto, con una generosità infinita, un cuore tenero ed una mente fuori dal comune! Grazie per avermi asciugato le lacrime anche tu, soprattutto nei momenti più difficili quando mi hai abbracciato e mi hai spinto ad andare avanti. Grazie per tutti i consigli, sia a livello scientifico ma anche personale. Grazie per essermi stata vicino anche quando eravamo lontane.

Grazie di cuore ai miei colleghi/amici di laboratorio, Fra Vaghi, Raffa, Leti, Matteo, Sabri, Crash e Antonia che siete stati i primi a sopportarmi, aiutarmi, passarmi la passione per la chimica ed insegnarmi dei trucchetti. Mi avete fatto sentire a casa dall'inizio, mi avete accettato e abbracciato come una famiglia. Avete anche sopportato i miei 'good morning' che urlavo ogni mattina. Grazie anche a Tommy, la nostra ultima 'new entry' che è subito diventato un collega (anche se lui dice che non siamo colleghi) e un amico. Grazie ragazzi, per tutti gli aperitivi, tutte le cene, tutte le ricette italiane, tutte le pause caffè, tutte le chiacchere.

Grazie a tutti i compagni di laboratorio che ho avuto in questi tre anni, a tutti i miei studenti, con cui ho condiviso dei momenti bellissimi, incluse le difficoltà che mi hanno fatto crescere tantissimo.

Grazie Giordi, amor de mi corazón, di tutte le belle esperienze che abbiamo avuto insieme, tutte le uscite, i pranzi, le sere, le risate.

Grazie alle mie zie, Kena e Shefi e a mia cugina, Martina, per avermi aiutato tantissimo da ogni punto di vista. Grazie Kena, per essermi stata vicina, perché sei

come la sorella che non ho mai avuto, sei una delle persone che mi ha ispirato di più, mi sento proprio fortunata ad essere tua nipote.

Non potrei non ringraziare Francesco. Sei nella mia vita solo da un anno, ma mi sembra di conoscerti da sempre. Grazie per tutte le volte che mi hai abbracciato, ricordandomi che va bene sbagliare delle volte, che mi ami così come sono con la tua tenerezza. Grazie anche a te per avermi passato la tua passione per la chimica. Grazie per tutte le volte che hai cucinato tu la cena perché io dovevo scrivere la tesi.

Και για το τέλος, θα ήθελα να ευχαριστήσω όλα τα άτομα που μου στάθηκαν, όχι μόνο αυτά τα τρία χρόνια του διδακτορικού, αλλά γενικότερα στην ζωή μου. Θα ήθελα να ευχαριστήσω την οικογένεια μου, τον πιο γλυκό μπαμπά του κόσμου, Αρμπεν ή Beni, όπως τον φωνάζει η μαμά. Σ'ευχαριστώ μπαμπά μου, για όλα όσα μου έχεις προσφέρει, για όλη την αγάπη και φροντίδα, για όσες φορές μου στάθηκες και με βοήθησες σε όλα τα επίπεδα. Ευχαριστώ και σένα, μαμά, Paqe που έχεις την πιο ζεστή αγκαλιά, και που καταλαβαίνεις τι έχω, μόνο από το πως θα σου πω καλημέρα. Σ'ευχαριστώ που με φροντίζεις ακόμα και στα 29 μου, που όταν έρχομαι στο σπίτι, είμαι πάντα το παιδί σου. Σας ευχαριστώ και τους δυό, που μου μάθατε τι είναι η ανιδιοτελής αγάπη. Θα ήθελα, επίσης, να ευχαριστήσω τον αδεφρό μου, Μάρκο, ο οποίος με τον δικό του μοναδικό τρόπο μου έχει σταθεί, είναι εκεί και ας είναι μακρυά και βλέπει ακόμα την μικρή Καλλιρόη, μα αγαπά την μεγάλη.

Τελευταίες και καλύτερες, οι κολλητές μου, τα κορίτσια μου, που πίστεψαν σε μένα, ακόμα και τις φορές που εγώ δεν πίστεψα, που με έκαναν να αγαπήσω τον εαυτό μου, που η κάθεμια τους μου δίδαξε κάτι διαφορετικό. Όλες τους αποτελούν πηγή έμπνευσης για μένα και χωρίς αυτές, δεν θα ήμουν ο άνθρωπος που είμαι σήμερα. Καλλιόπη, Ευαγγελία, Μαρία και Υρώ, σας ευχαριστώ για όλες τις στιγμές που ζήσαμε μαζί, για όλα τα τηλεφωνήματα, για όλες τις γκρίνιες μου, τα

ξεσπάσματα μου, για όλες τις φορές που έκλαψα και μου σκουπίσατε τα δάκρυα, με αγκαλιάσατε και με ωθήσατε να συνεχίσω. Ευχαριστώ για την ανιδιοτελή και ανεκτίμητη αγάπη και φιλία σας.